AUBURN

SAMUEL GINN
COLLEGE OF ENGINEERING

Research Report for ALDOT Project 930-738

SELF-CONSOLIDATING CONCRETE FOR PRESTRESSED APPLICATIONS—PHASE I: GIRDER FABRICATION AND PRE-ERECTION PERFORMANCE

Submitted to

The Alabama Department of Transportation

Prepared by

Samuel D. Keske, Robert W. Barnes, Anton K. Schindler,
Emily L. Dunham, Brandon R. Johnson, and Morgan A. Ellis

APRIL 2015

Highway Research Center
Harbert Engineering Center
Auburn, Alabama 36849

www.eng.auburn.edu/research/centers/hrc.html

1. Report No. FHWA/ALDOT 930-738	**2. Government Accession No.**	**3. Recipient Catalog No.**
4 Title and Subtitle Self-Consolidating Concrete for Prestressed Applications—Phase I: Girder Fabrication and Pre-Erection Performance		**5 Report Date** April 2015 **6 Performing Organization Code**
7. Author(s) Samuel D. Keske, Robert W. Barnes, Anton K. Schindler, Emily L. Dunham, Brandon R. Johnson, and Morgan A. Ellis		**8 Performing** FHWA/ALDOT 930-738
9 Performing Organization Name and Address Highway Research Center 238 Harbert Engineering Center Auburn, AL 36849		**10 Work Unit No. (TRAIS)** **11 Contract or Grant No.**
12 Sponsoring Agency Name and Address Alabama Department of Transportation 1409 Coliseum Boulevard Montgomery, AL 36130-3050		**13 Type of Report and Period Covered** Technical Report **14 Sponsoring Agency Code**

15 Supplementary Notes
Project performed in cooperation with the Alabama Department of Transportation

16 Abstract

Prior to statewide acceptance of self-consolidating concrete (SCC) in precast, prestressed bridge member production, the Alabama Department of Transportation sponsored an investigation of the material to be performed by the Auburn University Highway Research Center. Two parts of that research are presented in this report: a laboratory investigation of fresh stability test methods to quantify the unique fresh behavior of SCC, and a field investigation of as-built material and pre-erection structural behavior in the first full-scale SCC girders produced in Alabama for an in-service bridge.

During the laboratory investigation, the Visual Stability Index, Sieve Stability, and Surface Settlement tests correlated most strongly to multiple measures of hardened concrete uniformity; a testing protocol utilizing these test methods is recommended. Use of SCC in girder production was clearly beneficial. The utilized SCC mixture exhibited practically the same compressive strength, slightly reduced elastic stiffness, and increased time-dependent deformation (creep and shrinkage), at least in representative cylinders. However, the differences were expectable due to differences between the utilized SCC and vibrated concrete (VC). Also, SCC-girder transfer lengths, initial cambers, initial prestress losses, pre-erection time-dependent camber growth, and pre-erection time-dependent prestress force were found to be acceptably similar and at least as predictable as in companion, geometrically identical VC girders. Therefore, pre-erection behavior of SCC should not restrict its use in the production of precast, prestressed girders using current design and production procedures.

17 Key Words SCC, stability test methods, uniformity, transfer length, prestress transfer, creep, shrinkage, effective prestress, camber	**18 Distribution Statement** No restrictions. This document is available to the public through the National Technical Information Service, Springfield, Virginia 22161

19 Security Classification (of this report) Unclassified	20 **Security Classification (of this page)** Unclassified	**21 No. of pages** 303	**22 Price**

Form DOT F 1700.7 (8-72)

Research Report

ALDOT Research Project 930-738

SELF-CONSOLIDATING CONCRETE FOR PRESTRESSED APPLICATIONS—PHASE I: GIRDER FABRICATION AND PRE-ERECTION PERFORMANCE

Prepared by

Samuel D. Keske

Robert W. Barnes

Anton K. Schindler

Emily L. Dunham

Brandon R. Johnson

Morgan A. Ellis

Highway Research Center
and
Department of Civil Engineering
at
Auburn University

APRIL 2015

DISCLAIMERS

The contents of this report reflect the views of the authors, who are responsible for the facts and the accuracy of the data presented herein. The contents do not necessarily reflect the official views or policies of Auburn University or the Federal Highway Administration. This report does not constitute a standard, specification, or regulation.

NOT INTENDED FOR CONSTRUCTION, BIDDING, OR PERMIT PURPOSES

Robert W. Barnes, Ph.D., P.E.
Anton K. Schindler, Ph.D., P.E.
Research Supervisors

ACKNOWLEDGEMENTS

Material contained herein was obtained in connection with a research project "Implementation of Self-Consolidating Concrete for prestressed applications—Phase I: Girder fabrication and pre-erection performance," ALDOT Project 930-738, conducted by the Auburn University Highway Research Center. Funding for the project was provided by the Alabama Department of Transportation. The cooperation and assistance of the ALDOT Materials and Tests Bureau, Bridge Bureau, and Maintenance Bureau, Hanson: Pelham Prestress, BASF Construction Chemicals, and Racon General Contractors are gratefully acknowledged. The contributions of Wes Bullock and Levent Isbiliroglu to this work are greatly appreciated. The authors particularly acknowledge the contributions of the following individuals:

Buddy Black	ALDOT, State Bridge Engineer
Buddy Cox	ALDOT, State Materials and Tests Engineer
Lyndi Blackburn	ALDOT, Assistant Bureau Chief – Materials and Tests Bureau
Sergio Rodriguez	ALDOT, Special Projects Engineer, Montgomery
Craig Philips	ALDOT, Hillabee Creek Bridge Project Manager
Daniel Jones	ALDOT, Maintenance Bureau
Nathan Emmerich	Hanson: Pelham Prestress, Quality Control Manager
Dwain Hamby	Hanson: Pelham Prestress, Engineering Manager
Frankie Smith	Hanson: Pelham Prestress, Plant Manager
Rickey Swancey	BASF, Senior Sales Representative

ABSTRACT

Self-consolidating concrete (SCC) is a high-performance concrete in the fresh state—because of its highly fluid fresh behavior, it requires no mechanical consolidation during placement. Prior to statewide acceptance of SCC in precast, prestressed bridge member production, the Alabama Department of Transportation (ALDOT) sponsored an investigation of the material to be performed by the Auburn University Highway Research Center. Multiple aspects of that investigation are synthesized in this report, including material stability behavior evaluated in a laboratory setting and material and structural behavior evaluated in full-scale girders to be placed in an in-service bridge. In both settings, SCC was evaluated relative to vibrated concrete (VC) and considering existing design standards and construction practices.

The laboratory investigation focused on quantification of SCC stability, a unique property of the material that is important to assess during construction. Five fresh concrete stability tests were conducted on nine SCC mixtures each placed in walls of heights equaling 54, 72, and 94 inches. Fresh test results were then compared to the results of hardened uniformity testing conducted on the concrete walls. Analyses indicate that some SCC fresh stability tests correlate well with hardened concrete uniformity. Suitable fresh SCC tests and acceptance criteria are recommended, as is a testing protocol for use during implementation of SCC in the production of precast, prestressed elements.

The full-scale implementation of precast, prestressed SCC girders consisted of seven BT-54 bulb-tees and seven BT-72 bulb-tees placed in a bridge in rural Alabama. Companion girders were constructed with vibrated concrete. Fresh concrete properties and early-age structural properties including initial responses to transfer and time-dependent growth of camber and prestress loss were evaluated until prior to the addition a cast-in-place deck over the girders.

After accounting for differences in elastic stiffness at transfer, SCC girders exhibited approximately the same transfer length as VC girders; all were shorter than predicted using current design provisions. SCC appeared to exhibit a lesser stiffness (5–15% less relative to the square root of its strength) and greater time-dependent deformability (approximately 5–10% greater creep and 30% greater shrinkage) than VC in representative cylinders, but full-scale time-dependent and elastic responses (camber and prestress maintenance) were practically identical in the SCC and VC girders. Furthermore, full-scale SCC structural behavior was no less predictable than that of VC according to typical material and structural-behavior models.

All measured behaviors were accurately or conservatively predicted, and the use of design material properties in place of measured values led to distinct under-prediction of structural performance. Based on the results of this laboratory and full-scale testing, it is concluded that SCC is an acceptable alternative to vibrated concrete in the construction of precast, prestressed bridge girders using current design and production procedures.

TABLE OF CONTENTS

LIST OF FIGURES

LIST OF TABLES

LIST OF ABBREVIATIONS AND SYMBOLS

$A_{subscript}$	Area, described by “subscript”
AASHTO	American Association of State Highway and Transportation Officials
AEA	Air-entraining admixture
ALDOT	Alabama Department of Transportation
AMS	Average maximum strain, used to quantify transfer length
AUHRC	Auburn University Highway Research Center
BT-54	Bulb-tee girder 54 inches in height
BT-72	Bulb-tee girder 72 inches in height
cgp	Center of gravity of bottom-bulb prestress
CI	Confidence interval, a statistical measure of reliability of a measurement
CTE	Coefficient of thermal expansion
d_b	Nominal bar diameter, as of (where appropriate) the diameter of non-prestressed steel or prestressing strand reinforcement
DEMEC	Demountable mechanical strain gauge
DOT	Department of Transportation
e	Eccentricity of prestress force, as in relation to the centroid of the transformed area, e_{tr}, or gross area, e_{pg}
E	Modulus of elasticity, as of concrete, E_c, concrete specifically at transfer, E_{ci}, prestressed reinforcement, E_p, or deformed steel reinforcement, E_s
f_c	Measured compressive strength (or f_{ci} specifically for measured compressive strength at the time of prestress transfer)
f'_c	Specified compressive strength (or f'_{ci} specifically for specified compressive strength at the time of prestress transfer)
f_{cgp}	Concrete stress at the center of gravity of prestressing
f_{ct}	Splitting tensile strength
f_{pe}	Effective prestress in prestressing strands after all losses
f_{pj}	Jacking stress in prestressing strand
f_{pt}	Stress in the prestressing strand immediately after release
f_{pbt}	Stress in the prestressing strand immediately prior to release

HRWRA	High-range water-reducing admixture
I	Moment of inertia, as of the gross section, I_g, or transformed section, I_{tr}
$J(t,t_i)$	Compliance at a time, t, due to a load applied since an earlier time, t_i (also known as J)
k	Correction factor for nonstandard concrete composition or conditions, used by the *AASHTO LRFD* provisions to model time-dependent deformation
K_1	Aggregate modification factor used in calculation of E_c
L	Length, (where appropriate) of ultrasonic pulse path or girder length
l_t	Transfer length
M	Bending moment at a given cross section due to an applied load
MC	Model Code, specifically the European CEB-FIB Model Code 2010
n	Modular ratio, used in transformed-section analysis to transform areas of different materials based on relative E
NMSA	Nominal maximum size aggregate (also known as nominal aggregate size)
pcy	Pounds per cubic yard, used for concrete batch proportions
R^2	Regression coefficient of determination, used (as noted) to describe linear or non-linear strength of fit
s/agg	Sand-to-total-aggregate ratio by mass
SCC	Self-consolidating concrete
SCM	Supplementary cementitious material
SSD	Saturated surface-dry
t	Time, used in various predictions of time-dependent material and structural behavior
T_{50}	Time for SCC slump flow to reach a diameter of 50 cm (20 in.)
UPV	Ultrasonic pulse velocity
VC	Vibrated concrete (also known as conventionally vibrated concrete)
VMA	Viscosity-modifying admixture
V/S	Volume-to-surface-area ratio
VSI	Visual stability index
v_t	Time-correction factor as determined in Equation 5-2
v_u	Ultimate creep coefficient as determined in Equation 5-1

VWSG	Vibrating-wire strain gauge
w/cm	Water-to-cementitious material ratio, by mass
w_c	Weight of concrete, unreinforced
WRA	Water-reducing admixture
X	Independent variable, used in various equations related to the measurement or prediction of time-dependent deformation
y	Vertical distance from the centroid to the location at which strain or stress is determined, as with respect to the transformed section, y_{tr}
Y	Dependent variable, used in various equations related to the measurement or prediction of time-dependent deformation
α	Constant of proportionality used to normalize transfer length per Equation 4-1, or α' as alternatively derived in Equation 4-9
β_c	Coefficient to account for development of creep over time after loading, used by the European Model Code provisions
γ	Correction factor for nonstandard concrete composition or exposure conditions, used in Equation 5-1 or Equation 5-6
δ	Camber, particularly midspan camber (positive results represent upward deflection)
Δ	Change, as in change in temperature, ΔT, stress, Δ*f*, or strain, Δ*ε*
ε	Strain, used or calculated in various applications related to time-dependent or elastic deformation (or microstrain με, equal to $\varepsilon(10)^{-6}$)
$\varphi(t,t_o)$	Creep coefficient at a time *t* due to a load maintained since an earlier time t_o, used by the European Model Code provisions
$\psi(t,t_i)$	Creep coefficient at a time *t* due to a load maintained since an earlier time t_i, used by the *AASHTO LRFD* provisions
ω_{BP}	Bazant-Panula coefficient of variation, a statistical indicator of strength of curve fitment (always positive; results approaching 0 indicate better fit)

CHAPTER 1: INTRODUCTION

1.1 BACKGROUND ON SCC FOR PRECAST, PRESTRESSED GIRDERS

ACI 237 (2007) defines self-consolidating concrete (SCC) as a highly fluid, non-segregating concrete that can spread through reinforcement and completely fill formwork without the use of mechanical consolidation. Because of its fluid nature, SCC can efficiently fill congested or irregularly shaped members more easily than vibrated concrete (VC) while providing an improved surface finish. Its use also eliminates the need for vibratory consolidation efforts and associated construction labor and hazards and reduces wear and tear on formwork and equipment. Therefore, one of the most advantageous uses of SCC is in the production of precast, prestressed bridge girders, where reinforcement congestion and member shape can make filling and consolidation of VC difficult.

SCC achieves its unique fresh characteristics through the use of different constituent materials, proportions, or both. However, research concerning the effects of these mixture changes on the material has produced some mixed results, both with regard to fresh behavior and hardened-material and structural behavior. Understanding these effects is critical in the especially demanding environment associated with the production of precast, prestressed girders. Consequently, prior to statewide acceptance of SCC in precast, prestressed bridge member production, the Alabama Department of Transportation (ALDOT) sponsored a comprehensive investigation of SCC to be performed by the Auburn University Highway Research Center (AUHRC).

Past AUHRC laboratory-based research projects associated with this investigation have included formulation of SCC mixture proportions (Schindler et al. 2007), studies of the structural behavior when prestressed (Boehm et al. 2010; Levy et al. 2010), and evaluation of time-dependent properties (Kavanaugh 2008). The final phase of the investigation was to produce Alabama's first in-service bridge with precast, prestressed SCC girders, a task which took place from September, 2010 to November, 2011. AUHRC personnel monitored the entire process from the plant production through the addition of a cast-in-place concrete deck over the girders. Some of the girders, as they were erected over Hillabee Creek, are shown in Figure 1.1.

Figure 1.1: Erection of precast, prestressed girders over Hillabee Creek

1.2 STATEMENT OF OBJECTIVES

The primary objective of this research was to determine the acceptability of SCC for use in ALDOT precast, prestressed applications, particularly concerning fabrication and early-age behavior. Topics reported include evaluation of the

- Assessment and quantification of the fresh concrete stability of SCC,
- Effects of construction practices on the behavior of precast, prestressed members constructed with SCC,
- Differences in hardened material behavior in response to changes in the mixture proportions, as well as their predictability and significance, and
- Differences in structural performance prior to deck addition due to changes in material behavior, as well as their significance and predictability relative to current design and construction practices.

1.3 REPORT METHODOLOGY AND OUTLINE

The work documented in this report was conducted in two parts. The first involved the evaluation of fresh concrete stability test methods during the production of many different SCC mixtures and

the second involved the evaluation of a variety of behaviors in a one-to-one comparison of the SCC and VC girders produced for the Hillabee Creek Bridge with minimal researcher interference or direct involvement. Thus, different investigative approaches were associated with each part.

The laboratory investigation, which is presented in Chapter 2, focused on quantification of SCC fresh stability, a unique property of the material that has been difficult to rapidly and accurately assess previously. In the investigation, five fresh concrete stability tests were conducted on a variety of prestressed-suitable SCC mixtures each placed in walls of heights equaling 54, 72, and 94 inches. Walls were also constructed with control VC mixtures of similar proportions and materials, and the in-place concrete uniformity of each group of walls was evaluated nondestructively and destructively. Fresh SCC test results were then compared to the results of the hardened concrete uniformity testing to evaluate the correlations between these tests.

The evaluation of the full-scale project production took a different approach—researcher involvement in the design of the bridge, selection of mixtures, and production of the girders was minimized specifically so that the as-produced results of the process would be assessed. Furthermore, only one SCC and one VC mixture were used throughout production. The plant personnel used the implemented VC mixture regularly and were familiar with its expected behavior, so the producer chose to create an SCC using the same aggregate source (but a different gradation), cementitious materials, and water-to cementitious material ratio (*w/cm*) as in the VC for convenience. Thus, this research involved the assessment of a variety of fresh-material, hardened-material, and structural behaviors of comparable SCC and VC on a one-to-one basis. Topics relevant to girder fabrication and pre-erection performance that are assessed include

- Mechanical properties of SCC, including compressive strength and modulus of elasticity,
- Girder responses to the transfer mechanism, including transfer length, initial elastic prestress loss, and initial camber,
- Time-dependent deformation of concrete materials, particularly due to creep and shrinkage effects, and
- Time-dependent structural behavior of precast, prestressed girders, particularly regarding camber and maintenance of prestress.

The laboratory analysis involved the intentional varying of fresh concrete properties and proportions (frequently to intentionally yield concretes of a poor stability), so results from it should be considered separately from the results of the evaluation of full-scale trial production that are presented in Chapters 3–6. Conversely, while conclusions regarding the acceptability of SCC for full-scale implementation are derived from the latter part of this investigation, the results should

not be considered to be universal to all SCC. Self-consolidating behavior can be achieved in mixtures of infinitely varying constituents and proportions, so the presented results are most directly applicable to concretes made using comparable mixture constituents, proportions, and construction practices as employed in this project. Equally important are conclusions regarding whether the behavioral differences between SCC and VC are *expectable* or *predictable* in response to differences in their mixture properties, as these conclusions are more widely applicable.

CHAPTER 2: ASSESSMENT OF FRESH STABILITY

2.1 INTRODUCTION

SCC differs from VC primarily in the fresh state, and it can be proportioned to achieve practically any behavior in the hardened state (Bartos 2005). The unique, self-consolidating nature of SCC is practically described by three fresh properties: filling ability, passing ability, and stability. ACI 237 (2007) defines these properties:

- Filling ability (or unconfined flowability) refers to SCC's ability to fill formwork under its own weight,
- Passing ability (or confined flowability) refers to SCC's ability to pass through constricted spaces and around obstacles without blockage, and
- Stability (or segregation resistance) refers to SCC's ability to maintain a uniform distribution of its constituents during flow and setting.

Much research has been conducted to show that properly proportioned and prepared SCC can behave acceptably similarly to VC in the hardened state. Many researchers (Cussigh 1999; Daczko 2003; Khayat et al. 1997; and Soylev and Francois 2003) have determined that SCC exhibits acceptably similar hardened properties to those of their vibrated counterparts in concretes for many different applications; however, investigations continue concerning SCC in some especially demanding applications such as the production of precast, prestressed girders, where many properties and aspects of structural behavior need additional consideration.

With regard to the effect of fresh properties on structural behavior, the primary concern must be the *hardened uniformity* of the final product. Hardened properties of concrete (strength, stiffness, etc.) are affected by mixture proportioning, but that concept is not unique to SCC. Instead, the unique fresh nature of SCC is inherently only capable of affecting hardened concrete uniformity. Considering the three fresh properties described above, the effect of filling and passing ability on hardened concrete uniformity can be assessed visually or using widely accepted, standardized test methods. Both fresh properties depend on the intended application (ACI 237 2007)—elements with minimal confinement, congestion, or filling restriction require relatively less filling and passing ability. Elements with heavy reinforcement congestion, irregularly shaped formwork, or long flow distances (such as precast, prestressed girders) require relatively high filling and passing ability.

Like filling and passing ability, the degree of stability required of SCC can depend on the application (ACI 237 2007). However, assessment of this property in the fresh state and determination of its effects on hardened concrete properties may not be intuitive or easily tested.

Furthermore, the relevance of fresh property testing and in-situ uniformity testing to global structural behavior of concrete is unclear. The testing of in-place hardened properties can be difficult to interpret or time- and labor-intensive and can only be performed after completion of the placement. Therefore, proper identification of stability in the fresh state, as well as understanding of the relationship between fresh stability results and hardened concrete uniformity, is paramount to the successful implementation of SCC. Thus, the primary objectives of this research were to

- Identify fresh test methods that provide a quantitative assessment of the degree of stability of SCC for precast, prestressed applications, and
- Recommend the testing protocol that the Alabama Department of Transportation (ALDOT) should implement to address SCC stability during the production of precast, prestressed elements.

2.2 LITERATURE REVIEW

2.2.1 Fresh Concrete Stability Test Methods

Test methods that have been used in the assessment of fresh SCC stability (segregation resistance) are described in this section. They may be categorized by many traits: field- or laboratory-suitability, standardization status, segregation mechanism identified, speed of assessment, or others. Each of these considerations is discussed in the following test-specific subsections.

2.2.1.1 Visual Stability Index

The visual stability index (VSI) is the most widely used test to assess the stability of SCC (Lange et al. 2008) and was included in the first SCC-specific test to be standardized by ASTM. The VSI involves assigning a rating to the level of segregation seen in a sample of SCC. This sample, the patty left after testing the slump flow according to ASTM C1611 (2005), is inspected for visible signs of segregation. A rating from 0–3 is then assigned based on appearance: 0 showing no signs of segregation; 1 showing some bleed water on the SCC surface; 2 showing a slight, defined mortar halo (< 0.5 in.) and noticeable bleeding; and, 3 showing clear segregation with aggregate piling in the center and with a well-defined mortar halo (> 0.5 in.) (ASTM C1611 2005). PCI (2004) also gives advice on the half-increments of 0.5 and 1.5. In those Guidelines, a 0.5 rating is applicable when light bleeding is noticeable on otherwise non-segregating SCC, while a 1.5 rating is applicable when minor mortar separation and aggregate piling are visible.

The VSI is qualitative in nature and is subject to each technician's assessment. Therefore, while it is useful for rapid quality assurance during production, the VSI should not be

used to determine prequalification acceptance or rejection of a mixture (ACI 237 2007). Several summary reports (EPG 2005; Ozyildirim and Lane 2003) suggest that the VSI is sufficient for initial segregation inspection. Other researchers (Bonen and Shah 2004; 2005; Lange et al. 2008) suggest that a low VSI (showing good segregation resistance) does not ensure adequate stability.

Bonen and Shah (2004; 2005) and Lange (2007) state that the VSI is inadequate to study *static* stability because performance of the slump flow test imparts kinetic energy into the SCC, which can affect the appearance of static segregation. In fact, Tregger et al. (2010) suggest that the VSI from the slump-flow patty should only be used to assess dynamic stability. Furthermore, mixtures that do not bleed (one form of segregation) are less sensitive to the VSI (ACI 237 2007). This was confirmed by Khan and Kurtis (2010), Khayat and Mitchell (2009), and Peterman (2007), who have found unacceptable mechanical performance in SCCs with VSI values that indicated acceptable stability (VSI less than 2).

2.2.1.2 Column Segregation Test

The column segregation test (ASTM C1610 2006) was the second SCC stability test to be standardized by ASTM and is, therefore, often used to assess the static stability of SCC. Illustrated in Figure 2.1, this test involves pouring SCC into a cylindrical mold consisting of three detachable sections and allowing it to rest for 15 minutes. SCC from the top and bottom portions of the mold is then washed over a No. 4 sieve, leaving only the coarse aggregate. The coarse aggregate is then brought to the saturated surface dry (SSD) state and weighed. The weights of coarse aggregate in the top section and the bottom section are then compared to quantify segregation using a segregation index (I_{seg}). I_{seg} is calculated according to the following equation, in which *CA* is the weight of SSD coarse aggregate in the weighed section:

$$I_{seg} = 100\left[\frac{2(CA_{top} - CA_{bot})}{(CA_{top} + CA_{bot})}\right]$$

According to Koehler and Fowler (2010), the calculated I_{seg} may be less than zero due to test variability. ASTM C1610 (2005) states that, when that occurs, the value should be recorded as zero.

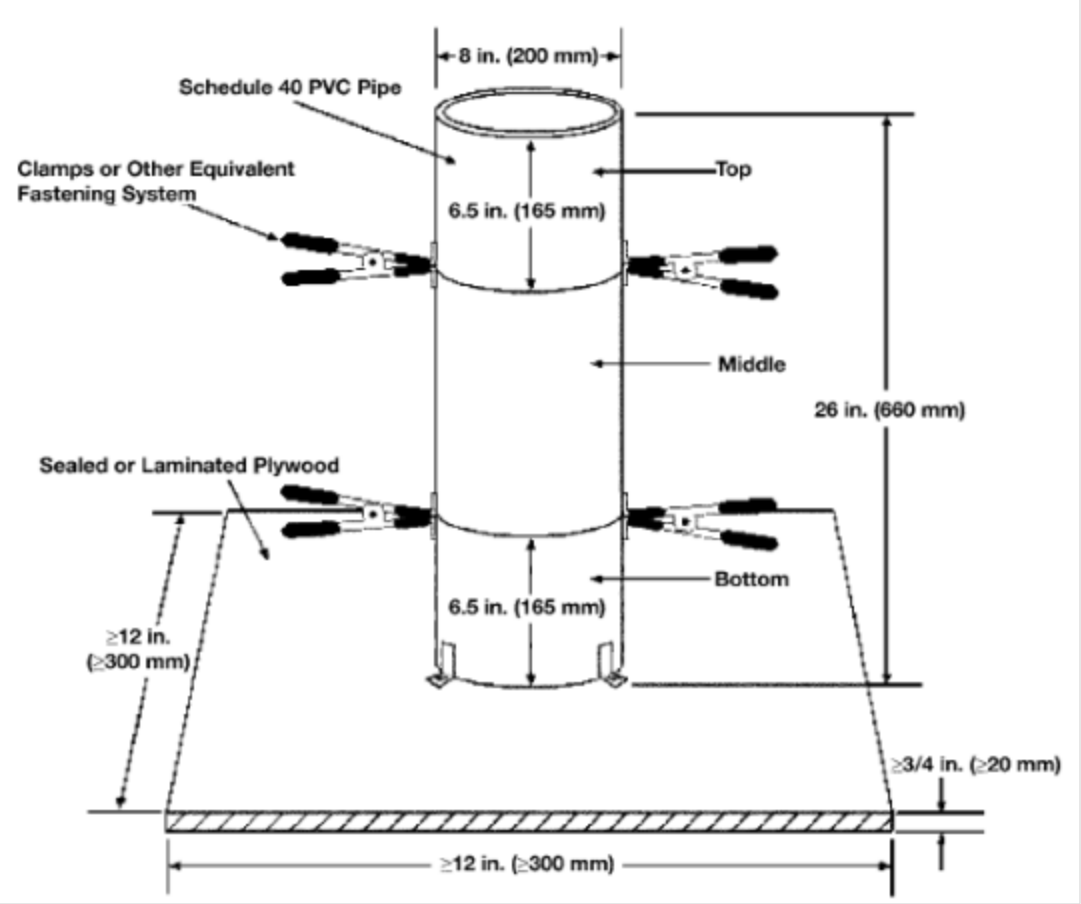

Figure 2.1: Standardized column segregation apparatus (ASTM C 1610 2006)

Assaad et al. (2004) and Khayat and Mitchell (2009) recommend using the column segregation test in conjunction with the surface settlement test described in Section 2.2.1.5, as the two tests may be sensitive to different forms of segregation. Similarly, Mouret et al. (2008) recommend using it in conjunction with the sieve stability test described in Section 2.2.1.4, as they found that the column segregation and sieve stability tests respond differently to segregation.

Many researchers (Bui et al. 2007; Koehler and Fowler 2010) have found the column test to be too slow and laborious to implement for quality assurance due to the 15-minute testing period and difficulty of separating and wet-sieving the test sample. However, Assaad et al. (2004), Khayat and Mitchell (2009), and Mouret et al. (2008) recommend using it for quality assurance testing of SCC stability.

2.2.1.3 Rapid Penetration Test

The rapid penetration test (ASTM C1712 2009) was developed to be a quicker, technician-friendly alternative to the column segregation test (Bui et al. 2007). To that effect, the test is run on SCC already placed in the inverted slump cone for VSI and slump flow testing. After allowing the sample to settle for 80 seconds, a weighted hollow penetration cylinder, shown in Figure 2.2, is placed on the top surface and allowed to settle under its own weight. After 30 seconds, the penetration depth (Pd) of the cylinder is read to the nearest millimeter, which may be related directly to the mortar layer depth at the top of the sample and indirectly correlated to segregation resistance. According to ASTM C1712 (2009), Pd relates to stability by the following:

- Samples with Pd < 0.4 in. are resistant to segregation,
- Samples with 0.4 in. ≤ Pd < 1.0 in. are moderately resistant to segregation, and
- Samples with Pd > 1.0 in. are not resistant to segregation.

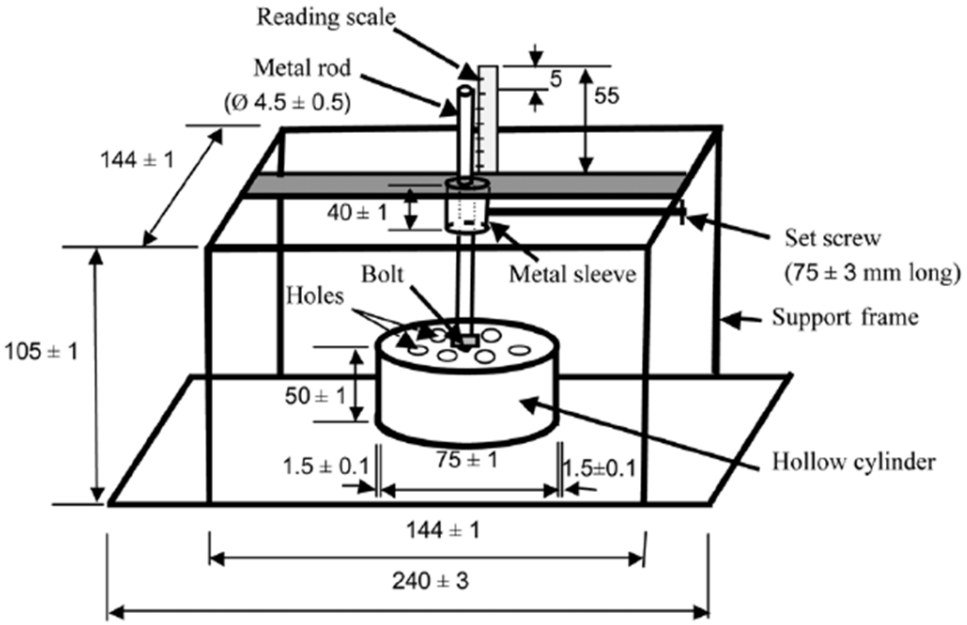

Figure 2.2: Standardized rapid penetration test apparatus (ASTM C1712 2009) (*Note: All units in millimeters; 1 in. = 25.4 mm*)

ASTM C1712 (2009) was developed by establishing a relationship between its results and those of the column segregation test (Bui et al. 2007). A relationship between the column segregation test results and the mortar layer depth at the top of hardened cylinders was also determined after vertically cutting the cylinders and measuring the depth to the first coarse aggregate particle. Bui et al. (2007) found that mortar depth relates to segregation index and penetration depth, thereby allowing use of the penetration test in place of the column test. According to ASTM C1712 (2009) and Bui et al. (2007), the test is useful for both mixture

prequalification and quality assurance, as it is faster than the column segregation test and is not subjective like the VSI.

ASTM C1712 (2009) recommends establishing a new correlation between the penetration and column segregation tests whenever dealing with new mixture proportions; penetration depth limits discussed earlier are only applicable to mixtures with less than 65% total aggregate volume. Koehler and Fowler (2010) have found the rapid penetration test to be poorly related to both the column segregation test and sieve stability test (described in the next section). The Self-Compacting Concrete European Project Group (EPG 2005) found the rapid penetration test to have greater scatter than the sieve stability test, and they recommend it as a secondary alternative to the sieve stability test. The test's use in peer-reviewed research has been limited, although similar tests (described in Sections 2.2.1.6 and 2.2.1.7) have been used elsewhere.

2.2.1.4 Sieve Stability Test

The current form of the sieve stability test (a.k.a. sieve segregation resistance test, sieve test, or GTM screen stability test) was standardized by the SCC European Project Group (EPG 2005) following a three-year study by the EPG representative organizations. The test, shown in Figure 2.3 and detailed in Appendix B.1, requires an approximately fifty pound sample of SCC and approximately eighteen minutes of testing time. After sitting for fifteen minutes, the top portion of the sample is poured from a specified height (usually with the assistance of a pouring apparatus) onto a sieve and pan. It then rests on the sieve for two minutes to allow separation of mortar and aggregate. After those two minutes, the sieve and retained SCC are removed from above the pan, and the sieved fraction (S) is calculated by dividing the weight of SCC passing onto the pan by the total weight of SCC tested according to the following equation:

$$S = \frac{[(pan + SCC\ sieved\ fraction) - (pan)]}{[(sieve + pan + SCC\ total) - (sieve + pan)]} \times 100$$

Figure 2.3: Sieve stability test apparatus

The EPG Guidelines (2005) specify the use of a 5 mm sieve, but the PCI guidelines (2004) allow a No. 4 (0.25 in.) sieve to be used in place of a 5 mm sieve because the No. 4 sieve is more common in the U.S. The EPG Guidelines (2005) recommend a sieved fraction 5% ≤ S ≤ 15%, as SCC with a sieved fraction less than 5% may begin to lack the flowability necessary to prevent bugholes and provide a good surface finish. More specifically, the guidelines classify sieve stability using the following classes (EPG 2005):

- S ≤ 20% for Class 1, which is applicable for slabs and applications with limited flow distances and clear spacing greater than 3 in.,
- S ≤ 15% for Class 2, which is applicable for vertical applications with limited flow distances and clear spacing greater than 3 in., and
- S ≤ 10% in demanding applications with greater flow distances and clear spacing less than 3 in., such as for precast, prestressed girders.

Because SCC is dropped from a height of 20 in. onto the sieve, El-Chabib and Nehdi (2006) and Koehler and Fowler (2010) question what form of segregation the sieve stability test identifies. Gravity causes an increase in kinetic energy as the SCC falls, resulting in forced

segregation of mortar from aggregate. Also, mixtures with a high mortar fraction and low coarse aggregate fraction may be more susceptible to testing poorly, as more mortar is present to pass through the sieve (El-Chabib and Nehdi 2006; Schwartzentruber and Broutin 2005).
Ng et al. (2006) contradict this observation regarding mixture proportioning. They found that mixtures with a high coarse aggregate fraction are more susceptible to testing poorly. For the same reason that the column segregation test becomes less sensitive as coarse aggregate content increases (see Section 2.2.1.2), the sieve test becomes *more* sensitive if it is able to identify bleeding and separation of mortar from aggregate. Mouret et al. (2008) found that the sieve test identifies segregation that the column test does not and vice versa, while others (EPG 2005; Koehler and Fowler 2010) have found the two tests to be highly correlated.

During a comprehensive study of SCC behavior, the sieve stability test was the best indicator of segregation when compared with the column segregation test and the rapid penetration test (EPG 2005). Although the form of segregation it identifies is unclear, EPG (2005) and Koehler and Fowler (2010) found that the sieve test seems to relate well with in-situ segregation. Johnson et al. (2010), on the other hand, present mixed results when comparing sieve stability results to results of core testing. They found the two to relate well in some trials and not in others. A lack of correlation was more frequently observed in mixtures with ¾ in. aggregate (Johnson et al. 2010).

Because of its simple nature, EPG (2005) recommends the sieve stability test as the primary on-site quality assurance measure of stability for SCC projects in the European Union. PCI (2004) found the sieve test to be unsuitable for on-site use due to its prolonged test duration.

2.2.1.5 Surface Settlement Test

The surface settlement test (a.k.a. surface settlement segregation test) was recommended by Khayat and Mitchell (2009) as the primary stability test for SCC in precast, prestressed bridge element production. The test has not been standardized by ASTM or by other European equivalents, but it has been used in SCC research for several years (Khayat 1998; Khayat et al. 1997; Khayat et al. 2003). The test is illustrated in its current form in Figure 2.4.

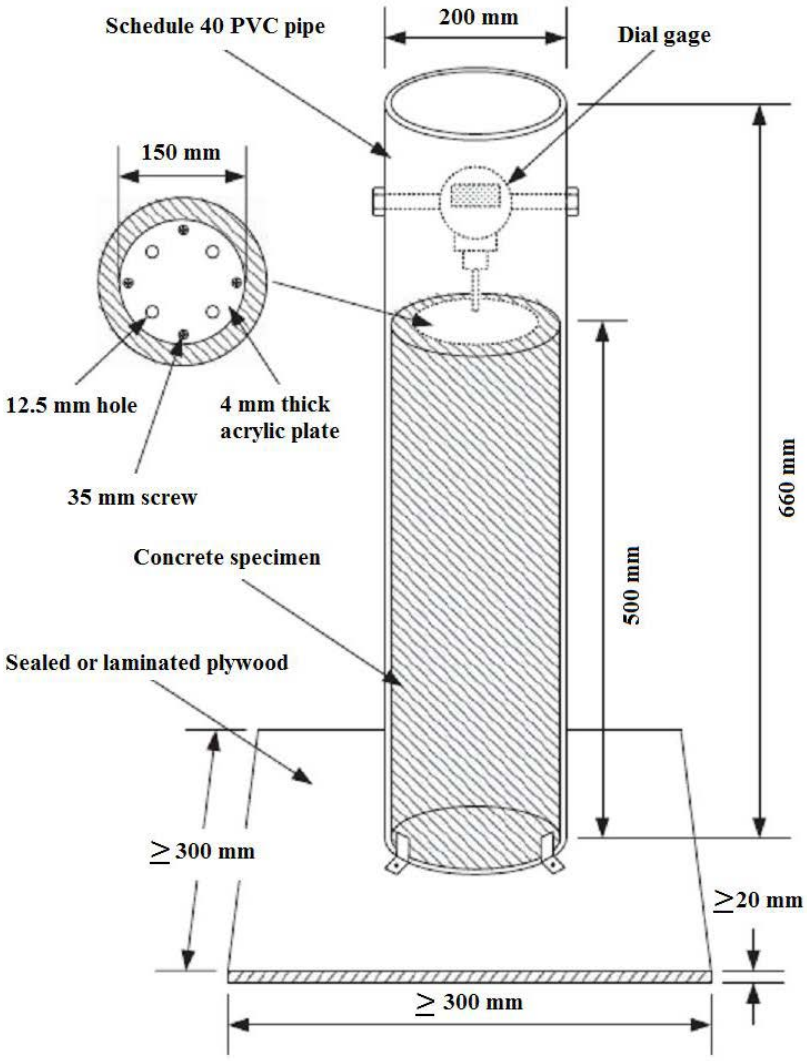

Figure 2.4: Surface settlement test apparatus (Khayat and Mitchell 2009)
(*Note: All units in millimeters; 1 in. = 25.4 mm*)

The principle of the test is simple: measure the settlement of a thin acrylic plate as it settles into a column of fresh SCC. The maximum settlement is recorded as a percentage of the height of the column of SCC, and the rate of settlement is calculated as a percentage of column height penetrated per hour. Either by settlement rate or maximum settlement, the test aims to study the presence of bleed water and paste at the top surface of the column and the settlement of the uppermost coarse aggregate particles.

The test was originally created to compliment in-situ uniformity testing of concrete walls (Khayat et al. 1997). Confirmed by pullout testing and visual examination of hardened cores, Khayat (1998; 1999) and Khayat et al. (1997) showed that the maximum settlement measured before the SCC sets indicates the level of static stability. Since this can take hours to determine, though, further testing was conducted that suggested the use of a rate of settlement calculated

over a five-minute interval of (10:00–15:00) or (25:00–30:00) minutes after test initiation (Hwang et al. 2006). The relationships they found are shown in Figure 2.5. Because of these relationships, Khayat and Mitchell (2009) recommend assessment by rate in order to improve testing convenience.

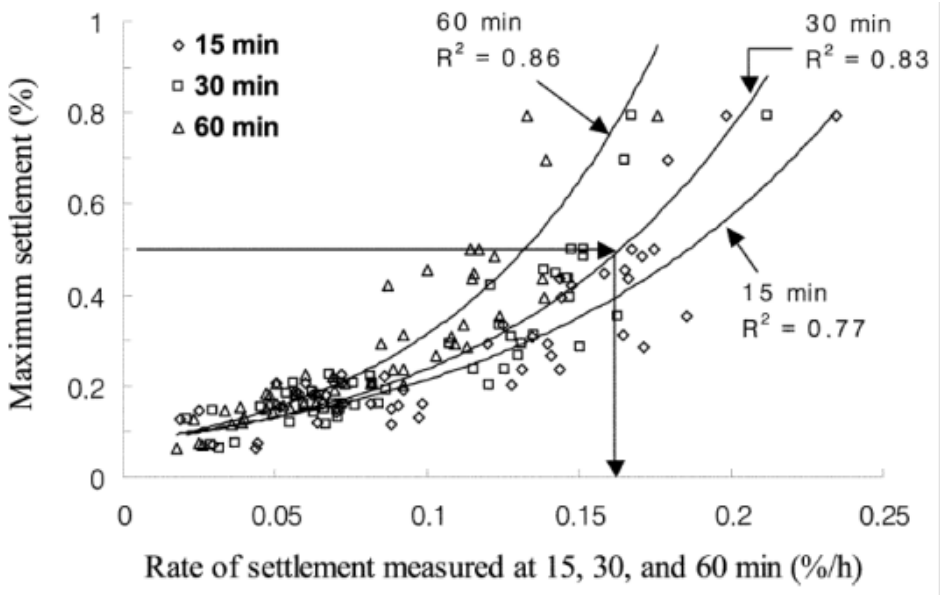

Figure 2.5: Relationships between rate of settlement and maximum settlement measured during the surface settlement test (Hwang et al. 2006)

Assaad et al. (2004) and Sonebi and Bartos (2002) have shown that the surface settlement test gives a good measurement of the development of bleeding, which they confirmed by comparison to other concrete stability tests and uniformity tests. Like the column segregation test and sieve test, though, surface settlement can be affected by the binder content and coarse aggregate content (Khayat 1999; Khayat et al. 2000; Sonebi and Bartos 2002). Increasing coarse aggregate content makes aggregate settlement more difficult, but at the expense of higher bleeding risk. Sonebi and Bartos (2002) also found that the test is sensitive to fine aggregate content, grading, and surface roughness, as these properties affect the bleeding potential of the mixture. Assaad et al. (2004) and Khayat and Mitchell (2009) therefore recommend that the settlement test compliment the column segregation test, as the two tests can be used to identify different forms of segregation.

2.2.1.6 Wire-Probe Penetration Test

The wire-probe penetration test (wire test) was designed to be a simpler, more repeatable replacement to the rapid penetration test (Lange et al. 2008; Shen et al. 2007). The test

equipment, shown in Figure 2.6, is constructed of a single piece of metal wire, twisted into a ring and vertical rod, with markings at every millimeter along the vertical rod. The wire is placed atop SCC in the inverted slump flow cone and allowed to settle for one minute, and the settlement of the metal ring is measured along the vertical rod left protruding from the sample.

Similar to other penetration-measurement tests, the wire test was created to measure the mortar layer at the top of a sample (Shen et al. 2007). The developers confirmed the test's ability to do so by analyzing DIA results from cores. They also compared its results those of the column segregation test, which showed an *exponential* increase in segregation as the wire test's settlement increased. The test has been standardized for use by the Illinois DOT (IDOT 2005), although its use in peer-reviewed research publications has been limited. Bui et al. (2007) suggested that the test may be less accurate than ASTM C1712 because of its lack of a lateral guide, as nothing forces the metal ring to sink directly downward into the sample.

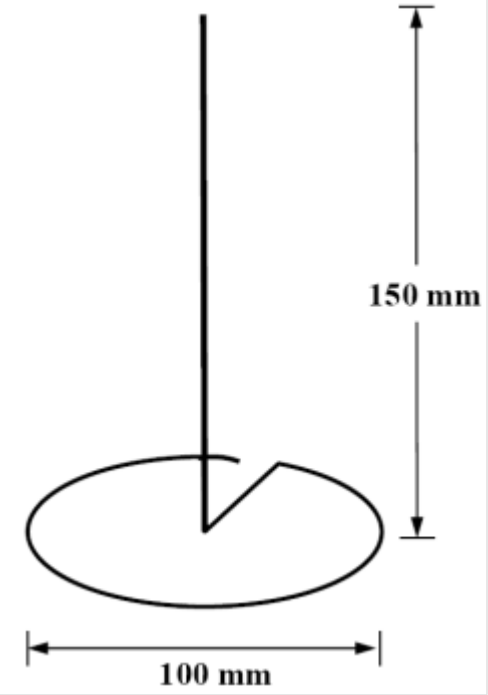

Figure 2.6: Wire penetration probe apparatus (adapted from Shen, Struble, and Lang 2007)

2.2.1.7 Multiple-Probe Penetration Test

Similarly to the wire test, the multiple-probe penetration test was originally based on the rapid penetration test (El-Chabib and Nehdi 2006). A schematic of the test is shown in Figure 2.7. The main difference between the multiple-probe test and the other penetration-based tests described above is that the multiple-probe test incorporates four solid penetration probes instead of one larger probe. El-Chabib and Nehdi (2006) suggest that averaging the displacement of four

probes atop the sample can reduce the variability of results. Random packing of coarse aggregate may allow very few coarse aggregate particles to resist the penetration of a large probe, but four probes should more closely represent the average mortar layer present on the sample (El-Chabib and Nehdi 2006).

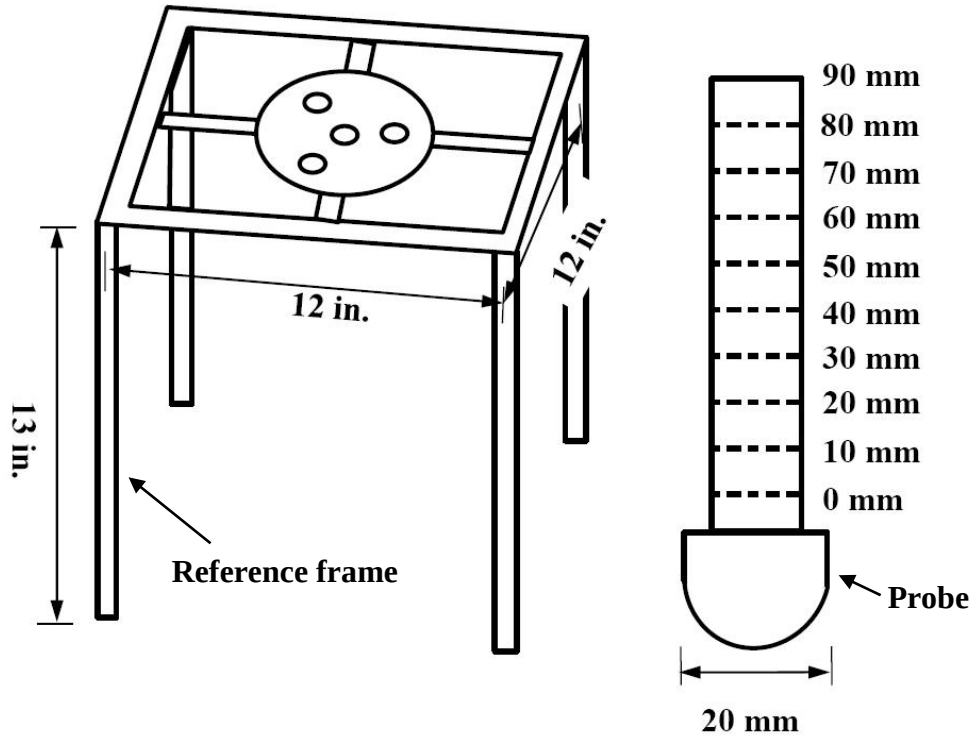

Figure 2.7: Multiple-probe penetration test apparatus (adapted from El-Chabib and Nehdi 2006)

During its development, the multiple-probe test was run in conjunction with the sieve stability test and a variant of the column segregation test. The researchers were able to relate its performance to these two tests in 123 SCC mixtures of varying aggregate contents and strengths. However, the multiple-probe test did not relate well with these tests, several other fresh concrete stability tests, or hardened uniformity of large-scale hardened specimens during preliminary testing for this research (Keske 2011). As shown in Figure 2.8, the four probes were subject to irregular settlement due to a lack of adequate lateral stabilization.

Figure 2.8: Multiple-probe penetration apparatus in use

2.2.1.8 Rheological Tests

Converse to the other fresh concrete stability tests described, rheological testing of SCC does not directly measure the segregation in a concrete sample. Instead, this class of tests measures the fundamental rheological properties of the sample (viscosity and yield stress) under the assumption that those properties are related to segregation. Conflicting conclusions have been drawn concerning the relationship of rheology to stability: some have found no statistically significant correlation (Assaad et al. 2004; Bartos 2005; Ozyildirim and Lane 2003; Sahmaran et al. 2007), while others have shown a tendency to segregate as viscosity decreases (Koehler et al. 2007; Saak et al. 2001).

As with the other fresh concrete stability tests described in this section, consideration must be given to how these conclusions were reached. In some past studies that incorporated the use of rheological testing, the fresh stability tests described above (including the column segregation test and VSI) were used as a basis for identifying segregation of concrete (Assaad et al. 2004; Bartos 2005; Koehler et al. 2007; Ozyildirim and Lane 2003). Elsewhere, hardened

concrete tests, including pullout testing and visual examination of aggregate distributions, were used to identify segregation.

In testing of bond quality, Peterman (2007) showed that rheological tests were no better a predictor of bond quality than other fresh concrete stability tests. Koehler et al. (2007) found excessive scatter in comparisons of rheology to aggregate distribution in cores, and Sahmaran et al. (2007) found similar excessive scatter between rheological and UPV testing. Saak et al. (2001) related rheology to settlement of a weight on the surface of SCC, but only settlement of aggregate was studied, not the bleeding of excess water.

2.2.2 Hardened Concrete Uniformity Test Methods

To effectively evaluate the fresh concrete stability test methods, the results from those tests were compared to measures of in-situ hardened concrete uniformity. Of the hardened properties of SCC most frequently affected by segregation, two were selected for identification of hardened concrete uniformity: ultrasonic pulse velocity and bond to reinforcement. Ultrasonic pulses sent through large hardened concrete specimens can show changes in elastic properties and composition (Mindess et al. 2003). Bond to reinforcement is affected by many forms of segregation: aggregate settlement, air migration, and bleeding (Castel et al. 2006; Soylev and Francois 2003). The details of these tests, as well as past research in which they have been employed, are described in the following subsections.

2.2.2.1 Ultrasonic Pulse Velocity Test

While strength testing and bond testing can show the effects of segregation on hardened performance, nondestructive ultrasonic pulse velocity testing (UPV) can directly measure changes in the overall quality of hardened concrete (Abo-Qudais 2005; Naik et al. 2004; Sahmaran et al. 2007). The test is conducted by placing two metal couplers on flat surfaces of the concrete specimen, initiating rapidly repeating ultrasonic pulses at one coupler, and measuring the average time required for the pulses to reach the other coupler. Once the travel length between couplers is determined, the average speed of pulses through that travel path is calculated. A typical configuration of this test is shown in Figure 2.9. The speed of the ultrasonic pulse is affected by several factors:

- Density and porosity, in which speeds are higher in denser, less porous material (Lin et al. 2007; Lin et al. 2003; Sahmaran et al. 2007),
- Interface quality between mortar and coarse aggregate, in which a better interface results in better transmission of waves (Abo-Qudais 2005; Soshiroda et al. 2006),

- Aggregate size, in which presence of larger aggregate results in reduced speed (Abo-Qudais 2005),
- Moisture content and concrete saturation, in which the water-filled pores transmit faster pulses (Abo-Qudais 2005; Mindess et al. 2003), and
- Strength and elasticity, in which speeds are higher in material of a higher strength or higher stiffness (Abo-Qudais 2005; Lin et al. 2007; Soshiroda et al. 2006).

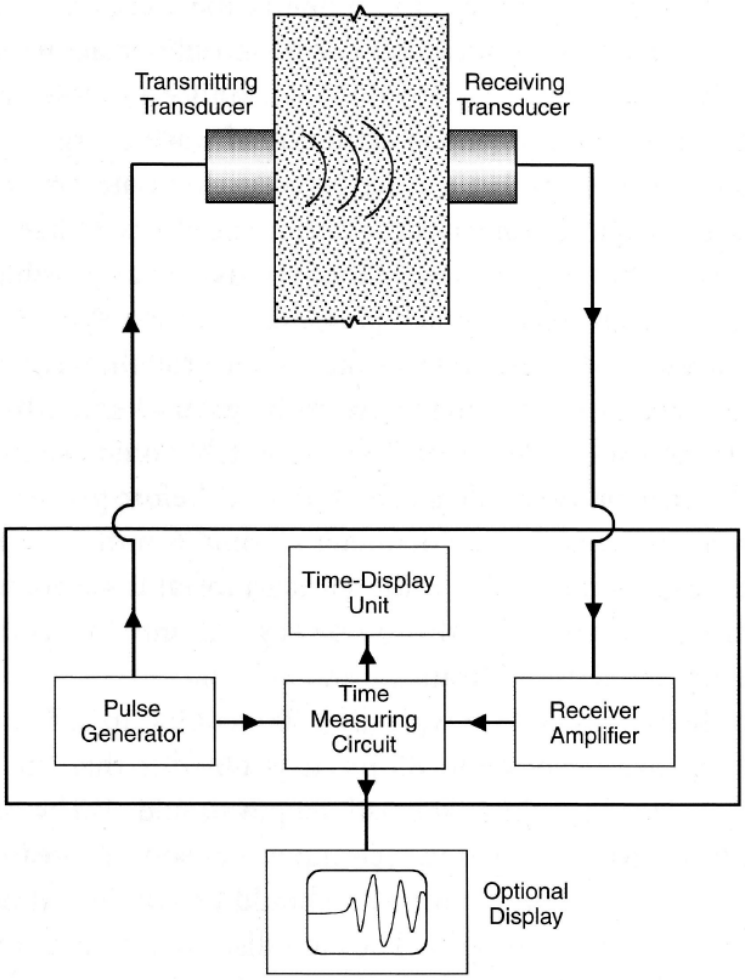

Figure 2.9: Ultrasonic pulse velocity testing equipment (Naik et al. 2004)

The factors that affect UPV results are all related to SCC uniformity: strength and elasticity relate to *w/cm*, density relates to distribution of constituents and mortar quality, and interface quality relates to presence of excess water (Mehta and Monteiro 2006). The ability to simultaneously account for these factors makes the UPV very useful for assessing the effects of possible segregation and for detecting changes in concrete quality at different locations within a concrete element.

To effectively use the UPV to study uniformity of concrete, care should be exercised in avoiding other sources of UPV variability. Variability can come from

- Reinforcement, which can either accelerate pulses by transmitting sound more quickly or attenuate pulses by scattering waves as they pass (Mindess et al. 2003; Naik et al. 2004),
- Large aggregate, which can scatter higher frequency waves as they pass through the material (Abo-Qudais 2005; Naik et al. 2004), and
- Cracks, which distort or block the travel of ultrasonic waves (Abo-Qudais 2005; Soshiroda et al. 2006).

Past research (Abo-Qudais 2005; Gaydecki et al. 1992) and guides for testing (ASTM C597 2002; Naik et al. 2004) have thoroughly outlined how to avoid these sources of variability. The first line of defense against irregularity is selection of the configuration and frequency of the equipment to be used. The direct transmission method, shown in Figure 2.10, is the preferred configuration of all groups referenced in this section because the travel length and form of transmission are easily defined.

For testing concrete, Gaydecki et al. (1992) recommend a frequency of 55–85 kHz and ASTM C597 (2002) recommends a frequency range of 40–80 kHz, both with a preference for higher frequencies when using shorter path lengths. There is no upper or lower limit to the path length, *L*, but Naik et al. (2004) recommend *L* be between 4 in. and 28 in. for 54 kHz transducers (the frequency used in this research). Cussigh (1999) used an *L* of 10 inches. At a frequency of 54 kHz, aggregate should have nominal dimensions no greater than 2.75 in., which is not a concern for precast, prestressed SCC. For reinforcement parallel to the direction of pulse transmission to not influence the signal, the bars must generally be laterally spaced at least 0.25*L* away from the test point, with a conservative estimate of 0.35*L* (Naik et al. 2004).

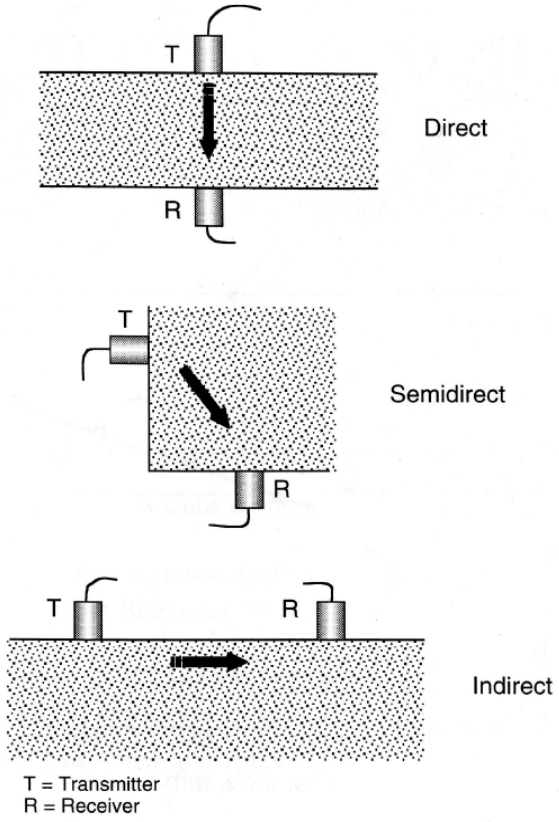

Figure 2.10: Ultrasonic pulse velocity testing transmission methods (Naik et al. 2004)

Unavoidable sources of UPV variability include cracking and degree of saturation (ASTM C597 2002). Good curing conditions, safe handling, and prevention of thermal cracking lessen the risk of cracking and non-uniform saturation. Readings through cracked concrete are drastically different than those taken through uninterrupted travel paths, making it easy to recognize them.

The influence of degree of saturation can only be normalized by testing samples at a consistent degree of saturation. Soshiroda et al. (2006) recommend taking readings at the earliest age possible after the concrete achieves final set because, over time, the strength of the mortar phase approaches that of the encapsulated coarse aggregate, resulting in faster UPVs that are less capable of differentiating between coarse aggregate contents. Later-age testing is, therefore, less useful for studying air, water, and aggregate distribution (Soshiroda et al. 2006).

2.2.2.2 Pullout Testing

Bond between reinforcement and concrete is a material mechanical property of broad applicability to structural performance. Although many configurations have been used to test it, the principle

is the same: apply tension to steel reinforcement cast into concrete specimens while recording the force applied. If the total bonded surface area is known, the bond stress is determined by dividing the pullout force by the surface area.

Pullout failure (also known as shear failure), occurs when sufficient confinement prevents splitting rupture of the concrete. In this failure mode, planes of shear stress caused by the mechanical interlock of reinforcement deformations and concrete develop parallel to the reinforcement. Microcracks develop in these planes, eventually coalescing until pullout failure occurs (ACI 408 2003). This failure mode shows a gradual buildup of bond stress as cracks form and a gradual decay as friction resists the pullout over extended displacements. Pullout testing that results in pullout failure can give a measure of concrete quality and uniformity not affected by inadequate cover or steel quality (Khayat et al. 2003), which makes it useful for studying the potential effects of segregation in SCC.

Researchers have related pullout failure to concrete quality using several variations of shortly bonded pullout specimens. Some researchers (Chan et al. 2003; Hassan et al. 2010) achieved adequate confinement by inclusion of confining reinforcement. To avoid the need for confining steel reinforcement, other researchers (Cattaneo et al. 2008; Girgis and Tuan 2005) achieved adequate confinement by increasing the lateral cover of the concrete surrounding the pullout bars. They (Cattaneo et al. 2008; Girgis and Tuan 2005) found that the minimum lateral cover that ensures pullout failure during pullout testing is eight times the nominal diameter of the steel bars pulled out (8 d_b).

Multiple researchers (Alavi-Fard and Marzouk 2004; Girgis and Tuan 2005; Khayat et al. 1997; Khayat and Mitchell 2009) have found that utilizing a bond length of 2.5 d_b to 3 d_b yields a satisfactory balance between achieving a uniform bond stress and having repeatable results . During that research, the bonded region of steel was isolated by debonding the remainder of the bar with commercially available plastic sheathing. A typical configuration of this style of pullout test is shown in Figure 2.11.

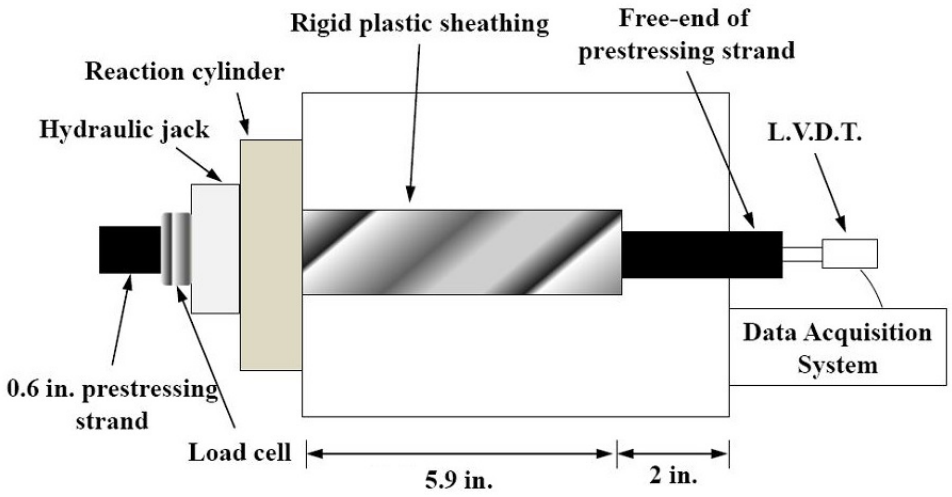

Figure 2.11: Configuration of shortly bonded pullout test (adapted from Khayat and Mitchell 2009)

The stresses in the concrete surrounding the pullout bar must also be considered in determining the test configuration. While the deformed steel reinforcement is tensioned, the concrete on which the tensioning jack rests is compressed. This compression can provide load-dependent, unnatural confining pressure around the steel bars, resulting in mechanically enhanced bond capacity. To avoid this effect, two steps are taken to disperse the compressive forces: seat the hydraulic jack at an adequate lateral distance from the pullout point, and place the bonded region of steel away from the loaded face of the concrete. Khayat (1998) embedded the bonded region 5 in. from the loading surface of the concrete, Khayat and Mitchell (2009) embedded it 6 in. from it, and Sonebi and Bartos (1999) embedded it 3 in. from it.

It would seem most appropriate to study the bond capacity of SCC used in precast, prestressed applications by pulling out seven-wire prestressing strand instead of deformed steel reinforcement. Many researchers have studied the interaction between strand and concrete in large specimens with long bonded lengths. This type of testing, which was also conducted during the research described in this report, is described in detail in Chapter 4. Khayat et al. (2003), Khayat and Mitchell (2009), and Stocker and Sozen (1970), on the other hand, tested bond to strand using a shortly bonded, pullout-failure-inducing configuration.

Stocker and Sozen (1970) confirmed that bond capacity of vibrated concrete is more significantly affected by bleeding and settlement than by strength, and Khayat et al. (2003) confirmed that stable SCC has better strand bond uniformity over height than VC. Stocker and Sozen (1970) point out two differences between testing strand and testing deformed reinforcing steel:

- Strand cast into concrete while unstressed does not employ the same bond mechanism as strand that is prestressed and then released after the concrete is cast. Axial

expansion of prestressed strand after it is released (due to Poisson's effect) increases the lateral pressure in the surrounding concrete, causing confinement that is not easily replicable in shortly bonded pullout specimens. This expansion-induced confinement does not occur while using deformed reinforcing steel.

- While bond of deformed bars depends on longitudinal shear interlock to its fixed deformations, seven-wire strand depends on torsional interlock to its spiral of six outer wires. The strand twists as it is pulled out of the concrete, and torsional bond occurs when the outer wires twist out of concrete keys formed during casting. It is difficult to prevent this twisting mechanism within a shortly bonded length of strand.

2.2.3 Existing Acceptance Criteria

All of the fresh concrete stability tests described earlier have been used either to confirm the stability of tested SCC or to establish a level of segregation above which SCC should not be accepted. The measures of hardened concrete uniformity described in the previous subsection (from which many of these fresh test criteria were derived) can also be used to determine acceptable in-place uniformity. Test outputs at which tests indicate that problems with segregation may occur, as well as the origins and applicability of these outputs, are discussed in the following sections.

2.2.3.1 Fresh Property Test Criteria

Table 2.1 includes the outputs at which each fresh concrete stability test method indicates that problems associated with segregation may occur. While not all of these tests were chosen for further evaluation in this research, their results illustrate general trends for acceptability criteria—acceptable penetration depths tend to be less than or equal to 0.4 in., for example. Rheological test results are not provided, as they depend on the type of rheometer utilized and were not incorporated in this research.

Table 2.1: Acceptance limits for various stability test methods

Test Method	Acceptability Criteria		Recommended By
Visual Stability Index (ASTM C1611)	VSI ≤ 1		Khayat and Mitchell (2009)
	VSI ≤ 1.5		PCI (2004)
Column Segregation (ASTM C1610)	I_{seg} ≤ 15 %		Khayat and Mitchell (2009), Koehler and Fowler (2010)
	I_{seg} ≤ 10%		ACI 237 (2007)
Rapid Penetration (ASTM C1712)	Depth ≤ 0.4 in. = Seg. Resistant ≤ 1 in. = Moderately Resistant		Bui et al. (2007), ASTM C1712 (2009)
Sieve Stability	S ≤ 20% (Class 1) S ≤ 15% (Class 2) S ≤ 10% (demanding[1])		EPG (2005)
	5% ≤ S ≤ 15%		PCI (2004)
Surface Settlement	NMSA ≤ ½ in.	Set. rate ≤ 0.27 %/hr Set. max ≤ 0.5%	Khayat and Mitchell (2009)
	NMSA > ½ in.	Rate ≤ 0.12 %/hr Max ≤ 0.3%	
Multiple-Probe Penetration	Average Depth ≤ 0.4 in.		El-Chabib and Nehdi (2006)
Wire-Probe Penetration	Depth ≤ 0.25 in.		Shen et al. (2007)

Note: [1] = when flow exceeds 15 ft or clear spacing is less than 3 in.

Acceptance criteria for the VSI were originally established as qualitative estimates (Daczko 2003), and the determination of the VSI is considered non-mandatory during slump flow testing (ASTM C1611 2005). Although Khayat and Mitchell (2009) recommend the VSI, they and others (Koehler and Fowler 2010; Peterman 2007; Khan and Kurtis 2010) found the VSI to erratically predict hardened performance of SCC.

Acceptable column segregation results have previously been based on visual assessment (ACI 237 2007), but the most recent recommendation was based on comparison to the surface settlement test (Khayat and Mitchell 2009). The acceptance criteria for the surface settlement test were also established by Khayat and Mitchell (2009); they were based on correlations to in-place core strength uniformity and pullout bond uniformity. The relationship between maximum surface settlement and top-bar effect is shown in Figure 2.12 (shown as

"modification factor"). Because pullout bond uniformity was utilized in this research, it is discussed further in Section 2.2.3.2.

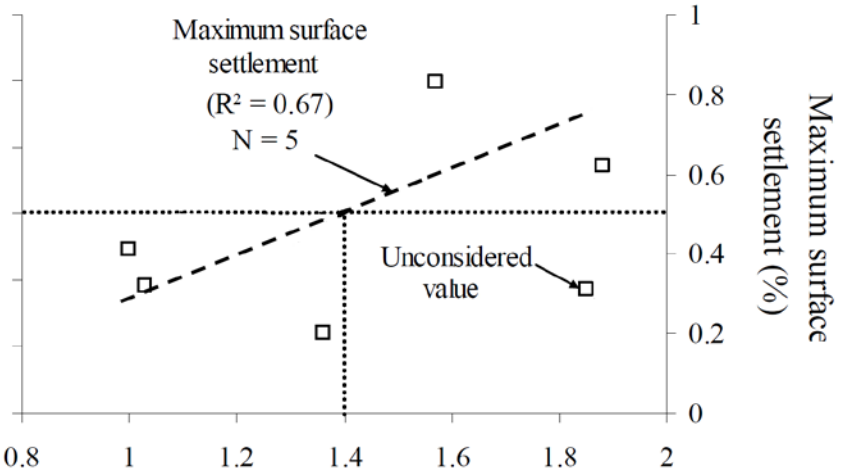

Figure 2.12: Relationship between top-bar effect and maximum surface settlement determined from surface settlement test (Khayat and Mitchell 2009)

As stated earlier, Bui et al. (2007) recommend that the column segregation test be replaced by the rapid penetration test based on a correlation between column segregation results and penetration test results. That correlation is shown in Figure 2.13. The recommended penetration depth limit of 0.4 in. (10 mm) is based on a segregation index limit of 10%, although penetration depths up to 1 in. (25 mm) may be acceptable if a segregation index limit of 20% is employed (Bui et al. 2007).

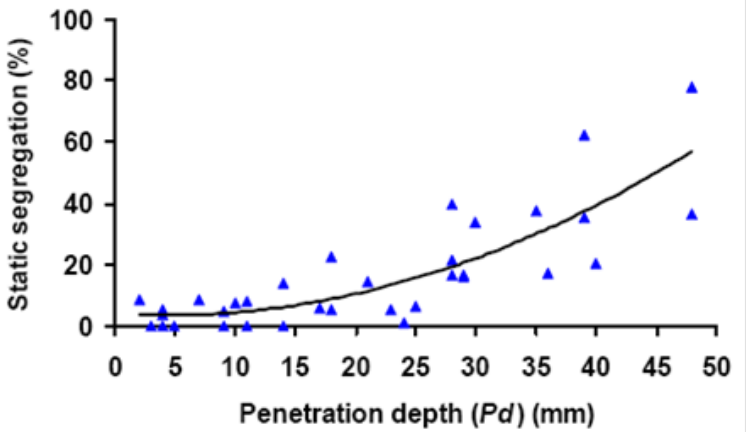

Figure 2.13: Relationship between penetration and column segregation (Bui et al. 2007)

Acceptance criteria for the sieve stability test were determined by visual observation and coring of hardened concrete during comprehensive testing (EPG 2005). European researchers

(Kwan and Ng 2009; Ng et al. 2006; Sahmaran et al. 2007) have frequently used the sieve stability test to verify SCC stability. These researchers allowed sieved fraction (S) values of up to 20%. EPG (2005) recommends only allowing sieved fractions of less than 10% for SCC used in demanding placements of greater than 15 ft of lateral flow or through spaces less than 3.0 in. wide, such as in the production of precast, prestressed elements.

Shen et al. (2007) based their acceptance criterion for the wire test on the column segregation test and visual examination of hardened SCC. They found that penetration depths less than 0.25 in. (7 mm) corresponded to column segregation results of less than 15% and were correlated well with in-situ mortar depths. They verified the effect of mortar layer depth, and an acceptable tolerance for it, through finite element modeling of differential shrinkage stresses due to paste-layer formation.

Note in Figure 2.12 and Figure 2.13 that, when it was even reported, the correlation, R^2, between fresh concrete stability test result datasets varied from 0.65–0.84. Notably, Khayat and Mitchell (2009) also excluded one of their six measurements prior to identifying a strong correlation between the surface settlement test and top-bar effect (shown in Figure 2.12). Very few other publications have shown the correlation between fresh test results and other fresh or hardened test measures. Others that reported R^2 include:

- Johnson et al. (2010), whose relationship between sieve stability results and digital image analysis only exceeded $R^2 = 0.50$ sporadically, and
- Hwang et al. (2006), whose relationship between rate of settlement and maximum settlement within the surface settlement test exhibited a nonlinear $R^2 = 0.77$ when comparing the rate at 15 min. (the time recommended based on their research).

The relative strength and scarcity of these R^2 correlations indicate that a threshold in the order of $R^2 \geq 0.50$ is acceptable when evaluating datasets involving fresh SCC stability tests. The literature reviewed in this chapter indicates that collection of fresh SCC stability test results may be cumbersome, especially when coupled with hardened concrete uniformity testing. Furthermore, as described by Johnson et al. (2010) and shown in Figure 2.12 (from Khayat and Mitchell 2009), the occurrence of outliers is likely when comparing concrete stability results to measures of hardened uniformity.

2.2.3.2 Hardened Concrete Uniformity Criteria

Hardened concrete uniformity tests are rarely used to prove the stability of individual SCC mixtures, as these test methods can be very time-consuming compared to fresh concrete stability testing. Even when possible to prequalify a particular mixture, hardened test methods are of minimal value for on-site batch acceptance, as their results would only become known after the

concrete was already placed and hardened. As mentioned in Section 2.2.2, hardened tests have frequently been used to prove the uniformity of high-quality SCC, though.

An acceptable level of concrete quality has been established using UPV results, but only for one known aggregate source (Solis-Carcano and Moreno 2008). To establish what UPV results would be acceptable in cast members, Solis-Carcano and Moreno (2008) recorded velocities in cylinders prepared from 100 mixtures of varying compositions, and then they matched velocities to strengths in the mixtures. In subsequent tests of as-cast members, the pulse velocities measured in as-cast members were used to determine acceptable strength uniformity. Meanwhile, Cussigh (1999) did not directly determine a UPV variation that would be acceptable, but instead compared VC of varying degrees of consolidation and SCCs of varying stability. Whatever level of UPV variation was observed in conventionally accepted VC would serve as the benchmark for SCC UPV acceptability (Cussigh 1999).

The UPV values determined to be acceptable in those research projects cannot be applied universally because of the multitude of variables affecting UPVs, and because UPVs measure underlying hardened properties of SCC that can have varying effects on mechanical performance. Pullout testing, on the other hand, directly assesses the mechanical performance of hardened concrete.

Section 2.2.2.2 described how the top-bar effect determined by pullout testing may be related to segregation of fresh concrete. Although not unique to SCC (the top-bar effect can occur in all concretes), AASHTO (2013) and ACI 318 (2011) recognize the top-bar effect and account for it with a single factor, commonly known as the 'top-bar factor.' The top-bar factor is used in each code's equation for development length and applies to top-cast bars with greater than 12 in. of concrete cast below them. In these top-cast bars, the development length is multiplied by the top-bar factor in order to ensure the same bond capacity as in bottom-cast bars. The factor is defined as equaling

- 1.4 in *AASHTO LRFD* (2013) Section 5.11.2.1.2, and
- 1.3 in ACI 318 (2011) Section 12.2.4.

The top-bar factor was experimentally determined and refined by testing vibrated concrete, although ACI 408 (2003) notes that both the 12 in. depth limit and the single-increment top-bar factor seem arbitrary considering the contributing research. Regardless, recent research has shown that stable SCC exhibits similar bond behavior (in both bond capacity and top-bar effect) as VC (Hassan et al. 2010; Khayat et al. 2007).

The top-bar factor was not created to limit the heterogeneity of SCC, but it does allow for a certain level of in-situ variability. If the top-bar effect present in an SCC is less than the code-accepted top-bar factor, then whatever heterogeneity is present must be acceptable for issues related to bond strength. Using this assumption, researchers have compared top-bar effects to

the code-accepted top-bar factor to test the viability of SCC as a replacement for VC (Almeida Filho et al. 2008; Esfahani et al. 2008), or to determine acceptance criteria of fresh SCC stability test methods (Khayat and Mitchell 2009).

2.3 EXPERIMENTAL PROGRAM

2.3.1 Summary of Work

Of the fresh concrete stability test methods described in Section 2.2.1, five were selected for evaluation during this research:

- Visual stability index (ASTM C1611 2005),
- Column segregation test (ASTM C1610 2006),
- Rapid penetration test (ASTM C1712 2009),
- Sieve stability test (EPG 2005), and
- Surface settlement test (Khayat and Mitchell 2009).

To assess in-situ concrete uniformity, 3 yd^3 batches of concrete were delivered by ready-mixed concrete trucks to the Auburn University laboratory, and they were then placed in walls of three heights: 54 in., 72 in., and 94 in. The three specimen heights selected are approximately incremental in height difference and correspond to the heights of typical precast bridge elements. This made it possible to study the potential correlation between section height and segregation.

The walls were tested using UPV testing and pullout testing in order to determine the in-situ effects of segregation. As summarized in Section 2.2.2.1, UPV testing is a nondestructive test method to evaluate the relative uniformity of hardened concrete specimens, and, as summarized in Section 2.2.2.2, the pullout testing is a direct, destructive method for evaluation of the bond strength of concrete. Segregation can affect constituent dispersion and bond quality, and tests of these properties have been used to study the uniformity of SCC (see Section 2.2.2). During this research project, the test methods were used as complimentary, but independent, assessments of in-situ concrete uniformity. Therefore, each result was used to independently assess the ability of the fresh concrete stability test methods to identify hardened concrete uniformity.

The researchers desired to assess the fresh stability tests over the full range of segregation severity, so a total of nine precast, prestressed-suitable SCC mixtures and two VC mixtures were placed that would provide varied fresh stability test results and degrees of in-situ uniformity. The SCC mixtures were divided into two approximately equal groups, each of which was tested over a range of segregation severity. The VC mixtures were intended to serve as

control mixtures for the SCC groups. Full-scale testing was conducted on a seven- to eight-day cycle.

2.3.2 Mixture Preparation

To accommodate the fresh concrete stability testing and wall casting for this research, approximately 2.25 yd^3 of concrete were needed for each concrete batch. To account for waste and ensure sampling uniformity, 3 yd^3 were produced for each testing cycle. As it was impossible to mix such a large volume in a single batch at the Auburn University (AU) Structural Engineering Laboratory in the Harbert Engineering Center (“the laboratory”), the majority of batching and mixing took place at the Twin City Concrete plant (“the plant”) in Auburn, Alabama. Certain aspects of mixture preparation thus required the cooperation of Twin City Concrete, while other aspects of concrete production unique to the research project were conducted at the laboratory upon receipt of each batch.

2.3.2.1 Ready-Mixed Concrete Plant Mixing Procedures

Prior to batching, AU staff gathered samples of coarse and fine aggregate to determine their moisture content at the laboratory. Plant staff then batched all materials except HRWR admixture, VMA, and a predetermined amount of additional water into a ready-mixed concrete truck for mixing and delivery. AU staff added hydration-stabilizing admixture directly into ready-mixed concrete truck before it departed for delivery to the laboratory. Additional mixing took place as the truck drove to the laboratory, a trip that took approximately fifteen minutes. Per AU staff requests, the ready-mixed concrete trucks used minimal mixer rotation during transport.

2.3.2.2 Laboratory Mixing Procedures

Upon arrival of the ready-mixed concrete truck at the laboratory, several activities were conducted before discharging the concrete for placement:

1) Add a predetermined amount of water (if desired to adjust stability and filling ability) using five-gallon buckets,
2) Add an initial dose of HRWRA (every mixture) and VMA (if desired to adjust stability),
3) Mix the concrete in the ready-mixed concrete truck for 30 drum revolutions at half of the truck’s maximum rotational speed,
4) Wait two minutes to allow the dispersed chemical admixtures to take effect, and

5) Rotate the mixer to bring the concrete up to a visible level in the truck, and either add additional HRWRA (if visibly necessary to achieve required filling ability), add additional VMA (if visibly necessary to further adjust stability), or dispense a small sample for acceptance testing.

Once the mixture reached the apparent level of filling ability desired, the truck's chute was positioned above a waste container, and a five-gallon bucket of concrete was captured directly from the chute as concrete was discharged into the waste container. The mixer was not rotated during acceptance testing of the sample, which took approximately four minutes. The chute of the ready-mixed concrete truck was washed before any additional concrete was dispensed in order to remove deleterious material.

Acceptance of each batch of SCC was based on the filling ability and stability as determined by the slump flow test and VSI, and acceptance of each VC batch was based on the slump test. The goal for the various SCC mixtures was to create concretes that achieved high levels of filling ability (slumps exceeding 25 in.) while exhibiting VSI values ranging from 0.0–3.0. The goal for the four VC mixtures was to obtain the workability necessary for precast, prestressed applications with slumps of 3.5–7.0 inches.

Air content was also tested, although it alone did not disqualify a concrete batch. For example, one SCC mixture arrived with an air content of 9.5%, but slump flow and VSI values were similar to previously prepared concretes of the same proportions, and later testing confirmed that the high-air-content mixture reached a slightly lower but still acceptable strength.

In mixtures that did not achieve a minimum of 25 in. of slump flow, or that were more stable than desired for a particular testing cycle, HRWRA was added in 1–3 oz/cwt increments until the SCC exhibited the desired fresh properties. Similar to initial mixing, the adjusted mixture was mixed for thirty revolutions at a slow speed and allowed to rest for two minutes before retesting. Partly because chemical admixture effectiveness would diminish over time, and partly because remixing added air content, no batch was accepted that required more than three dosages of chemical admixture (consisting of an initial dosage plus two additions).

2.3.2.3 Sampling for Required Tests

Once a desirable combination of slump flow and VSI was achieved, the batch was dispensed from the ready-mixed concrete truck into a 1.5 yd^3 placement bucket. During SCC placements, the following placement order was followed:

1) Fill a sampling container with enough concrete to perform all fresh concrete stability tests and start to fill strength cylinders.
2) Cast the 94-inch-tall wall in a single lift.

3) Refill the bucket from the ready-mixed concrete truck.
4) Cast the 72-inch-tall wall in a single lift.
5) Refill the bucket from the ready-mixed concrete truck.
6) Refill the sampling container to finish casting of all strength cylinders.
7) Cast the 54-inch-tall wall in a single lift.

During VC placements, the above order of placement was adjusted to accommodate consolidation efforts. Following the recommendations set forth by PCI (2004), lifts of approximately 18 in. were placed and then consolidated using a 1-inch-diameter internal vibrator. The same order of wall placement was followed as previously described for the placement of SCC.

2.3.3 Fresh Testing

From the test methods described in Section 2.2.1, the VSI was chosen because it is the most frequently specified on-site quality assurance test method. The column segregation test was chosen because it is the only considered test that involves physically determining the aggregate distribution over the height of a sample, and it is an ASTM standardized test method for characterization of the static stability of SCC. The rapid penetration test was chosen because it the fastest test offering a completely objective result and is the most recently ASTM standardized test to assess SCC stability.

The sieve stability test was selected because it is recommended by a European consortium of concrete producers as the primary stability test in Europe (EPG 2005). The surface settlement test was selected because it is recommended in NCHRP Report 628 (Khayat and Mitchell 2009) as the primary stability test for precast, prestressed SCC. All fresh concrete stability tests were conducted in accordance with the recommendations set forth in Section 2.2.1 or, where available, their respective ASTM standards. The test procedures given in Appendix B were derived from the most current version of test instructions available to the researcher at the beginning of testing in November 2009.

Pairs of each of these five tests were used in conjunction with the casting of the three walls described in Section 2.3.4. A total of 10 ft^3 of concrete was needed to perform all fresh stability testing, so wheelbarrows and plastic-lined boxes with a volume exceeding 16 ft^3 were filled for sampling. The first tests begun were the tests for air content, unit weight, and temperature, all of which were conducted with a single sample. The tests for air content, unit weight, and temperature were conducted only once.

The two slump flow and VSI tests were run consecutively. The two iterations were conducted consecutively so that a single operator could conduct them (to eliminate between-user

variation) while ensuring that the time spent evaluating the VSI of the first sample would not interfere with evaluation of the second sample. Also, rapid penetration testing was conducted on the same sample as the slump flow and VSI, as allowed by the guidelines for operation of the rapid penetration test (ASTM C1712 2009). The order of filling and initiation of the other tests, in which pairs of samples were tested simultaneously, was as follows:

1) Rapid penetration test (when conducted separately),
2) Sieve stability test,
3) Column segregation test, and
4) Surface settlement test.

This order of preparation and initiation was used during every testing cycle. Although fresh properties may not have been identical at the beginning of each fresh test, all tests were initiated quickly enough (within ten minutes) that very little change was expected in fresh concrete behavior. Also, to reduce the risk of time-sensitive changes in the material during the initiation of all tests, hydration-stabilizing admixture was added to each batch in the ready-mixed concrete truck to delay setting until long after wall casting. Information on the hydration-stabilizing admixture, as well the other mixture constituents, is located in Section 2.3.4.4.

2.3.3.1 Slump Flow, Rapid Penetration Test, and Visual Stability Index

During SCC placements, the slump flow test was first performed prior to initiating wall placement (as part of acceptance testing). It was performed again to coincide with the other fresh concrete stability tests, and only the result of that second test was used for analysis. During this second round of testing (after beginning the casting of walls), the slump flow was tested in conjunction with the rapid penetration test and the VSI. Performing all three of these tests simultaneously met the individual time requirements specified for each, so it was convenient to conduct all three tests on the same sample.

The apparatus used to perform the slump flow, rapid penetration, and VSI tests are shown in Figure 2.14, reading of the penetration depth during the rapid penetration test is shown in Figure 2.15, and a slump flow test in progress following removal of the rapid penetration test apparatus is shown in Figure 2.16. The rapid penetration test apparatus could not be purchased from a commercial concrete laboratory equipment supplier, so the equipment was manufactured by an Auburn University machinist to meet all of the requirements of ASTM C1712 (2009).

Figure 2.14: Inverted slump cone and rapid penetration apparatus

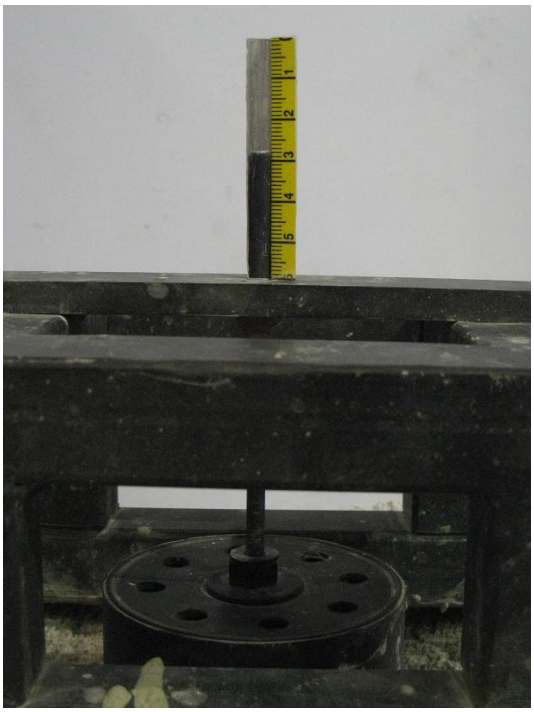

Figure 2.15: Penetration depth of 28 mm (1.1 in.) using the rapid penetration test method

Figure 2.16: Performance of slump flow test

2.3.3.2 Column Segregation Test

The column segregation test was conducted in accordance with ASTM C1610 (2006) using the apparatus shown in Figure 2.17. The two column segregation tests were started simultaneously using concrete collected from a single sampling container. Although the white column segregation mold shown has four segments, only the top and bottom portions of concrete were collected for comparison—four-part segmentation improved the ease of testing, but ASTM C1610 only requires comparison of aggregate volumes of the top and bottom quartiles.

Figure 2.17: Two column segregation molds used during simultaneous testing

2.3.3.3 Sieve Stability Test

The sieve stability test, which measures the percentage of SCC passing through a sieve as it falls from a predetermined height, was conducted according to the procedure outlined in Appendix B.1. As suggested in the European Guidelines for SCC (EPG 2005) to ensure a consistent pouring height, the sieve stability test was operated with the use of the pouring apparatus shown in Figure 2.18.

Figure 2.18: Sieve stability test with pouring apparatus, sieve, and scale

The bucket shown in the figure was marked with a dashed line to indicate the level to which concrete should be filled to meet the required sample volume of ten liters (0.35 ft^3). The hinging mechanism for the bucket was attached parallel to the forward lip of the bucket so that, regardless of the angle at which the concrete fell from the bucket onto the sieve, the drop height would remain constant at approximately twenty inches.

A waterproof, rubberized scale with a precision of 0.005 lb was used for the sieve stability test. The European Project Group (2005) recommended using a 5 mm (0.20 in.) sieve, but the American equivalent, a No. 4 (0.25 in.) sieve was used instead. This was deemed acceptable considering the literature reviewed in Section 2.2.1.4, as well as considering the practicality of using a US standard sieve more commonly available in the US than a metric sieve.

2.3.3.4 Surface Settlement Test

The surface settlement test, which measures the settlement of an acrylic plate into a column of concrete, was conducted according to the procedure outlined in Appendix B.2 and recommended by NCHRP 628 (Khayat and Mitchell 2009). A linear variable differential transformer (LVDT) was recommended by Khayat and Mitchell (2009) to continuously record the settlement of the acrylic plate. However, readings were only necessary every five minutes, and the Auburn University researchers desired to use a measurement instrument offering the least risk of either applying downward pressure or resisting settlement of the surface settlement plate. Therefore, a springless digital dial gauge was used. One of these gauges is shown in Figure 2.19.

Figure 2.19: Surface settlement test equipment with digital indicator

The gauges displayed displacements of up to 2 in. with a precision of 0.0001 in., which met the requirements of Khayat and Mitchell (2009). The gauges were supplied by Chicago Dial Instruments. Removal of the return spring meant the measurement rod was able to fall freely as the plate settled. The rod weighed one gram, which was accounted for in manufacturing an acrylic settlement plate of the required weight.

The surface settlement testing apparatus shown in Figure 2.20 consisted of four pieces. The main column portion of the mold was split vertically and then sealed with a rubber gasket. The removable base was also sealed with a rubber gasket. This made it possible to disassemble the apparatus after each sample hardened in the mold. The portion of the mold housing the dial indicator was detachable and was attached after filling the mold. This made quick filling and strike-off of the concrete at the top of the mold possible without risk of damaging the indicator, and it made disassembly and removal of the hardened sample more convenient.

Figure 2.20: Four-piece constructed surface settlement test apparatus

2.3.3.5 Other Fresh Concrete Stability Tests Considered

Rheological testing, which involves testing of fresh SCC or sieved mortar to determine yield stress and viscosity, was considered for use as both a potential indicator of stability and as a benchmark against which to assess the fresh concrete stability tests. However, after reviewing the literature described in Section 2.2.1, the research team decided against using rheological testing for the following reasons:

- Rheological testing would only indirectly assess stability, and the relationship between rheological properties and stability is unclear (Assaad et al. 2004; Koehler et al. 2007)
- The least expensive rheological testing equipment available to the research team would have cost more than all other equipment combined, and
- For similar equipment costs, the researchers felt that UPV testing would be more valuable because it could comparatively assess as-placed concrete uniformity.

The wire-probe penetration test, like the rapid penetration test and the multiple-probe penetration test, involves measuring the settlement of a probe into a sample of SCC. The research team decided not to incorporate the test because it offered little advantage over the rapid penetration test. Reasons for its exclusion were that

- The test method is specified by only one state DOT, and documentation of its use is limited,
- It measures the same segregation mechanism as an alternative (the rapid penetration test) whose use is standardized by ASTM, and
- It does not incorporate any form of stabilization to ensure that the wire probe would settle directly downward into the sample.

The multiple-probe penetration test is similar to both the rapid penetration and wire-probe penetration tests in that it involves measurement of a probe's settlement into SCC (El-Chabib and Nehdi 2006). After preliminary testing for this research (Keske 2011), the research team decided not to evaluate the test further because it performed relatively poorly compared to the other evaluated tests. Reasons for its abandonment were that

- The test method is not specified or standardized by any organization and documentation of its use is limited,
- It measures the same segregation mechanism as an alternative (the rapid penetration test) whose use is standardized by ASTM, and
- It was found during preliminary testing (Keske 2011) to lack adequate stabilization to ensure that the probes would settle vertically into the sample.

2.3.4 Hardened Concrete Testing

During each testing cycle, hardened concrete testing (UPV and pullout) was conducted on walls to establish the level of in-situ uniformity of each concrete mixture, and strength cylinders were cast to establish each concrete's strength profile. The construction and testing considerations for these activities are described in the following subsections.

2.3.4.1 Large-Scale Walls

Since section height can potentially affect the degree of segregation, specimens of three heights were cast, each matching the height of a typical precast component:

- 54 in. to match an AASHTO Type IV or AASHTO/PCI BT-54 bridge girder,
- 72 in. to match an AASHTO Type VI or AASHTO/PCI BT-72 bridge girder, and
- 94 in. to match an AASHTO-PCI-ASBI 2400-1 standard segment.

The wall heights selected changed in approximately even increments, making it possible to observe height-based trends in segregation. While some dynamic segregation could occur

during the filling of the walls, height trends were primarily due to static segregation rather than variable dynamic effects of free-fall placement because a trunk was used to place concrete in the 94 in. and 72 in. walls. This trunk limited the free-fall drop height in those walls to less than 60 in., in accordance with the guidelines for free-fall placement of concrete set forth in *AASHTO Bridge Construction Specifications* (2010) Section 8.7.3.1.

Thirty-six in. walls were also cast, as further described by Keske (2011). The 36 in. walls did not contain any pullout specimens, and they were only tested for UPV uniformity. During preliminary testing described in Keske (2011), their uniformity never varied as greatly as that of the taller walls. The absence of pullout bars also limited their value for comparison to fresh concrete stability test results, so they are not considered during the analyses reported here.

A consistent width and thickness of 40 in. and 8 in., respectively, was utilized in all walls. These dimensions, as well as the location of form ties and hoist anchors permanently cast into the walls, were selected primarily in consideration of the hardened concrete testing configuration desired. The details of those configurations are described in Sections 2.3.4.2 and 2.3.4.3. As explained in those sections, a lateral distance of at least 4 in. was kept between each UPV reading location and the nearest pullout bar, form tie, or wall edge, and 8 in. was kept between pullout bars.

Selection of a wall width of 40 in. thus made it possible to test five vertical lines of UPV measurement locations and four vertical lines of pullout bars, alternating each vertical line with a lateral spacing of 4 in. on-center. A thickness of 8 in. was selected for all walls based on past studies and testing configurations identified in Sections 2.2.2.1 and 2.2.2.2 and on the calculation that unreinforced walls of that thickness would be structurally sound under flexural and tensile loads encountered during maneuvering and testing.

Threaded-rod form ties were used to control the outward deflection of forms under the pressure exerted by the fresh concrete. The 94 in. wall used eight ties, the 72 in. wall used six, and the 54 in. wall used four. These ties, and hoist anchors cast into the walls to assist in lifting and moving, were all placed to keep at least 4 in. clear spacing to any UPV measurement location and at least 3 in. clear spacing from the nearest pullout bar. The minimum clear spacing between parallel reinforcement required by ACI 318 (2011) to allow uninhibited placement was 1 in., which was exceeded in all cases.

As described in Section 2.2.2.1, UPV testing for the purpose of comparative uniformity testing is most effective at very early ages. A testing age of two days was selected as a compromise between early-age testing needs and strength needs to ensure that the walls would be sufficiently strong during form removal and moving. As seen in Figure 2.21, two parallel lines were used during this testing: one for form erection and casting and one for wall storage and testing. During each casting cycle, the walls were lifted by the still-attached formwork in the first line, moved to the second line, anchored into place, and then stripped of all formwork. Work

crews began stripping the formwork from each wall while the next wall was being moved and anchored, which allowed for UPV testing of the walls to be conducted continuously at as close to an age of forty-eight hours as possible. Although the completion of form removal typically took two hours, all form ties and joints were loosened at 48 hours to allow exposure to laboratory humidity and temperature conditions.

After the forms were removed, wax construction pencils were used to mark a UPV measurement location grid onto each wall, and UPV testing was conducted as soon as possible thereafter. The walls were then left in this position until an age of at least six days, after which they were moved to a third location and laid horizontally in order to conduct pullout testing at a concrete age of thirteen days. The walls were left in a vertical orientation for as long as possible in order to limit the risk of damage from loads that could occur either while being moved or while supported horizontally prior to testing.

To tip the walls from their as-cast vertical orientation to the horizontal orientation needed to conduct pullout testing, metal plates were loosely attached to hoist anchors that were cast horizontally near the top of each wall (points of bracing attachment in Figure 2.21). The walls were then lifted by the plates with an overhead crane, moved into place on concrete blocks, and tipped over to lie horizontally on the concrete blocks. Local stresses from lifting were only experienced near the points where hoist anchors were cast into the walls, which were always at least 8 in. from the nearest pullout specimen location. While on the blocks, the walls rested on rubber pads that were aligned near their corners. This support system was used to limit the flexural stresses experienced by the walls while in a horizontal orientation and to ensure adequate clearance for instrumentation during pullout testing.

Figure 2.21: Parallel lines of cast walls and formwork

2.3.4.2 Ultrasonic Pulse Velocity Testing

Ultrasonic pulse velocity (UPV) testing was conducted on each group of walls two days after casting. The testing equipment used, shown in Figure 2.22, was a Pundit Plus portable ultrasonic instrument from Germann Industries. Following the testing recommendations of Section 2.2.2.1, the Pundit Plus was configured for continuous 54 kHz testing. It displayed ten readings per second at a precision of ± 0.1 microseconds. An alcohol-based ultrasound jelly was used between each metal coupler and wall surface to create a continuous ultrasound path, and the couplers were pressed firmly against the wall surfaces until an unchanging reading was observed.

Figure 2.22: Ultrasonic pulse velocity testing equipment

Rows of UPV and pullout testing were approximately uniform, with slight variations to avoid pullout bars and form ties. As mentioned in Section 2.2.2.1, UPV testing through concrete at 54 kHz requires a minimum of 2.8 in. of clear spacing to the nearest obstacle oriented parallel to the direction of wave transmission. Typical spacing between UPV measurement points was six to eight inches, and no point was located less than four inches from the nearest edge or obstacle. The configuration used during this testing is shown in Figure 2.23.

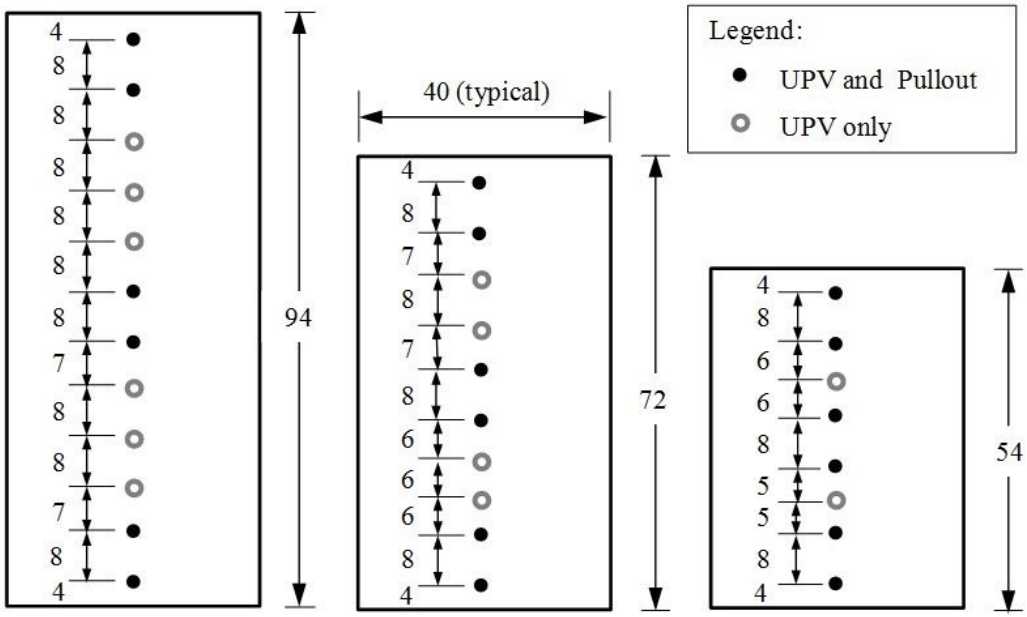

Figure 2.23: Location of UPV measurement and pullout testing locations (*Note: All measurements in inches*)

UPV measurement points were labeled to ensure proper location of wall thickness measurements necessary to calculate pulse velocities. The caliper used to measure wall thicknesses is shown in Figure 2.24. The caliper was constructed by welding parallel rectangular steel tubing 9 ± 0.01 in. apart. One leg of the caliper was laid flush with one side of the 8 in. thick wall, and a 1/100th in. gradation steel ruler was used to read the distance from the other side of the wall to the inner face of the second leg. Using this system, the wall thickness at each UPV test location was measured with a precision of ± 0.02 in., which falls well within the precision required by ASTM C597 (2002).

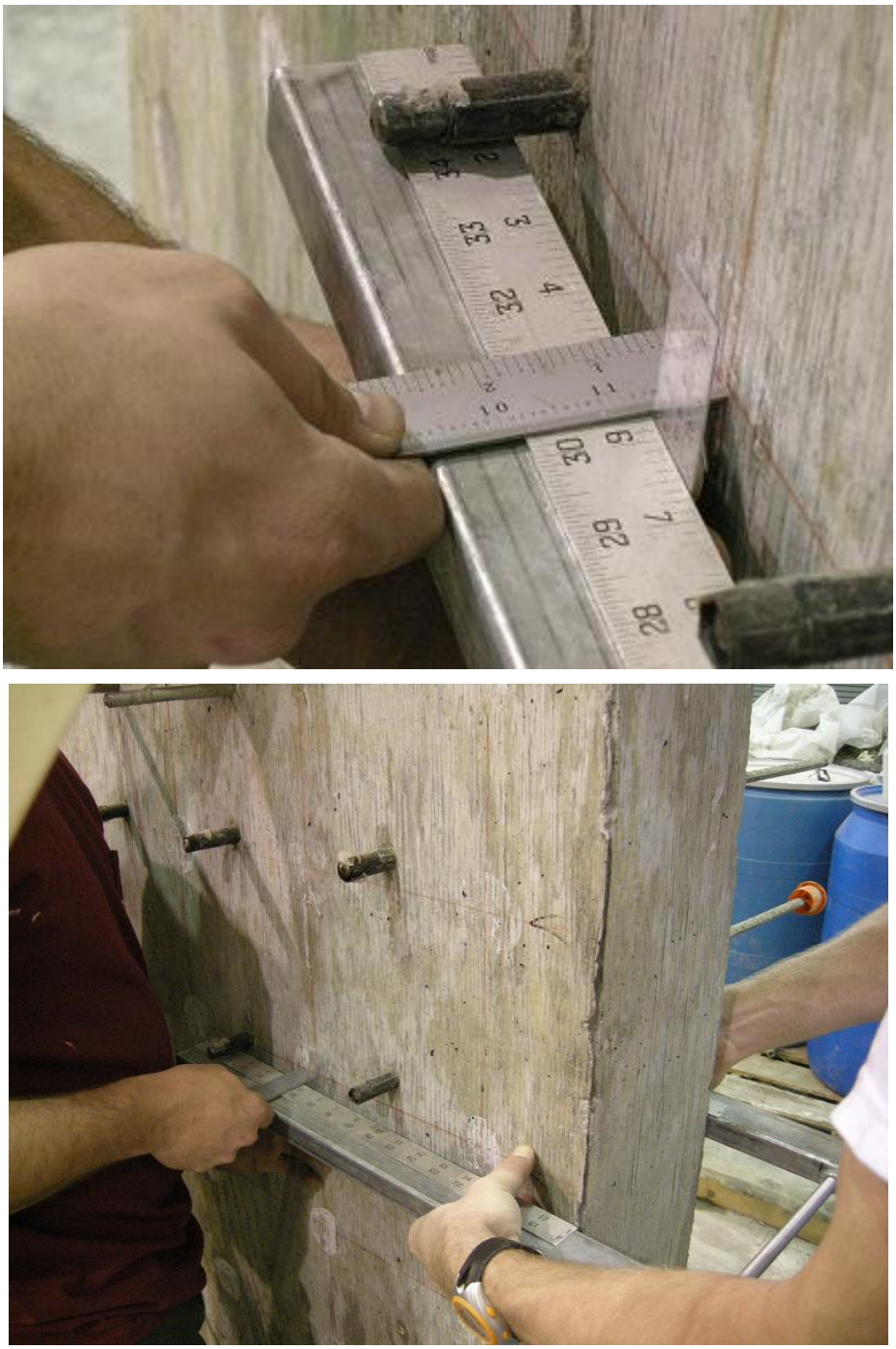

Figure 2.24: Measurement of wall thickness using (*top*) a caliper and 1/100th in. gradation ruler and (*bottom*) orientation of caliper

2.3.4.3 Pullout Testing

Pullout testing was conducted on the walls thirteen days after casting. The location of each four-bar row of pullout bar specimens is noted in Figure 2.23. To ensure adequate cover as described

in Section 2.2.2.2, the top and bottom rows of bars were located four inches from the top and bottom of each wall. A distance of eight inches was employed between each vertical line of bars so that

- An 8 in. wide reaction frame would be equally spaced between the bar being pulled out and the nearest adjacent bars,
- A 4 in. radius would be kept between the reaction frame and pullout bar in order to dissipate potential confining forces, and
- A 4 in. radius would be kept between the nearest UPV testing location and any pullout bar, as previously explained in Section 2.3.4.2.

2.3.4.3.1 Configuration of Bars

Pullout testing for this project was conducted using No. 4 reinforcing bars from two batches provided by Nucor Steel, Inc. of Birmingham, Alabama. The batches exhibited a yield stress of 68 ksi in tensile testing by Nucor, which was confirmed by the AU researchers through the tensile testing of randomly selected bars from the batch.

Based on the past research described in Section 2.2.2.2, a bonded length of 2.5 d_b, or 1.25 in., was selected in order to ensure a shearing pullout failure of the concrete, instead of splitting or conical failure. The short bonded length also limited the possibility of steel yielding due to the bond strength of this high-strength concrete. A pullout specimen prepared with a 1.25 in. long debonded region is shown in Figure 2.25. This preparation involved several steps:

1. Nonabsorbent paper was first cut into 1.25-inch-wide strips after being marked with a 1/100th in. gradation steel ruler.
2. After the bar was cleaned, the paper was taped to the desired location along the length of the pullout specimen,
3. At least one inch on either side of the paper was coated with Type I silicone,
4. After allowing the silicone to dry for at least one day, the paper was peeled away, leaving an exposed length of 2.5 d_b enclosed on both ends by permanent silicone.
5. Lastly, commercially available strand-debonding sheathing was placed on both sides of the exposed section (over the silicone) and securely taped into place using electrical tape.

Figure 2.25: 1.25 in. bonded region of a No. 4 rebar ready for casting into concrete

Once it was encapsulated in concrete, the bonded region of steel began 4 in. away from the loaded face of the concrete wall, similar to the configurations used by Khayat (1998) and Sonebi and Bartos (1999). Unlike those configurations, the end of the bonded region was not flush with the unloaded face of the wall. It was decided that placing the bonded region close to the middle of the wall thickness would remove the risk of uncharacteristic pullout behavior from two sources: different collection of bleed water and aggregate at the face of the wall, and flexural stresses experienced by the wall under its own weight. The surface friction and the preferred orientation of aggregate at the face of the wall could lead to irregularity at this face, and flexure experienced by the wall in a horizontal, simply supported orientation could place the concrete near the top face in compression while reducing the compression at the bottom face of concrete.

To both accommodate sealing the other joints and avoid contaminating the pullout bars with form release agent, the pullout bars were placed in the erected formwork after the forms had been sealed and sprayed. Consequently, insertion of the bars was the last activity performed before placement of concrete, leaving at least twenty-four hours between when the bars were sealed with Type I silicone on the outer face of the formwork and when the concrete was cast.

2.3.4.3.2 Configuration of Pullout Testing Equipment

Both the 8 in. tall reaction chair and the center-hole hydraulic cylinder (jack) used in this research project, as well as the aluminum load cell and chuck placed above them, are shown in Figure

2.26. This configuration was based on the configuration used by Khayat and Mitchell (2009), which was shown in Figure 2.11. The load cell had a precision of ± 0.5 lb and was capable of resisting up to 40,000 pounds of compressive force. The jack, with a capacity of 120,000 pounds, was operated with an air-powered hydraulic pump.

Figure 2.26: Chuck, load cell, hydraulic jack, and 8-inch-tall reaction chair

Loading was displacement-controlled by controlling the airflow into an air-powered hydraulic pump serving a 120,000-pound center-hole hydraulic cylinder (jack). Displacement of the unloaded end of the pullout bar was measured using a linear displacement potentiometer. Loading was not discontinued until the free-end slip of the bar was more than double the slip at maximum pullout force. Only one of the more than 700 tested bars yielded before reaching its maximum pullout force. In that occurrence, pullout force plateaued and free-end slip ceased

while the jack continued to extend. That result was not used in analysis, as the uniformity of bond stress could have been affected by yielding of the steel bar.

The pullout testing apparatus, illustrated in its entirety in Figure 2.27, made it possible to pull out each bar with minimal additional confining pressure, without damaging the surrounding concrete, and without causing dynamic loading effects. An Optim MEGADAC data acquisition system was utilized for all data collection. Time, load, and slip were instantaneously displayed by the acquisition system and were viewable during testing, which made it possible to monitor and record load and free-end slip. The research team was thus immediately made aware of equipment malfunction, bar yielding, or testing completion.

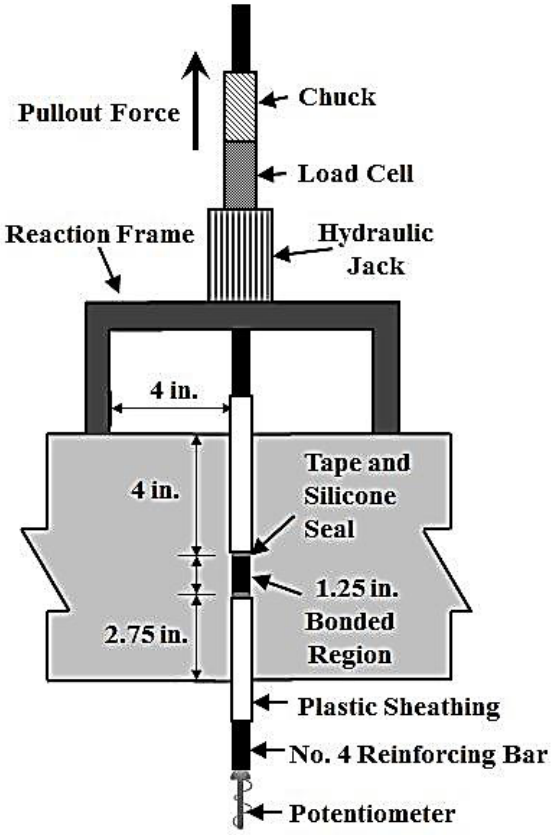

Figure 2.27: Pullout testing configuration

Based on small-scale trial pullout testing, a relationship between bond strength and concrete compressive strength was determined to estimate the necessary minimum yield strength of the rebar (68 ksi) and maximum compressive strength of the concrete (12,000 psi) that would prevent steel yielding during testing. This relationship was corroborated by research results from Khayat (1997) and Stocker and Sozen (1970). These strengths were taken into consideration when selecting concrete mixture proportions, which are described in Section 2.3.5, and when choosing to use deformed bars instead of seven-wire strand.

2.3.4.3.3 Use of Deformed Bars Instead of Seven-Wire Strand

SCC to be used for precast, prestressed applications was the primary focus of this project, so seven-wire prestressing strand was the first choice for pullout testing. Although Khayat et al. (2003) and Stocker and Sozen (1970) tested strand, the Auburn University researchers were unable to prevent an unwinding failure of seven-wire strand when a bonded length of 2.5 d_b was used. As described in Section 2.2.2.2, bond to seven-wire strand depends on torsional forces exerted as the strand attempts to rotate through the concrete. The Auburn University researchers observed visible twisting of strand as it was removed, and maximum pullout force observed was only a small percentage (less than 10%) of the force observed when pulling out deformed steel reinforcement of the same diameter (0.5 in.).

As mentioned by Stocker and Sozen (1970), a pullout failure of this type indicates that the concrete surrounding the strand is only bonded to the strand by adhesion and surface friction, not by mechanical interlock. Deformed steel reinforcement, on the other hand, is mechanically locked into the surrounding concrete because of its deformations. Because an unwinding, slipping failure cannot occur in this situation, shear failure occurs in the surrounding concrete, which is ideal for studying the quality of that concrete (or lack thereof, if affected by segregation). For that reason, it was decided that, as also done by Khayat (1998), Khayat et al. (1997), and Sonebi and Bartos (1999), deformed steel reinforcement would be used for pullout testing in this research program.

Concrete failure may have been induced by using longer bonded lengths of strand, which was possible in consideration of the strength of the strand (longer bond lengths would not yield the strand). However, because short bonded lengths were preferred in order to approximate a uniform bond stress, the use of deformed bars was deemed acceptable and appropriate for this project.

2.3.4.4 Compressive Strength Assessment

Standard 6-inch-diameter by 12-inch-high cylinders were cast for each mixture. They were used for compressive strength testing at each of the following ages: two days, to coincide with form removal and UPV testing; thirteen days, to coincide with pullout testing; and twenty-eight days, to establish a standard compressive strength for each mixture. SCC cylinders were cast in a single lift by pouring the concrete from a five-gallon bucket in a steady motion, filling the molds in 3 ± 1 seconds. No rodding or consolidation was used, but the outside of each mold was lightly tapped with a rubber mallet to remove any air pockets caught against the inside of the mold walls.

Molds were removed from the cylinders at the same time as form removal, at two days. The cylinders were then left adjacent to the walls so that they would be exposed to similar laboratory drying and curing conditions.

2.3.5 Mixtures and Raw Materials

The self-consolidating concrete mixtures used for this research, SCC-1 and SCC-2, were based on mixture proportions developed by Schindler et al. (2007) for precast, prestressed applications. The primary mixtures used the same aggregate type (crushed limestone typical of Alabama precast, prestressed construction) but different *s/agg*, *w/cm*, and SCMs. These primary mixtures were accompanied by several mixtures that were deliberately adjusted to obtain varying levels of stability, as well as VC control mixtures. A total of eleven concrete mixtures were used—nine SCC mixtures and two VC mixtures.

2.3.5.1 Mixture Design

SCC-1 was proportioned to achieve relatively higher strength but less flowability, and SCC-2 was proportioned to achieve moderate strength and higher flowability. Both primary mixtures contained aggregate fractions above 65%, as a large total aggregate fraction is frequently used in precast, prestressed concrete. From each of these primary mixtures, other mixtures of the same cementitious content, aggregate content, and aggregate proportioning were created with varying stabilities. The stability was adjusted by changing the water content, HRWRA dosage, or VMA dosage, or by changing a combination of them. The majority of the mixtures were proportioned with stabilities whose acceptance would be marginal. This is the apparent stability at which the use of quantitative, less subjective fresh concrete stability tests should be most beneficial.

VC mixtures were selected as control mixtures to mimic each primary SCC mixture. The control mixtures employed a higher *w/cm*, lower *s/agg*, and different coarse aggregate gradation than the SCC mixtures. These changes were selected because VCs typically employ a larger gradation of stone (¾ in.) and lower *s/agg* than recommended for SCC. Still, the following were expected: that each mixture's slump and early-age compressive strength would be relevant to the represented SCC, and their proportions relative to each other would mirror the differences between the SCCs. A hydration-stabilizing admixture was used in all mixtures. This dosage was not varied, and it was the minimum effective dosage recommended by the manufacturer. The proportions used are shown in Table 2.2 at the end of Section 2.3.

2.3.5.2 Raw Materials and Proportions

Lafarge Type I portland cement was used because Type III portland cement is characterized by rapid setting and early-age strength gains. This could have jeopardized the researcher's ability to initiate all fresh tests while the concrete was still in the dormant period, and the use of Type III portland cement offered no long-term benefits over Type I portland cement in terms of testability.

All SCC-2 mixtures incorporated a 30% replacement of Type I portland cement with Class C fly ash. This offered the possibility of producing concrete with a different characteristic workability and reaction to adjustments in stability modifiers (water, HRWRA, and VMA). The crushed limestone coarse aggregate used for both SCC mixtures matched the No. 78 gradation crushed limestone used in earlier studies of SCC conducted at Auburn University. It was supplied by Vulcan Materials of Calera, Alabama, while fine aggregate was well-graded natural sand taken from the ready-mixed concrete plant's general supply.

Table 2.2: Concrete mixture proportions

Mixture ID	Cement (pcy)	Fly Ash (pcy)	Water (pcy)	*w/cm*	Coarse Agg. (pcy)	Fine Agg. (pcy)	*sand/ total agg*	*total agg. vol.* (%)	HRWRA (oz/cwt)	VMA 1 (oz/cwt)	VMA 2 (oz/cwt)
VC-1	640	0	270	0.42	1,977	1,167	0.37	67.6	11	0	0
SCC-1A	750	0	270	0.36	1,680	1,342	0.44	66.9	6	2	0
SCC-1B	750	0	310	0.41	1,680	1,342	0.44	67.1	6	2	0
SCC-1C	750	0	295	0.39	1,680	1,342	0.44	62.8	11	2	0
SCC-1D	750	0	270	0.36	1,680	1,342	0.44	60.8	9	0	0
VC-2	450	190	290	0.45	1,935	1,125	0.37	67.4	2	0	0
SCC-2A	475	200	270	0.40	1,663	1,360	0.45	64.8	11	0	0
SCC-2B	475	200	270	0.40	1,663	1,360	0.45	66.4	12	0	0
SCC-2C	475	200	270	0.40	1,663	1,360	0.45	67.6	13	0	2
SCC-2D	475	200	290	0.43	1,663	1,360	0.45	66.7	5	0	0
SCC-2E	475	200	270	0.40	1,663	1,360	0.45	66.5	9	0	2

Notes: HRWRA = Glenium 7500, VMA 1 = Rheomac 362, and VMA 2 = Rheomac 450

2.4 PRESENTATION AND ANALYSIS OF RESULTS

2.4.1 Concrete Production

Using the proportions shown in Table 2.2, eleven concretes were produced and tested with five fresh concrete stability and two hardened concrete uniformity test methods. Because of the varied proportions, as well as because of fluctuations in batching, mixing, handling, and ambient conditions, the concretes achieved different fresh and hardened properties. Some of these properties are shown in Table 2.3.

When comparing Table 2.2 and Table 2.3, mixtures that were proportioned to be very similar exhibited different fresh and compressive strength behaviors. The research team assumes that this inconsistency was the result of batching fluctuation at the ready-mixed concrete plant. This suspicion was supported by evidence of incorrect batching (wrong aggregate or gradation) observed upon receipt of some batches; batches that were obviously incorrect were rejected, while others of questionable proportioning were included. Minor inconsistency from specified proportions was deemed acceptable because the proportions used in each mixture were less important than the resulting stability of each. In other words, fluctuations from the proportions listed in Table 2.2 do not affect the viability of the data collected.

Table 2.3: Fresh properties and compressive strengths of concrete mixtures

Mixture ID	Fresh Concrete Properties				Compressive Strength, f_c (psi)		
	Slump Flow (in.)	T_{50} (sec.)	Total Air (%)	Unit Wt. (lb/ft^3)	2 day	13 day	28 day
VC-1	5.5[1]	-	4.0	149.5	4,680	6,700	7,440
SCC-1A	27.5	2.3	2.0	152.8	4,690	7,110	7,390
SCC-1B	25.5	6.9	1.7	150.8	5,230	8,030	8,460
SCC-1C	27.0	1.5	5.5	144.2	4,340	6,320	6,780
SCC-1D	26.0	1.3	9.5	138.5	3,200	4,790	5,190
VC-2	7.0[1]	-	2.3	148.9	2,460	5,000	5,390
SCC-2A	28.0	1.5	6.0	144.6	2,510	5,010	5,530
SCC-2B	27.5	2.1	3.6	148.5	1,820	4,160	4,410
SCC-2C	26.0	8.0	1.8	148.8	2,620	5,300	5,880
SCC-2D	25.5	1.5	2.3	145.2	2,200	4,370	5,060
SCC-2E	26.0	4.0	3.5	145.3	2,720	4,890	5,290

Note: [1] = conventional slump

Mixture SCC-1D exhibited a high air content of 9.5%, which was attributed to the addition of the HRWRA to the ready-mixed concrete truck at the laboratory followed by rapid on-site mixing prior to discharge. However, the compressive strength of SCC-1D was deemed high enough to be included in this study. Additionally, it was deemed necessary to include mixtures with various ranges of air content in this study, as the air content can impact stability and mechanical properties (i.e. pullout strength) (Castel et al. 2006; Soylev and Francois 2003) and both these properties are directly assessed in this study.

2.4.2 Fresh Concrete Stability Tests

Summary results of the five fresh concrete stability tests conducted on each mixture are presented in Table 2.4. In the table, each fresh test result represents the average of two tests conducted simultaneously, except that VSI and rapid penetration depth values are always the average from two consecutive tests (per discussion of Section 2.3.3.1). For consistency, it was deemed best to have a single operator conduct both repetitions of the VSI test. Notably, the standard rest period required for the rapid penetration test appeared to occasionally affect the VSI test during the testing.

Table 2.4: Fresh concrete stability test results

Mixture ID	VSI	Segregation Index (%)	Rapid Penetration (in.)	Sieve Fraction (%)	Rate of Settlement (%/hr)	Maximum Settlement (%)
SCC-1A	2	5.6	0.26	N.A.	0.15	0.60
SCC-1B	0.75	0.0	0.20	6.5	0.15	0.35
SCC-1C	1.25	8.4	0.12	8.2	0.11	0.03
SCC-1D	1.25	17.5	0.33	15.8	0.02	0.01
SCC-2A	1.75	8.0	0.35	13.8	0.05	0.02
SCC-2B	3	20	0.30	30.5	0.25	0.14
SCC-2C	1.75	3.0	0.30	9.0	0.12	0.09
SCC-2D	1.25	11.1	0.10	5.2	0.25	0.13
SCC-2E	1.75	16.6	0.14	14.3	0.17	0.18

Note: N.A. = not available because sieve fraction result was recorded incorrectly

In Table 2.4, visual stability index values other than the discrete values discussed earlier (0, 0.5, 1, 1.5, 2, or 3) indicate average values in instances in which the two VSI tests yielded different results. Although the two samples were obtained from the same sampling container,

identical test results were not guaranteed. The research team took measures to avoid between-user variability (see Section 2.3.3.1), so occurrence of nonmatching VSI test results is simply a possible result of the test method.

The acrylic settlement plate of one surface settlement test apparatus sank unevenly into the test sample during placement of SCC-1A, which nullified the result obtained from that apparatus during the respective cycles. This problem, which is shown in Figure 2.28, probably occurred because the SCC being tested was so unstable that the thin acrylic plate was unevenly engulfed as it settled. In this instance, the result of the second surface settlement test indicated unacceptably high segregation according to the recommendation of Khayat and Mitchell (2009), which reinforces the possibility that failure of the first apparatus was due to the use of a highly segregating mixture and not testing error.

Figure 2.28: Acrylic settlement plate sinking unevenly during surface settlement testing

Each concrete's fresh stability results were compared to each other in order to identify any correlations between the fresh stability test methods. Table 2.5 is a correlation matrix that shows the linear-regression coefficients of determination (R^2) between each fresh stability test when comparing all eleven SCC mixtures. A nonlinear model was also applied to each relationship, and only one test's was R^2-value significantly improved by its use—the relationship between the rate of settlement and maximum settlement results obtained from the surface settlement test. In the table, R^2-values are highlighted to show relative strength—the smallest bold value is at least 50% greater than all non-highlighted R^2-values, thus indicating a division of relative correlation strength.

Table 2.5: Fresh concrete stability result linear-regression coefficients of determination

Test Result	VSI	Seg. Index	Rapid Pen.	Sieved Fraction	Rate of Settlement	Max. Settlement
Maximum Settlement	0.00	0.00	0.00	0.00	**0.47***	-
Rate of Settlement	0.15	0.03	0.00	0.04	-	
Sieved Fraction	**0.77**	**0.54**	0.36	-		
Rapid Penetration	0.12	0.07	-			
Segregation Index	0.26	-				
VSI	-					

* = nonlinear regression coefficient of determination

In the table, the linear correlations having the greatest R^2-values were the correlations between the sieve stability test and the VSI and column segregation tests, as well as the test correlation between rate of settlement and maximum settlement determined from the surface settlement test. These three strong correlations are illustrated below in Figure through Figure. Meanwhile, the rapid penetration test and surface settlement test do not exhibit a reasonable correlation with the VSI, column segregation test, sieve stability test, or each other.

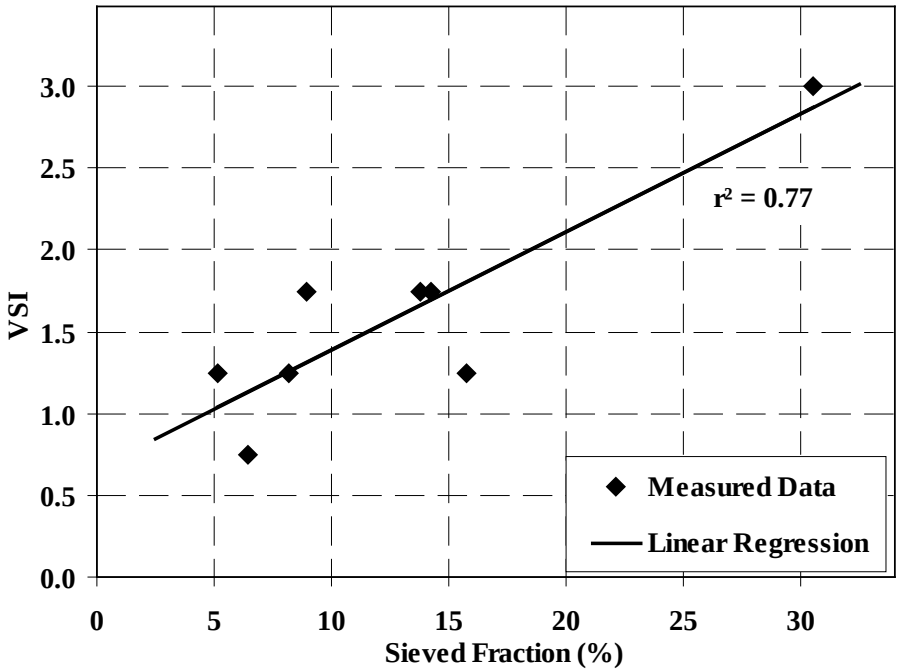

Figure 2.29: Acrylic settlement plate sinking unevenly during surface settlement testing

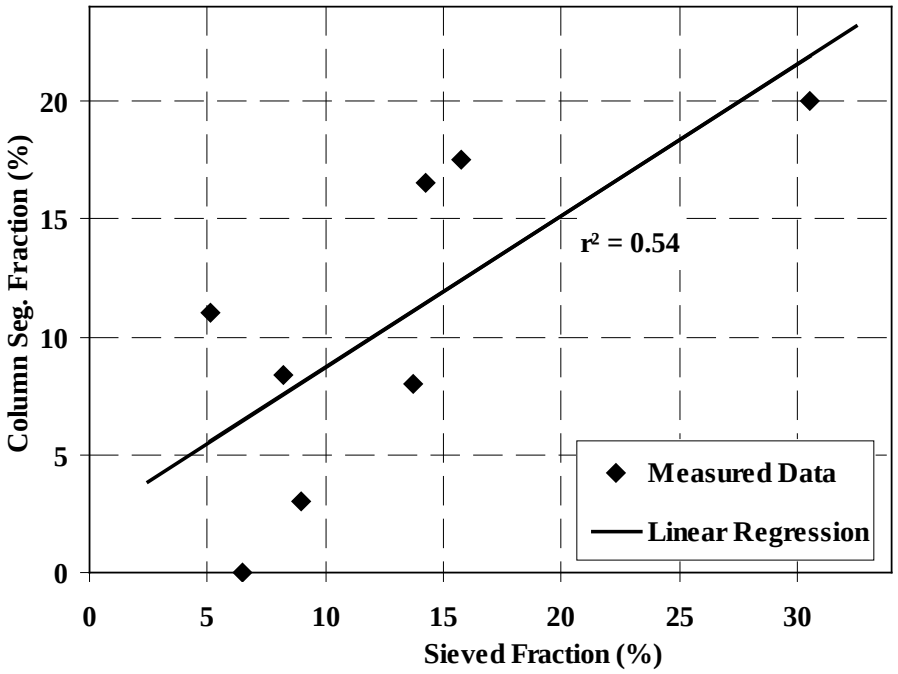

Figure 2.30: Acrylic settlement plate sinking unevenly during surface settlement testing

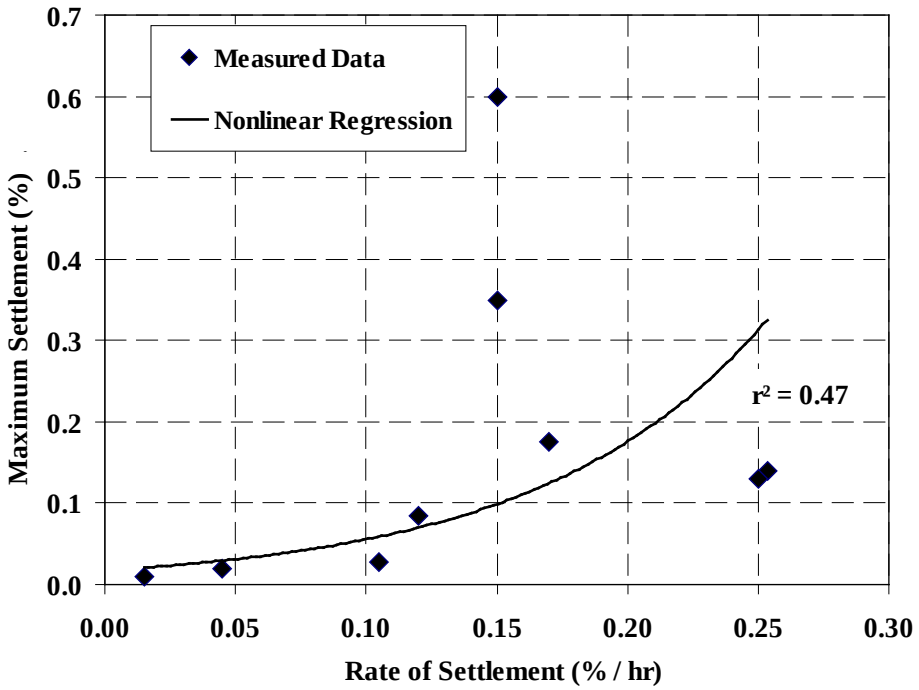

Figure 2.31: Acrylic settlement plate sinking unevenly during surface settlement testing

Conclusions that can be drawn from these correlations include that

- When assessed by trained personnel, the VSI gives results that are relatable to more time-consuming but less subjective tests,
- Since the VSI is already used extensively for quality assurance applications, the sieve stability test is a well correlated and quantitative alternative when determining stability acceptance by the VSI,
- The linear relationship between sieve stability and column segregation result found during this research is similar to the relationship found by Kohler and Fowler (2010),
- The sieve stability test is a viable alternative to the column segregation test, especially considering its increased technician-friendliness, and
- The nature of the relationship between rate of settlement and maximum settlement from the surface settlement test is similar to the relationship found by Hwang, Khayat, and Bonneau (2006).

2.4.3 In-Situ Concrete Uniformity Tests

In-situ hardened concrete uniformity test results (UPV and pullout) obtained during this research are presented in Table 2.6. The way these values were determined for each test is discussed in

the following subsections. In the last subsection, correlations between these hardened concrete uniformity results are presented and discussed.

Table 2.6: Hardened concrete uniformity test results

Mixture ID	UPV Segregation Index	Top-Bar Effect
VC-1	1.036	1.28
SCC-1A	1.073	1.24
SCC-1B	1.039	1.56
SCC-1C	1.034	1.16
SCC-1D	1.038	1.09
VC-2	1.066	1.75
SCC-2A	1.042	1.27
SCC-2B	1.114	2.80
SCC-2C	1.030	1.30
SCC-2D	1.056	2.05
SCC-2E	1.034	1.56

2.4.3.1 Ultrasonic Pulse Velocity Testing

The five UPV measurements in each row of measurements (discussed in Section 2.3.4.2) were averaged to determine an average UPV for that height. Surface defects and human error in either testing or recording of measurements occasionally caused outliers in the determined pulse velocities within a wall. Outliers were identified as any pulse velocity greater than three standard deviations away from the average of the other four velocities at a given height. Outliers, which were removed prior to further evaluation of results, were found in less than 11% of measurements.

UPV measurements for several of the 94 in. walls are shown in Figure 2.32. Complete UPV data for each wall and mixture are reported in Appendix A. As shown in the figure, the measured velocities tend to decrease with increasing height, but the fastest and slowest velocities were not always measured at the very top or bottom of each wall.

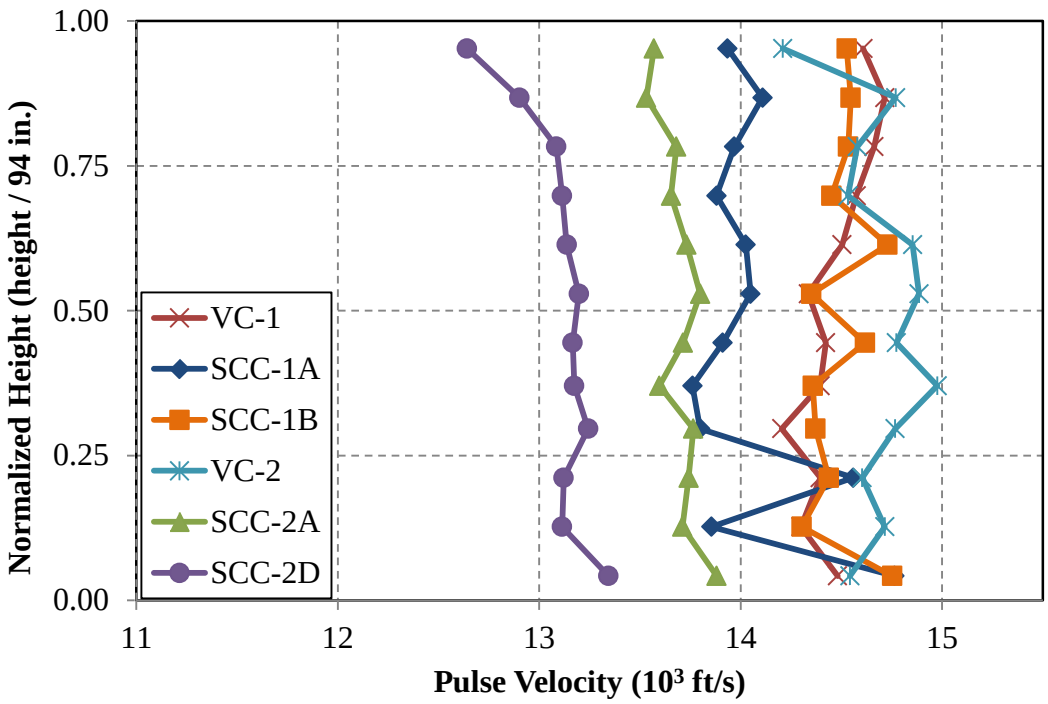

Figure 2.32: Sample of UPV results over normalized height, in 94 in. walls

Many properties affected by segregation, including distribution of air voids, aggregate, and excess water, can affect the measured UPV, and these properties do not necessarily fluctuate linearly. Therefore, although the UPV measurements in a wall may not consistently vary over the wall's height, the maximum and minimum velocities likely indicate the level of non-uniformity within the wall. To quantify that non-uniformity, a "UPV segregation index" was determined for each wall and mixture by dividing the maximum row-average UPV by the minimum. The UPV segregation indices for each wall and mixture are shown in Figure 2.33 and are presented in Appendix A.

Since the UPV segregation indices presented in Figure 2.33 do not vary consistently with wall height, the largest magnitude UPV segregation index for each mixture was used for all analyses. These mixture-maximum UPV segregation indices are presented in Table 2.6.

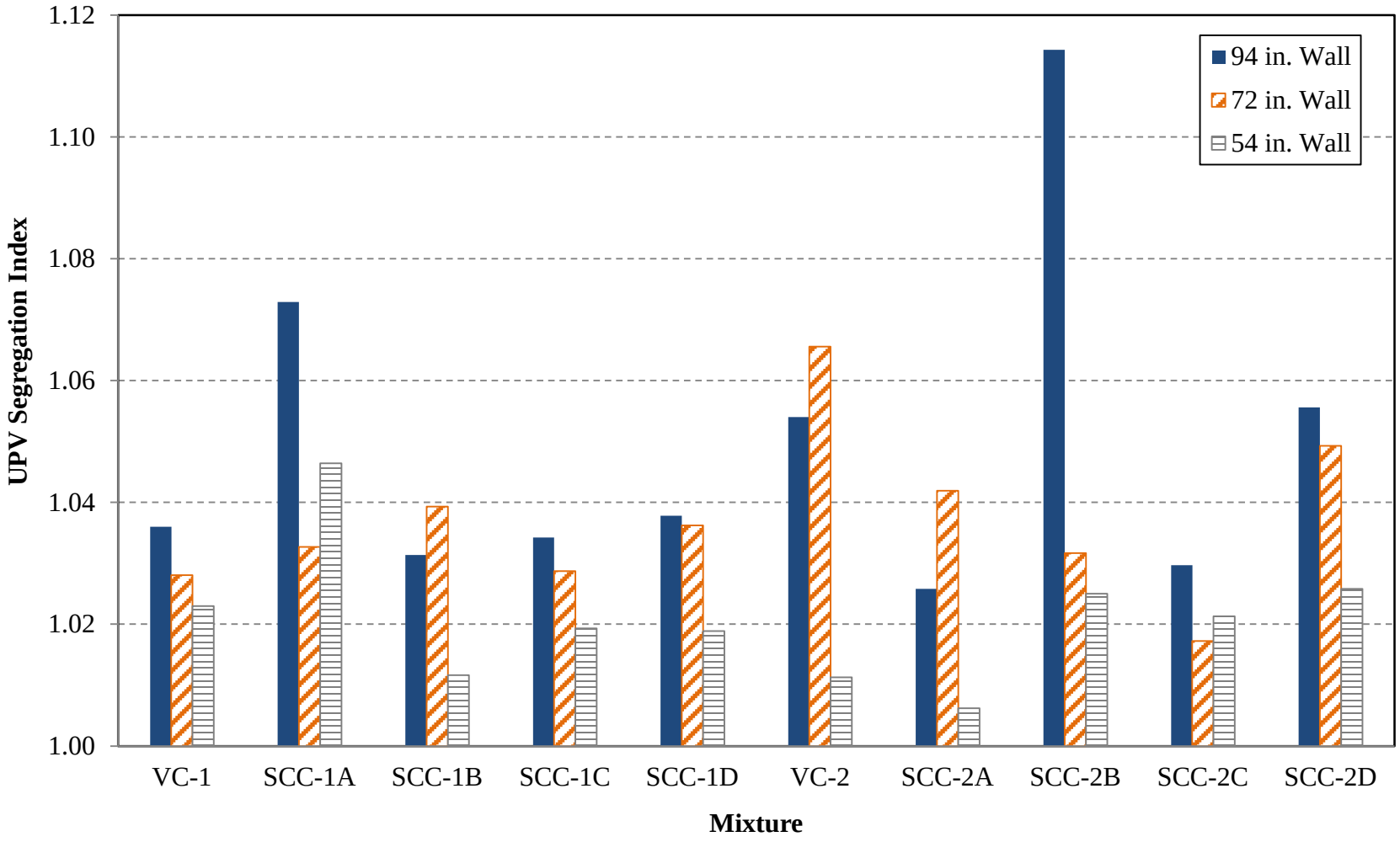

Figure 2.33: UPV segregation indices by wall height and mixture

2.4.3.2 Pullout Testing

The average pullout force was determined for the eight bars closest to each other at the top, bottom, and approximate midheight of each wall. Eight-bar groups were used because of the inherent scatter involved with short-embedment pullout testing and because the eight bars at each location were much closer to each other than to the other groups of eight.

Pullout testing outliers were identified and removed from consideration. Outliers were identified as any value greater than two standard deviations away from the average of the other seven results in a given group. Outliers were found in less than 13% of measurements, which was similar to the percentage found during UPV testing. A sample of pullout strength results from the same 94 in. walls shown in Figure 2.32 is given in Figure 2.34. Complete pullout force data for each wall and mixture are reported in Appendix A.

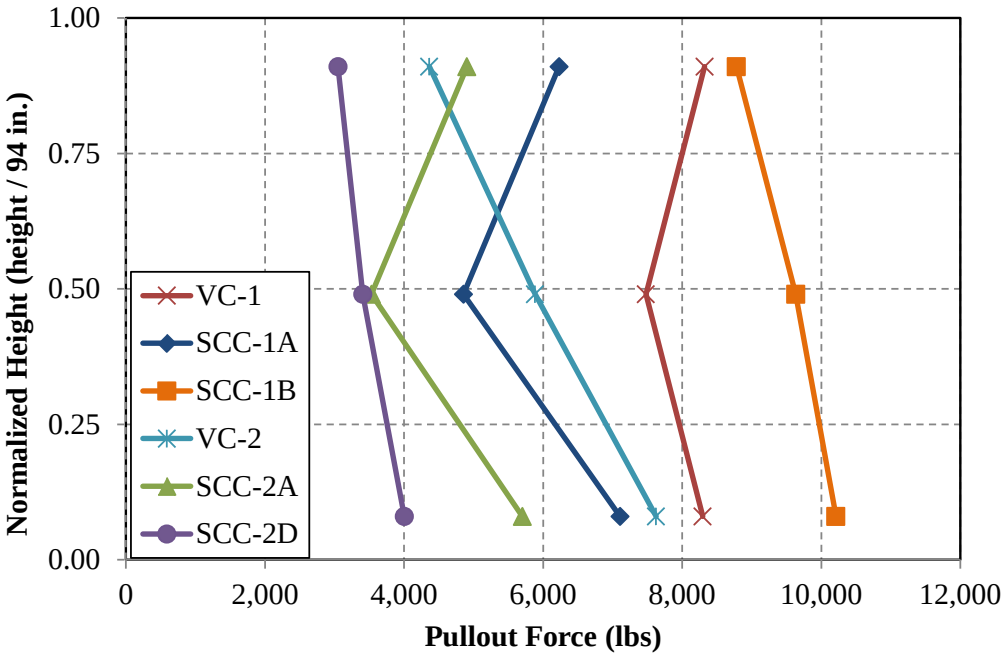

Figure 2.34: Sample of pullout strengths over normalized height, in 94 in. walls

In accordance with the convention of Khayat and Mitchell (2009) and others (Khayat et al. 1997; Stocker and Sozen 1970), the top-bar effect was calculated by dividing the pullout force in the bottom group of bars by the lesser average pullout force of the midheight group or top group (but never taken less than 1.00). The top-bar effects for each wall and mixture are summarized in Figure 2.35 and are presented in Appendix A. Because the top-bar effects presented in Figure 2.35 do not vary consistently with wall height, the mixture-maximum top-bar effect was used as the pullout benchmark result for all analyses. These values are summarized in Table 2.6.

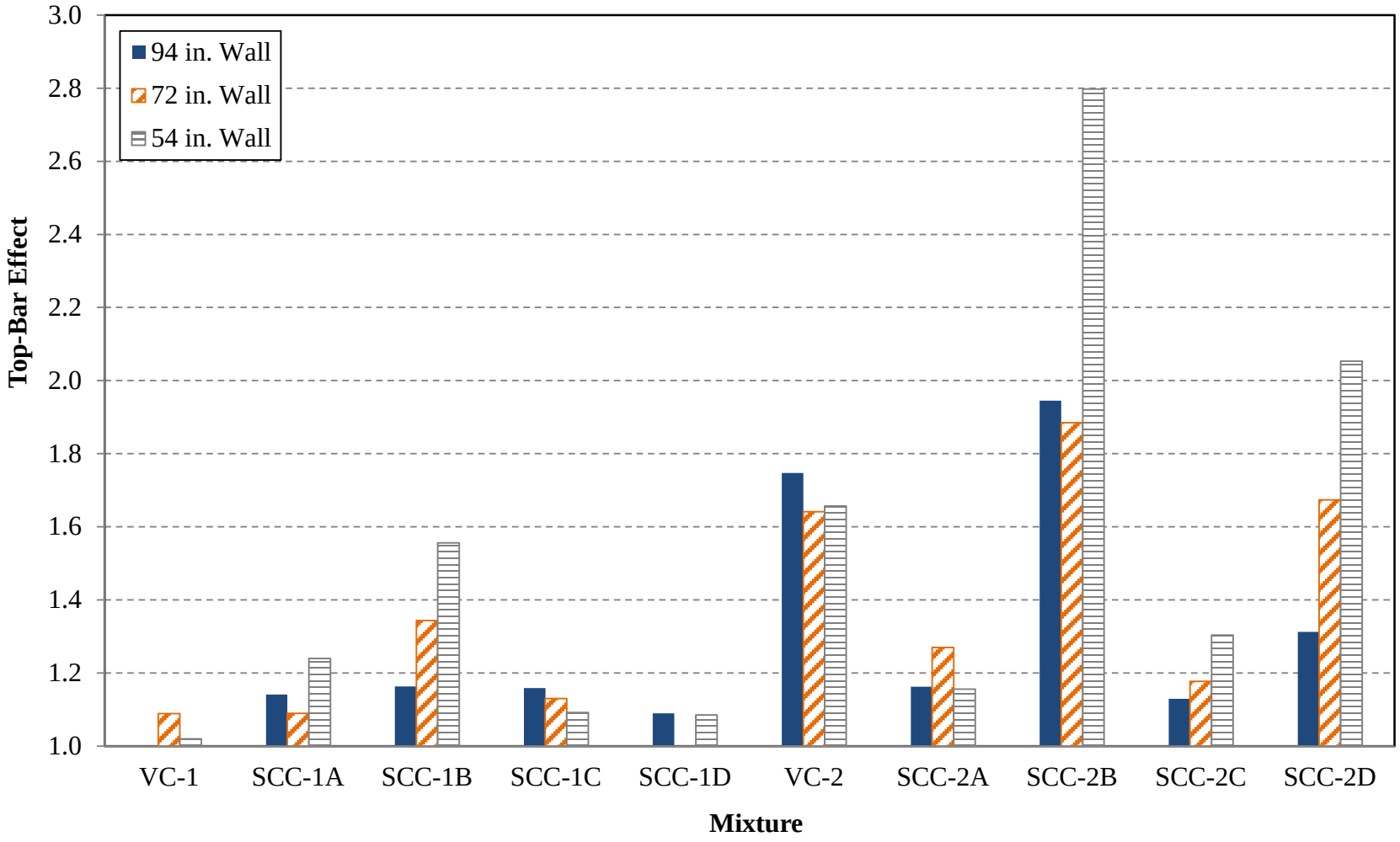

Figure 2.35: Top-bar effects by wall height and mixture

2.4.3.3 Alternative Approaches for Result Determination

Alternative approaches were considered when choosing how to compare the UPV and pullout measures to each other and to each fresh concrete stability test result. In additional to simple ratios of maximum results to minimum results, hardened uniformity results were alternatively tabulated as the ratio of the maximum result difference divided by the average of all measurements. This was considered because of the inconsistency between measurement location and result illustrated in Figure 2.32 and Figure 2.34. However, the alternative did not significantly affect the relationships found.

While mixture-maximum UPV segregation index and top-bar effect results identify the most severe heterogeneity present among multiple walls, *average* uniformity values for each mixture were considered because of the inconsistency between wall height and uniformity shown in Figure 2.33 and Figure 2.35. However, these alternatives did not significantly affect the relationships found.

2.4.3.4 Correlations between Hardened Test Results

A correlation between UPV results and pullout testing results was evaluated by comparing each mixture's maximum UPV segregation index and maximum top-bar effect. VC results were included in this comparison, as the comparison does not concern fresh concrete stability test results. This comparison is illustrated in Figure 2.36, in which a reasonable correlation exists between the results (R^2 = 0.54). A nonlinear model was also applied, but the R^2-value was not improved through the use of a nonlinear model.

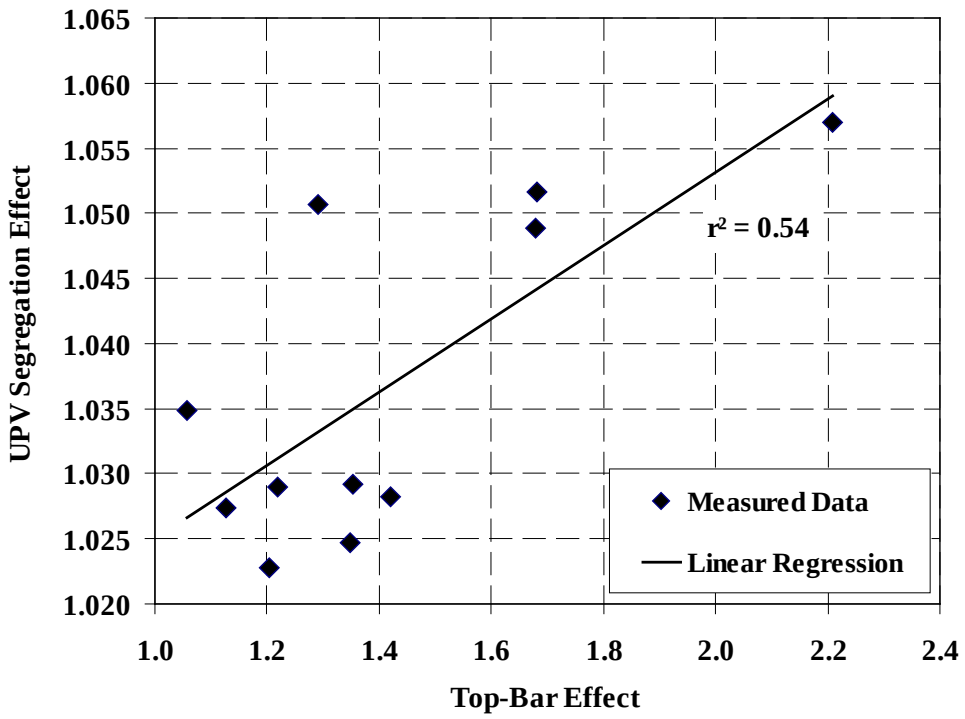

Figure 2.36: Comparison between top-bar effect and UPV segregation index

Based on this comparison, the types of in-situ non-uniformity identified by the UPV (air void stability, aggregate gradation, localized w/cm, etc.) appear to also affect the bond between concrete and horizontally-embedded reinforcement. This is in line with the findings of Castel et al. (2006), Esfahani et al. (2008), and Khayat et al. (1997), who all found that weakened bond surfaces develop as a result of irregular constituent dispersion. Regardless of the correlation, though, both test methods are given equal consideration in this research as independent measures of in-situ uniformity to determine the ability of fresh stability tests to assess stability.

2.4.4 Correlations between Test Results

Table 2.7 consists of linear-regression coefficients of determination (R^2) between each fresh stability and hardened uniformity test result when comparing all available SCC results. In the table, R^2-values are highlighted to show relative strength—the smallest bold value is at least 50% greater than all non-highlighted R^2-values, thus indicating a division of relative degree of correlation strength.

Table 2.7: Linear correlation R^2-values between fresh concrete stability and hardened concrete uniformity test results (all available SCC results)

Hardened Uniformity Test Result	Fresh Concrete Stability Test Result					
	VSI	**Seg. Index**	**Rapid Pen.**	**Sieved Fraction**	**Rate of Settle.**	**Max. Settle.**
UPV Segregation Index	0.19	0.16	0.01	0.17	**0.44**	0.14
Top-Bar Effect	**0.46**	0.21	0.01	**0.41**	**0.65**	0.00

Highlighted in the table, the linear test correlations having the greatest R^2-values were the correlations relating the VSI and sieved fraction to the top-bar effect and relating the surface settlement rate to the UPV segregation index and top-bar effect. The rapid penetration test and surface settlement test (maximum settlement) do not exhibit a reasonable correlation with either hardened concrete uniformity test results. A nonlinear model was also applied to each relationship, but no R^2-value was improved by more than 0.10 through the use of a nonlinear model.

2.4.4.1 Surface Settlement Test Correlations

Two sets of results were analyzed from the surface settlement test: the rate of settlement experienced between 10 and 15 minutes, and the maximum settlement experienced. Only the rate of settlement results correlated well with both the UPV segregation index and top-bar effect, and the ultimate settlement results did not correlate well with either. The correlations between rate of settlement and each in-situ uniformity measurement are shown in Figure 2.37 and Figure 2.38.

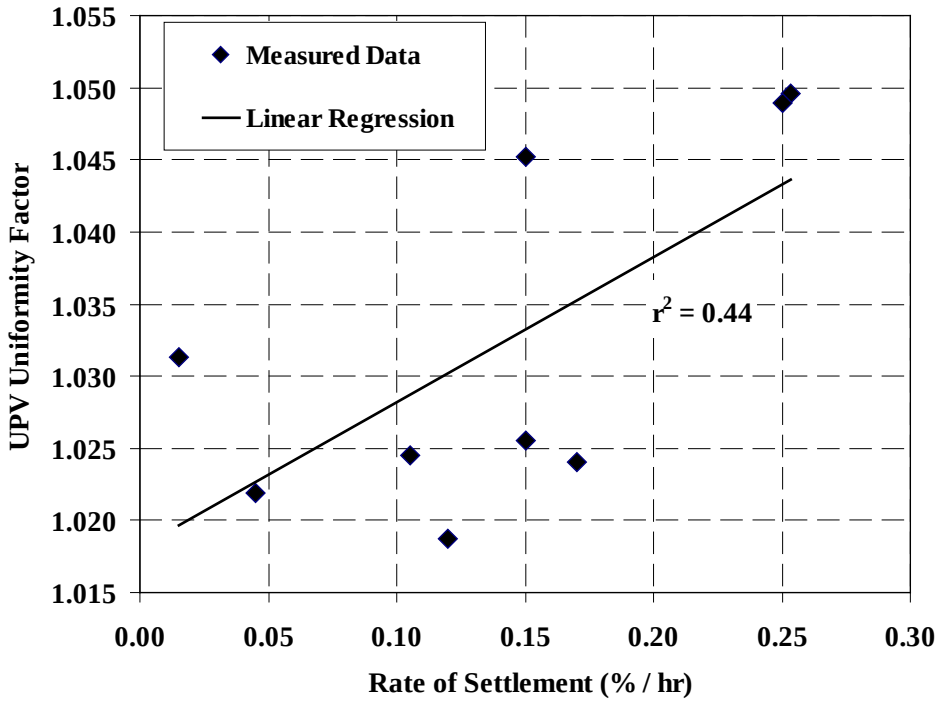

Figure 2.37: Comparison between rate of settlement results and UPV segregation index

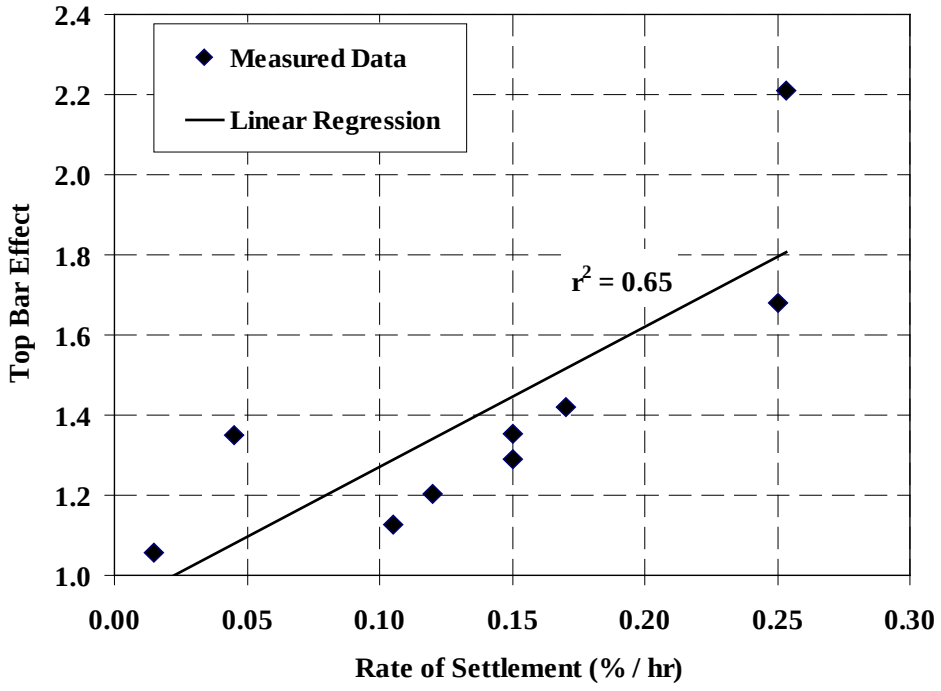

Figure 2.38: Comparison between rate of settlement results and top-bar effect

The coefficients of determination between rate of settlement and each in-situ uniformity measure were the highest among fresh stability tests ($R^2$of 0.44 with UPV segregation index and

R^2 of 0.65 with top-bar effect). Because the maximum settlement results from the test were not well related to either measure, only the rate of settlement should be necessary to assess mixture stability while using the surface settlement test.

2.4.4.2 Sieve Stability Test Correlations

The results of the sieve stability test correlated well with both the VSI and column segregation test results, and the sieve stability results also correlated reasonably well with the top-bar effect. The correlation between the sieved fraction and top-bar effect is shown in Figure 2.39, and it exhibited an R^2-value of 0.41, which is the third highest R^2-value between any fresh stability test and the top-bar effect.

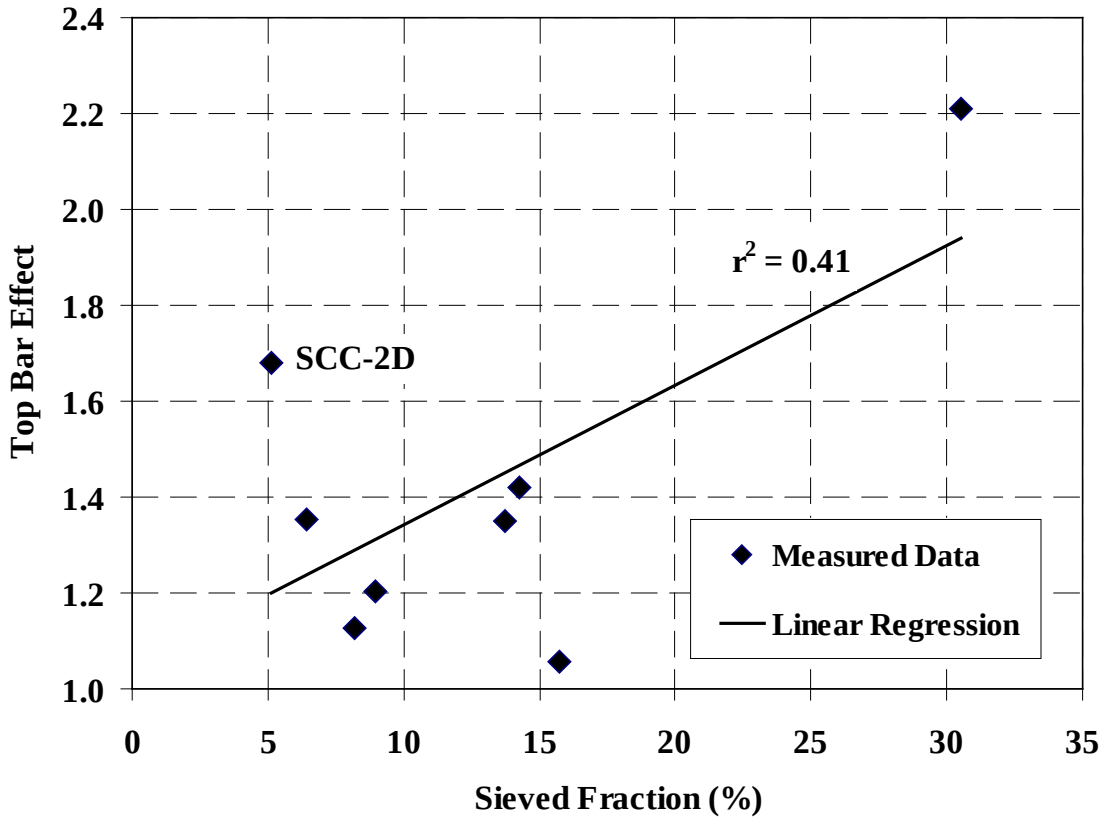

Figure 2.39: Comparison between sieved fraction and top-bar effect

Sieve stability test results and the UPV segregation index were also correlated, except in results from mixture SCC-2D. UPV uniformity and top-bar values from SCC-2D fit the correlation between UPV segregation index and top-bar factor that is shown in Figure 2.36, but SCC-2D's segregation indices did not fit the correlation between sieve stability results and top-bar effect or between sieve stability results and UPV segregation index (see data point [5.15, 1.68] on Figure

2.39). Therefore, exclusion of mixture SCC-2D was not permissible in analyzing the correlation between sieve stability results and UPV results.

2.4.4.3 Visual Stability Index Correlations

The VSI exhibited the second strongest correlation to the top-bar effect of any fresh concrete stability test. This relationship is shown in Figure 2.40.

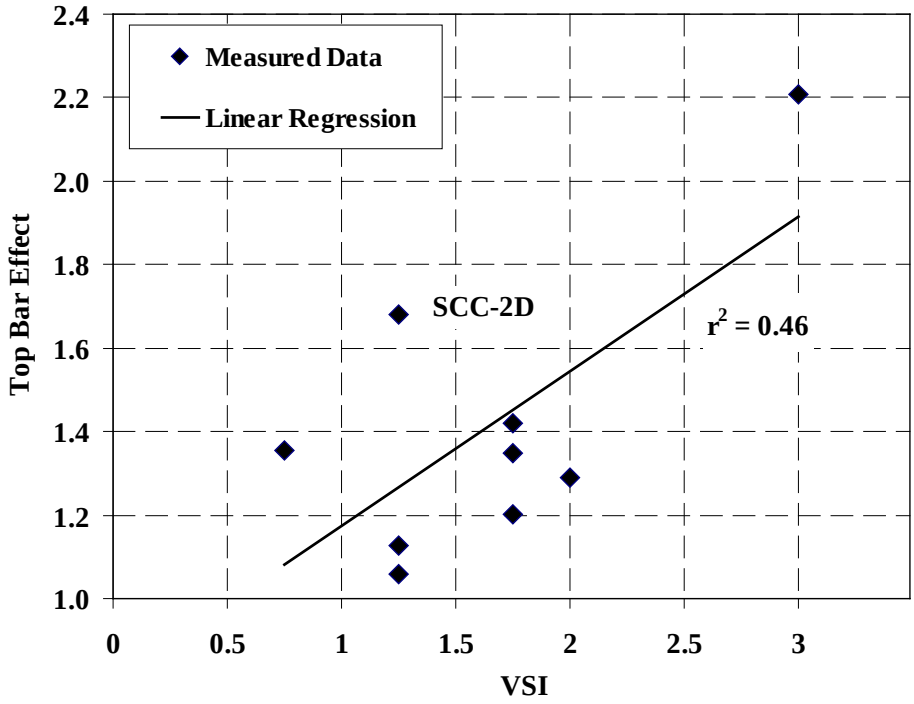

Figure 2.40: Comparison between VSI and top-bar effect

Similar to the sieve stability test results, the VSI and the UPV segregation index were also correlated, except in results from mixture SCC-2D. As in the previous comparison, SCC-2D's segregation indices did not fit the correlation between VSI and top-bar effect or between VSI and UPV segregation index (see data point [1.25, 1.68] on Figure 2.40). As already stated in Section 2.4.4.2, the results from SCC-2D could not be excluded from comparisons with in-situ uniformity measures, which greatly reduced the correlation factor between those measures and all fresh stability measures except the rate of settlement from the surface settlement test.

2.4.4.4 Fresh Concrete Stability and Hardened Concrete Uniformity Tests Exhibiting Weak Correlations

The results from the rapid penetration and column segregation test methods did not correlate well with either measure of in-situ uniformity, as can be inferred from their low coefficients of determination. Conclusions concerning the inaccuracy of the rapid penetration test must take into consideration the fresh stability tests that were successful. Both the VSI, which is faster to conduct, and the surface settlement test, which measures the settlement of a specified weight into a sample of SCC, were more accurate. Therefore, either the specific form of segregation measured by the penetration test cannot be sufficiently studied in such a short time, or the precision of the test is insufficiently low.

The column segregation test, which takes more time to conduct than the sieve stability or surface settlement (rate of settlement) test methods, is not as well correlated to in-situ uniformity measures as either. Therefore, it is likely that the form of segregation identified by the column segregation test does not correlate to in-situ performance as well as the other two measures, at least in the mixtures studied in this research project. Furthermore, the column segregation test correlates well with the sieve stability test, and the sieve stability test is easier to conduct. For those reasons, the column segregation test should be replaced with the sieve stability test for determining the fresh concrete stability of SCC.

2.4.5 Stability Testing Protocol and Criteria

2.4.5.1 Test Method Recommendations

The use of the VSI, sieve stability test, and surface settlement test in determining SCC stability is warranted from the discussions presented in the previous sections. Considering the technician-friendliness of these tests, the use of the VSI and sieve stability test are recommended for use in on-site quality assurance, while the surface settlement test (rate of settlement) is recommended for mixture prequalification in a laboratory setting. The VSI test provides quick feedback and should be the first test used to screen a load of SCC for quality assurance. If the VSI result exceeds acceptable limits (discussed in the next subsection), then the slower sieve stability test can provide a quantitative result for final determination of batch acceptance or rejection.

Different limiting VSI and sieve fraction values have been previously recommended; regardless, using the sieve stability test result can remove undesirable subjectivity from batch acceptance decisions in borderline VSI situations. This approach requires simultaneous initiation of the VSI and sieve stability tests, but the sieve stability test may be discontinued if the SCC exhibits a clearly acceptable VSI result. The two test methods are strongly correlated, and this simple approach provides a quantitative means for field quality assurance testing.

2.4.5.2 Test Result Recommendations

In accordance with the discussion of Section 2.2.3.2 and the practice of Khayat and Mitchell (2009), acceptance criteria for these three tests were determined based on limiting measured top-bar effects to less than 1.4. This top-bar-effect limit is based on the top-bar factor applied by AASHTO (2013) and ACI 318 (2011); a UPV segregation index limit of 1.046 was utilized based on the relationship between top-bar effect and UPV segregation index discussed in Section 2.4.3.4. The two in-situ measures are strongly correlated, so fresh concrete stability criteria based on the UPV segregation index should affirm the criteria determined based on the top-bar effect.

Table 2.8: Fresh concrete stability test acceptance criteria

Fresh Test Result	In-Situ Measurement		Recommended Test Criteria[1]
	UPV Seg. Index = 1.046	Top-Bar Effect = 1.4	
VSI	-	1.61	≤ 1.5
Sieved Fraction	-	12.0	≤ 10.0%
Rate of Surface Settlement	0.27	0.14	≤ 0.15 %/hr

Note: - = result not applicable because of relative weakness of correlation; 1 = recommendations subject to update in Keske et al. (2015)

The applicability of these recommendations is limited by the number and variety of mixtures tested to derive them, and the results from additional mixtures are presented in a forthcoming report regarding ALDOT Project 930-799 by Keske et al. (2015). Results presented in that report supersede these results, but several conclusions were reached concerning the mixtures reported here:

- The limiting rate of settlement recommended by Khayat and Mitchell (2009) for ½ in. NMSA concrete was too large, as every mixture exhibited an acceptable rate of settlement but some exhibited unacceptably high top-bar and UPV effects,
- A sieved fraction limitation of 15% recommended by EPG (2005) for Class 2 (vertical construction) applications was too high, although their recommendation for constrained flow applications (10%) was reasonably accurate, and
- The VSI limitation of 1.5 recommended by PCI (2004) would reasonably identify acceptance in all but one tested mixture (SCC-2D), although the applicability of this VSI limitation are unclear because of the subjectivity of the test method.

2.5 SUMMARY AND CONCLUSIONS

2.5.1 Summary

The research described in this chapter was undertaken as part of a larger research project funded by ALDOT to study the behavior of SCC used in the production of precast, prestressed bridge girders. This laboratory phase was undertaken to address the assessment of fresh SCC stability, as this is a concern that may limit the use of SCC in precast, prestressed applications. Five fresh concrete stability tests were selected for further study:

- ASTM C1611 Visual Stability Index (described in Section 2.2.1.1),
- ASTM C1610 Column Segregation Test (described in Section 2.2.1.2),
- ASTM C1712 Rapid Penetration Test (described in Section 2.2.1.3),
- Sieve Stability Test (described in Section 2.2.1.4), and
- Surface Settlement Test (described in Section 2.2.1.5).

To assess these tests, they were conducted concurrently with the casting of three concrete walls with heights of 54, 72, and 94 inches. Walls were cast and fresh concrete stability tests were conducted on a total of eleven mixtures, nine of which were SCC. The SCC mixtures were divided into two approximately equal groups, and each mixture was adjusted to exhibit different fresh behavior and stability. The adjustments to stability were controlled by varying water content, HRWRA content, VMA content and type, or a combination of the variables.

The two VC mixtures were proportioned similarly to the SCC mixtures but using a higher *w/cm*, lower *s/agg*, and larger aggregate gradation typical of VC used in precast, prestressed applications. Only in-situ uniformity tests were conducted on VC mixtures, as the fresh concrete stability test methods could only be assessed in SCC mixtures.

Two test methods were selected to measure in-situ uniformity of the concrete walls: ultrasonic pulse velocity (UPV) testing and pullout bond testing. UPV testing was used primarily to identify changes in overall uniformity of concrete, including changes in air void distribution and aggregate distribution. Pullout testing was conducted on eight-specimen groups of deformed steel bars cast horizontally through the walls at the bottom, approximate midheight, and top of each. This method was used primarily to identify changes in bond uniformity.

Results from the five fresh concrete stability tests were compared with each other and with the results of each in-situ hardened concrete uniformity test. The observations and conclusions made during the collection and analysis of these results are summarized in Section 2.5.2. The recommendations made based on this research are given in Section 2.5.3.

2.5.2 Research Observations and Conclusions

2.5.2.1 Fresh Concrete Stability Tests

- The strongest correlations between fresh tests were those between the sieve stability, and both the VSI and column segregation tests (two paired correlations), and between the rate of settlement and maximum settlement determined from the surface settlement test.
- The rate of settlement determined during the surface settlement test correlated well with the maximum settlement found during the same test (R^2 = 0.47) when compared using a nonlinear regression model. This closely resembled the nature of the relationship reported by Hwang et al. (2006).
- The sieve stability test correlated well with the column segregation test. This suggests that both tests are similarly affected by SCC segregation.
- The rapid penetration test did not show any reasonable correlations to other fresh concrete stability tests.

2.5.2.2 Hardened Concrete Uniformity Tests

- Pulse velocities decreased with increasing height in both VC and SCC, but the trend was not consistently related to the height of the specimen or relative location within the specimen.
- Pullout bond strengths decreased with height in a majority of walls in both VC and SCC, but the reduction was not consistently related to specimen height.
- The UPV segregation index and top-bar effect are strongly correlated (R^2 = 0.65). The correlation may be attributed to the similarity in what properties affect each test: air void distribution, aggregate distribution, and presence of bleeding.
- Although only relatively small variations were observed in UPV measurements compared to pullout measurements (up to 5% versus up to 121%), either test method can be independently used to assess in-situ uniformity.
- Mixture SCC-2D was determined to be unstable by both the UPV and pullout tests, but, among the fresh stability tests, the mixture was only identified as unstable by the rate of settlement from the surface settlement test method.

2.5.2.3 Relationships between Fresh Concrete Stability and Hardened Concrete Uniformity Test Results

- The rate of settlement determined by the surface settlement test was found to have a reasonable correlation to both UPV uniformity results and pullout strength uniformity results (R^2-values of 0.44 and 0.65, respectively), and it was the only fresh stability test strongly correlated to both measures of in-situ uniformity.
- The sieve stability test exhibited a reasonable correlation to pullout bond uniformity (R^2-value of 0.41), as did the VSI (R^2-value of 0.46).
- The rapid penetration and column segregation test methods did not correlate well with either measure of in-situ uniformity.
- No correlations between fresh stability test methods and either measure of in-situ uniformity was improved through the use of nonlinear regression models.

2.5.3 Recommendations

2.5.3.1 Test Method Recommendations

- The rapid penetration test and column segregation test may not be able to accurately assess the stability of fresh SCC, and further research would be necessary before recommending their use for this application.
- Because it correlates well with both measures of in-situ uniformity (UPV testing and pullout testing) but is not well suited for field use due to the sensitivity of the test apparatus, the surface settlement test should be the primary test used to determine SCC mixture stability acceptance during prequalification.
- It is only necessary to measure the rate of settlement determined between 10 and 15 minutes while conducting the surface settlement test.
- Because it correlates well with pullout testing results and both the VSI and column segregation tests and provides a quantitative result, the sieve stability test should be the primary stability test method used for QA batch acceptance.
- Because it correlates well with the column segregation test, requires less time to conduct, and is better correlated to in-situ uniformity measurements, the sieve stability test should be used in place of the column segregation test when testing SCC stability.
- Because it correlates well with the quantitative but more time-consuming sieve stability test, as well as with pullout testing results, the VSI is a viable quality assurance test method in the field.

2.5.3.2 Stability Testing Protocol and Criteria

During mixture prequalification in a laboratory setting, the rate of settlement determined during the surface settlement test should be used alongside the sieve stability test to determine SCC mixture stability. The two measures, both of which provide a quantitative result and relate well with in-situ measures of hardened concrete uniformity, may be differently affected by mixture composition and should together provide comprehensive identification of mixture stability. The fresh stability results at which to determine acceptance may vary by application, mixture, and reinforcement type, but, when evaluating SCC for precast, prestressed applications, a rate of settlement of 0.15%/hr and sieved fraction of 10% should be acceptable.

Because it provides quick feedback, the VSI test should be the first test used to screen a load of SCC for quality assurance during full-scale production. If the VSI result exceeds 1.0, then the sieve stability test can provide a quantitative result for final determination of batch acceptance or rejection while removing undesirable subjectivity from batch acceptance decisions in borderline VSI situations. This approach requires simultaneous initiation of the VSI and sieve stability tests, but the sieve stability test may be discontinued if the SCC exhibits a VSI less than or equal to 1.0. Despite the additional effort, this approach is simple and provides a quantitative means for field quality assurance testing.

CHAPTER 3: PRODUCTION AND MECHANICAL PROPERTIES OF FULL-SCALE GIRDERS

3.1 INTRODUCTION

The final phase of the AUHRC investigation of SCC for precast, prestressed construction was to produce Alabama's first bridge with precast, prestressed SCC girders. This full-scale implementation of SCC precast, prestressed girders consisted of the production of seven 97 ft-10 in. AASHTO-PCI BT-54 bulb-tees and seven 134 ft-2 in. BT-72 bulb-tees to be placed in a rural highway bridge over Hillabee Creek in Alexander City, Alabama alongside an equal number of companion VC girders. The most recent estimate of average daily traffic at this location (2011) was reported to equal 3,290 with approximately 10% heavy truck traffic (ALDOT 2014). Production of some of the girders is shown in Figure 3.1.

Figure 3.1: Removal of formwork following

Full-scale production was conducted with minimal researcher interference or direct involvement, which provided the AUHRC researchers a unique opportunity to connect laboratory-investigated findings concerning the use of SCC to various aspects of as-built, full-scale structural behavior. Furthermore, because each property and full-scale structural behavior was assessed in

the same members, correlations between these properties and behaviors were directly evaluated. Several properties, behaviors, and their correlations are discussed in Chapters 4–6 of this dissertation:

- Transfer behavior of full-scale girders (Chapter 4),
- Time-dependent material deformability (Chapter 5), and
- Time-dependent behavior of full-scale girders (Chapter 6).

Many aspects of the full-scale project are of importance to all of these correlations and must be considered first to effectively understand the comparisons made in Chapters 4–6. Furthermore, valuable insight is gained by reviewing the production process, which was expected to be different when using SCC. Thus, the primary objectives of this chapter are to

- Describe and assess the geometry and production of the precast, prestressed SCC girders produced in Alabama's first full-scale SCC implementation, and
- Describe and assess mechanical properties and production practices from the full-scale production that are of overarching significance to the material and structural behaviors described in the subsequent chapters of this report.

3.2 LITERATURE REVIEW

When evaluating a new material, it is important to understand *how* results should be compared to meet the objectives of the test. If the new material is to be used as a direct replacement for another, then a direct comparison of mechanical properties is warranted. This type of one-to-one comparison is of limited value when comparing two concretes of the same constituents, though, because many factors (mixture proportions, concrete age, and curing history) are known to have an effect on hardened concrete mechanical properties including compressive strength (f_c), splitting tensile strength (f_{ct}), and modulus of elasticity (E_c). More important when assessing a new material such as SCC is assessment of whether its performance is as predictable or reliable as that of a conventional VC material after accounting for known differences in material properties.

In this section, research is reviewed concerning common differences between SCC and VC hardened mechanical properties and whether those differences affect the applicability of existing prediction models. Lastly, because it appears to be of concern especially during the production of precast, prestressed girders, documented differences between predicted and measured properties are reviewed.

3.2.1 Effects of Mixture Proportioning on SCC Mechanical Properties

Mixture changes common to produce SCC are necessary primarily to create a mixture with stable, self-consolidating properties in the fresh state. Common changes from equivalent-use vibrated concrete include decreased *w/cm*, increased paste content (and decreased aggregate content), decreased coarse aggregate size, increased *s/agg*, and increased HRWRA use. In *all* concrete, these changes can affect strength and modulus of elasticity, although to different degrees (Mehta and Monteiro 2006).

Comparisons of mechanical properties in SCC and VC have been mixed. ACI 237 (2007) suggests that SCC frequently exceeds the strength of comparable-use VC due to lowered *w/cm*, and Naito et al. (2005) found that SCC of the same *w/cm* exhibited higher compressive strength and tensile strength than those of VC. Both ACI 237 (2007) and Khayat and Mitchell (2009) indicate that SCC can reasonably be expected to exhibit E_c of up to 20% lower than that of comparable-strength VC. Many researchers (Bonen and Shah 2004; Kim et al. 2012; Naito et al. 2005; Panesar and Shindman 2011; Parra et al. 2011; Zia et al. 2005; Ziehl et al. 2009) have reported such, while Almeida Filho et al. (2010), Erkmen et al. (2008), and Schindler et al. (2007) found SCC E_c to be similar or within the expected variability of testing according to ASTM C469. Findings of SCC f_{ct} are mixed, as well: Kim et al. (2012), Naito et al. (2005), and Ozyildirim (2008) found that SCC exhibits comparable or better f_{ct} than VC, while others (Almeida Filho et al. 2010; Parra et al. 2011; Zia et al. 2005) found that it was slightly reduced.

3.2.2 Code Provisions for the Prediction of Mechanical Properties

As mentioned in the previous section, many parameters can influence the mechanical properties of SCC. However, only a few parameters that can be controlled in the design phase, well before construction, are typically considered by structural engineers. For that reason, minimum f'_c is usually specified, while prediction models for other properties such as splitting tensile strength (f_{ct}) and modulus of elasticity (E_c) are greatly simplified and based on assumed correlation with f'_c (Al-Omaishi et al. 2009). Since SCC can be proportioned very differently to achieve the same f'_c, the applicability of these prediction models has been studied frequently. In the following subsections, literature is reviewed concerning two particular mechanical properties: f_{ct} and E_c.

3.2.2.1 Splitting Tensile Strength Prediction Models

In American practice, splitting tensile strength (f_{ct}) is tested according to ASTM C496 (2010) and is correlated to uniaxial tensile strength and compressive strength. Coarse aggregate source is not commonly integrated (despite an apparent dependence) due to low likelihood of engineer knowledge of coarse aggregate type. ACI 318 (2011) reports average f_{ct} according to Equation 3-1 (from R8.6.1 of the code), and AASHTO (2013) and ACI 363 (1992) report average f_{ct} according

to Equation 3-2 (from C5.4.2.7 of AASHTO 2013 or Section 5.6 of ACI 363 1992). In both equations, f_{ct} is calculated in psi based on f'_c reported in psi.

$$f_{ct} = 6.7\sqrt{f'_c} \tag{3-1}$$

$$f_{ct} = 7.4\sqrt{f'_c} \tag{3-2}$$

Kim et al. (2012) recommend the use of Equation 3-2 for SCC f_{ct}, and Khayat and Mitchell (2009) found it acceptable for precast, prestressed SCC. Many other researchers (Almeida Filho et al. 2010; Naito et al. 2005; Ozyildirim 2008) have found that SCC and VC f_{ct} exceed values predicted by Equations 3-1 and 3-2. Myers (2008) found that these models especially under-predict f_{ct} in high-strength concrete used for precast, prestressed girders, as the relationship may be more related to the cubic root of f_c. It is for this reason that Kim et al. (2012) recommend the use of Equation 3-2 during the design of precast, prestressed girders utilizing SCC—it predicts higher f_{ct} than Equation 3-1 but is still conservative. Almeida Filho et al. (2010) and Parra et al. (2011), on the other hand, found that the models tend to over-predict f_{ct} of SCC.

3.2.2.2 Modulus of Elasticity Prediction Models

In American practice, E_c is typically predicted using models that incorporate three or fewer variables: f'_c, concrete unit weight, w_c, and coarse aggregate source. The most-widely used of these equations is from ACI 318 Section 8.5.1 (2011), in which E_c is calculated in psi, f'_c is in psi, and w_c is in lb/ft^3:

$$E_c = 33{w_c}^{1.5}\sqrt{f'_c} \tag{3-3}$$

Frequently, the unit weight of concrete is not known to the engineer, so ACI 318 (2011) allows a simplification of Equation 3-3 based on w_c equal to 145 lb/ft^3. That yields Equation 3-4:

$$E_c = 57{,}000\sqrt{f'_c} \tag{3-4}$$

The prediction model used by AASHTO (2013) (Equation 5.4.2.4-1 of the *LRFD* provisions) is identical to Equation 3-3 except that AASHTO takes coarse aggregate type into account with a multiplication factor, K_1. This modification factor accounts for the effect of aggregate properties on concrete elasticity and can vary between 0.70 and 1.30 (Al-Omaishi et al. 2009; Mehta and Monteiro 2006; Myers 2008). Because Equation 3-3 is directly multiplied by this factor, higher K_1 values are assigned to concretes utilizing stiffer coarse aggregate. AASHTO (2013) recommends using K_1 = 1.0 unless the mechanical properties of concrete made with a specific aggregate type are tested directly or are known from research on this aggregate type.

ACI 363 (1992) found that Equation 3-3 over-predicts E_c of concrete whose f'_c exceeds 6,000 psi. They recommended Equation 3-5 in the committee's state-of-the-art report on high-strength concrete (Equation 5-1 in ACI 363 1992):

$$E_c = 40{,}000\sqrt{f'_c} + 1(10)^6 \quad (3\text{-}5)$$

ACI 237 (2007), Khayat and Mitchell (2009), and PCI (2004) recommend the use of Equation 3-3 for SCC E_c prediction but suggest trial-batch evaluation of E_c according to ASTM C469 when E_c is important to the application (such as for camber prediction of precast, prestressed girders). Many other researchers (Almeida Filho et al. 2010; Kim et al. 2012; Naito et al. 2005; Panesar and Shindman 2011; Schindler et al. 2007; Storm et al. 2013) have found that SCC E_c is equally or more predictable than that of VC according to Equation 3-3. Among them, Kim et al. (2012) and Naito et al. (2005) state that SCC E_c was more predictable because VC exhibited an elastic modulus in excess of what would be predicted when using the equation; Ozyildirim (2008) found it more predictable because VC exhibited an elastic modulus less than what would be predicted (a weak coarse aggregate was used, and less of it was used in SCC). Meanwhile, Ziehl et al. (2009) found that E_c of SCC and VC were equally predictable, but that both fit better with Equation 3-5 among mixtures with compressive strength exceeding 6,000 psi. Erkmen et al. (2008) found that Equation 3-4 was well suited for SCC and VC E_c prediction for concrete using materials available in Minnesota.

Trejo et al. (2008) recommend the use of Equation 3-3 with K_1 values 0.95–1.05 for precast, prestressed SCC girder design when using Texas aggregates, while Storm et al. (2013) recommend using K_1 = 0.85 for all precast, prestressed girder design based on an evaluation of VC data from several states. These authors (Trejo et al. 2008 and Storm et al. 2013) also recommend the use of w_c = 150 lb/ft^3 in Equation 3-3. Al-Omaishi et al. (2009) noted that this w_c is expectable for precast, prestressed concrete because of the mixture proportioning tendencies—low *w/cm* and high aggregate content—typical of this application.

Ziehl et al. (2009) noted that the use of K_1 factors other than 1.0 cannot be expected in general design practice, as engineers would be unaware of the need or aggregate source. They also found that, while lightweight SCC mixtures fit well with Equation 3-3 when the unit weight is known, higher strength (f'_c exceeding 6,000 psi) normal-weight SCC and VC properties were more accurately predicted using Equation 3-5. Notably, Ziehl et al. (2009) assessed the elastic modulus equations among SCC mixtures with an average w_c equaling 146 lb/ft^3. Many other researchers (Al-Omaishi et al. 2009; Khayat and Mitchell 2009; Kim et al. 2012; Myers 2008) state that Equation 3-5 under-predicts E_c in precast, prestressed concrete.

3.2.3 Differences between Design and Measured Properties

The applicability of the E_c and f_{ct} prediction methods discussed in this section clearly depends on the values of $\sqrt{f_c}$, w_c, and K_1 used in them. In concrete structural design practice, design f'_c serves only a as a minimum value to be met by the contractor. Concrete producers must exceed this minimum, and the risk of construction cost overruns (in delayed production or removal of unacceptable concrete) frequently leads them to produce concrete far exceeding f'_c. European

prediction models similar to the equations shown above take this into account by requiring that a mean f_c be used in service-state design predictions in place of the specified minimum compressive strength (*fib* 2010).

As discussed earlier, SCC is likely to be proportioned in such a way that it more greatly exceeds f'_c than does VC, although less so when dealing with precast, prestressed concrete. Compounding this, Storm et al. (2013) found that precast, prestressed girder producers typically exceed specified prestress-release and 28-day compressive strengths (f'_{ci} and f'_c) by 25% and 45%, respectively, at least when utilizing VC.

3.3 EXPERIMENTAL PROGRAM

3.3.1 Girder Description

The bridge selected for study has four spans—two outer spans each consisting of seven AASHTO-PCI BT-54 bulb-tees, and two inner spans each consisting of seven AASHTO-PCI BT-72 bulb-tees. One span of BT-54s and one span of BT-72s were made with SCC while the companion spans were constructed with VC girders. SCC girders support the first and second spans, while VC girders support the third and fourth spans, as displayed in Figure 3.2.

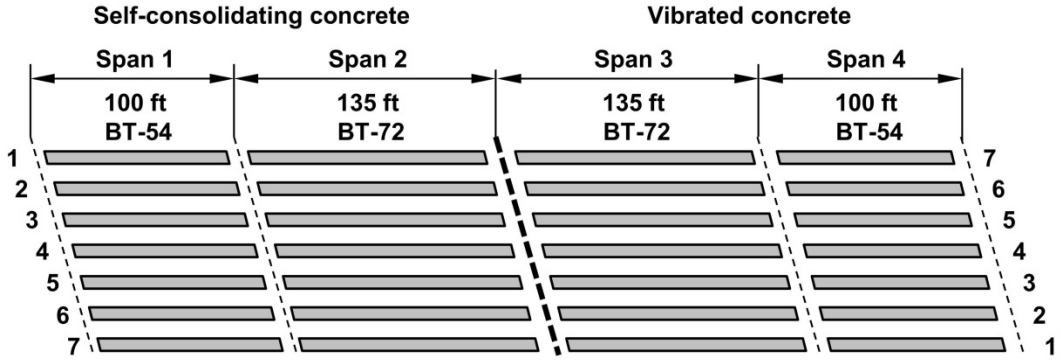

Figure 3.2: SCC and VC girders placed in the bridge over Hillabee Creek

The twenty-eight girders for the Hillabee Creek Bridge were produced at Hanson Precast of Pelham, AL during the months of September and October of 2010. The plant employed a central rotational mixer, and concrete was delivered to the prestressing bed in 4 yd^3 loads. Three BT-54 bulb-tees were cast in each of four days (two days of VC placements and two days of SCC placements), and the seventh VC and seventh SCC girders were cast on the same bed during a fifth production day. Following the completion of BT-54 production, two BT-72 bulb-tees were cast in each of six days (three days of VC placements and three days of SCC placements). Similar to the production of the BT-54s, the seventh VC and SCC girders were cast on the same

bed during a seventh production day. Thus, twelve SCC and VC production days alternated throughout the production, starting with SCC girders on September 21, 2010. Production days alternated between SCC and VC such that each matched pair of spans would exhibit a similar average age and ambient exposure history. After the girders were placed at the bridge site in early May of 2011, the bridge deck over each span was cast on four days during August of 2011. All findings related to the in-place performance of the composite bridge are reported in a separate report prepared by Keske et al. (2015).

3.3.1.1 Girder Dimensions

Standard dimensions of BT-54 and BT-72 girders are shown in Figure 3.3 and Figure 3.4. Cross-sectional areas are 789 in.^{2} and 1,085 in.^{2} for these two girder sizes. At lengths of 97 ft-10 in. and 134 ft-2 in., respectively, the girders approached the upper length limits allowed by *AASHTO LRFD* (2013) of 114 ft and 146 ft for BT-54 and BT-72 girders, respectively.

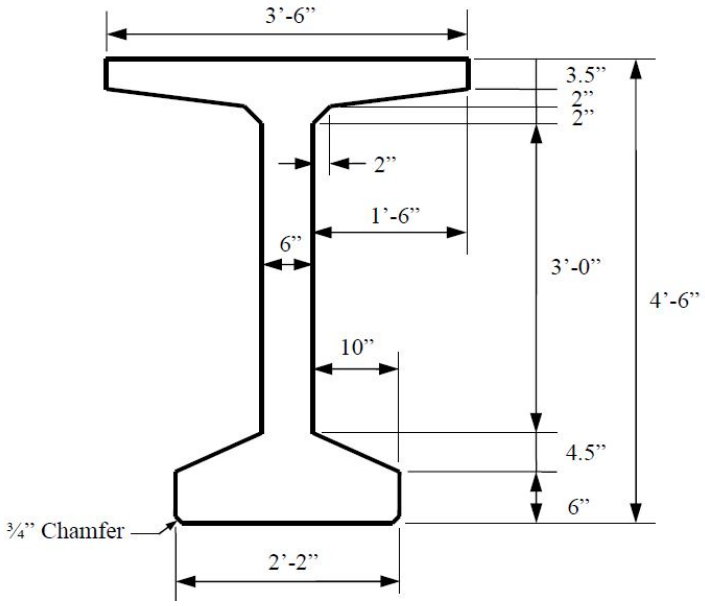

Figure 3.3: Typical BT-54 girder cross-sectional dimensions

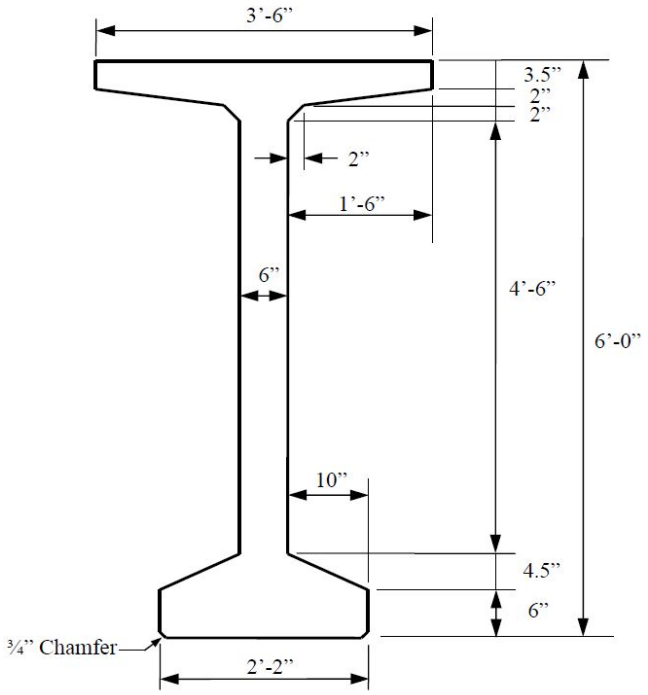

Figure 3.4: Typical BT-72 girder cross-sectional dimensions

All girders were heavily reinforced with seven-wire, Grade 270, low-relaxation strands. BT-54 girders included only ½-inch strands, and BT-72 girders included mostly ½-inch 'special' strands. The BT-54 girders contained a total of forty strands: twenty-eight strands in the bottom of the section tensioned to 30,980 pounds each, eight strands draped along the length of the member and tensioned to 30,980 pounds each, and four top strands lightly tensioned to 5,000 pounds each and used to support non-prestressed mild steel reinforcement.

The BT-72 girders had the same strand arrangement plus ten additional draped strands. Specifically, each contained twenty-eight ½ in. 'special' strands in the bottom of the section tensioned to 33,800 pounds each, eighteen ½ in. 'special' strands draped along the length of the member and tensioned to 33,800 pounds each, and four ½ in. top strands lightly tensioned to 5,000 pounds each.

In both strand sizes, the jacking force corresponded to a specified jacking stress (f_{pj}) of 202.5 ksi for the draped and the bottom strands and 32.7 ksi for the top strands. The specific location of each strand at the girder ends and midspan is illustrated in Figure 3.5. In addition, the draping profiles are presented in Figure 3.6.

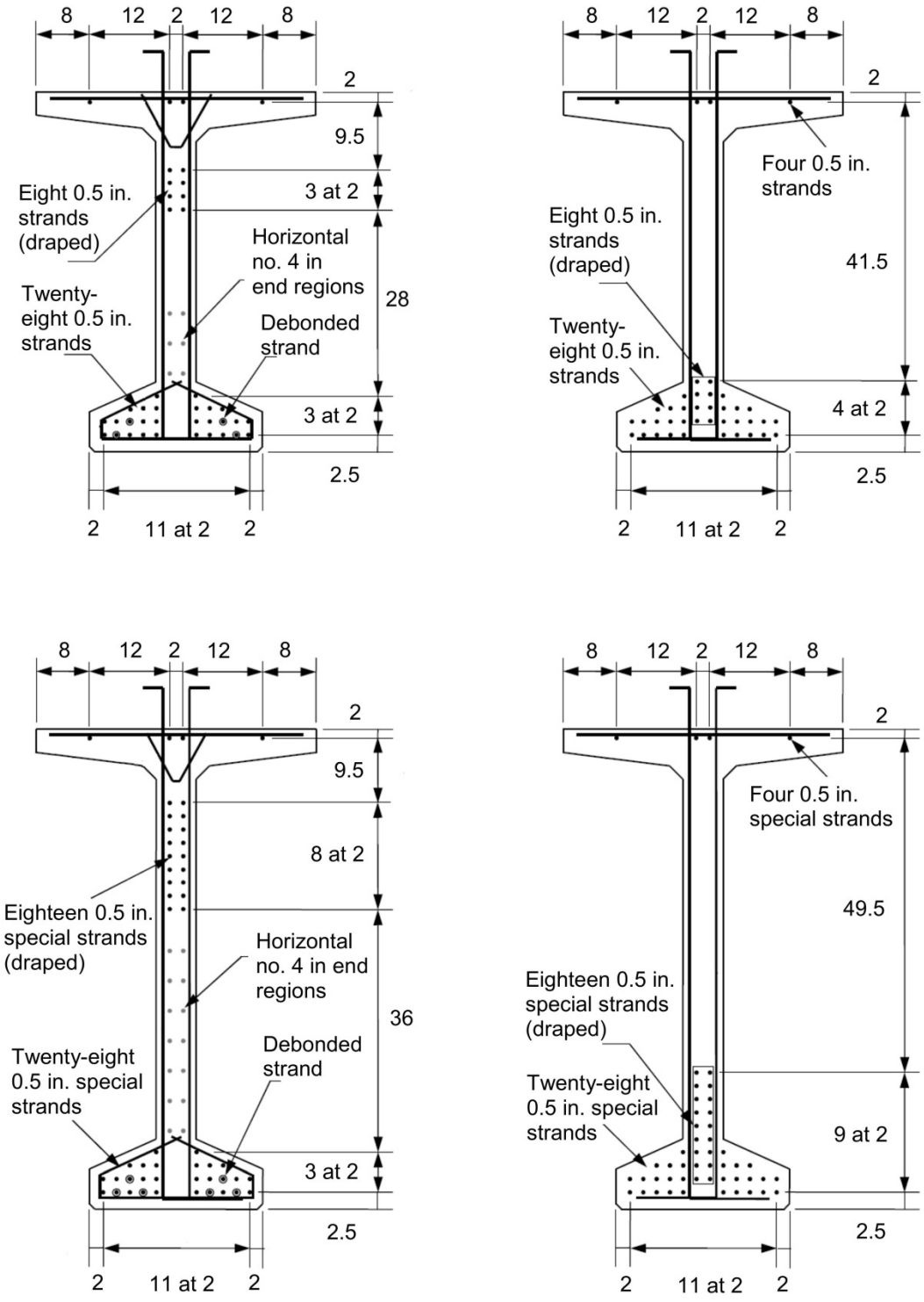

Figure 3.5: Strand arrangement for (*top left and right*) BT-54 girder at girder ends and midspan and (*bottom left and right*) BT-72 girder at girder ends and midspan

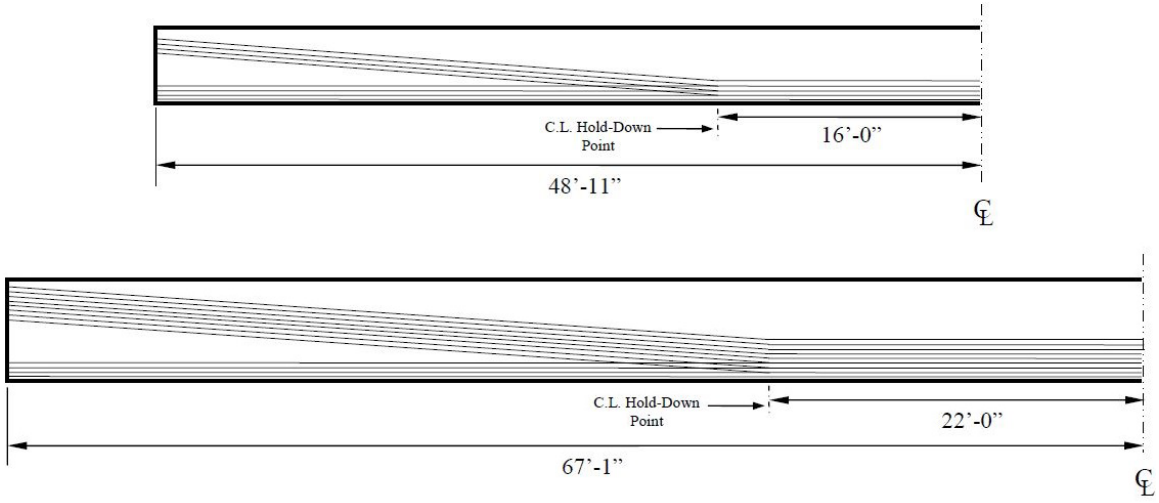

Figure 3.6: Profile of draped strands for (*top*) BT-54 girder and (*bottom*) BT-72 girders

In addition to draping some strands, it was also necessary to debond some strands to satisfy allowable stress limits. Consequently, four straight strands were debonded for a distance of 10 ft at each BT-54 girder end, and six straight strands were debonded for the same length in the BT-72 girders. This was accomplished by sheathing the strands with a plastic casing and sealing the casing with tape. The debonded strands are denoted with a circle around the strand in Figure 3.5.

3.3.1.1 Girder Nomenclature

In order to distinguish the twenty-eight girders, a specimen identification system was implemented as shown in Figure 3.7. Previously completed theses associated with this research (Dunham 2011; Ellis 2012; Johnson 2012) have each incorporated a different numbering scheme to identify production and geometric considerations of specific importance to them. The primary girder identification system selected for this research report was chosen to unify and clarify those previous identification schemes.

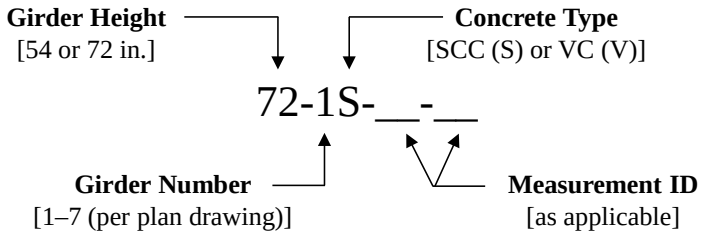

Figure 3.7: Girder identification scheme

Additional suffixes are appended to the girder identification depending on the property or behavior being analyzed. Different girders and samples within each production day were

assessed for the properties and behaviors discussed in this and subsequent chapters. Thus, not only is girder identification necessary, but so is identification of production groups. The primary production group identification system selected for this research report was chosen based on the sequential days of concrete production (seven days each of SCC and VC production). As discussed earlier, only two mixtures were utilized throughout this research—one SCC and one VC—so the identification scheme shown in Figure 3.8 does not distinguish between girder sizes.

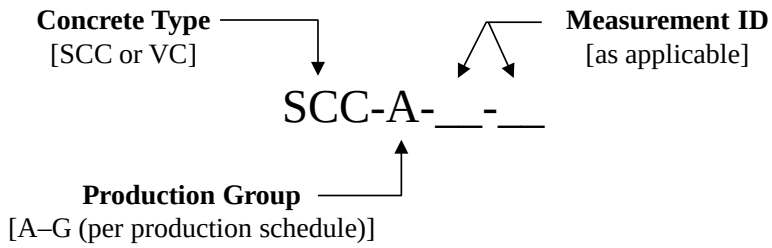

Figure 3.8: Production group identification scheme

3.3.1.2 Mixture Proportions

While the minimum compressive strengths were the same for SCC and VC mixtures, the precast producer was free to proportion each mixture in any way that would satisfy the project specification requirements. The producer chose to proportion the mixtures to achieve similar mechanical properties while using similar constituent materials because the plant personnel were familiar with the selected VC. The mixtures utilized are shown in Table 3.1, in which results are the average of weights and proportions from all batches placed during this research.

Table 3.1: SCC and VC mixtures used in girders for bridge over Hillabee Creek

Item	BT-54 Girders		BT-72 Girders	
	SCC	VC	SCC	VC
Cement content (pcy)	758	696	760	708
Slag cement content (pcy)	134	124	135	125
Water content (pcy)	266	238	265	234
w/cm	0.30	0.29	0.30	0.28
SSD Coarse aggregate #78 (pcy)	1,528	0	1,550	0
SSD Coarse aggregate #67 (pcy)	0	1,923	0	1,950
Fine aggregate (pcy)	1,384	1,163	1,370	1,179
sand/total aggregate (by volume)	0.48	0.38	0.47	0.38
***Total aggregate volume* (%)**	63	66	63	67
Air-entraining admixture (oz/cwt)	0.3	0.3	0.2	0.2
HRWRA (oz/cwt)	11	8	11	7
VMA (oz/cwt)	2	0	4	0
Hydration-stabilizing ad. (oz/cwt)	2	1	2	1
Measured air content (%)	4.1	4.2	4.0	3.2
Measured unit weight (lb/ft^3)	150.6	153.5	151.1	155.5
Specified transfer f'_{ci} (psi)	5,200	5,200	5,800	5,800
Specified 28-day f'_c (psi)	6,000	6,000	8,000	8,000

The producer chose an already-prequalified VC mixture and then proportioned the SCC mixture to exhibit similar hardened properties. Besides differences in the amounts of chemical admixtures added, SCC contained #78 (½ in.-NMSA) dolomitic limestone, while VC contained #67 (¾ in.-NMSA) dolomitic limestone. Both coarse aggregates came from the same quarry. SCC was also proportioned with a higher *s/agg* (0.47 versus 0.38 in VC) and lower total aggregate volume (63% versus 67% in VC). Specific gravities (SG) of #78 limestone, #67 limestone, and sand were 2.82, 2.87, and 2.66, respectively. SCC and VC both utilized low *w/cm* (ranging from 0.28–0.30).

Notably, while distinctly different minimum compressive strengths were specified for each girder size (28-day f'_c = 6,000 and 8,000 psi for BT-54s and BT-72s, respectively), essentially only one SCC and one VC mixture were utilized. SCC for BT-72s incorporated more VMA (4 oz/cwt versus 2 oz/cwt in the BT-54 mixture) to improve stability, but all other variations between BT-54 and BT-72 VC mixtures are slight and are the result of differences in measured air content during production. This difference in air content was most noticeable in the VC BT-72 batches, in which lower air content led to reduced volumetric yield and higher concrete unit weight.

3.3.2 Production and Testing

BT-54 girders consisted of approximately 17 yd^3 of concrete apiece, and BT-72 girders consisted of approximately 27 yd^3 of concrete apiece. Because concrete was delivered to the prestressing bed in 4 yd^3 batches, many loads of concrete were placed per girder and production day. The

first batch of concrete was always tested prior to initiating placement in the girders, and subsequent batches were infrequently sampled for quality control and quality assurance purposes or at the request of the Auburn University researchers.

Up to two batches were placed at the same approximate time and location along the length of the prestressing bed. SCC and VC placement followed the standard practices for VC placement—filling from one end, with delivery trucks able to move further along the prestressing bed as the formwork was filled. Only one line of girders was produced in a given production day, but two prestressing beds were utilized to allow back-to-back production days. Because of the difference in length, up to three BT-54 girders could be produced on the same bed, while only two BT-72 girders could be produced on the same bed. Configurations of the prestressing beds are shown in Figure 3.9. The researchers documented which end was cast first for each girder (East or West, Inner or Outer), which did not follow a pattern by production day or material due to the use of two prestressing beds.

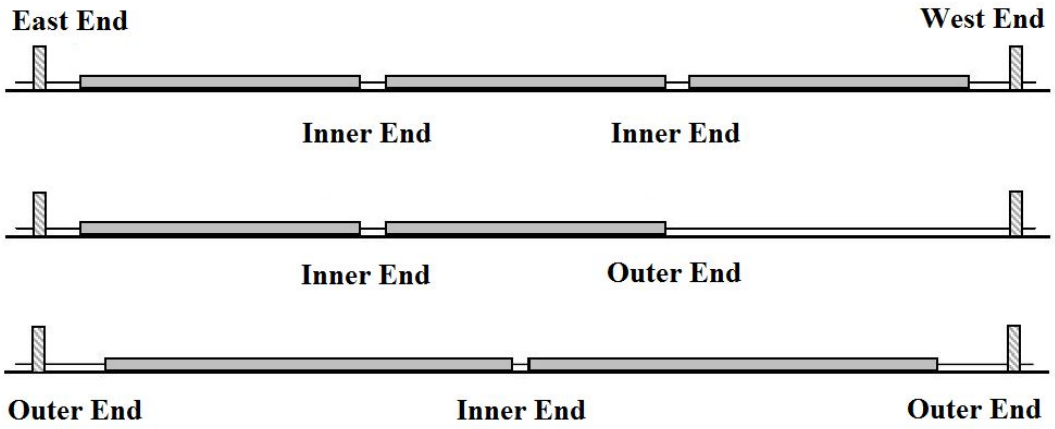

Figure 3.9: Prestressing bed configuration for production of (*top*) three BT-54 girders, (*middle*) two BT-54 girders, and (*bottom*) two BT-72 girders

After all the concrete had been placed, the top surface was roughened and any embedded accessories required for the particular girder were added. The surface was roughened to approximately ¼ in. by running a metal rake with several fingers across the wet concrete as seen in Figure 3.10. Unlike the VC girders, the SCC girders were only able to retain a roughened surface after the top concrete surface had started to set slightly. Consequently, SCC top-surface roughening was delayed. Total production time prior to covering the girders with a steam-curing tarp was approximately the same for SCC placements, as a delay was always necessary to position the tarp after completing concrete placement.

Figure 3.10: Application of transverse, top-surface roughening with a metal rake

Compressive strength cylinders were tested by the precast producer early the next morning after each placement to verify that the concrete had achieved the required f'_{ci}. Productions spanning a weekend were specifically avoided. After the forms were removed, the AUHRC researchers were given access to the girders for pre-release behavioral measurements (baseline camber, prestress transfer, and hardened mechanical properties, all of which are described further during this report). Instrumentation for and measurement of these behaviors caused an approximately one- to two-hour delay between removal of the formwork and detensioning. Placement and detensioning schedules were determined by the precast producer's schedule; the time between placement and detensioning varied from 18–25 hr, with a median time of 23 hours.

The tests conducted on each girder and sample are summarized in Table 3.2. Details concerning the instrumentation required for each test are described in the appropriate section and chapter. As further discussed in Sections 3.3.3 and 3.3.4, certain tests relate only to production groups and *not* unique girders. While up to eight batches were placed in each girder, only a few batches were sampled for material property testing, and their placement was rarely isolated to a known girder location.

Table 3.2: Summary of tests performed on each casting group and girder

Material	Member Size	Batch Tests			Girder Tests		
		Product. Group	f_c	Creep & Shrink.	Girder ID	Transfer Length	Temp. & Strain
SCC	BT-54 (Span 1)	A	28-Day	-	54-2S	Yes	Bot. Flange
					54-5S	-	Full Depth
					54-6S	-	Full Depth
		B	28-Day	Yes[1]	54-1S	-	Bot. Flange
					54-3S	-	Bot. Flange
					54-4S	Yes	Full Depth
		C	1-Year	Yes	54-7S	Yes	Full Depth
	BT-72 (Span 2)	D	28-Day	-	72-1S	-	Bot. Flange
					72-7S	Yes	Full Depth
		E	1-year	Yes	72-3S	-	Bot. Flange
					72-4S	Yes	Full Depth
		F	28-Day	-	72-2S	Yes	Bot. Flange
					72-5S	-	Full Depth
		G	28-Day	-	72-6S	-	Full Depth
VC	BT-54 (Span 4)	A	28-Day	-	54-2V	Yes	Bot. Flange
					54-5V	-	Full Depth
					54-6V	-	Full Depth
		B	1-Year	Yes	54-1V	-	Bot. Flange
					54-3V	-	Bot. Flange
					54-4V	Yes	Full Depth
		C	28-Day	-	54-7V	Yes	Full Depth
	BT-72 (Span 3)	D	28-Day	-	72-1V	-	Bot. Flange
					72-7V	Yes	Full Depth
		E	28-Day	-	72-2V	Yes	Bot. Flange
					72-5V	-	Full Depth
		F	1-Year	Yes	72-3V	-	Bot. Flange
					72-4V	Yes	Full Depth
		G	28-Day	-	72-6V	-	Full Depth

Notes: [1] = match-curing apparatus malfunctioned; N.A. = not applicable; - = not tested

3.3.3 Fresh Property Evaluation

3.3.3.1 Fresh Concrete Stability Test Methods

A total of five fresh concrete stability test methods were used during full-scale production: the VSI, sieve stability, column segregation, rapid penetration, and surface settlement tests. After

evaluating these five tests in a laboratory environment (see Chapter 2), the researchers determined that the VSI and sieve stability test were the best suited tests for use in plant quality-assurance testing, while the surface settlement test was best suited for assessing segregation risk during mixture prequalification testing. Nonetheless, all five tests offered potential advantages, so they were all chosen for further study during this full-scale project. The proposed fresh concrete stability testing protocol described in Section 2.4.5 was also evaluated during the full-scale project.

3.3.3.2 Fresh Testing Procedure

As mentioned previously, the full-scale project was conducted with minimal researcher interference or direct involvement. The research team provided training to the ALDOT inspectors and plant personnel prior to production, but ALDOT personnel were responsible for quality-assurance testing and Hanson plant personnel were responsible for quality-control testing. Batch acceptance was determined based on the results of the testing required in the Special Provision and specifications (slump flow or slump, air content, temperature, and, where applicable, VSI).

Although they did not influence these tests, the Auburn University researchers were present to observe all testing and to conduct their own testing for research purposes. Results obtained by the researchers were not shared with the plant technicians in order to avoid biasing their assessments. While the ALDOT technicians were only required to test the VSI once per 50 yd^3 for quality-assurance purposes, the Auburn University researchers independently conducted the VSI and the sieve stability test at least twice per SCC production day. The rapid penetration test was also conducted at least twice per SCC production day because of its relative speed of testing.

Except during production groups C and G (when one SCC and one VC girder were cast on the same bed), three cycles of these fresh tests were conducted each production day (of both SCC and VC production)—once from the first accepted batch of the day, once at the approximate middle of production for the day, and once near completion of production for the day. During production groups C and G, the first batch was still tested, and the second cycle of testing was conducted on one of the last batches placed for the day. The exact placement location of the second and (where applicable) third batches could not be precisely controlled by the researchers due to the mandate to avoid interfering with the production process. However, general locations can be inferred from the production sequence (see Section 3.3.2).

The column segregation test and surface settlement test, which are more time-consuming and labor-intensive, were conducted once per SCC production day to coincide with the first cycle of testing of the other three SCC stability test methods. All testing by ALDOT technicians, plant personnel, and Auburn University researchers was conducted on a slab on grade outside of the plant's materials testing laboratory located along the path between the mixer

and the prestressing bed. The only exception was that the surface settlement test was conducted inside the laboratory and away from any other testing in order to limit interference that could affect its results. A pair of each of the five stability tests was conducted simultaneously during each testing cycle, and the results obtained from two apparatuses were averaged before analysis.

3.3.4 Hardened Material Property Evaluation

3.3.4.1 Cylinders for Evaluation of Strength and Modulus of Elasticity

Samples of concrete were collected during each production day for strength and elastic modulus testing according to ASTM C39 (2010), C496 (2011), and C469 (2010), as well as for creep and shrinkage testing described in Chapter 5. Sampling was intentionally coordinated to coincide with fresh property testing cycles. The cylinders were produced alongside the prestressing bed and were stored there (and were exposed to some degree of steam-curing like the girders), and they were always taken from the same batches of concrete that had been tested for fresh property evaluation.

Since representative 6 in. by 12 in. cylinders were produced in conjunction with the cycles of fresh testing described in Section 3.3.3.2, at least two sets of cylinders were produced during each production day. The second set of cylinders was always the largest set produced. The number of cylinders produced during each production day varied depending on whether time-dependent deformation testing would be conducted on samples from that production group. The second set of cylinders was chosen for evaluation of hardened properties because the researchers assumed that it would be representative of the majority of concrete placed during a production day.

Batches sampled near the middle of the day's production exhibit the average maturity of all concrete placed, while the first and last few batches could be subject to adjustments to account for changing material and weather conditions. Consequently, the first and (where applicable) third sets of cylinders were only produced to confirm the 28-day f_c of the second set of cylinders; E_c was not tested in these confirmation cylinders, so strengths were only used to capture between-batch variability.

All representative field-cured cylinders were exposed to essentially the same temperature profile as the represented girders. The cylinders were capped immediately after being struck off and, as shown in Figure 3.11, all were then placed in recesses within the girder formwork to be covered by the tarp. In this way, they would receive steam-curing exposure alongside the girders.

Figure 3.11: Storage of representative 6 in. by 12 in. cylinders within girder forms

To further ensure that the cylinders would be exposed to the same ambient conditions as the girders, all cylinders were uncapped and demolded at the same times as when the tarps and formwork were removed from the girders. Some were tested immediately to coincide with the girder detensioning, and all other cylinders were left in a sheltered outdoor location adjacent to the girders for at least two weeks. After being stored at the plant for at least two weeks, the remaining cylinders were transported to the AUHRC laboratory approximately 110 miles southeast of the precast plant. There, they were stored in a sheltered outdoor location with humidity and temperature conditions not dissimilar from at the plant. Cylinders prepared in this way were tested at various ages up to one year after production, which coincided approximately with the addition of the concrete deck to the girders at the bridge.

In addition to these cylinders, cylinders were produced from five production groups for creep and shrinkage testing at the AUHRC laboratory. Upon reaching a concrete age of three years, all cylinders that had been loaded for creep testing or stored for free shrinkage testing were then tested for f_c and E_c according to ASTM C39 and C469. While these cylinders did not experience the same ambient conditions as the girders, valuable conclusions could still be drawn from comparing them—twenty-eight sets of SCC and VC cylinders were exposed to uniform, controlled drying conditions for at least two years, and half of those sets had been loaded to 40% of f_c for that time. Thus, long-term compressive strength and elastic behavior were compared, as were the predictability of E_c and any effects of long-term precompression.

3.4 PRESENTATION AND ANALYSIS OF RESULTS

Results and discussion relevant to the objectives of this chapter are presented in this section. First, girder production observations are summarized. Then, fresh properties are given, and their relationship to laboratory results and the proposed SCC testing protocol (from Chapter 2) are discussed. Finally, strength and E_c data are reviewed.

3.4.1 Production Observations

Each SCC placement required fewer than half as many laborers as each VC placement. All production activities were conducted at least as quickly during SCC placements (see Table 3.4 on page 120 for batching times) until top-surface scratch roughening and covering of the girders for steam-curing. A delay was required before roughening the top surface of the SCC girders to ensure that the concrete would set sufficiently to hold the desired texture. Early efforts to apply transverse roughening had difficulties similar to those documented by Boehm et al. (2010)—the SCC reconsolidated, so roughening had to be reapplied later. Despite the delay, total production times were similar during SCC placement, and production times noticeably decreased (improved) between SCC productions as crews became more familiar with the material.

Some cracking in the girders was observed after the removal of the formwork and prior to prestress transfer. Every girder had two or three evenly distributed cracks that ran from the top surface down into the web. Cracks were widest at the top of the girder; most were approximately 0.02 in. wide, with the largest crack equaling 0.04 inches. There did not seem to be any difference between VC and SCC girders in the cracking pattern or number of cracks. In Figure 3.12, typical cracks have been highlighted with a marker for enhanced visibility.

Figure 3.12: Cracking of girders constructed with (*left*) SCC and (*right*) VC

Cracking was frequently observed immediately after formwork removal, but all cracks closed during prestress transfer. The cracking was likely due to a temperature gradient present after removal of the tarp, which allowed the exposed top flange to rapidly cool. ALDOT production inspectors commented that the occurrence of these cracks was not uncommon to this type of production. This type of cracking has also been documented in long-span prestressed girders by Baran et al. (2003) and Erkmen et al. (2008), who found that it does not noticeably affect service-load performance as long as cracks reclose after prestress transfer. Occurrences of pre-release cracking did not seem to be affected by the concrete type, age at time of transfer, or ambient temperature at the time of transfer (which varied widely over the two-month production schedule).

Also, hold-down points frequently appeared to become hung up in the casting bed during prestress transfer. The hold-down points were flame-cut, but there were times when it was obvious that the girder was trying to lift itself up off of the casting bed and was instead being kept down by the base of the bed. The specific girders that were affected by this were not recorded

because there were times when it was unclear whether or not the hold-down was affecting the girder behavior; occurrences were random and did not appear to be related to the concrete type.

Despite the absence of consolidation efforts during SCC placements, the SCC girders exhibited a much better surface finish than companion VC girders. Examples of the surface finish achieved with each concrete type are shown in Figure 3.13 through Figure 3.16. In those figures, bug holes were both deeper and more prevalent in VC girders, while the primary undesirable surface features in the SCC girders were shallow bleed channels and surface bubbles that occurred in the bottom bulb where bleed water and air bubbles were trapped against the inclined upper surface of the bottom bulb formwork. These undesirable surface features of SCC girders are similar to the appearance described by Ozyildirim (2008).

Figure 3.13: Shallow bleed channels in SCC girder (U.S. quarter for scale)

Figure 3.14: Shallow surface flaws in SCC girder (U.S. quarter for scale)

Figure 3.15: Bugholes in VC girder (U.S. quarter for scale)

Figure 3.16: Surface flaws in VC girder (U.S. quarter for scale)

According to the precast plant's engineering manager, the improved surface finish of the SCC girders was the single largest advantage gained through use of the material. The plant's quality control manager was confident that continued adjustments to the SCC mixture would eventually result in a surface finish that would require no improvement or repair prior to shipment. Aesthetic quality was confirmed by ALDOT, who found that these full-scale SCC girders already met the state's standard specification for surface finish. According to the ALDOT standard specifications for the production of precast, prestressed elements, only surface defects deeper than 0.25 in. covering an area of at least 1.5 ft^2 or deeper than 0.5 in. with a 0.75 in. diameter must be repaired prior to shipment.

The plant engineering manager was also confident that eliminating resurfacing measures would provide a cost savings that would exceed any savings realized from removal of the consolidation efforts currently required for VC construction. He went on to state that the company would prefer to use SCC for all precast, prestressed placements. Again, these observations are similar to those of Ozyildirim (2008)—SCC can be an economically preferable material over VC at least as much for its tendency to produce products of a high aesthetic quality and uniformity as for its improved ease of placement.

3.4.2 Fresh Properties

3.4.2.1 Fresh Concrete Material Tests

Summary results of the fresh concrete tests conducted by the ALDOT quality assurance inspectors during each production day are presented in Table 3.3. The fresh concrete property values shown in the table were used to monitor the acceptability of fresh concrete properties and were not influenced by the AUHRC research team.

Comparing the above results to the specifications and Special Provision (ALDOT 2010a; 2010b) concrete batches were regularly acceptable. Occasionally, the first batch of concrete (both types) was rejected by ALDOT inspectors because its properties fell outside of the acceptable range. SCC batches were generally rejected that exhibited too *low* of a slump flow while VC batches were generally rejected that exhibited too *high* of a slump. After consideration of slump flow results from accepted batches and the resulting high-quality surface finish achieved in the SCC girders, it was suggested by the precast plant's quality-control manager that the specified slump flow of SCC for precast, prestressed girders be decreased in future revisions of the SCC provisions to 26 in. ± 2 in. (from 27 in. ± 2 in.).

Table 3.3: Fresh concrete material properties from ALDOT batch-acceptance testing

Mix ID	Production Date	Time of Test	Fresh Concrete Properties			
			Slump or Flow (in.)	VSI	Total Air (%)	Concrete Temp. (°F)
SCC-A	9/21/10	10:18	28.0	1.5	3.3	85.0
		11:20	25.5	1.0	4.5	87.0
SCC-B	9/28/10	9:20	27.5	1.5	2.6	73.0
		9:48	27.5	1.0	3.0	77.0
SCC-C	10/5/10	10:54	26.0	1.5	5.5	76.0
		11:04	26.0	1.5	4.2	75.0
SCC-D	10/14/10	10:17	27.0	1.5	2.0	78.0
		11:15	26.5	1.5	4.2	83.0
SCC-E	10/19/10	14:30	26.0	1.5	3.3	82.0
		15:07	27.0	1.5	3.7	81.0
SCC-F	10/25/10	10:17	25.5	1.0	4.2	77.0
		11:01	25.0	1.0	3.7	77.0
SCC-G	10/28/10	13:04	28.0	1.0	3.8	83.0
		13:25	28.0	1.0	3.7	83.0
SCC Avg.			*26.7*	*1.29*	*3.7*	*79.7*
VC-A	9/23/10	9:25	9.0		3.9	82.0
		10:35	8.75		4.0	87.0
VC-B	9/29/10	11:25	8.5		4.2	75.0
		12:30	8.75		4.4	88.0
VC-C	10/5/10	9:56	9.0		4.5	69.0
		10:07	8.75		3.9	72.0
VC-D	10/18/10	10:25	8.75	N.A.	4.0	72.0
		11:10	9.0		3.4	77.0
VC-E	10/21/10	10:20	9.0		3.1	73.0
		10:58	9.0		2.5	79.0
VC-F	10/26/10	12:50	8.5		3.6	84.0
		13:35	9.0		3.5	73.0
VC-G	10/28/10	11:20	9.0		2.2	80.0
		11:31	8.25		3.2	81.0
VC Avg.			*8.8*	*N.A.*	*3.6*	*78.0*

Note: N.A. = not applicable

Summary results of the fresh concrete tests conducted by the AUHRC research team during each production day are presented in Table 3.4. In the table, all fresh concrete property

values were obtained by averaging all available data for the given production group. Note that these results were only used for research purposes and were not shared with the producer during production.

Table 3.4: Fresh concrete material properties

Mix ID	Casting Duration (min.)	Average Fresh Concrete Properties				
		Slump or Flow (in.)	T_{50} (s.)	VSI	Total Air (%)	Unit Wt. (lb/ft^3)
SCC-A	98	27.2	N.A.	1.17	4.1	151.1
SCC-B	76	26.7	7.0	1.0	3.4	151.7
SCC-C	50	26.0	7.5	1.5	4.9	148.9
SCC-D	97	24.0	11.3	0.0	4.0	151.2
SCC-E	82	25.0	10.3	0.33	4.1	151.0
SCC-F	79	22.8	10.3	1.0	3.9	151.2
SCC-G	54	27.0	N.A.	1.25	3.8	151.2
SCC Avg.	*77*	*25.5*	*9.3*	*0.9*	*4.0*	*150.9*
VC-A	72	9.3	-	-	4.0	153.7
VC-B	89	8.8	-	-	4.4	153.2
VC-C	33	8.9	-	-	4.2	153.6
VC-D	68	8.8	-	-	3.9	154.1
VC-E	98	9.1	-	-	2.9	155.7
VC-F	94	8.9	-	-	3.4	155.2
VC-G	82	8.6	-	-	2.7	156.9
VC Avg.	*77*	*8.9*	-	-	*3.6*	*154.6*

Notes: N.A. = not available; - = not tested

In addition to these average results, batch-specific properties are presented by Keske (2014). Among the measurements obtained by the AUHRC research team, SCC slump flows ranged from 22.0–28.0 in. and averaged 25.5 inches while VC slumps ranged from 8.5–10 in. and averaged 9.0 inches. These results are different from those presented in Table 3.3 because some of the AUHRC-tested batches overlapped with those tested by ALDOT, but not all. Also, the order of test initiation may have also affected the results. It would be difficult to assess the impact of the difference between ALDOT and AUHRC results, but the results suggest expectable changes in fresh behavior over time (reduced workability but improved SCC fresh stability). Regardless, all testing for research purposes was initiated consistently for comparative purposes.

The doubling of the VMA dosage used during SCC BT-72 production groups (SCC-D–SCC-G) led to an increase in T_{50}. This effect was tributary to the intended purpose of improving stability (which is discussed in the next section). Contrary to the recommendations of Khayat and Mitchell (2009), girders of both sizes exhibited a high-quality surface finish despite being constructed with a highly viscous SCC. Viscosity of SCC mixtures utilized in precast, prestressed girder production should not, therefore, be restricted for constructability purposes.

All mixtures exhibited air contents within the specified limits, and SCC appeared to exhibit comparable variability in air content to that of VC (COV equaled 4.7% versus 4.1% in VC). Overall variability may be misleading though—SCC air content variation appeared to be random, but there was a noticeable trend in the variation in VC air content. All of the VC BT-72 production groups (VC-D–VC-G) exhibited lower air contents, which led to a higher w_c among these mixtures.

All VC batches exhibited higher w_c than SCC batches, averaging 154.6 lb/ft^3 versus 150.9 lb/ft^3 in SCC batches (a 2.5% increase). This systematic difference in w_c is likely due to three VC mixture attributes discussed earlier: 1) lower measured air contents, 2) increased aggregate content (67% versus 63% in SCC), and 3) decreased *s/agg* (0.38 versus 0.47 in SCC) with higher SG of coarse aggregate than that of sand. When comparing SCC and VC values in Table 3.4, even SCC and VC mixtures of the same air content exhibited a systematic difference in w_c.

The w_c of both types of concrete exceeded the observations of Storm et al. (2013) and Al-Omaishi et al. (2009), and they were very similar to the SCC and VC unit weights observed by Trejo et al. (2008) (150 and 153 lb/ft^3 for SCC and VC, respectively). SCC w_c was consistently closer to the value recommended by Trejo et al. (2008) of w_c = 150 lb/ft^3, although this comparison is limited. Regardless, the difference between predicted and measured w_c could have an influence on structural properties (elastic modulus, self-weight, etc.).

Care should be exercised when choosing the w_c to use in predictive and design equations for precast, prestressed applications. Determination of w_c based on the utilized proportions and materials may be useful in lieu of a larger analysis of this tendency in concretes typical of a particular region or application. Measured w_c was, on average, greater than that calculable from the proportions listed in Table 3.1 because the as-produced concrete regularly exhibited less than the target air content (4.5%). Still, calculated w_c equaled 150.7 and 154.2 lb/ft^3 in SCC and VC, respectively, based on the target air content and previously listed constituent specific gravities and proportions. Since any variation in measured w_c due to air content would not be consistently predictable, the previously recommended 150 lb/ft^3 should be sufficient for mixtures utilizing similar aggregates and proportions to those presented in Table 3.1.

3.4.2.2 Fresh Self-Consolidating Concrete Stability Tests

Summary results of the five fresh SCC stability tests conducted on each SCC production group are presented in Table 3.5. In the table, VSI, sieved fraction, and rapid penetration results were obtained by averaging the results from at least two batches of SCC; column segregation and surface settlement results, which require more time and labor to obtain, were obtained during the first cycle of testing of the other three stability test methods. All results shown are those obtained while utilizing standard test procedures; the use of alternative rest periods was assessed in Chapter 2, but only as a result of the full-scale project testing described here and discussed further in Section 3.3.3. Furthermore, pairs of each fresh test were conducted simultaneously, except that the VSI test was always conducted twice consecutively. For consistency, it was deemed best to have a single operator conduct both repetitions of the VSI test.

Table 3.5: Production day-specific fresh concrete stability test results

Mix ID	Avg. Results from Multiple Batches			Results from First Batch		
	VSI	Rapid Pen. (in.)	Sieved Fraction (%)	Seg. Index (%)	Rate of Set. (%/hr)	Maximum Set. (%)
SCC-A	1.2	0.43	5.3	6.0	0.25	0.22
SCC-B	1.0	0.26	7.5	7.9	0.27	0.37
SCC-C	1.5	0.18	5.5	7.0	0.10	0.16
SCC-D	0.0	0.22	0.2	3.0	0.13	0.11
SCC-E	0.3	0.13	1.6	3.9	0.10	0.16
SCC-F	1.0	0.17	0.3	1.3	0.13	0.12
SCC-G	1.3	0.28	4.6	5.9	0.07	0.18

In Table 3.5, visual stability index values other than the discrete values discussed previously (0, 0.5, 1, 1.5, 2, or 3) indicate instances in which the multiple tests and batches yielded different results. As with all fresh tests, identical test results were not guaranteed for test pairs or between batches of concrete. Batch-specific results from the VSI, rapid penetration, and sieve stability tests are shown in Table 3.6. In it, slump flows are also given for reference (recall that VSI and slump flow results presented here were used only for research comparisons, not to determine batch acceptance).

Table 3.6: Batch-specific fresh concrete stability test results

Mix ID	Batch #	Slump Flow (in.)	VSI	Rapid Pen. (in.)	Sieved Fraction (%)
SCC-A	1	28.0	1.5	0.43	7.8
	2	27.5	1.0	0.51	4.9
	3	26.0	1.0	0.35	3.2
SCC-B	1	27.0	1.0	0.31	10.4
	2	26.0	1.0	0.31	8.0
	3	27.0	1.0	0.16	4.2
SCC-C	1	26.0	1.5	0.20	6.0
	2	26.0	1.5	0.20	4.9
SCC-D	1	25.0	0.0	0.16	0.0
	2	23.0	0.0	0.12	0.5
	3	24.0	0.0	0.20	0.0
SCC-E	1	26.0	1.0	0.35	3.0
	2	26.0	0.0	0.20	1.1
	3	23.0	0.0	0.08	0.7
SCC-F	1	22.5	1.0	0.12	0.2
	2	24.0	1.0	0.12	0.4
	3	22.0	1.0	0.12	0.4
SCC-G	1	26.0	1.0	0.28	1.6
	2	28.0	1.5	0.28	7.5

From Table 3.6, SCC used to produce BT-72 girders (SCC-D–SCC-G) yielded fresh concrete stability test results that would indicate somewhat improved stability. Previously, Khayat (1999) concluded that increased SCC stability may be attributed to the use of larger dosages of VMA. The plant's quality-control manager commented that stability was improving because the plant personnel gained experience concerning SCC use during the duration of this project. By the end of production in late October, they were more aware of the batching sensitivity and chemical admixture use necessary to achieve flowable and stable SCC.

Among the fresh concrete stability tests in which multiple batches were tested (VSI, rapid penetration, and sieve stability tests), results were frequently classified as satisfactory or borderline according to the protocol recommended in Chapter 2 (VSI ≤ 1.0 or sieved fraction ≤ 7.5%). The results shown in Table 3.5 and Table 3.6 suggest that SCC stability generally improved during the duration of this project, but the inconsistency of this trend (see SCC-G)

confirms that the same levels of quality assurance and quality control currently employed for VC placements should be maintained during the utilization of SCC.

Fresh concrete stability test results were compared to each other on a batch-specific basis for all SCC produced at the plant. Comparisons yielded correlation values similar to those discussed in Chapter 2:

- Strong correlations were observed between the sieve stability test and both the VSI and column segregation tests (R^2 = 0.41 and 0.70, respectively),
- A strong correlation was observed between the rate of settlement and maximum settlement when using the surface settlement test (R^2 = 0.53), although improvement through the use of a nonlinear model was unclear, and
- The rapid penetration test did not correlate well with the other fresh concrete stability tests.

Fresh test results from the full-scale project are illustrated in Figure 3.17 through Figure 3.19 alongside results from AUHRC laboratory mixtures of similar coarse aggregate NMSA and aggregate volume. As a reminder, the laboratory-assessed results in those figures varied more widely because stability was intentionally varied during the laboratory phase.

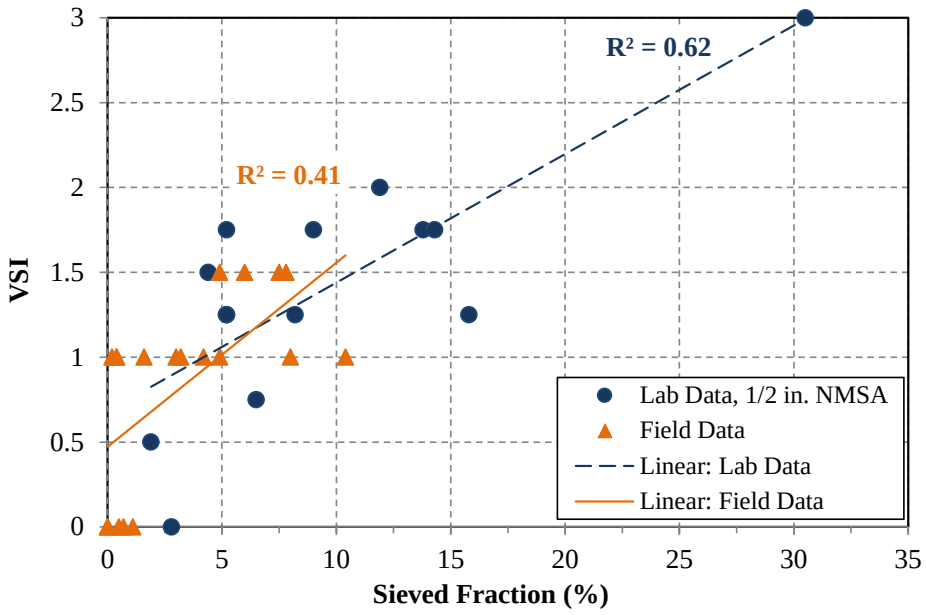

Figure 3.17: Comparison between sieved fraction and VSI results (field data and comparable laboratory data from Chapter 2)

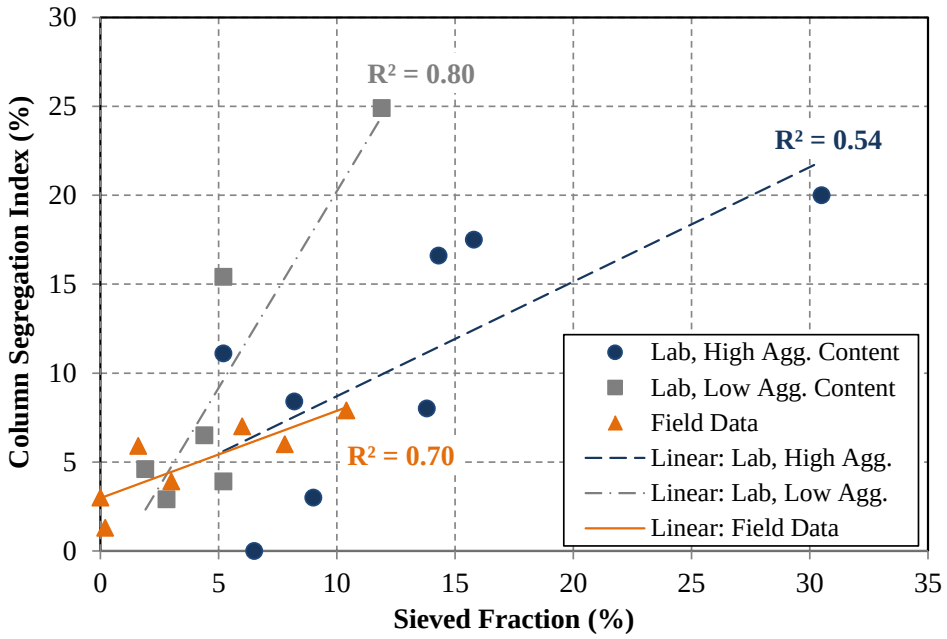

Figure 3.18: Comparison between sieved fraction and column segregation index results (field data and comparable laboratory data from Chapter 2)

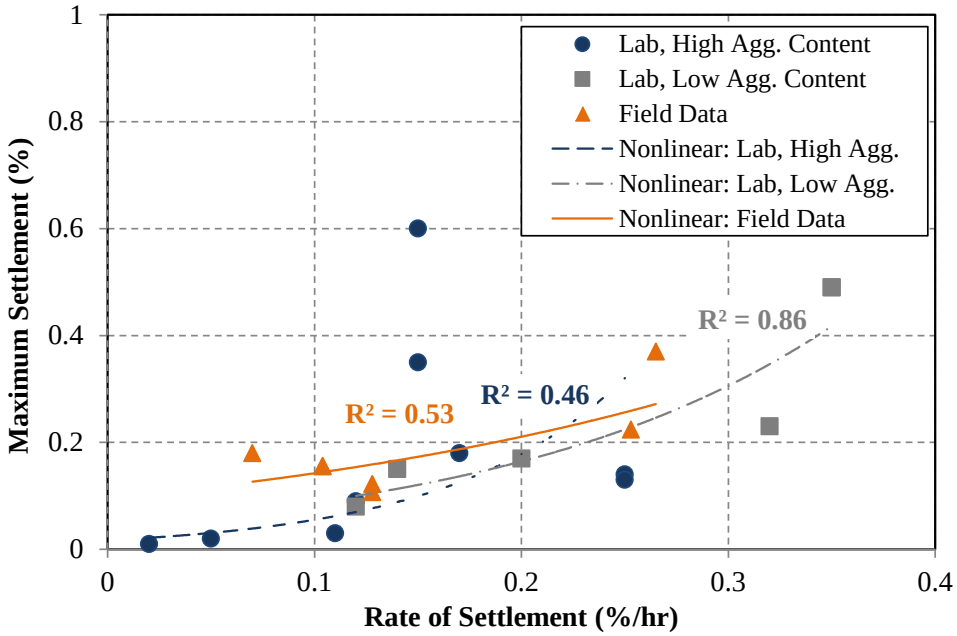

Figure 3.19: Comparison between rate of settlement and maximum settlement results (field data and comparable laboratory data from Chapter 2)

In these figures, the laboratory- and field-assessed relationships between sieved fraction and VSI and between rate of settlement and maximum surface settlement are very similar. The field-assessed relationship between the sieved fraction and column segregation index is distinctly similar to the "high aggregate content" AUHRC laboratory data. The high-aggregate-content

laboratory mixtures in that figure included total aggregate fractions greater than 65%, while the field mixture was proportioned for 63% total aggregate. In light of this, the exact point at which to distinguish between high- and low-aggregate-content mixtures is unclear. As discussed in Section 2.5.2.1, the exact nature of the relationship between the column segregation index and sieved fraction is not as important as the fact that they are related in all cases.

3.4.3 Strength and Modulus of Elasticity

Summary results of the strength and modulus of elasticity testing conducted on field-cured specimens are presented in Table 3.7. In the table, all results were obtained from the second batch of concrete tested in each production group, when results were expected to be representative of the majority of concrete in the girders. Also, “age at transfer” for each production group is the average age of the girder concrete at detensioning. While this age approximately matches that of the cylinders whose properties are shown in Table 3.7, it should be noted that total production times varied widely (see Table 3.4). Therefore, the difference in ages between the first concrete and last concrete produced vary by as much as 1.6 hours.

Table 3.7: Strength and modulus of elasticity of field-cured cylinders

Mix ID	Transfer Age (hr)	Compressive Strength (psi)		Splitting Tensile Strength (psi)		Modulus of Elasticity (ksi)	
		Transfer f_{ci}	28-Day f_c	Transfer f_{ct}	28-Day f_{ct}	Transfer E_{ci}	28-Day E_c
SCC-A	**24**	9,010	10,240	510	710	6,200	6,350
SCC-B	**24**	8,680	10,800	690	900	6,350	6,600
SCC-C	**23**	7,940	10,180	580	690	6,050	6,150
SCC-D	**23**	8,120	10,490	640	760	5,750	6,300
SCC-E	**20**	7,860	10,770	670	790	5,850	6,350
SCC-F	**23**	8,220	10,550	650	820	5,850	6,350
SCC-G	**18**	6,930	10,070	610	720	5,650	6,000
SCC Avg.	***22***	*8,110*	*10,440*	*620*	*770*	*5,950*	*6,300*
VC-A	**25**	8,790	10,590	590	800	7,100	7,350
VC-B	**23**	7,860	9,670	690	740	6,650	6,850
VC-C	**24**	8,760	10,360	650	860	6,450	6,850
VC-D	**23**	8,290	10,770	580	830	6,700	7,000
VC-E	**23**	8,770	10,850	660	690	7,050	7,300
VC-F	**20**	8,320	11,050	650	880	6,800	7,650
VC-G	**20**	7,710	10,510	640	840	6,550	6,850
VC Avg.	***22.5***	*8,360*	*10,540*	*640*	*810*	*6,750*	*7,100*

Noted in Table 3.2, concrete from four production groups (SCC-C, SCC-E, VC-B, and VC-F) was also tested at one year; these results are presented by Keske (2014). Property evolution was as expected: compressive and splitting tensile strengths increased by approximately 10% in these four batches, while modulus of elasticity had limited to negligible growth. Compressive strengths (28-day only) were also evaluated in batches from the beginning and approximate end of each production day to capture between-batch variability. Those results are also presented by Keske (2014). Despite the potential for differences resulting from concrete age (average length of each production was 77 min.), no consistent pattern was visible in f_c of the first, second, and (where applicable) third batches of concrete. Ranges of 28-day f_c between batches produced on the same day were up to 860 psi (averaging 2.6% COV) in SCC and 1,170 psi (averaging 4.1% COV) in VC. This agrees with the conclusion of Khayat et al. (2007) and Zhu et al. (2001) that SCC compressive strength is at least as uniform as that of vibrated concrete in large-scale production.

In addition to the field-cured specimens evaluated above, the cylinders used to study long-term time-dependent deformability were tested for f_c and E_c at a concrete age of approximately three years. Those results are presented in Table 3.8, divided by the time at which each set was loaded (to coincide with transfer, at a consistent age of twenty-six hours, and at the time of deck addition). In the table, all results were obtained from the second batch of concrete tested from each production group (like those presented in Table 3.7). Prior to strength testing, cylinders subjected to sustained compressive loading were unloaded and monitored for unloading deformation tendencies (instantaneous and gradual length increase following removal of the sustained load) for three weeks. They are labeled "L" for loaded in the table. Cylinders that were never loaded prior to destructive testing for this evaluation are labeled "U" for unloaded. The loaded and unloaded cylinders were tested on the same day, three weeks after removing the load from the loaded cylinders.

Table 3.8: Compressive strength and modulus of elasticity of cylinders subjected to controlled drying shrinkage or sustained compressive loading

Mix ID	Time of Load	3-Year f_c (psi)		Ratio (L/U)	3-Year E_c (ksi)		Ratio (L/U)
		U	L		U	L	
SCC-B	**Transf.**	11,890	12,010	1.01	6,350	6,850	1.08
	26 hr	11,620	11,610	1.00	6,300	6,650	1.06
SCC-C	**Transf.**	10,870	10,590	0.97	6,000	6,100	1.02
	26 hr	10,470	10,540	1.01	6,150	6,400	1.04
	1 yr	10,930	11,490	1.05	6,050	6,300	1.04
SCC-E	**Transf.**	10,540	10,940	1.04	6,150	6,400	1.04
	26 hr	11,160	11,070	0.99	6,100	6,350	1.04
	1 yr	11,310	11,490	1.02	6,250	6,300	1.01
SCC Avg.	***All***	*11,100*	*11,220*	*1.01*	*6,150*	*6,400*	*1.04*
VC-B	**Transf.**	10,090	10,090	1.00	6,450	6,600	1.02
	26 hr	10,450	10,340	0.99	6,550	6,700	1.02
	1 yr	10,290	10,420	1.01	6,250	6,550	1.05
VC-F	**Transf.**	11,620	11,390	0.98	6,500	7,050	1.08
	26 hr	11,640	11,650	1.00	6,260	6,850	1.09
	1 yr	11,960	11,900	0.99	6,850	6,950	1.01
VC Avg.	***All***	*11,010*	*10,970*	*1.00*	*6,500*	*6,800*	*1.05*

Notes: U = Unloaded; L = Loaded in sustained compression for at least two years

3.4.3.1 Compressive Strength Comparisons

From Table 3.7, the SCC and VC utilized in this bridge appeared to exhibit very similar compressive strengths. For reference, ASTM C39 (2010) states that the average compressive strength of concrete from the *same batch* is expected to range up to 14% of the average in multi-laboratory testing, and ASTM C94-11a states that the range between batches of ready-mixed concrete shall not exceed 7.5%. Thus, differences (SCC compressive strengths were 0–6% less than those of VC) were insignificant.

Practically identical compressive strengths were achieved in the SCC and VC despite a distinct difference in *s/agg* between the two (SCC was proportioned with 20% more sand than was the VC). This reinforces the conclusions of Khayat and Mitchell (2009), Mehta and Monteiro (2006), and Schindler et al. (2007): *s/agg* does not appear to affect f_c when similar coarse and fine aggregate are used. Similarly, the differences were insignificant despite slight differences in *w/cm* (SCC *w/cm* averaged 0.30 while VC *w/cm* averaged 0.29), coarse aggregate NMSA (NMSA equaled ½ in. in SCC versus ¾ in. in VC), and total aggregate content (SCC aggregate content equaled 63% of total volume while that of the VC equaled 67%).

In both materials, prestress-transfer f_{ci} was strongly correlated to concrete age at the time of transfer. This correlation is illustrated in Figure 3.20. In it, SCC and VC f_{ci} are indistinguishable once accounting for concrete age. Analysis of the materials' linear correlations revealed that, at a 95% CI, the relationships between f_{ci} and concrete age were not significantly different (P-value equaled 0.4248). This indicates that SCC and VC f_{ci} would be indistinguishably different if all had been tested at the same age.

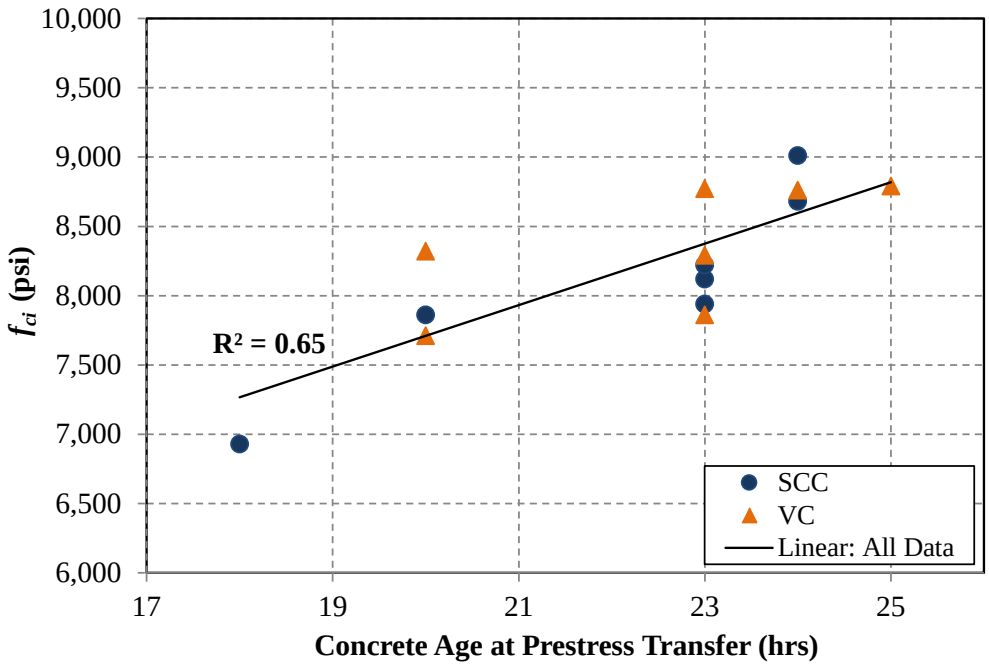

Figure 3.20: Prestress-transfer compressive strength versus concrete age at transfer

From Table 3.8, all loaded and unloaded SCC and VC cylinders appeared to exhibit practically similar compressive strengths at an age of three years. Differences (SCC compressive strengths were up to 2% higher than those of the VC) were insignificant and reversed the behavior observed at earlier ages (SCC compressive strength had been 0–6% less than that of the VC at earlier ages). Considering the dependence of f_{ci} on the age at release, these results further suggest that the SCC and VC used in the Hillabee Creek Bridge exhibit virtually identical early-age and long-term f_c.

Also from Table 3.8, sustained precompression appeared to have no effect on f_c, regardless of the age at which the sustained compressive loading was applied. This matches the conclusions of Buettner and Hollrah (1968) and Garner and Tsuruta (2004): long-term, elastic-level sustained compression does not noticeably affect ultimate f_c.

Minimum compressive strength is frequently the only hardened mechanical property specified during the project design phase, and this was the case in this project. In Table 3.9, the specified minimums are compared to measured compressive strengths. Groups are divided by girder size within the table because different compressive strengths were specified in these groups.

Table 3.9: Difference between measured and specified compressive strength

Property	Compressive Strength			
	SCC BT-54	VC BT-54	SCC BT-72	VC BT-72
Meas. Transfer (psi)	8,540	8,470	7,780	8,270
Spec. Transfer (psi)	5,200	5,200	6,000	6,000
Meas./Design Transfer	*1.64*	*1.63*	*1.30*	*1.38*
Meas. 28-Day (psi)	10,410	10,210	10,470	10,800
Spec. 28-Day (psi)	6,000	6,000	8,000	8,000
Meas./Spec. 28-Day	*1.73*	*1.70*	*1.31*	*1.35*

The difference between measured compressive strength and specified compressive strength was much greater than the difference between SCC and VC. Both materials exhibited compressive strengths 30–64% greater than specified for release f'_{ci} and 31–73% greater than specified for 28-day f'_c. Because the same mixture was utilized in both girder sizes, all BT-54 f_c values exceeded specified values by a larger margin than did BT-72 f_c values. In general, this occurrence mirrors the observation of Storm et al. (2013) that as-produced concrete for precast, prestressed applications can exhibit f_c well in excess of specified f'_c values.

3.4.3.2 Splitting Tensile Strength Comparisons

From Table 3.7, the SCC and VC utilized in this bridge appeared to exhibit very similar f_{ct}. Differences (SCC splitting tensile strengths were 3–5% less than those of the VC) were minor, despite differences in proportions as previously discussed. Any difference not explained by testing variability could be explained by these mixture proportioning differences. It is concluded that the two concretes, which exhibited similar compressive strengths, also exhibit similar splitting tensile strengths. Unlike compressive strength, prestress-transfer f_{ct} did not correlate to concrete age at the time of testing.

The predictability of f_{ct} when calculated using Equations 3-1 and 3-2 was also evaluated. Results from that evaluation are summarized in Figure 3.21 and Figure 3.22, and supplemental information is given by Keske (2014). In the figures, prestress-transfer and 28-day properties are plotted versus the values predicted according to the respective expressions. Values nearer to the line of equality indicate better predictability. Bars indicating ± 10% error are also included considering the expected variability of compressive strength (7.5% of average f_c); between-batch variability of f_{ct} is not reported in ASTM C496 (2004).

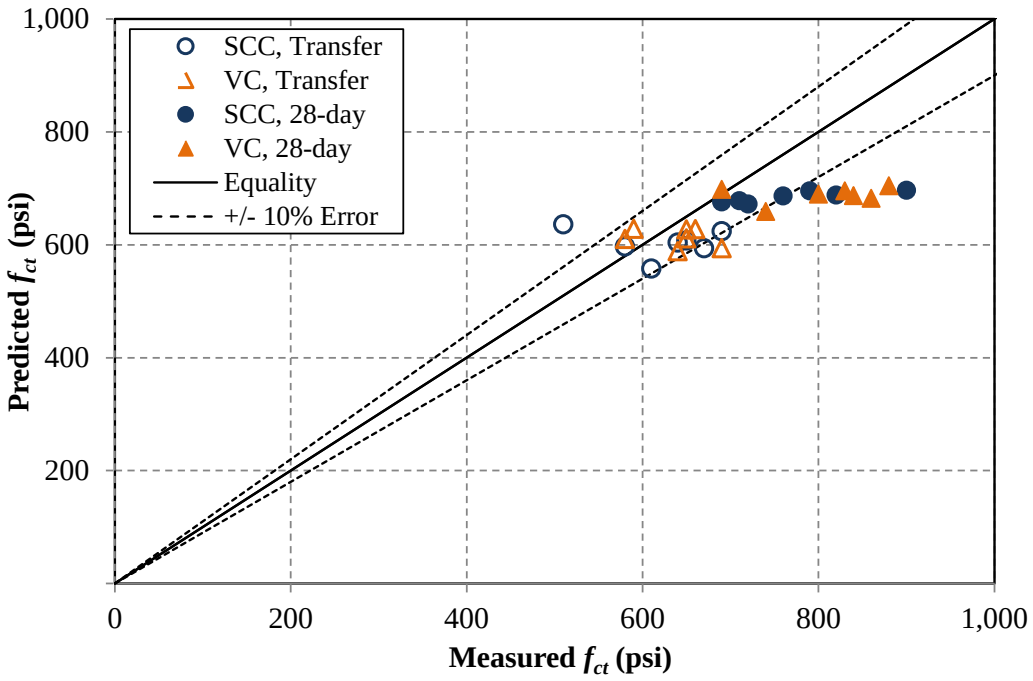

Figure 3.21: Measured f_{ct} versus f_{ct} predicted by Equation 3-1

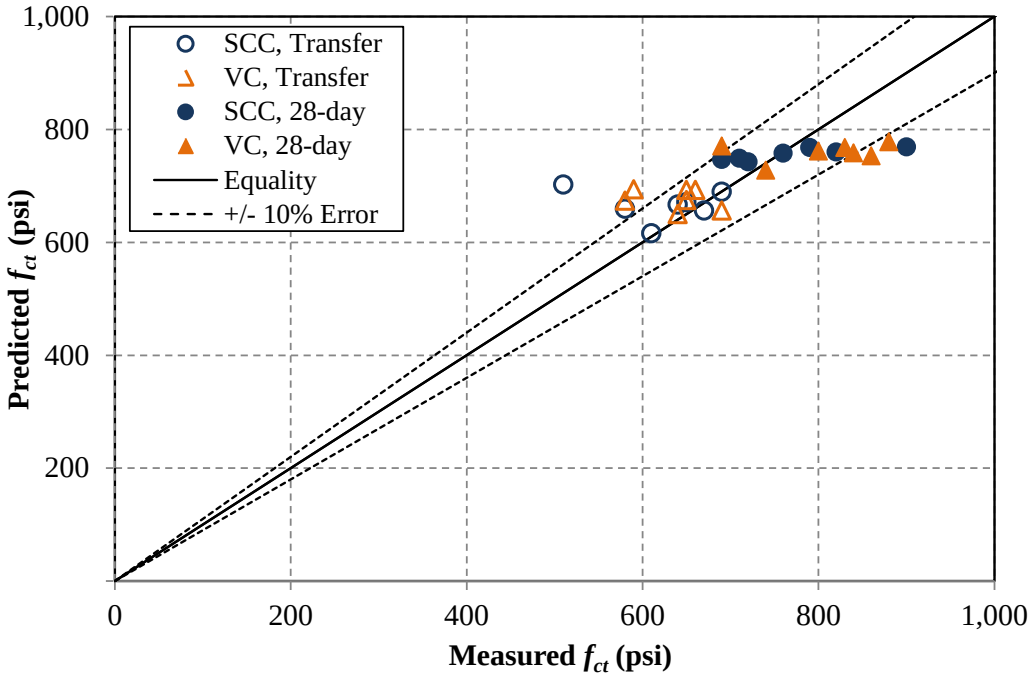

Figure 3.22: Measured f_{ct} versus f_{ct} predicted by Equation 3-2

Several conclusions are drawn from these figures, at least with respect to these two mixtures prepared using Alabama crushed dolomitic limestone and the proportions listed in Section 3.3.1:

- Overall, both equations provided conservative estimates of f_{ct}, but Equation 3-2 was more accurate to predict average f_{ct},
- Predictions of SCC and VC prestress-transfer f_{ct} were less conservative than those of 28-day f_{ct}, and
- SCC f_{ct} is at least as predictable as that of VC when calculated using measured $\sqrt{f_c}$.

To compare to the f_{ct} values that an engineer would have available at the time of design, f_{ct} values were compared in a similar fashion as done in Table 3.9 for compressive strength. Results are compared with f_{ct} calculated according to the ACI 318 (2011) equation for normal-weight concrete (Equation 3-1) in conjunction with the design f'_c for this project. Those values and ratios of measured to design values are shown in in Table 3.10. In the table, groups are divided by girder size because different compressive strengths were specified for the different sizes.

Table 3.10: Difference between measured and design splitting tensile strength

Property	Splitting Tensile Strength			
	SCC BT-54	**VC BT-54**	**SCC BT-72**	**VC BT-72**
Measured Transfer (psi)	590	640	640	630
Design Transfer (psi)	540	540	580	580
Meas./Design Transfer	*1.10*	*1.19*	*1.11*	*1.09*
Measured 28-Day (psi)	770	800	770	810
Design 28-Day (psi)	580	580	670	670
Meas./Design 28-Day	*1.32*	*1.38*	*1.15*	*1.21*

The difference between *measured* and *design* f_{ct} was larger than the difference between SCC and VC measured results. Both materials exhibited f_{ct} exceeding the specified limit set forth by ACI 318, but the percentage by which they exceeded the design f_{ct} was less than the amount by which f_c exceeded the specified minimums. This is due to the relationship between f_c and f_{ct}, in which f_{ct} is only expected to increase at the square root of the rate at which f_c increases. Still, existing predictions for f_{ct} appear to be acceptable considering these results.

3.4.3.3 Modulus of Elasticity Comparisons

From Table 3.7, the SCC cylinders routinely exhibited E_c approximately 10–15% less than of equivalent-strength VC cylinders. Considering that the between-batch variability of E_c in the *same material* is expected to be up to 4.25%, the difference in E_c is minor. It is also in line with the literature reviewed in Section 3.2.2.2; the difference is expected between any two concretes that differ in *s/agg*, total aggregate content, or coarse aggregate NMSA, so it should be expected when proportioning SCC with higher *s/agg*, lower total aggregate content, *and* smaller coarse aggregate NMSA than an equivalent-strength VC mixture.

The predictability of the modulus of elasticity when calculated using Equations 3-3 through 3-5 was also evaluated. Results from that evaluation are summarized in Figure 3.23 through Figure 3.25, and supplemental information is given by Keske (2014). In the figures, prestress-transfer and 28-day properties are plotted versus the values predicted according to the respective expressions. Values nearer to the line of equality indicate better predictability. Bars indicating ± 10% error are also included considering the expected variability of compressive strength (7.5% of average f_c), which would impact the predictability of E_c.

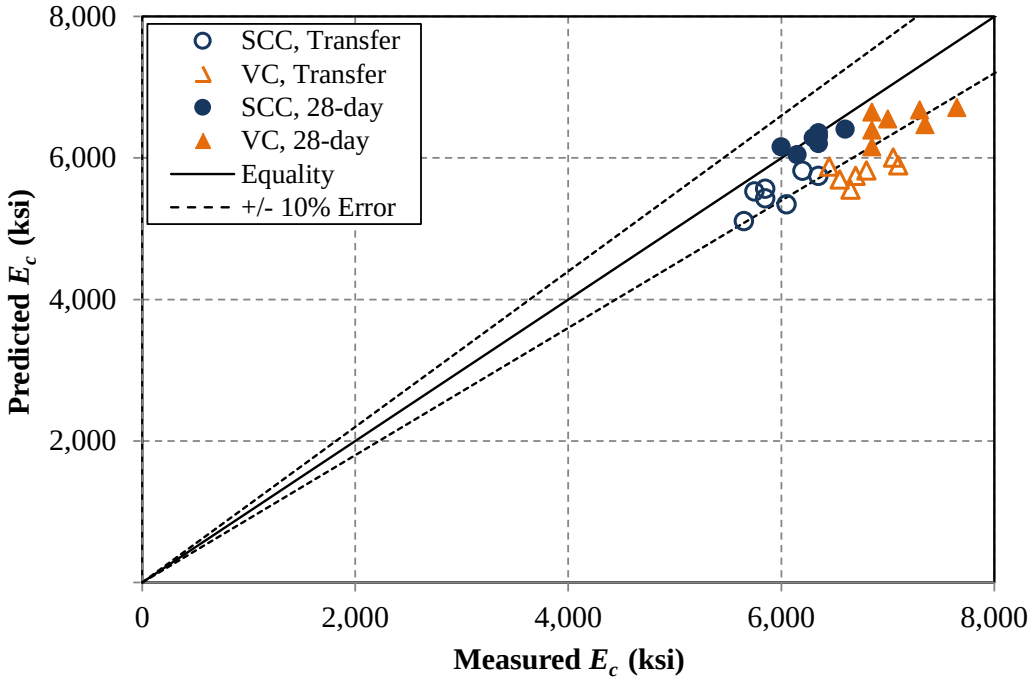

Figure 3.23: Measured E_c versus E_c predicted by Equation 3-3

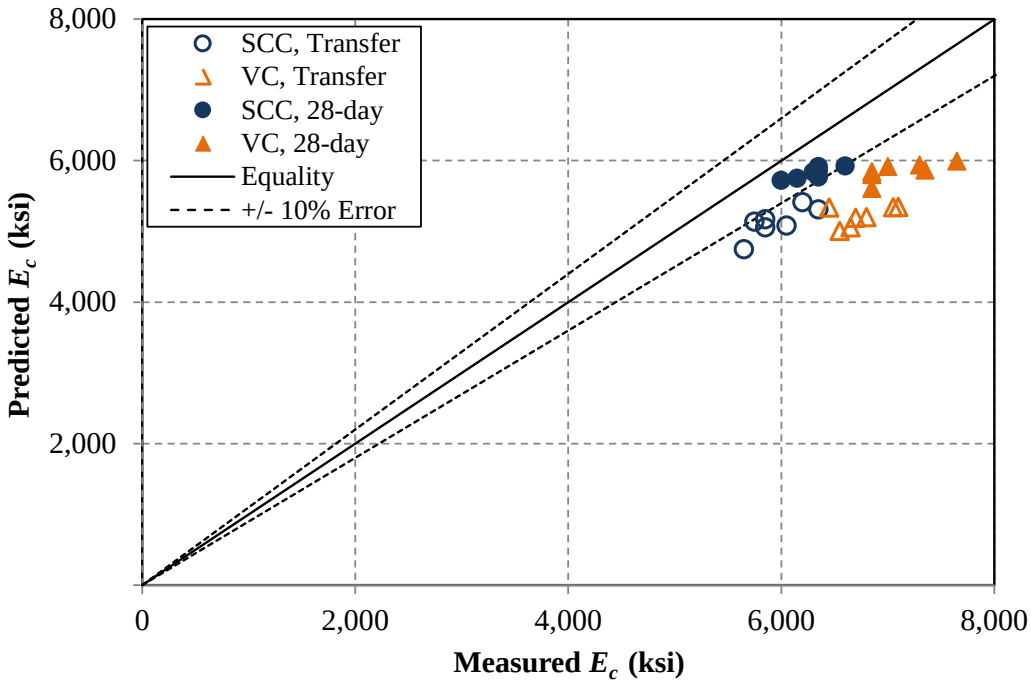

Figure 3.24: Measured E_c versus E_c predicted by Equation 3-4

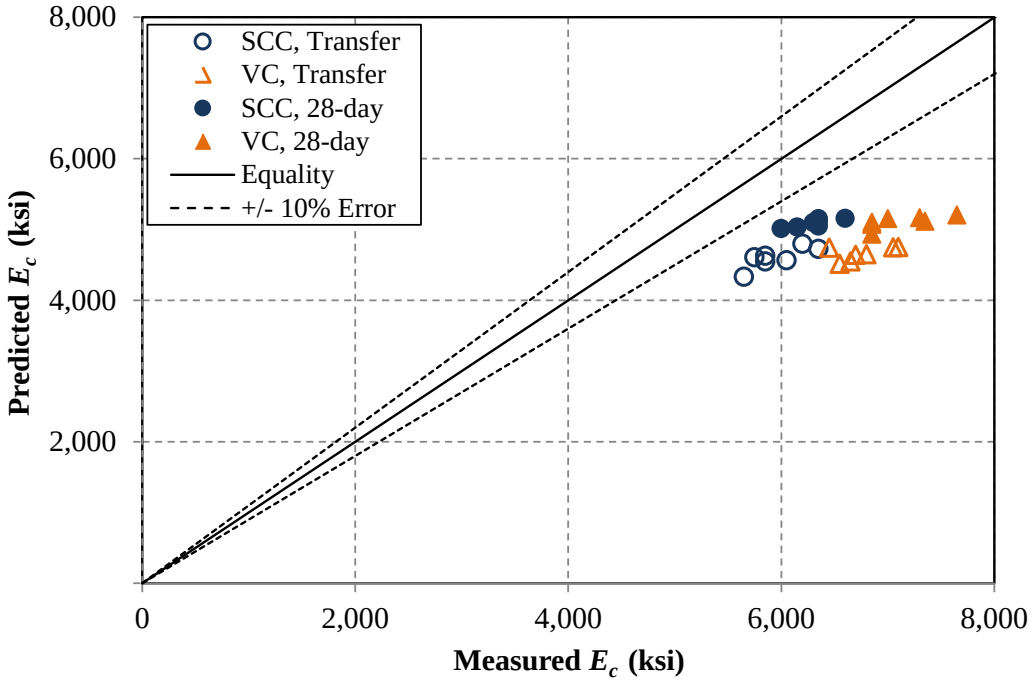

Figure 3.25: Measured E_c versus E_c predicted by Equation 3-5

Several observations and conclusions are drawn from these figures, at least with respect to these two concretes prepared using Alabama crushed dolomitic limestone and the mixture proportions listed in Section 3.3.1:

- Equation 3-3, which incorporates w_c and f_c, more accurately predicts E_c than either Equation 3-4 (a simplification of Equation 3-3 using w_c = 145 lb/ft^3) or Equation 3-5 (ACI 363 equation for concrete with f'_c greater than 6,000 psi),
- Equation 3-3 was more accurate than the model specifically developed for high-strength concrete (Equation 3-5) despite being applied to concretes with f_c of up to approximately 11,000 psi and w_c of up to approximately 154.5 lb/ft^3,
- SCC and VC both consistently exhibit E_c values greater than predicted when using measured properties, and
- SCC E_c is at least as predictable as that of VC when using measured properties.

In addition to the comparison of batches from all production groups at ages up to twenty-eight days, the four mixtures evaluated through an age of one year exhibited similar trends—SCC E_c was essentially equal to predicted using Equation 3-3 (measured divided by predicted equaled 0.99), and VC E_c approached the value predicted using Equation 3-3 (ratio of 1.03). These results are presented by Keske (2014). At all ages, Equation 3-3 was most accurate at predicting E_c when using measured properties.

K_1 values were determined to refine Equation 3-3 (as allowed by AASHTO 2013). SCC K_1 values equaled 1.08 and 1.01 at transfer and twenty-eight days, respectively; VC K_1 values equaled 1.17 and 1.09 at transfer and twenty-eight days, respectively. SCC K_1 values were similar to those suggested by Trejo et al. (2005) for SCC used in precast, prestressed applications, and all values exceeded the value (0.85) recommended by Storm et al. (2013).

From Table 3.8, the difference between SCC and VC E_c discussed above appeared to be less pronounced in the cylinders exposed to controlled drying or sustained compressive loading. SCC cylinders exhibited E_c approximately 6% less than of VC cylinders at three years, compared to being 10–15% less at earlier ages. SCC 3-year values appear to be in line with 28-day and 1-year values, but VC values were reduced by approximately 7% from 28-day and 1-year results. Three-year VC results suggest a more gradual or plateauing elastic modulus evolution similar to that of the SCC cylinders. Because many more cylinders were tested at three years (sixteen sets of SCC cylinders and twelve of VC cylinders) than at one year (two sets each of SCC and of VC), these results suggest that the SCC and VC used in the Hillabee Creek Bridge girders exhibit very similar long-term E_c, with expectable and insignificant reductions in SCC E_c due to mixture proportioning.

Sustained precompression appeared to have a minor but consistent effect on E_c in both materials—fourteen sets of cylinders that were precompressed for an extended time (at least two

years) consistently exhibited approximately 5% greater E_c than fourteen sets of cylinders that were never previously loaded. These results suggest that sustained precompression experienced by the actual girders would only provide improvements in long-term E_c.

Using only Equation 3-4 with the design minimum compressive strengths specified for this project (conservative assumption of the process used during design), E_c design values were calculated and compared to measured values in Table 3.11. In the table, groups are divided by girder size because different compressive strengths were specified for the different sizes.

Table 3.11: Difference between measured and design modulus of elasticity

Property	Modulus of Elasticity			
	SCC BT-54	**VC BT-54**	**SCC BT-72**	**VC BT-72**
Measured E_{ci} (ksi)	6,200	6,750	5,800	6,800
Design E_{ci} (ksi)	4,100	4,100	4,400	4,400
Meas./Design Transfer	*1.51*	*1.64*	*1.31*	*1.53*
Measured E_c (ksi)	6,350	7,000	6,250	7,200
Design E_c (ksi)	4,400	4,400	5,100	5,100
Meas./Design 28-Day	*1.44*	*1.59*	*1.23*	*1.41*

The difference between *measured* and *design* modulus of elasticity was much larger than the difference between SCC and VC, especially considering the long-term E_c results discussed in the previous subsection. The difference between measured and design values was marginally improved by use of Equation 3-3 with w_c equal to 150 lb/ft^3 (as recommended for precast, prestressed concrete)—measured values equaled 1.15–1.54 of design values derived in this way.

Because the same mixture was utilized in both girder sizes, all BT-54 elastic modulus values exceeded design values by a larger margin than BT-72 values. In light of these results, consideration of the actual E_c expected during production is strongly recommended for use during design and prediction of precast, prestressed girder behavior (especially camber and prestress losses, which are discussed in Chapters 6 and 7).

3.5 SUMMARY AND CONCLUSIONS

3.5.1 Summary

The final phase of the investigation was to produce Alabama's first bridge with precast, prestressed SCC girders. This full-scale implementation of SCC precast, prestressed girders consisted of seven 97 ft-10 in. AASHTO-PCI BT-54 bulb-tees and seven 134 ft-2 in. BT-72 bulb-

tees to be placed in a rural highway bridge over Hillabee Creek in Alexander City, Alabama. An equal number of companion girders were constructed with VC in order to allow for a direct comparison of the construction operations and hardened properties associated with each type of concrete. Production required fourteen production groups—seven each for SCC and VC girders. Production was completed with minimal researcher involvement; the only interference was an approximately one- to two-hour delay prior to detensioning required to complete work involving the assessment of pre-release material and structural behavior.

Fresh concrete samples were sampled at least twice in each production group to evaluate fresh properties (air content, slump or slump flow, etc.) and hardened mechanical properties including strength and modulus of elasticity. Additional cylindrical specimens were produced from several production groups to evaluate time-dependent material properties. Observations from the production and results from the fresh and hardened mechanical testing were then made. The observations and conclusions made during the collection and analysis of these results are summarized in Section 3.5.2. The recommendations made based on this research are given in Section 3.5.3.

3.5.2 Observations and Conclusions

3.5.2.1 Production of Precast, Prestressed Girders

- Each SCC placement required fewer than half as many laborers as each VC placement. Batching and placement of SCC took approximately as much time as that of VC.
- A longer delay was required before texturing the top surface of the SCC girders to ensure that the concrete would set sufficiently to hold the desired texture. This did not seem to affect construction times because a delay was already incorporated between concrete placement and tarp covering of the girders.
- Batching and placement time varied widely: SCC and VC placements varied from 68–98 min. when casting multiple girders on the same bed and from 33–82 min. when casting a single girder on a production day.
- Cracking was observed in the top flange and web of every girder prior to prestress transfer. Temperature gradients experienced after tarp removal were the likely cause. A delay required to complete measurements for this research may have affected the severity of girder cracking, but cracks were frequently visible either before or immediately after removal of the formwork.
- Cracking did not seem to be affected by concrete type, age at transfer (which varied from 18–25 hr), or ambient temperature at transfer.
- The primary undesirable surface features in the SCC girders were shallow bleed channels and surface bubbles that occurred in the bottom bulb where bleed water and air

bubbles were trapped against the inclined upper surface of the bottom bulb formwork. These surface defects were shallow enough (less than 0.25 in. deep) to not require repair prior to shipment.

- SCC girders exhibited a much better surface finish than companion VC girders. The precast plant's engineering manager stated that the economic advantage of SCC over vibrated concrete would be at least as much due to its tendency to produce products of a high aesthetic quality and uniformity as due to its improved ease of placement.

3.5.2.2 Fresh Properties

- SCC slump flows for some batches were less than specified for this project, while VC slumps were occasionally greater than specified. Still, SCC girders were more easily constructed and exhibited better surface finish than VC girders, despite the use of high-slump VC (slump averaged 9.0 in.) and the use of high-viscosity SCC.
- A high-quality surface finish was achieved in the SCC girders but it was occasionally difficult to meet the required minimum slump flow without also causing a reduction in fresh concrete stability. It was therefore recommended by the precast plant's quality-control manager that the specified slump flow of SCC for precast, prestressed girders be decreased in future SCC provisions to 26 in. ± 2 inches.
- SCC exhibited fresh w_c of approximately 151 lb/ft^3, while VC exhibited fresh w_c of approximately 154.5 lb/ft^3. Both materials achieved high unit weights expectable for concrete to be used in precast, prestressed girder production, which exceeded the unit weight of 145 lb/ft^3 incorporated in simplified E_c design expressions.
- SCC stability generally improved during the course of the two-month production as plant personnel became more familiar with the sensitivity of SCC fresh properties to batching practices and chemical admixture dosages. All SCC placed during this production met the minimum stability requirements set forth in the SCC Special Provisions for the project.
- No more rigorous quality assurance and quality control of SCC was required to achieve batch uniformity comparable to that of vibrated concrete, but the occasional occurrence of borderline test results confirms that the levels of quality assurance and quality control currently implemented when using VC should be maintained during the use of SCC.
- Several fresh concrete stability test correlations (or lack thereof) observed in the laboratory testing described in Chapter 2 were replicated during the full-scale project. Such observations included strong correlations between the sieve stability test and both VSI and column segregation and between the rate of settlement and maximum settlement from the surface settlement test, as well as a relatively weak correlation between the rapid penetration test and any other fresh concrete stability test.

- Total aggregate volume appeared to affect some fresh concrete stability results, in which field results followed a pattern similar to that of the high-aggregate-content laboratory results. Because the SCC used in the full-scale project was proportioned with 63% total aggregate volume while the results of Chapter 2 suggested delineation of acceptance criteria by total aggregate volumes greater or less than 65%, the point at which to delineate SCC mixtures by total aggregate volume is not clear.

3.5.2.3 Compressive Strength

- Compressive strengths of SCC and VC used in this bridge were virtually identical at all ages up to three years despite distinct differences in mixture proportions between the two concretes. SCC was proportioned with a higher *s/agg* (0.47 versus 0.39 in VC), smaller coarse aggregate (½ in. versus ¾ in. in VC), and lower total aggregate content (63% versus 67% in VC).
- The prestress-transfer f_{ci} of both materials exhibited a significant dependence on the age of the concrete at transfer. The dependence was statistically indistinguishable between the two materials.
- At twenty-eight days, between-batch consistency of SCC f_c was similar to that of vibrated concrete: batches within the same production day varied by as much as 860 psi (averaging 2.6% COV) in SCC and 1,170 psi (averaging 4.1% COV) in VC cylinders.
- No change in concrete f_c was observed during the course of each production day—the compressive strength of the first placed batch was indistinguishable from those of batches at the middle and end of each production day.
- Compressive strength in both materials greatly exceeded specified release and 28-day values: 30–64% greater than specified for f'_{ci} and 31–73% greater than specified for 28-day f'_c. Because the same mixture was utilized in both girder sizes while different compressive strengths were specified for each size, BT-54 f_c values exceeded specified values by a larger margin than BT-72 f_c values.

3.5.2.4 Splitting Tensile Strength

- Splitting tensile strengths of SCC and VC used in this bridge were very similar, both in relation to f_c and in a direct comparison. SCC f_{ct} was 3–5% less than that of VC at prestress transfer and twenty-eight days despite having different proportions.
- Prestress-transfer f_{ct} did not correlate well with concrete age at the time of transfer.
- Both evaluated f_{ct} prediction models yielded acceptably conservative predictions of f_{ct} based on measured f_c in SCC and VC. The expressions given by AASHTO (2013) and ACI 363 (1992) over-predicted prestress-transfer f_{ct} by 6% and under-predicted 28-day f_{ct}

by 2–6%, while that used by ACI 318 (2011) under-predicted prestress-transfer f_{ct} and 28-day f_{ct} by 3–4% and 12–17%, respectively.

- Measured splitting tensile strength in both concrete materials exceeded the design values determined using the expression from ACI 318: by 9–19% at release and 15–38% at twenty-eight days, at least when evaluated using f'_c. Because the same mixture was utilized in both girder sizes while different compressive strengths were specified for each size, BT-54 f_{ct} values exceeded design values by a larger margin than did BT-72 f_{ct} values.

3.5.2.5 Modulus of Elasticity

- E_c of SCC was slightly (10–15%) less than that of VC used in this bridge at prestress transfer and twenty-eight days. Three-year E_c results from sixteen sets of SCC cylinders and twelve sets of VC cylinders suggest that long-term E_c of SCC and VC used in the Hillabee Creek Bridge girders are very similar with only a minor, expectable reduction (less than 6%) in SCC due to mixture proportioning.
- Prestress-transfer E_{ci} did not correlate well with concrete age at the time of transfer. Since f_{ci} did correlate well with age at the time of transfer, the weaker correlation to E_{ci} is likely due to the implicit variability of the test measurement.
- The E_c prediction model given by AASHTO (2013) and ACI 318 reasonably predicted E_c in both materials when using measured w_c and f_c, and the model given by ACI 363 (1992) more distinctly under-predicted E_c. SCC E_c was at least as accurately predicted as that of VC when using measured properties.
- Measured E_c greatly exceeded design values in both materials: 31–64% greater than expected at release and 23–59% greater than expected for 28-day E_c, at least when using the simplified (and most commonly used) ACI 318 equation. Predictions were slightly improved when incorporating w_c = 150 lb/ft^3. Because the same mixture was utilized in both girder sizes while different compressive strengths were specified for each size, BT-54 E_c values exceeded design values by a larger margin than did BT-72 E_c values.
- SCC and VC cylinders exposed to sustained compressive loading equal to 40% of f_c for at least two years exhibited 5% greater E_c than in cylinders never previously loaded (in twenty-eight sets of cylinders). This stress-stiffening phenomenon is in agreement with previous findings of Buettner and Hollrah (1968), Gardner and Tsuruta (2004), and Yue and Taerwe (1993). Results suggest that sustained precompression experienced by the actual girders would only provide improvements in long-term E_c.

3.5.3 Recommendations

- Concerns about the effect of fresh SCC stability on uniformity of concrete appearance, strength, and stiffness should not restrict the implementation of SCC in precast, prestressed applications when adequate quality-assurance and quality-control programs are in place.
- Successful implementation of SCC in precast, prestressed applications can be accomplished using a similarly rigorous level of quality-assurance and quality-control operations as currently enforced for VC implementation.
- While the current ALDOT specification requiring SCC slump flow of 27 in. ± 2 in. was manageable, slump flows in the range of 26 in. ± 2 in. may also be acceptable considering the satisfactory placement of SCC exhibiting this lower slump flow range during this project.
- SCC viscosity should not be restricted for constructability considering the satisfactory placement of highly viscous SCC used during this project.
- During production, special attention may be required to ensure that adequate texture is applied to the top of SCC girders, as the applied texture can reconsolidate and diminish if applied too early.
- Unless more accurate trial batch data or known mixture proportions and constituent specific gravities are available, an *unreinforced* concrete unit weight, w_c, of 150 lb/ft^3 should be used during the design of precast, prestressed girders constructed with proportions similar to those utilized in this research.
- Unless a more thorough analysis of a variety of mixtures is performed, the use of K_1 = 1.0 in the AASHTO 2013 E_c estimator should be acceptable for SCC and VC proportioned for precast, prestressed applications using Alabama aggregates (dolomitic limestone and natural river sand).
- The use of *expected* mean compressive strength and unit weight in ACI 318 (2011) and AASHTO (2013) mechanical-property predictions for service-state design should yield more accurate results than the use of specified properties when using materials and proportions similar to those employed in this research.

Based on the results discussed in this chapter, concerns regarding SCC f_c, f_{ct}, and E_c should not restrict implementation of SCC in precast, prestressed applications. Differences between VC and SCC properties were minor expectable and in response to differences between the two evaluated concrete mixtures. Differences between the tested SCC and VC were no more significant than variability related to age at prestress transfer. Between-batch variability of SCC was also no greater than that of VC.

SCC properties were at least as accurately predicted using existing material and property relationships. While current f_{ct} and E_c prediction models appear to be equally applicable to SCC and VC in this project when using measured f_c and w_c, measured values far exceeded design values, which could be significant during design. The difference between measured and design values should be investigated further.

CHAPTER 4: PRESTRESS TRANSFER BEHAVIOR OF FULL-SCALE GIRDERS

4.1 INTRODUCTION

In the previous chapters of this report, self-consolidating concrete was shown to be different than vibrated concrete in the fresh state as a result of its different constituent proportions and chemical admixture use. Chapter 2 included an exploration of the correlations between measures of concrete fresh stability and hardened uniformity, and Chapter 3 included analyses of the differences in full-scale production and basic mechanical properties (f_c, f_{ct}, and E_c) expected during the use of SCC. These field analyses were conducted during the production of Alabama's first full-scale SCC precast, prestressed girders for an in-service bridge, and the fresh tests assessed in Chapter 2 were conducted throughout girder production. An evaluation of transfer behavior of the full-scale girders is presented in this chapter. Transfer may be affected by all of the previously discussed variables—fresh properties, production practices, and early-age hardened material properties.

Understanding that full-scale production practices may affect bond behavior as much as fresh concrete stability or hardened concrete properties, many researchers (Erkmen et al. 2008; Trejo et al. 2008; Zia et al. 2005; Ziehl et al. 2009) have incorporated some form of transfer bond measurement into their full-scale evaluations of SCC for precast, prestressed girder production. Investigations of SCC's bond to prestressed strand have also been conducted at the AUHRC (Boehm et al. 2010; Levy 2007; Swords 2005), but using smaller concrete specimens and amounts of prestressing. The work presented in this chapter builds upon all of these references for several reasons:

- The evaluated girders have larger cross sections (BT-54 and BT-72) and concrete volumes (approximately 17 yd^3 and 27 yd^3 per BT-54 and BT-72 girder, respectively) than in any previously documented studies of SCC transfer bond behavior,
- The evaluated girders have a higher prestress demand (40–50 strands, including draped strands and debonded strands) than in any previously documented studies of SCC transfer bond behavior,
- Extensive fresh properties, hardened material properties, and production practices were simultaneously tested or observed in the evaluated girders, and
- The evaluated girders were produced using similar concrete mixtures as used in the three previous AUHRC studies with increases in specimen size and prestress demand in successive studies, thus allowing for a direct between-study comparison of Alabama SCC.

The primary objective of the work documented in this chapter was to evaluate the acceptability of the transfer response behavior exhibited by the SCC girders made during Alabama's first full-scale implementation of SCC in an in-service precast, prestressed bridge. This evaluation required consideration of both the companion VC girders used in the bridge and the transfer-bond provisions set forth in ACI 318 (2011) and the *AASHTO LRFD Bridge Design Specifications* (AASHTO 2013).

4.2 LITERATURE REVIEW

In order to produce an effectively pretensioned member, the desired prestressing force must be transferred to the hardened concrete by releasing the strands that were tensioned prior to concrete placement. This action is referred to as prestress release or transfer. The prestress force is transferred over a finite distance of embedded strand defined as the transfer length, l_t (ACI 318 2011). Also, as the force is transferred and the strand and concrete contract, some prestress force is lost due to elastic shortening. Factors that affect the transfer response, previous findings regarding l_t of SCC, and provisions for the prediction of l_t and the elastic loss of prestress due to transfer are discussed in the following sections.

4.2.1 Transfer Bond

4.2.1.1 Factors Affecting Transfer Bond

Influences on the bond behavior of concrete include

- Reinforcement size and surface characteristics (Stocker and Sozen 1970; Barnes et al. 2003),
- Compressive strength, in which l_t is assumed to vary inversely to the square root of f_{ci} (ACI 318 2011; Barnes et al. 2003; Khayat et al. 2003),
- Concrete age at time of testing, in which bond to reinforcement is affected differently by aging than is f_{ci} (Chan et al. 2003; Hassan et al. 2010), and
- Weakness in the concrete surrounding the reinforcement that is caused by the accumulation of migrating air bubbles and bleed water (Castel et al. 2006; Soylev and Francois 2003).

In addition to these effects, the bond between prestressed reinforcement and the surrounding concrete is also directly related to the effective level of prestress being transferred, both at the time of release and after time-dependent changes have occurred in the surrounding concrete. Unlike the passive mechanism of bond to deformed reinforcement, transfer of prestress actively affects and is affected by the surrounding concrete. Concrete in the immediate

vicinity of the transfer zone is highly stressed in circumferential tension and radial compression, which leads to time-dependent reduction of the bond and increases in transfer length (Barnes et al. 2003). Therefore, l_t is expected to grow over time until prestress losses, evolution of concrete material properties, and external loads (such as girder self-weight) cause the strand bond length to stabilize.

Despite the occurrence of time-dependent growth of l_t, it is most convenient to continue to relate l_t to the stress in the prestressing strands immediately after release, f_{pt} (Barnes et al. 2003). Measured f_{pt} is less than the original jacking force due to losses from strand chuck seating, steel relaxation, and elastic shortening of the concrete, but it is calculated readily by estimating steel relaxation and seating losses and estimating the elastic shortening of concrete based on E_{ci}. Furthermore, Mitchell et al. (1993) proposed that l_t is inversely proportional to the square root of the concrete compressive strength, and Barnes et al. (2003) further hypothesized that this proportionality to $\sqrt{f_c}$ is related to both E_{ci} and f_{ct} because of the stress state induced by the transfer mechanism (circumferential tension and radial compression). Since both of these properties are widely considered to be related to $\sqrt{f_c}$ (see discussion of Section 3.2.1 for details), Barnes et al. (2003) recommended that l_t be described according to Equation 4-1, in which f_{pt} and f'_{ci} are reported in ksi:

$$l_t = \alpha \frac{f_{pt}}{\sqrt{f'_{ci}}} d_b \tag{4-1}$$

In Equation 4-1, α is a constant of proportionality that Barnes et al. (2003) found to equal 0.57 ksi$^{-0.5}$ as an upper-bound for long-term l_t for strength design calculations and 0.17 ksi$^{-0.5}$ as a lower-bound for allowable stress calculations. These α values were determined from measurement of l_t in thirty-six AASHTO Type I girders produced in Texas with high-strength VC. Pozolo and Andrawes (2011) summarized that many similar expressions for transfer length have been developed elsewhere and all expressions that incorporate initial prestress and f_{ci} are more accurate at describing l_t (with different constants of proportionality) than those that utilize effective prestress force after all losses or do not use concrete strength as an independent variable.

Method of prestress transfer has also been found to affect l_t. Prestress force is frequently transferred by flame cutting the tensioned strands with a torch. Cutting can be coordinated so that the same strand is cut at each girder end simultaneously, or all cutting can be done at one end of the specimen and then the other. The former method, called the simultaneous release method, is done to both distribute stresses more evenly and prevent the specimen from moving on the prestressing bed. In the latter, stresses are transferred suddenly at one end (as each strand is cut) and gradually at the other (where all strands are gradually stepped down as the opposite end is detensioned). Thus, this method produces a “live end” and “dead end”, respectively. Many studies have indicated that release methods that produce a live end causes

longer l_t, likely as a result of "the dynamic effect associated with the transfer of energy from the strand to the concrete member" (Barnes et al. 2003).

Barnes et al. (2003) reported that transfer lengths of simultaneously released specimens were comparable to those at the dead end of specimens released from one end. For comparison, Levy (2007) proposed the use of $\alpha = 0.78$ ksi$^{-0.5}$ and 0.64 ksi$^{-0.5}$ in Equation 4-1 when predicting the live- and dead-end transfer lengths, respectively, of Alabama concrete (both SCC and VC) made with slag cement.

4.2.1.2 Transfer Bond Behavior of Self-Consolidating Concrete

The early-age bond strength of SCC to prestressing strand has been found to be less than that of comparable VC (Chan et al. 2003; Pozolo and Andrawes 2011; Staton et al. 2009). Chan et al. (2003) state that early-age transfer length growth does not follow the same trend as the evolution of compressive strength over time, so bond capacity must depend more on the effect of chemical admixtures and SCMs. More specifically, Girgis and Tuan (2005) and Staton et al. (2009) both found that the use of VMA led to increased l_t. Chan et al. (2003) and Hassan et al. (2010) found that the effect of chemical admixture type and dosage on bond strength seems to stabilize at approximately fourteen days. Past work performed at the AUHRC (Boehm et al. 2010; Swords 2005) and elsewhere (Pozolo and Andrawes 2011; Staton et al. 2009) has also indicated that later-age l_t stabilized within a few weeks after prestress release, although the occurrence was not unique to SCC.

Many of the studies of SCC transfer bond behavior have involved the testing of small specimens with only a few prestressed strands. The single-live-end release method of prestress transfer is considered to be more prevalent in this setting than in full-scale production (Russell and Burns 1993), but researchers have not regularly documented the dead- and live-end transfer lengths separately when evaluating SCC in this setting. Furthermore, not all researchers normalized results by $\sqrt{f_{ci}}$ or other measures. Thus, results concerning SCC bond have been mixed. Those that reported live- and dead-end l_t separately (Levy 2007; Pozolo and Andrawes 2011; Swords 2005) indicated that SCC appeared to be similarly affected by the release mechanism as VC.

Results from full-scale evaluations have also been mixed: Staton et al. (2009), Pozolo and Andrawes (2011), and Trejo et al. (2008) found that SCC exhibited shorter later-age transfer lengths than comparable VC, while Erkmen et al. (2008) and Girgis and Tuan (2005) found that SCC transfer length was longer when comparing values normalized by equations similar to Equation 4-1. Elsewhere, Boehm et al. (2010), Khayat and Mitchell (2009), Naito et al. (2005), and Zia et al. (2005) found SCC and VC to be essentially identical after accounting for strength, especially considering the variability of transfer-length measurements. Hamilton et al. (2005) and

Staton et al. (2009) state that the inherent variability of the full-scale release mechanism alone is probably larger than any difference between SCC and VC.

4.2.1.3 Code Provisions for Anchorage of Prestressing Strands

The two primary guidelines for predicting l_t for design purposes are found in the ACI 318 *Building Code Requirements for Concrete Structures* (ACI 318 2011) and *AASHTO LRFD Bridge Design Specifications* (AASHTO 2013). Two equations are given by ACI 318 (2011) for l_t calculation—one regarding calculation of development length and one for calculation of shear strength. The first is based on the effective prestress after all losses (f_{pe}), while the second is a simplification of the first based on an assumed f_{pe} of 150 ksi (low considering modern practices). The equations are presented below:

$$l_t = \frac{f_{pe}}{3000} d_b \tag{4-2}$$

$$l_t = 50 d_b \tag{4-3}$$

The equation recommended in the *AASHTO LRFD* (2013) specifications is of a similar format to Equation 4-3, except that it was based on the use of Equation 4-2 in conjunction with an assumed f_{pe} of 180 ksi. This estimate of l_t is given in Equation 4-4:

$$l_t = 60 d_b \tag{4-4}$$

Numerous researchers (Ozyildirim 2008; Pozolo and Andrawes 2011; Staton et al. 2009; Ziehl et al. 2009) have found that measured SCC transfer lengths are regularly shorter than those predicted by the above equations, while Girgis and Tuan (2005) found them to underestimate SCC transfer length. Many have recommended that no changes be made to the equations, though, due to the high variability of transfer length. In past AUHRC research, Levy (2007) found that moderate-strength SCC did not meet the above specifications, although it was hypothesized that the deficiency could be related to the size of the tested specimens. Russell and Burns (1993) observed that specimens of a larger cross section produce shorter l_t, likely because they are better able to absorb the dynamic impact of released strands. Boehm et al. (2010) found a similar pattern in AUHRC SCC projects in which larger sections were used in successive studies.

The above guidelines were developed for the prediction of l_t in fully bonded strands. Provisions for debonded strands (which were used in this project) are less clear. The commentary to ACI 318 (2011) indicates that "for the analysis of sections with debonded strands at locations where strand is not fully developed, it is usually assumed that both the transfer length and the development length are doubled." Similarly, a modification factor of 2 is applied to the development length of debonded strands in the *AASHTO LRFD* guidelines (2013) (see Section 5.11.4.3), although it is not stated whether the associated transfer length is also doubled.

While there has not been much research reported concerning debonded strands in SCC, Barnes et al. (2000) found that debonded strands exhibited no greater l_t than did fully bonded strands in high-strength VC. Hamilton et al. (2005) observed longer l_t of debonded strands in SCC and VC girders; they hypothesized that the increase was likely related to the increased free length of the unbonded strands, as strand with a longer free length would release more energy when cut.

4.2.2 Elastic Prestress Loss

4.2.2.1 Iterative Approach to Determine Elastic Prestress Loss at Transfer

At the time of transfer, the prestressing force applied to the concrete member causes axial compression and, consequently, axial shortening of the member. This directly affects the effective prestressing force being applied. Therefore, the prestress loss due to the elastic shortening of the concrete, Δf_{pES}, can be iteratively calculated by equilibrating the change in concrete strain with the corresponding change in steel strain:

$$\Delta f_{pES} = E_p\left[\Delta\varepsilon_{cen,ES} + (\Delta\phi)_{ES}y\right] \quad (4\text{-}5)$$

In which

$\Delta\varepsilon_{cen,ES} = \frac{-N_o}{E_{ci}A_{tr}}$ is the change in strain at the centroid of the cross section due to transfer mechanism and

$(\Delta\phi)_{ES} = \frac{M_G - M_o}{E_{ci}A_{tr}}$ is the change in change in curvature of the cross section due to transfer mechanism,

And where

$N_o = (\Sigma E_p\varepsilon_{p,i})A_p$ is the axial load on the cross section due to the prestress transferred,

$\varepsilon_{p,i} = \frac{f_{pbt}}{E_p} = \frac{f_{pj} + \Delta f_{p,R}}{E_p}$ is the strain in the prestressing steel immediately before transfer, based on the jacking stress, f_{pj}, and pre-release relaxation loss,

M_G is the moment on a cross section due to self-weight, and

$M_o = \Sigma N_o y_{p,cen}$ is the moment on a cross section due to the prestress transferred.

4.2.2.2 Pre-Release Losses

Several mechanisms can lead to unidentifiable loss of prestress in the strands—steel stress relaxation, seating of the strand chucks, friction at draped-strand hold-downs, and differential heating prior to concrete set. Most of these mechanisms only occur prior to strand release, and

they may be compensated for by the producer or have not been found to be differently affected by the use of SCC (Erkmen et al. 2008). Meanwhile, time-dependent steel stress relaxation, or a reduction in steel stress without a corresponding change in strain, occurs over time and is difficult to accurately measure in the prestressing bed or once the steel is bonded to the concrete.

For the purpose of this study, the only assumed pre-release prestress loss was that due to the relaxation of the steel prestressing reinforcement prior to transfer. The effective stress in the prestressing strands just prior to transfer, f_{pbt}, is found by subtracting the relaxation before transfer from the jacking stress that was assumed to equal 202.5 ksi. Relaxation losses prior to transfer can be estimated according to the following equation from Nilson (1987) that was also used by Stallings et al. (2003):

$$f_{pbt} = f_{pj}\left\{1 - \left[\frac{\log(t_i)}{45}\right]\left[\left(\frac{f_{pj}}{f_{py}}\right) - 0.55\right]\right\} \quad (4\text{-}6)$$

Where

f_{pj} is the jacking stress (ksi),

f_{py} is the yield strength of the prestressing reinforcement (ksi), and

t_i is the time between jacking and prestress transfer (hours).

4.3 EXPERIMENTAL PROGRAM

In addition to the general fresh and hardened properties and production observations documented in Chapter 3, transfer length testing specifically involved measuring concrete surface strains at transfer zones in twelve girders (see Table 3.2 for details). Elastic prestress losses were measured using vibrating-wire strain gauges (VWSG) embedded at midspan of each girder. The experimental work related to each of these activities is summarized below. While initial camber was also measured and could be calculated, evaluation of this property required accounting for the potentially nonlinear thermal effects present in the girder. Evaluation of thermal effects is further discussed in Chapter 6, so evaluation of initial camber is discussed further in that chapter, as well.

4.3.1 Transfer Length

4.3.1.1 Transfer-Length Instrumentation

Transfer lengths were determined by analyzing the concrete surface strains measured in each transfer zone. Each girder had four transfer zones—one at each end of the girder and one at each region associated with the transfer of partially debonded strands (120 in. inward from the

ends of each girder, as shown in Figure 3.6). To minimize interruption of the production schedule, no more than one girder per day—twelve girders in total—were studied during this research program. Each end's transfer zone was examined for all twelve girders, as was one of the two debonded strand transfer zones for ten of the twelve girders. Thus, there were thirty-four measured transfer zones: twenty-four end zones and ten debonded-strand zones.

Concrete surface strains were measured through the use of demountable, mechanical (DEMEC) strain gauges that were applied to the bottom flange at each zone. Because of 1) the scale of the specimens being tested, 2) all testing was to occur within the precast plant, and 3) researcher interruption of production needed to be minimized, a system was devised to rapidly attach the DEMEC measurement targets to the girders. This system, which is shown in Figure 4.1 and Figure 4.2, was adapted from a similar method utilized by Dr. Ben Graybeal of the Federal Highway Administration.

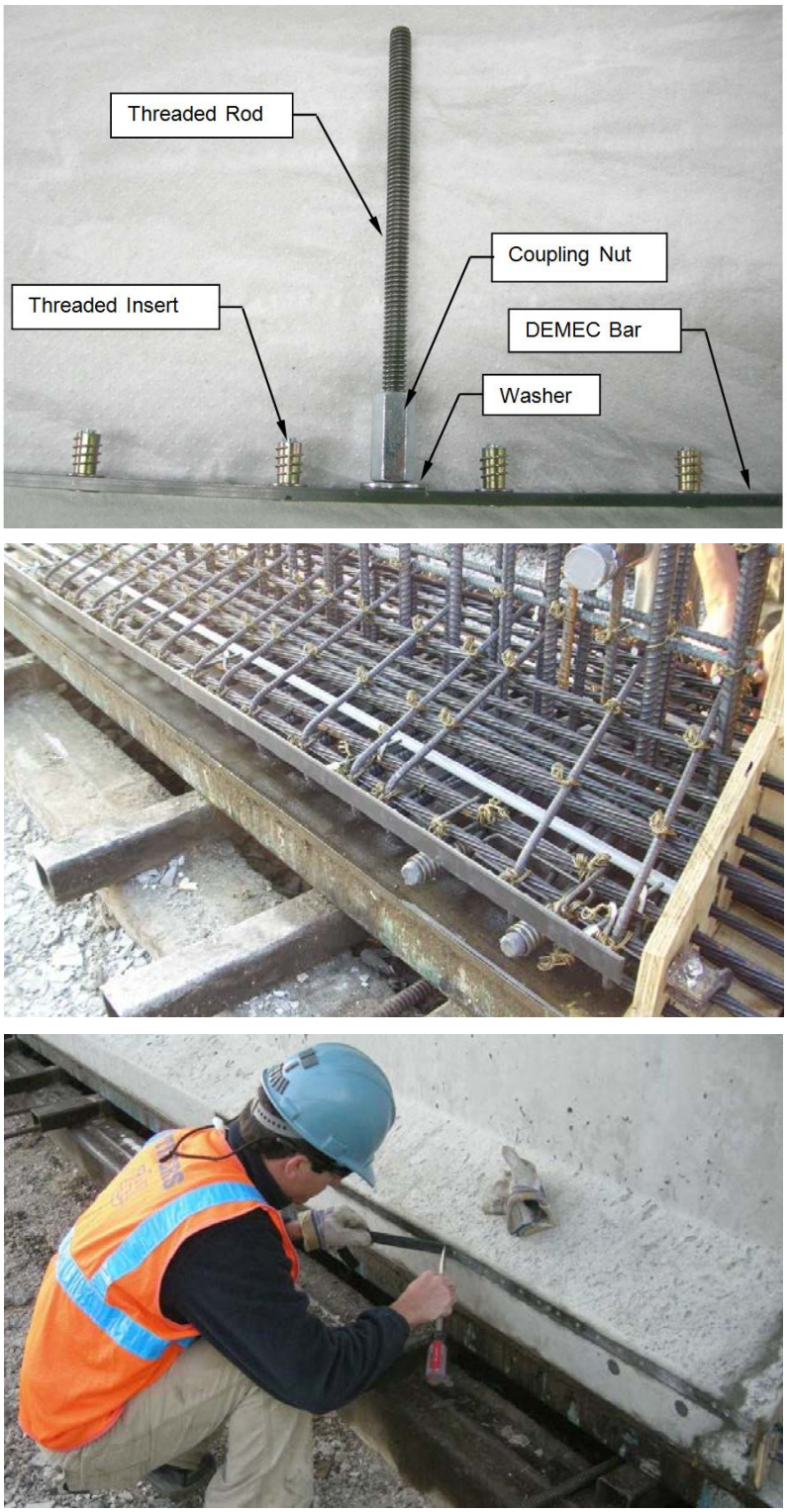

Figure 4.1: DEMEC mounting strips (*top*) and installation (*middle*) before closure of formwork and (*bottom*) following removal of formwork

Figure 4.2: DEMEC insert (*top*) installation within DEMEC mounting strips and (*bottom*) measurement using a DEMEC strain gauge

As shown in the figures, 6.0 ft strips of threaded inserts were cast into the bottom bulb of the girder and, following form removal, threaded DEMEC targets were rapidly screwed into the inserts and locked into place using a thread-locking compound. By mounting the DEMEC targets in this fashion, disruption of the normal girder prestressing operation was minimized. Further details concerning the fabrication of this system were documented by Dunham (2011).

4.3.1.2 Conversion of Concrete Surface Strains

Concrete surface strain results were interpreted through the use of the 95% average maximum strain (AMS) method, which was based on the method described by Barnes et al. (2000). In it,

transfer length is calculated by determining the distance to the intersection of the measured strain profile and the 95% AMS plateau. This concept is illustrated in Figure 4.3 below.

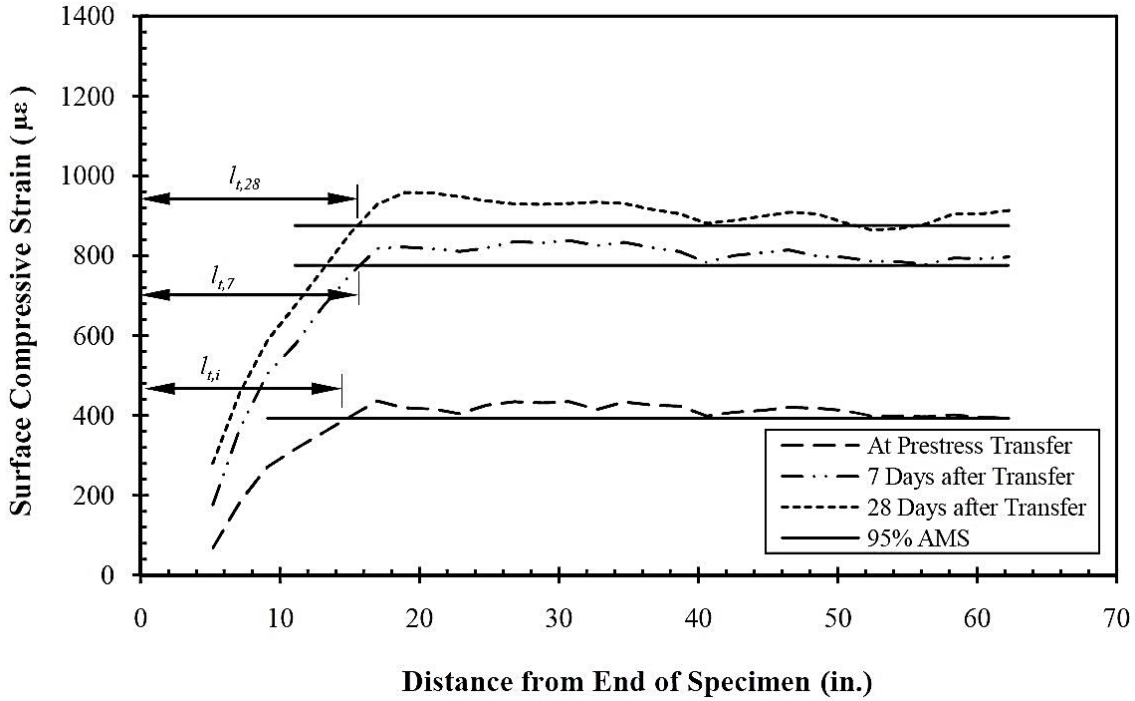

Figure 4.3: Use of 95% AMS method to determine l_t of fully-bonded strands

The first step required to create a surface compressive strain profile for any of the girders was to transform the measurements collected at the prestressing facility into strain values. The following steps were followed to perform this conversion.

1. Two deformation measurements were obtained for each 200 mm (7.87 in.) gauge length before and after transfer and at girder ages of seven and twenty-eight days; the average reading was determined at each location at each age.
2. A reference reading was taken (using a reference bar) prior to taking the surface DEMEC target measurement for every age throughout the study. The reference reading for each age was subtracted from the surface DEMEC target reading at each location for the same age. The resulting difference is described as the "relative reading" in the next step.
3. The change in compressive strain at each location was determined by subtracting the relative reading prior to transfer from the relative reading at the age of interest. The resulting difference was then multiplied by the appropriate gauge factor to determine the strain over the 200 mm gauge length. At this stage, each measured strain was assigned to the absolute position of the DEMEC point at the middle of the 200 mm gauge length measured.

4. As mentioned previously, the girders were skewed at 15 degrees. Consequently, the resulting strains were determined for the center line of the girder by averaging the strains from opposite faces of the girder at corresponding points (the first point on the north face was averaged with the first of the south face). The centerline distance from the end of the girder to each point was also calculated by averaging the distance from the end of the girder to the point on each face of the girder.
5. The strains were then smoothed: a single strain value was assigned to each distance along the centerline by averaging the strain assigned to a particular location with the strains assigned to the immediately adjacent locations. A visual aid depicting the smoothing portion of this process can be seen in Figure 4.4.

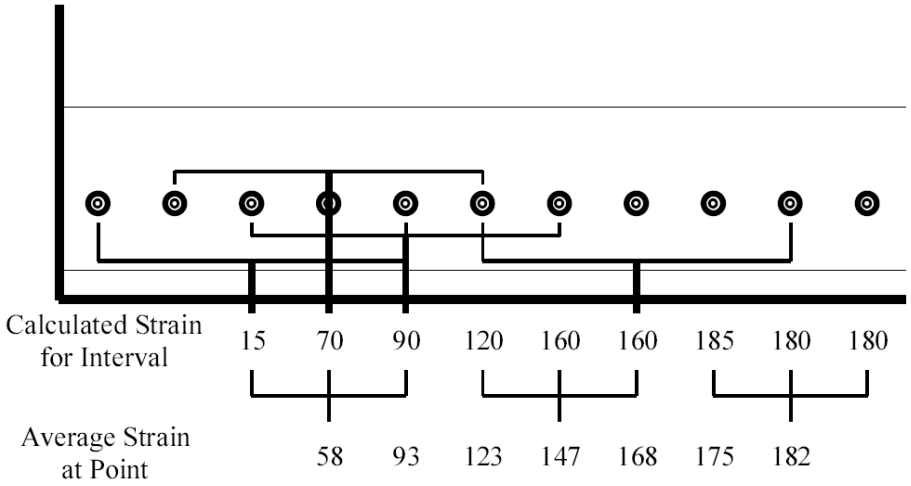

Figure 4.4: Assignment of Surface Compressive Strain Values (Barnes et al. 1999)

6. The smoothed strain values were then plotted in relation to their absolute values. The resulting graph (Figure 4.3) depicts the concrete strain along the centerline of the girder.

Once the strain profile is plotted, determination of l_t is complicated by several factors: strain due to the self-weight of the girders, strain due to the varying eccentricity of draped strands (see Figure 3.6), and selection of the appropriate AMS plateau. Strains due to strand draping were found to balance the strains due to self-weight in these girders so effectively that it was unnecessary to make any changes to the measured strain profiles for either (Dunham 2011).

Determination of l_t at later ages is complicated by creep associated with the prestressing force and self-weight of the girders, as well as shrinkage of the girders. Creep and shrinkage are described in greater detail in Chapters 5 and 6 of this report, but time-dependent deformations have a noticeable effect on l_t. Creep is hypothesized to be directly proportional to applied load

(Barnes et al. 2000), which would cause an *amplification* of all strain measurements over time. Changes in the later-age AMS due to creep do not artificially decrease the apparent l_t because all values are amplified proportionally to the applied load. Meanwhile, shrinkage is independent of load and causes a *translation* of the strain profile which would artificially decrease the apparent l_t (Barnes et al. 2000). Based on time-dependent deformation results that are discussed in Chapter 5 of this report, creep and shrinkage effects were estimated to cause 2/3 and 1/3 of time-dependent changes in l_t, respectively. Based on this estimate, the later-age 95% AMS was determined according to Equation 4-7, in which only creep-induced changes in the AMS are considered in the growth of l_t:

$$AMS_{95} = AMS_{100} - \left[\frac{1}{3} \times \left(0.05AMS_{100,i}\right) + \frac{2}{3} \times \left(0.05AMS_{100}\right)\right] \quad (4\text{-}7)$$

Where

AMS_{95} is the long-term 95% AMS value desired,
AMS_{100} is the long-term 100% AMS value at the time considered, and
$AMS_{100,i}$ is the 100% AMS value immediately after transfer.

Determination of l_t in debonded strands is complicated by these same issues and by the level of strain in the debonded region due to the fully bonded strands. It was only appropriate to consider the *change* in compressive strain resulting from the debonded strands, so the AMS at these zones was calculated by subtracting the AMS of the adjacent fully bonded strand transfer zone from the AMS measured further inward where debonded strands were bonded. The transfer length of the debonded strands was taken as the distance from the beginning of bonding (120 in. from the girder end) to the point where the measured strain profile crossed the 95% AMS threshold. This determination is illustrated in Figure 4.5.

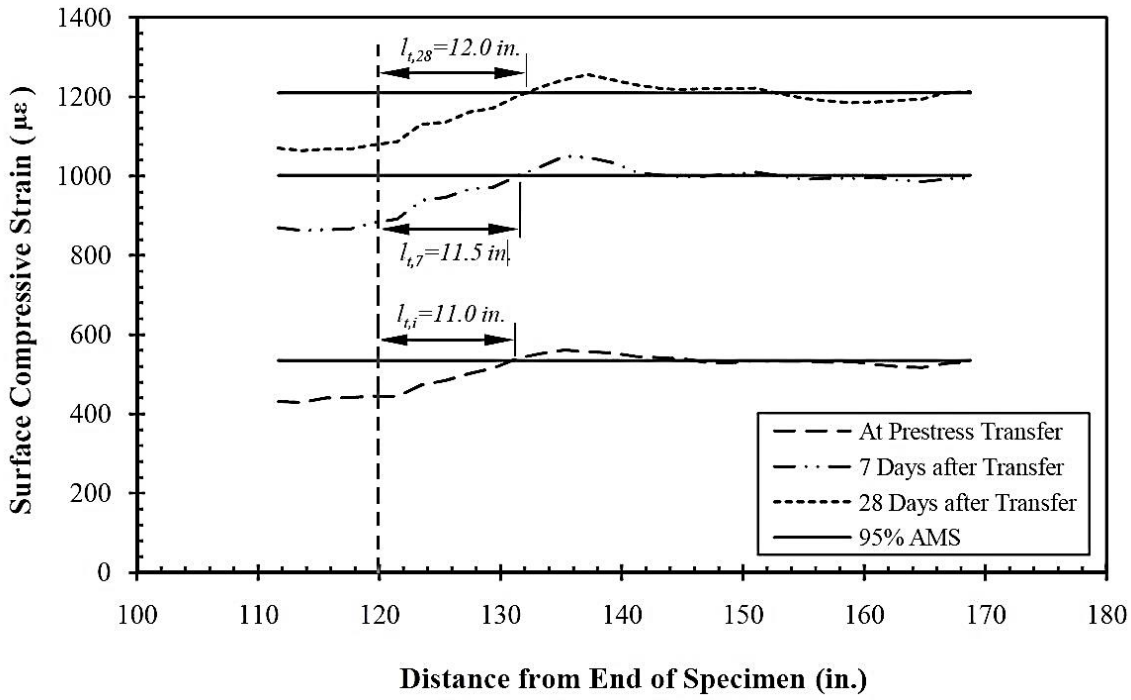

Figure 4.5: Use of 95% AMS method to determine l_t of debonded strands

In all measurements of AMS to determine l_t, the use of a 95% AMS value was used instead of 100% for two reasons. First, it provides a clearly identifiable intersection location between the compressive strain profile and the bounding horizontal line (Russell and Burns 1993). Second, the reduction in AMS, which may appear to artificially shorten the transfer length reading, actually compensates for the rounding of the strain profile that results from the smoothing process (Boehm et al. 2010). Considering the variables inherent in this research, it was determined that an l_t precision of 0.5 inches was suitable for individual measurements; consequently, a precision of ¼ in. was chosen for reporting of girder-average measurements. While DEMEC spacing and equipment precision could allow for more precise reporting, the field conditions and assumptions associated with the long-term analyses (creep and shrinkage) made the use of this precision most appropriate.

4.3.2 Prestress Loss

Prestress losses were not directly measured in this research. However, prestress losses were estimated based on the strain results from vibrating-wire strain gauges (VWSGs). Compatibility and the bond between the concrete and prestressing strand should mean that a strain change measured by the VWSG corresponds directly to a strain change in the prestressing strand at the level of the gauge. The stress in the prestressing steel remained well within the linear-elastic

behavior range, meaning that a change in measured concrete strain would also correspond directly to a change in stress in the strand. Based on linear-elastic stress-strain behavior and compatibility, the elastic prestress loss due to transfer was thus determined as follows:

$$\Delta f_{pES} = E_p(\Delta \varepsilon_{cgp}) \quad (4\text{-}8)$$

In Equation 4-8, $\Delta\varepsilon_{cgp}$ is the change in concrete strain at the center of gravity of the bottom-bulb prestressing steel, or *cgp* that was directly measured using VWSGs placed at the *cgp* of each girder. While the concrete strain would actually differ over the height of the cross section due to curvature of the girder, prestress loss is only calculated at the *cgp* during design. It is for this reason that VWSGs were placed at the approximate midspan *cgp* in every girder.

The data acquisition system used in this research was capable of recording VWSG strain readings at user-specified intervals as short as approximately two minutes. While readings were, consequently, incapable of identifying the truly instantaneous responses to the transfer loading, this load is not applied instantaneously. Transfer by flame-cutting was observed to require approximately 6–10 min. depending on the coordination of the plant personnel. Therefore, pre-release and post-release strain readings were taken approximately 14 min. apart. While measured results may include a small and unmeasurable amount of time-dependent deformation (creep, shrinkage, or thermal), these effects would be minimal over the 14-min. interval.

Also, cylinder-measured E_c is an approximation of the elastic stiffness of concrete because it is tested in unreinforced concrete subjected to uniaxial compression, with the testing variability described further in Section 3.4.3.3. The loading of concrete during E_c testing according to ASTM C469 occurs over less than three minutes, so this measurement is the best available estimate of elastic concrete stiffness. Thus, the direct comparison of measured results to those calculated using the E_c measured in representative cylinders was deemed acceptable, and transfer-load results are understood to include some inherent variability.

VWSGs were installed at various locations over the height of the girders, and the gauge locations were identical in companion SCC and VC girders. The VWSGs used in this project were Geokon, Inc. VCE-4200 gauges. Details showing the various components of these gauges are shown below in Figure 4.6 and described further by Johnson (2012).

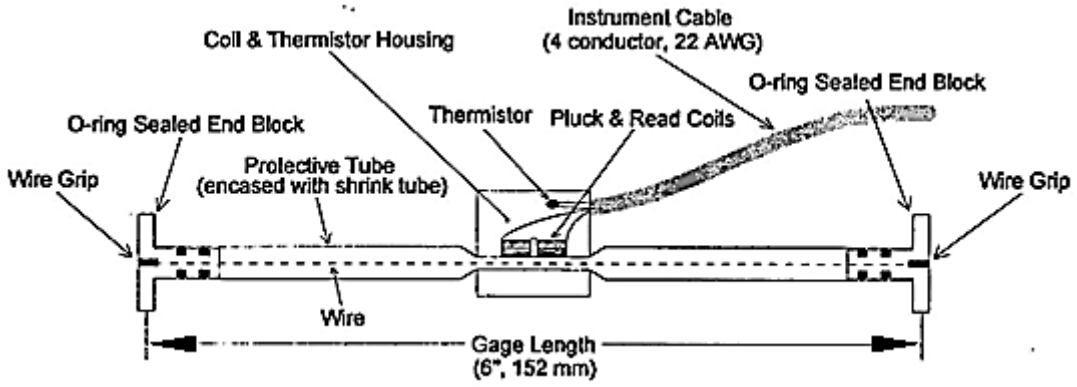

Figure 4.6: VCE-4200 vibrating-wire strain gauge schematic (Geokon 2010)

With reference to Figure 3.2 and Table 3.2, girders along lines 4–7 were instrumented for "full-depth" strain and temperature measurement, while girders in lines 1–3 were instrumented only for bottom-flange concrete strain and temperature measurement. VWSG locations are illustrated in Figure 4.7 and Figure 4.8. As shown in those figures, the VWSGs were placed so that they would be located (where applicable) at

- The midspan centroid of the bottom-flange prestressing strands located 6 in. from the bottom surface of the BT-54 girders and 8.8 in. from that of the BT-72 girders (all girders),
- One quarter of the web height above the bottom bulb as well as below the top flange (for full-depth measurements only), and
- The centroid of the lightly stressed prestressing steel in the top flange (for full-depth measurements only).

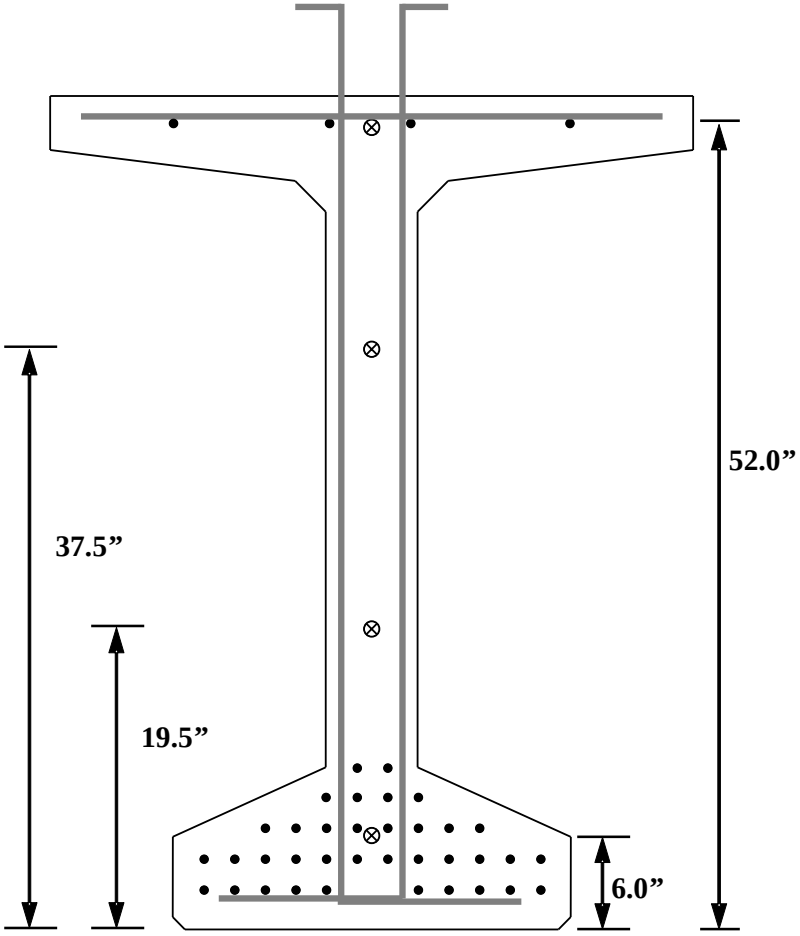

Figure 4.7: BT-54 VWSG configuration (where applicable)

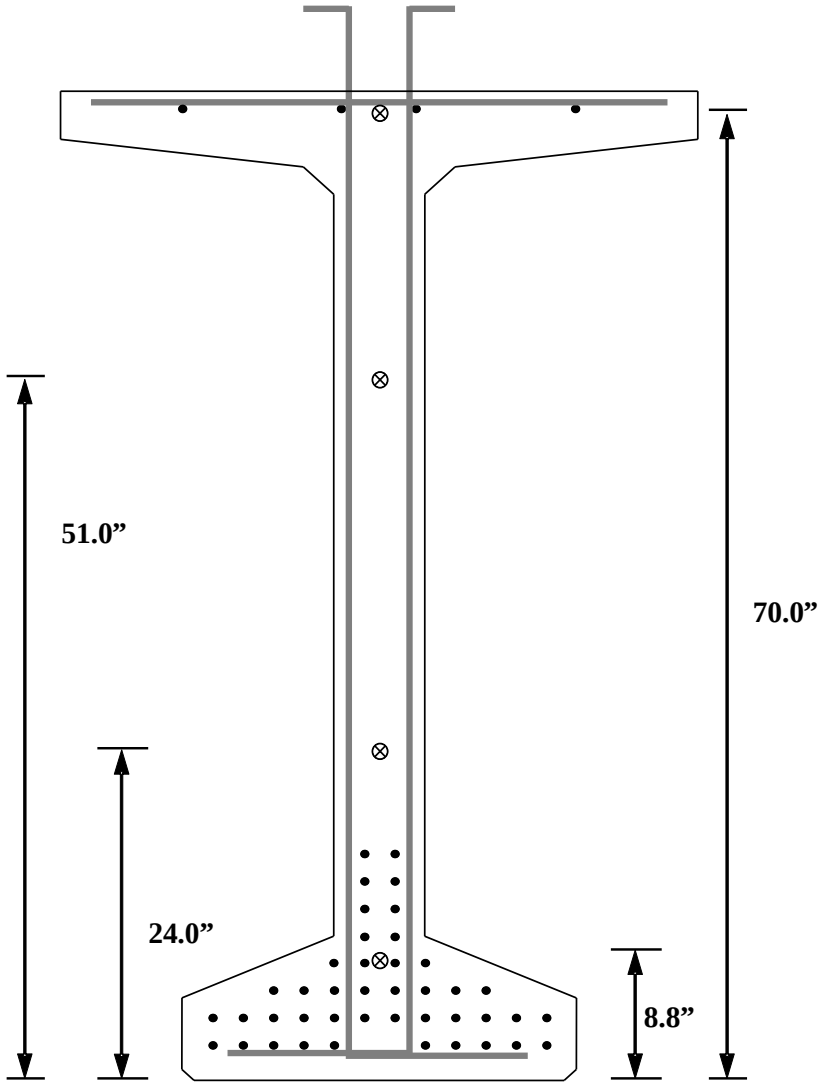

Figure 4.8: BT-72 VWSG configuration (where applicable)

The gauges were secured into place using various materials including plastic zip cable-ties, steel wire, and small segments of reinforcing steel. Gauges located in the bulb section of the girder were secured into place using zip-ties tied around the prestressing strand. Figure 4.9 shows a gauge located in the bottom bulb of a girder. Gauges placed in the top flange of a girder were secured in the same manner.

Figure 4.9: VWSG Secured in Bottom Bulb

Gauges placed within the web of a girder were more difficult to secure because there were no prestressing strands in the region. An assembly of small sections of reinforcing bar along with steel wire was fabricated in order to provide a stable suspension system without adding significant longitudinal reinforcement to the cross sections. Figure 4.10 shows a typical example of this method of securing the VWSGs. Wire ties were used to tie small sections of reinforcing steel to the stirrup sections used as reinforcement in the girder. Next, steel wire was wound around the steel sections to connect them together. Finally, zip-ties were used to secure the VWSG to the steel wire.

Figure 4.10: VWSG Secured in Web of a Bulb Tee Girder

Two data acquisition systems were used in this research. These systems were described in detail by Johnson (2012). The process by which gauge strains are determined is found in Appendix B of the Geokon Instruction Manual (2010) that was included with the gauges; this process was also described by Johnson (2012). In all reported results, the measured strains have been corrected for the actual temperature of the gauge according to the process described by those two references.

4.3.3 Additional Considerations and Nomenclature

As with the strength and E_c assessments of Chapter 3, the exact placement location of the sampled batches within the girders could not be determined. Samples taken at the midpoint of each production day (see Chapter 3) were assumed to be representative of the majority of concrete placed during that day. Furthermore, the way in which the average age of the girders was considered in relation to f_{ci} in Section 3.4.3.1 should be applied to comparisons of l_t. Isolation of the age at each transfer zone was not possible, although some inference is possible when considering the casting order. Likewise, fresh property results could not be isolated to a particular transfer zone; instead, fresh property results taken from the same mid-production batch were assumed to give a reasonable estimate of the stability of the concrete placed during that day.

Many transfer zones were assessed during this research (thirty-four zones), and the elastic release prestress loss was measured in every girder (twenty-eight girders). A single SCC and VC mixture were used throughout girder production, which could allow for a fairly well populated comparison of SCC and VC results. However, every girder was exposed to a slightly different curing and exposure history. Also, transfer length measurement can exhibit high variability, and the number of transfer zones that were exactly identical (girder size, zone location, casting order, and bed orientation) varied, which complicated comparisons.

The basic nomenclature shown in Figure 3.7 was sufficient for identifying elastic prestress losses; additional suffixes were necessary for identification of each transfer zone tested during this research. Casting orientation may affect transfer bond in full-scale girders because at least half an hour passed between the casting of the first end and second end of each girder (see the discussion of Section 3.4.3 and times shown in Table 3.4 for details). Furthermore, SCC may be affected differently by the casting process than VC due to the free-flowing nature of SCC. Casting orientation was documented as discussed in 3.3.2, so the first suffix added to the girder identification is based on the order of casting: -1 or -2 for the first end and second end placed, respectively.

The effects of the difference in age between girder ends and difference in filling could not be evaluated independently in this research, but they may both be of significance. Khayat and

Mitchell (2009) found that the filling method alone did not affect SCC performance: they filled some girders from a single point at the middle of the formwork and others from one end to the other to make this comparison.

Additionally, method of release may affect transfer length (see Section 4.2.1), especially when the method yields a dead and live end in each girder. This production utilized the simultaneous method of flame-cutting release described earlier (no explicitly live or dead end), but distinctly longer free lengths of strand were exposed at the outer ends of the prestressing bed than between the girders. Hamilton et al. (2005) pointed out that longer unbonded strand lengths release greater amounts of energy, so the occurrence of pseudo-live ends was possible in this project. Therefore, the second suffix added to the girder identification is based on bed orientation, as this is analogous with strand length and energy released: -E or -I for exterior and interior ends to coincide with longer (more energy) or shorter (less energy) exposed strand length, respectively. Finally, debonded zones are denoted with by the suffix "/D". These zones were always associated with adjacent, fully bonded transfer zones but varied unevenly between first-end, second-end, interior-end, and exterior-end orientations.

4.4 PRESENTATION AND ANALYSIS OF RESULTS

4.4.1 Measured Transfer Lengths

Girder-average transfer lengths are reported below in Table 4.1; these values are the long-term l_t values that were determined at twenty-eight days. It was previously seen and confirmed in this project by Dunham (2011) that there is a significant growth of transfer length within the first week after prestress transfer, especially in VC girders (approximately 20% growth in VC girders versus approximately 10% growth in SCC girders). However, lt changed less than approximately 2% after the first week, so 28-day values are of primary significance during this analysis, as they indicate the long-term transfer-length behavior of the girders.

Normalized results in terms of α (see Equation 4-1) are also presented in the table. To calculate these normalized α results, f_{pt} (the prestress in the prestressing strands immediately *after* release) was determined based on the use of a reasonable estimate of the strand stress immediately before transfer (f_{pbt}) and the average measured change in transfer-zone concrete surface strain at the time of transfer (equal to the 100% AMS). Transfer-zone surface strains were directly measured using the DEMEC instrumentation described in Section 4.3.1.1 and results from the same zone type, material, and girder size (fully-bonded SCC BT-54 zones, for example) were averaged to determine the local change in prestress. Thus, using an assumed jacking stress of 202.5 ksi and relaxation losses calculated using Equation 4-6, f_{pt} varied from 187–191 ksi (results are presented in Keske 2014).

Table 4.1: Measured transfer lengths and normalized coefficients of determination

Girder ID	End Transfer Zones				Debonded Transfer Zone			
	l_t (in.)	α (ksi$^{-0.5}$)	Average α (ksi$^{-0.5}$)		l_t (in.)	α (ksi$^{-0.5}$)	Average α (ksi$^{-0.5}$)	
54-2S	16.25	0.51			12.0	0.38		
54-4S	18.0	0.56	0.49		13.5	0.42	0.40	
54-7S	13.25	0.40		0.47	-	-		0.39
72-2S	17.25	0.50			14.0	0.41		
72-4S	16.75	0.48	0.46		12.0	0.35	0.38	
72-7S	13.75	0.40			13.5	0.40		
54-2V	12.5	0.39			10.5	0.33		
54-4V	13.25	0.39	0.41		12.0	0.35	0.34	
54-7V	13.75	0.45		0.40	-	-		0.33
72-2V	13.0	0.39			11.0	0.33		
72-4V	12.75	0.37	0.40		9.5	0.28	0.33	
72-7V	15.0	0.44			13.0	0.38		

The data in the above table illustrate that the use of SCC resulted in longer transfer lengths, both in direct comparison and after accounting for variations in strength, prestress intensity, and strand size. This is important because the transfer-length prediction equations discussed earlier (Equations 4-2 through 4-4) do not account for strength or prestress intensity in the determination of l_t. This topic is discussed further in Section 4.4.2.

The end-transfer α values presented in Table 4.1 represent the average of the results from both end transfer zones, while the debonded-transfer α values were obtained from a single debonded transfer zone. Average end-transfer results provide the best estimate of the overall tendencies of SCC and VC, while debonded-transfer results may exhibit more scatter because only one zone was measured per girder. In general, debonded transfer lengths were shorter than those of the *adjacent* fully-bonded strands (approximately 90% of l_t in the adjacent fully bonded zone, on average) and also experienced less time-dependent growth. The reductions could be the result of friction in the debonding sheathing, the relatively smaller change in prestress force resulting from transfer of the debonded strands, or other geometric considerations at these locations (such as different self-weight or eccentricity of the draped strands). Regardless, this confirms the findings of Russell and Burns (1993) and Barnes et al. (2000) and disagrees with the findings of Hamilton et al. (2005) regarding debonded strand transfer length.

On average, SCC α values were approximately 18% greater than in the VC girders (in both fully bonded and debonded zones). Considering the statement by Barnes et al. (2003) that

strand transfer may be related to both E_{ci} and tensile strength, this difference was expectable in lieu of the E_{ci} and f_{ct} results presented in Chapter 3—SCC E_{ci} was approximately 10–15% less than that of VC, relative to $\sqrt{f_c}$, and f_{ct} was insignificantly less (5%) relative to $\sqrt{f_{ci}}$.

4.4.1.1 Comparison of Alternatively Normalized Transfer Lengths

To further assess the hypothesis that transfer length differences could be expectable as a result of changes in E_{ci} and f_{ct}, the data in Table 4.1 were assessed according to the general form of Equation 4-9. In the equation, $Y_{measured}$ was the measured E_{ci} or f_{ct} (see Table 3.7 for values) that was substituted directly to eliminate the assumption of correspondence to the square root of compressive strength:

$$l_t = \alpha' \frac{f_{pt}}{Y_{measured}} d_b \tag{4-9}$$

The constants of proportionality (α') determined according to Equation 4-9 exhibit different units than the α values reported in Table 4.1; they depend upon the measured property in the denominator of the equation and are reported elsewhere by Keske (2014) to avoid confusion. Values of α' and α are compared graphically in Figure 4.11 below. Only fully bonded transfer length results are represented. Note that, within each SCC-versus-VC comparison, values have been normalized by the average of all SCC and VC results calculated within that particular comparison. In other words, material averages are equal distance from 1.0 on the normalized vertical axis.

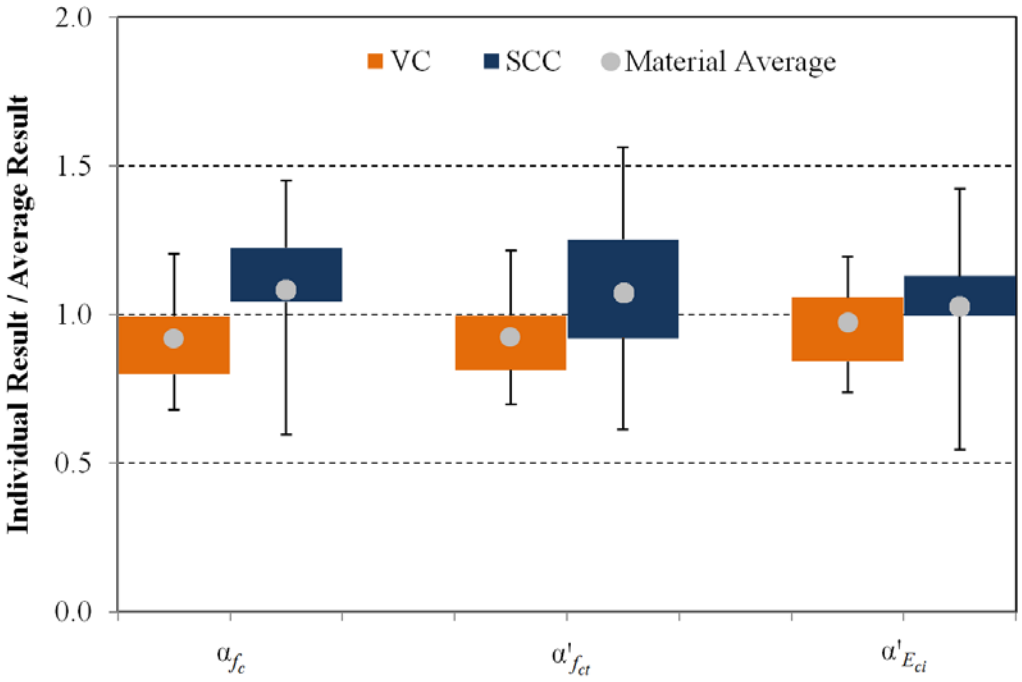

Figure 4.11: Comparison of SCC and VC normalized α and α' values

In the above figure, solid boxes indicate the range of the inner two quartiles of results, while unfilled plot "whiskers" indicate the maximum and minimum measured values within each dataset. Several conclusions are warranted based on Figure 4.11. First, SCC transfer lengths exhibit more variability (longer plot whiskers). Second, normalization by f_{ct} increased the variability of the results while normalization by E_{ci} did not (narrower boxes indicate decreased spread in results). Third, normalization by E_{ci} appeared to account for the majority of the difference between SCC and VC (material averages were less than 5% different when normalized by E_{ci}), while normalization by f_{ct} did not. Considering the first two conclusions, it is unclear whether this third distinction is due to testing variability, a difference in tensile behavior of the concrete in response to confinement, or a greater bond dependence on elastic stiffness (E_{ci}) than on the tensile capacity of the concrete (f_{ct}).

Values normalized through direct use of E_{ci} according to Equation 4-9 were well within the precision of the measurements obtained during this research (the 5% difference would equal approximately 0.7 inches of transfer length based on the average f_{pt}, f_{ci}, and E_{ci} from this research). Thus, while longer transfer lengths were present in these SCC girders, the difference may be largely attributable to differences in E_{ci} which could occur between any two concretes. In other words, while SCC E_{ci} may commonly be less relative to its $\sqrt{f_{ci}}$, such a difference could occur between *any* two concretes of different mixture proportions. Additional comparisons of ways in which SCC may uniquely affect transfer length are described in the following subsections.

4.4.1.2 Effect of Specimen Size (Comparison to Past AUHRC Studies)

Normalized BT-54 transfer lengths were compared to those in BT-72 girders via comparison of α, as well as to results previously measured by Swords (2005), Levy (2007), and Boehm et al. (2010). While actual transfer lengths are reported in Table 4.1, comparison of α values in the two girder sizes was necessary because different strand sizes were utilized in each girder size. Average ratios of BT-54 α to BT-72 α equaled 1.02–1.06 depending on zone and material. A two-sample t-test also yielded a statistically insignificant difference between girder sizes (P-values exceeded 0.65 in each material). Thus, in comparisons to past AUHRC studies and in comparisons of other variables in subsequent subsections regarding orientation and SCC stability, BT-54 and BT-72 results are combined prior to evaluation.

Summary results from previous AUHRC studies are shown below in Table 4.2; supplemental data regarding these previous studies are presented by Keske (2014). In the table and supplemental information, the following stipulations apply:

- Only fully bonded strands are compared because debonded strand transfer lengths were found to be noticeably shorter than those of fully bonded strands,
- Results used from the current study are those obtained at a concrete age of seven days because all previous studies involved measurement at these earlier ages, and
- Specimens are shown in order of increasing size; specimen descriptions are given in the cited references and by Dunham (2011).

Table 4.2: Summary of normalized transfer lengths in AL concrete

Study	Specimen Description and Height (in.)	Average Values		
		α_{SCC} ($ksi^{-0.5}$)	α_{VC} ($ksi^{-0.5}$)	α_{SCC}/α_{VC}
Swords 2005	**Prisms (4 in.)**	1.00	0.78	1.28
Levy 2007	**T-Beams (15 in.)**	0.71	0.64	1.12
Boehm et al. 2010	**AASHTO Type I (28 in.)**	0.50	0.49	1.03
Current Study	**Bulb-Tees (54, 72 in.)**	0.47	0.40	1.20

For both materials, transfer length clearly decreases as specimen size increases—average normalized l_t in the smallest specimens was approximately double that of the largest specimens. This corroborates the findings of Russell and Burns (1993) that larger specimens produce shorter transfer lengths as a result of larger specimens' ability to absorb more energy upon strand release. Because full-scale transfer lengths are likely to be shorter than those

measured in smaller experimental specimens, it is concluded that any findings regarding the transfer length of SCC determined using small specimens are likely to be conservative for larger specimens of similar material properties.

Upon further evaluation using measured E_{ci} (Equation 4-9) the same trend with specimen size was apparent, but the difference between SCC and VC was less noticeable than in Table 4.2. This trend is illustrated in Figure 4.12 and in Table 4.3. In the figure and table, α' is a unitless constant equal to 10^{-3} (per Equation 4-9 when using E_{ci} as the measured dependent variable $Y_{measured}$).

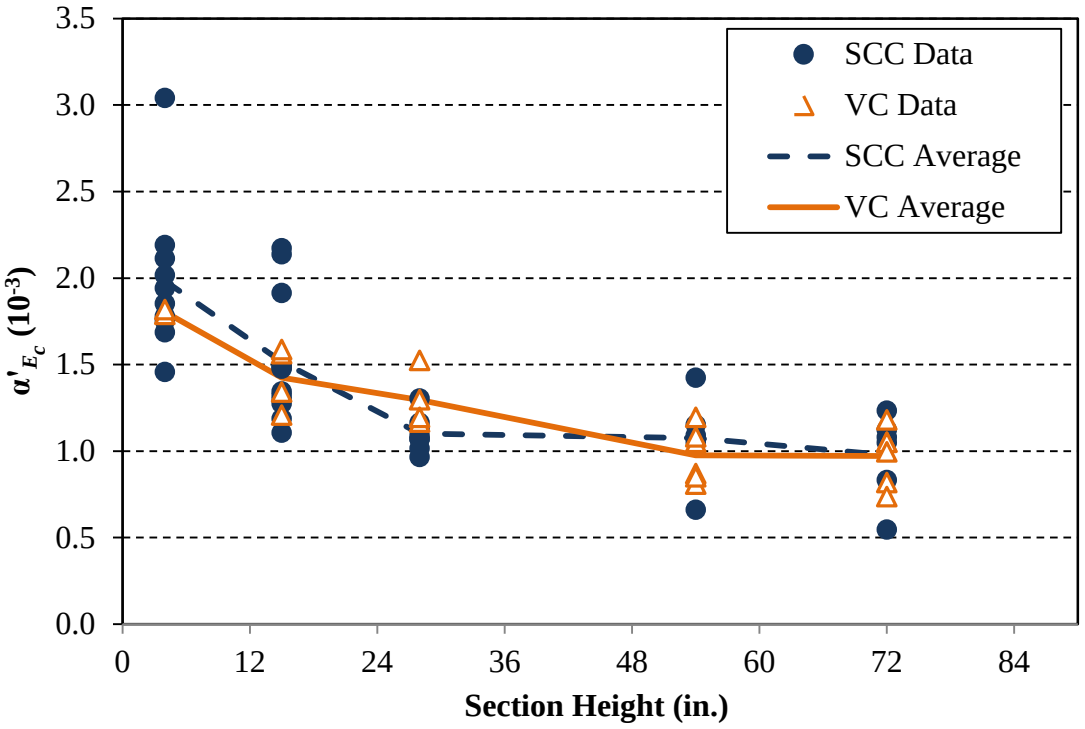

Figure 4.12: Comparison of SCC and VC normalized α' values by section height

Table 4.3: Summary of alternatively normalized transfer lengths in AL concrete

Study	Specimen Description and Height (in.)	Average Values		
		α'_{SCC} (10^{-3} ksi/ksi)	α'_{VC} (10^{-3} ksi/ksi)	$\alpha'_{SCC}/\alpha'_{VC}$
Swords 2005	**Prisms (4 in.)**	1.98	1.80	1.10
Levy 2007	**T-Beams (15 in.)**	1.52	1.42	1.06
Boehm et al. 2010	**AASHTO Type I (28 in.)**	1.10	1.30	0.85
Current Study	**Bulb-Tees (54, 72 in.)**	0.99	0.94	1.05

As discussed earlier regarding the full-scale girder results from the current study, these ranges (SCC results equaled 0.85–1.10 of average VC results) could be explained by the precision and variability of the measurements. Thus, it is concluded based on the data presented in this section that the effect of specimen size is more significant than the difference observed between the tested SCC and VC during each of these projects. While longer transfer lengths were present in some of the tested SCC specimens, the difference appears to be largely attributable to differences in E_{ci} that can occur between *any* concretes of different mixture proportions.

4.4.1.3 Effect of Orientation

Normalized transfer lengths could also be compared relative to casting order (1st or 2nd end) and bed orientation (internal or external end). Because BT-72 and BT-54 results were not statistically different in this project, comparisons are of the normalized α values that account for strand diameter. Comparisons of fully bonded transfer zones that were exactly identical with regard to girder size, casting order, and bed orientation are presented in Table 4.4. While zone identifications alone can be used to identify the unique comparisons, status as the 1st or 2nd end cast (-1 or -2) and external or internal end on the prestressing bed (-E or -I) is labeled for clarity.

Table 4.4: Comparison of identical SCC and VC transfer zones

Transfer Zones		1st or 2nd Cast	Exterior or Interior	α_{SCC}/α_{VC}
SCC	**VC**			
54-2S-1-E **54-4S-1-E** **54-7S-1-E**	**54-2V-1-E** **54-4V-1-E**	1	E	1.25
72-4S-1-E **72-7S-1-E**	**72-4V-1-E** **72-7V-1-E**	1	E	1.31
-	**54-7V-1-I**	1	I	-
72-2S-1-I	**72-2V-1-I**	1	I	1.66
-	**54-7V-2-E**	2	E	-
72-2S-2-E	**72-2V-2-E**	2	E	1.07
54-2S-2-I **54-4S-2-I** **54-7S-2-I**	**54-2V-2-I** **54-4V-2-I**	2	I	1.26
72-4S-2-I **72-7S-2-I**	**72-4V-2-I** **72-7V-2-I**	2	I	0.84

Note: - = no matching transfer zones

Within the above unique comparisons, SCC α was, on average, 23% greater than that of the directly comparable VC. This is very similar to 18% relative increase in SCC l_t that was discussed in reference to Table 4.1, and the difference could be explained by the smaller sample sizes present upon subdividing results this finely. There was high variability of these unique comparisons and no patterns were easily detectable, so broader grouping of all zones by casting order *or* bed orientation could provide better insight regarding their effects on l_t.

Several previous studies have shown that transfer methods that create live and dead ends noticeably affect transfer length (see discussion of Section 4.2.1), and Hamilton et al. (2005) suggested that the same trend occurs where longer exposed lengths of strand are present. To test this, the measured values were regrouped according to bed orientation (recall that exterior-end zones were always placed next to much longer exposed lengths of strand). Average results are presented below in Table 4.5, and individual results are presented by Keske (2014).

Table 4.5: Comparison of exterior and interior transfer zones

Transfer Zone	Average α	Exterior /Interior
SCC, Exterior Ends	0.54	1.32
SCC, Interior Ends	0.41	
VC, Exterior Ends	0.45	1.28
VC, Interior Ends	0.35	

As shown in the above table, external-end transfer lengths were approximately 30% longer than those in interior-end transfer zones, in both materials. The statistical significance of this bed-orientation effect was also determined in both materials at a 95% CI: P-values equaled 0.0316 and 0.0034 in SCC and VC, respectively. However, while the effect of bed orientation (and exposed strand length) is significant, SCC did not appear to be differently affected by the phenomenon.

This agrees with the finding of Hamilton et al. (2005) that transfer length is noticeably affected by the exposed strand length, although application of their observation is different—while debonded transfer lengths were shorter in this research than fully bonded transfer lengths, fully bonded l_t was distinctly affected by exposed strand length. Meanwhile, the shorter debonded strand transfer lengths were likely a result of variables discussed earlier such as friction within the debonding sheathing over the 120 in. of debonding at each girder end.

Because exposed strand length was a significant variable, evaluation of the effect of casting direction (and the half-hour difference in concrete age between girder ends) could only be evaluated after considering bed orientation. Thus, Table 4.6 includes results subdivided such that comparisons illustrate whether the statistically significant bed-orientation effect (which occurred in both SCC and VC) was different when also considering casting order. In other words, the effect of casting order must be inferred from whether the severity of the bed-orientation effect is different among transfer lengths at the first end cast versus those at the second end cast.

Table 4.6: Comparison of normalized transfer length by bed orientation and casting order

Zone	Average α Results and Ratios		
	SCC	VC	All Concrete
1-E	0.55	0.43	0.49
2-I	0.39	0.37	0.38
E/I	*1.39*	*1.16*	*1.29*
1-I	0.50	0.33	0.38
2-E	0.51	0.50	0.51
E/I	*1.03*	*1.53*	*1.32*

If casting order (and age difference between girder ends) had no effect, the four ratios of external-to-internal results shown above would approximately equal the effect observed due only to bed orientation (approximately 1.3). They do not (ranging 1.03–1.53), but the variability may be due to the limited sample size—in only one SCC girder was the first end cast also an interior end (bottom left comparison in the table). The "All Concrete" ratios presented in the table reinforce this sampling phenomenon: once sample size was increased, the bed-orientation effect was the same regardless of whether the exterior end was cast first or second.

Considering the variability of these four ratios and that the largest ratio occurred in VC (in girders where the exterior ends were also cast second), the results shown in Table 4.6 illustrate that SCC transfer bond is no more greatly affected by casting sequence than is VC transfer bond. Instead, the effect of bed orientation appears to be more significant: regardless of which end was cast first, exterior ends generally exhibited longer transfer lengths, in both materials.

Based on the results discussed in this section related to bed orientation and casting sequence, it is concluded that the difference between SCC and VC transfer length is less important than the variability caused by the full-scale construction process and transfer mechanism. This agrees with the findings of Hamilton et al. (2005) and Staton et al. (2009). Transfer lengths in both materials were significantly affected by bed orientation and may have been somewhat affected by casting order, but neither of these effects was more pronounced in SCC than in VC.

4.4.1.4 Effect of Other Variables

In addition to specimen size, bed orientation, and casting order, several other variables may have affected the observed transfer bond behavior:

- Average age at the time of transfer, which would affect the bond behavior of both SCC and VC,

- Admixture (VMA or HRWRA) use or dosage, which would affect SCC bond differently because the SCC was proportioned with greater amounts of HRWRA and varying dosages of VMA (see Table 3.1),
- Fresh concrete workability, as indicated by either the slump test when using VC or the slump flow test when using SCC, or
- Fresh SCC stability, which was tested daily (see Section 3.3.3.1).

It was difficult to isolate the effects of each of these variables, especially considering the inherent variability of the transfer length measurements. Analyses indicate that average age at the time of transfer and workability did not independently affect l_t in either material. It was impossible to completely rule out the effect of the *presence* of VMA on l_t in this project since the tested SCC always contained VMA while the VC contained none, but there is no evidence that the *quantity* of VMA included in the SCC had any effect on l_t. The amount of VMA used in the SCC BT-72s was doubled from the amount used in the BT-54 (see Table 3.1), but transfer lengths were insignificantly different in the BT-72 girders (see Section 4.4.1.2).

Recall from Section 4.4.1.1 that differences in E_{ci} appeared to explain the majority of the difference between SCC and VC transfer length observed in this project. While the remainder of the difference may have been a consequence of the presence of VMA in the SCC, fresh concrete stability may play an equally important role considering the findings presented in Chapter 2. It was impossible to isolate and test the batches of concrete placed at each transfer zone, but comparison of mid-production stability results (see Section 3.3.3) and girder-average transfer length results should indicate general trends.

Among the five fresh SCC stability tests conducted, the surface settlement test results correlated most strongly with SCC l_t. The rate of settlement and maximum settlement determined during the test were equally well correlated with l_t (R^2 equaled 0.56 and 0.54, respectively). The relationship between rate of settlement and transfer length is shown below in Figure 4.13. Per the earlier discussion that BT-54 and BT-72 results were not significantly different, these results are combined in the figure.

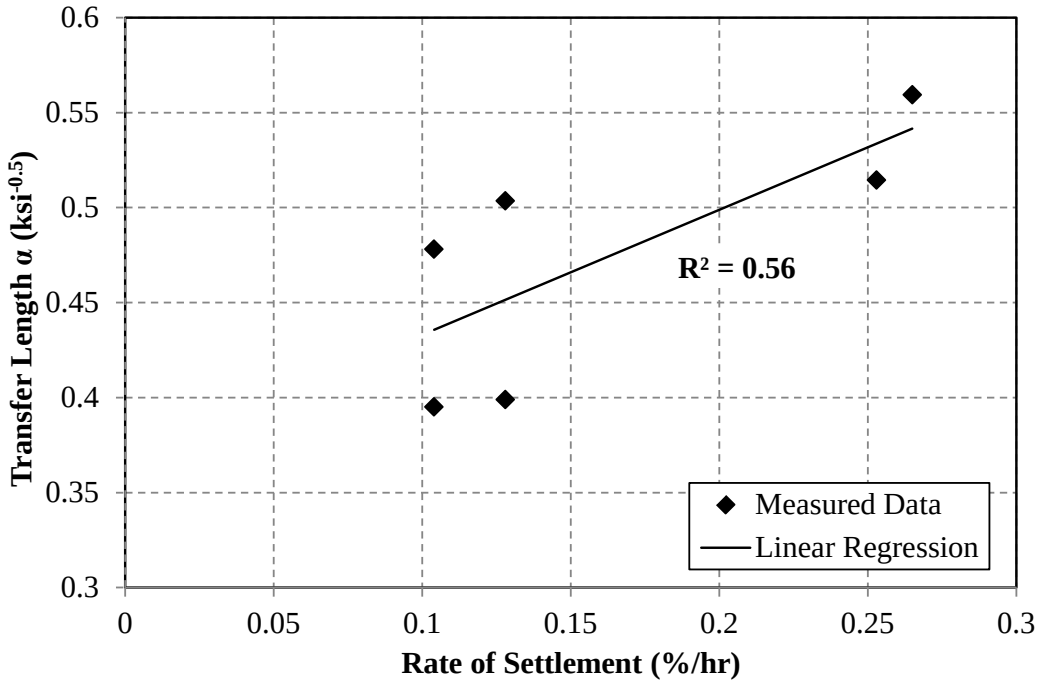

Figure 4.13: Correlation between rate of settlement and normalized SCC transfer length

The correlation shown in the above figure, which is at least as strong as the relationships discussed in Chapter 2, illustrates that SCC stability may affect bond behavior. The observed variability of these l_t results and in f_{ci} and E_{ci} must be considered, though—f_{ci} varied by as much as 2,000 psi between SCC production days only as a result of differences in the age at transfer. Therefore, it is concluded that the impact of fresh stability and the presence of VMA on l_t was minor relative to the variability due only to typical construction practices.

4.4.2 Comparison of Measured and Predicted Transfer Length

In contrast to the results analyzed in the previous section, comparisons to code provisions are based directly on the measured transfer lengths shown in Table 4.1. Most of the transfer-length prediction equations discussed earlier (Equations 4-2 through 4-4) do not account for concrete strength or prestress intensity in the determination of l_t. Ratios of the measured results to those predicted by Equations 4-2 through 4-4 are summarized below in Table 4.7. In the table, ratios less than 1.0 indicate that measured transfer lengths were shorter than predicted. Also, measured results are compared to those predicted using the expressions recommended by Barnes et al. (2003) and Levy (2007) because they (Barnes et al. 2003; Levy 2007) reported l_t in terms of the same constant of proportionality used in this research. Barnes et al. (2003) stated that transfer lengths in simultaneously released girders are more comparable to those at the dead

end of suddenly released specimens, so the dead-end α recommended by Levy (2007) is considered in the table.

Table 4.7: Comparison of measured and predicted transfer lengths

Prediction Method		Average Measured / Predicted l_t			
Equation	Source	Fully Bonded		Debonded	
		SCC	VC	SCC	VC
Equation 4-2	**ACI 318 (2011)**	0.57	0.48	0.46	0.40
Equation 4-3	**ACI 318 (2011)**	0.62	0.53	0.51	0.44
Equation 4-4	**AASHTO (2013)**	0.52	0.44	0.42	0.36
α = 0.64 (ksi$^{-0.5}$)	**Levy (2007)**	0.74	0.63	0.63	0.52
α = 0.57 (ksi$^{-0.5}$)	**Barnes et al. (2003)**	0.83	0.71	0.68	0.58

While the transfer lengths in SCC girders were slightly less over-predicted than in the VC girders, average transfer lengths were shorter than predicted by all of the evaluated models. To evaluate the most demanding of these—Equation 4-3 among code-based equations and the expression recommended by Barnes et al. (2003)—the individual transfer lengths are presented in Figure 4.14 and Figure 4.15.

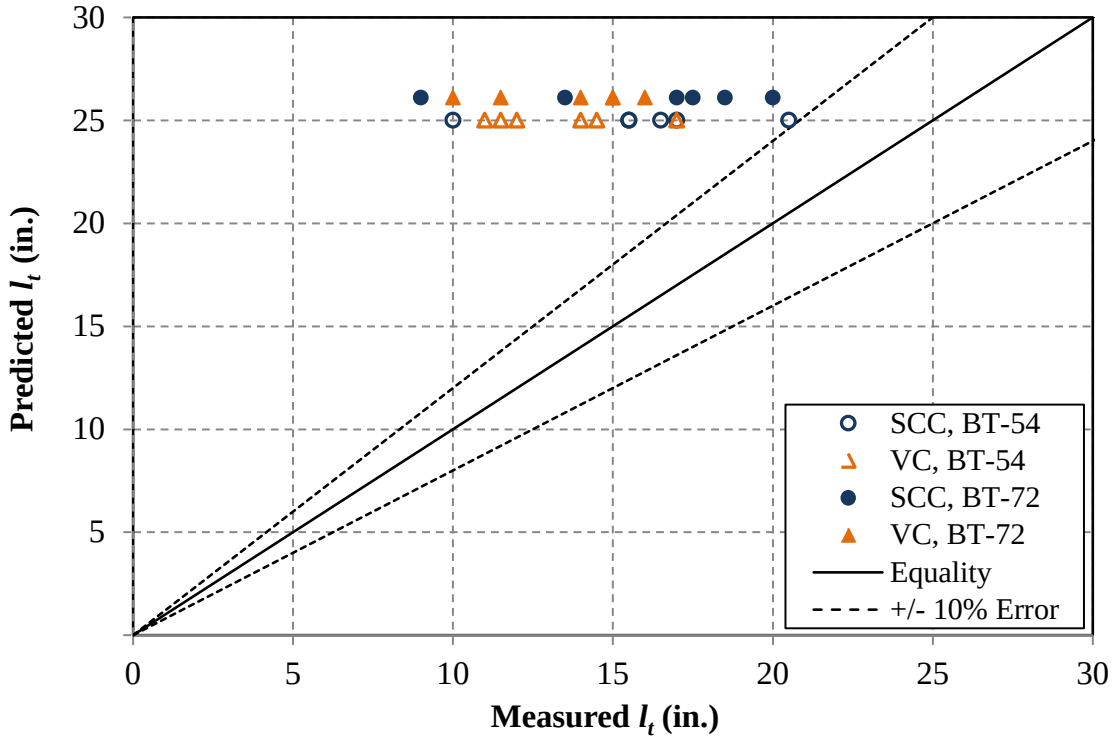

Figure 4.14: Comparison of measured l_t and l_t predicted according to Equation 4-3

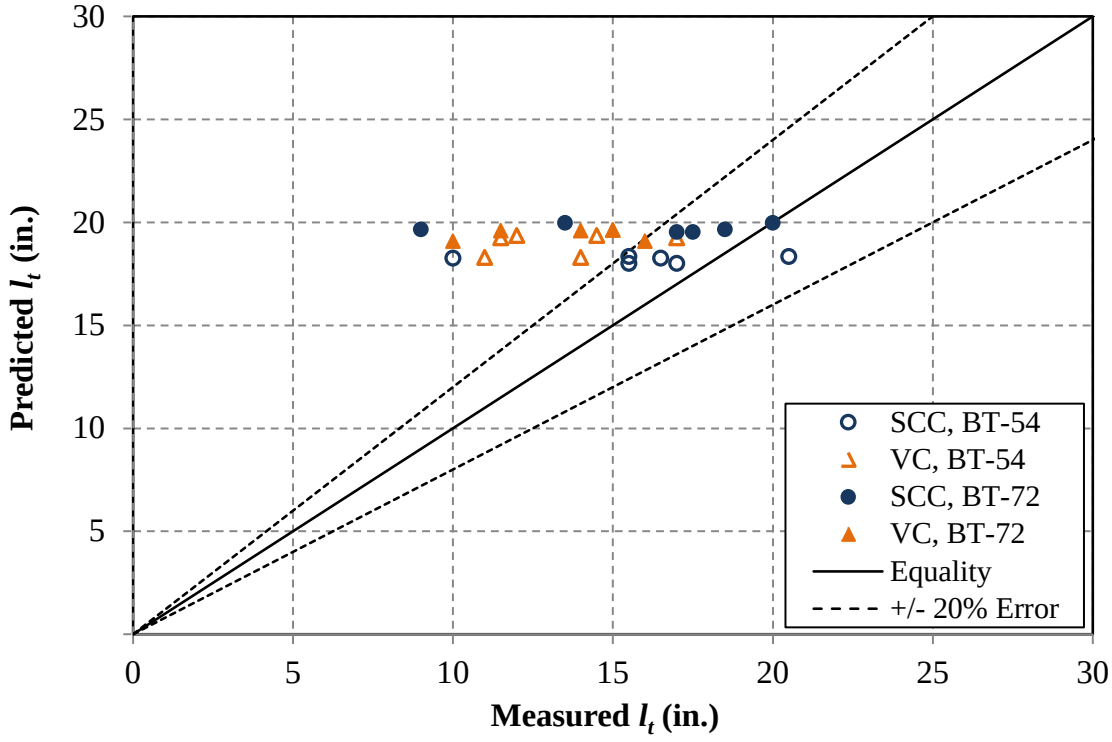

Figure 4.15: Comparison of measured l_t and l_t predicted according to expression proposed by Barnes et al. (2003)

As shown in the figures, no single transfer length at either end of any SCC girder was greater than 0.82 of the transfer length predicted through the use of Equations 4-3, and no VC transfer length was greater than 0.68 of the value predicted by that equation. Meanwhile, only one individual SCC transfer lengths exceeded the upper limit suggested by Barnes et al. (2003)—in 54-4S-1-E, by 12% (approximately 2 in.). No individual VC transfer length exceeded 93% of the upper limit suggested by Barnes et al. (2003).

Notably, the one under-predicted transfer length identified in Figure 4.15 was in the exterior-end zone of a BT-54. It was subjected to the most demanding release mechanism and was of the smaller size tested, which could have significant implications during the production of smaller prestressed specimens. Based on these results and on the findings of Levy (2007) regarding moderate-strength concrete (see Section 4.2.1.3), no changes to the existing predictions are recommended. While the methodology recommended by Levy (2007) and Barnes et al. (2003) provided the best predictions *on average*, the variability of transfer lengths and their dependence on exposed strand length and girder size preclude any reduction in the existing predictions at this time.

4.4.3 Initial Elastic Prestress Losses

In comparisons of initial elastic prestress losses, "measured" responses are those directly based on concrete strains measured in the girders; they do not account for observed differences in concrete properties (such as E_c). While the comparison of measured responses is limited for this reason, it is instructive because the SCC and VC girders were designed to be direct companions in an in-service bridge. Meanwhile, "predicted" responses are those calculated using the iterative approach described in Section 4.2.2.1 in conjunction with the material properties measured in representative cylinders. Comparisons of predicted responses to measured responses are only made *within* each material to assess the predictability of measured responses. Also, because no time-dependent deformation is included in this calculation, no distinction is required between the responses predicted using the three assessed time-dependent deformation models.

In addition to these measured and predicted results, "design" responses are those calculated using Equation 4-5 with design properties (f'_{ci}, f'_c, etc.). Thus, SCC responses were compared to measured VC responses and predicted SCC responses, and measured VC responses were compared to predicted VC responses. All measured and predicted responses were then compared to the design responses (which are equally applicable to SCC and VC responses). Some of these comparisons are summarized below in Figure 4.16 and Table 4.8; the individual girder responses are summarized by Keske (2014).

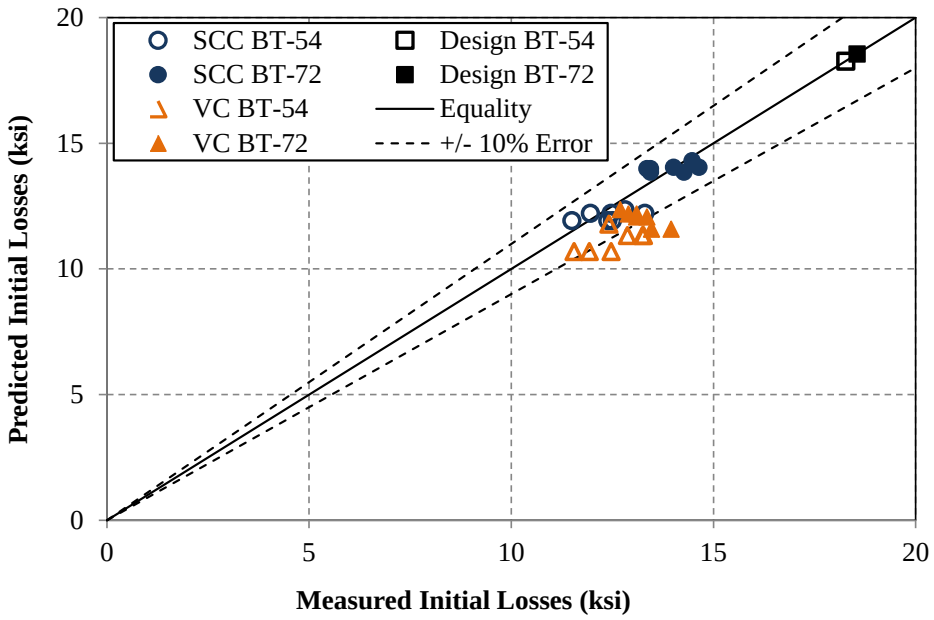

Figure 4.16: Comparison of measured elastic prestress losses and losses predicted from iterative elastic calculation

Table 4.8: Comparison of initial elastic prestress loss

Average Result	Initial Elastic Prestress Loss (ksi)		Measured/ Predicted	SCC/VC Response	
	Measured	Predicted		Measured	Predicted
54-S	-12.4	-12.1	1.03	0.99	1.09
54-V	-12.5	-11.1	1.13		
72-S	-13.9	-14.0	1.00	1.05	1.17
72-V	-13.2	-12.0	1.10		
SCC	-	-	1.01	1.02	1.13
VC	**-**	**-**	1.12		

In the above table, elastic prestress losses in response to the transfer mechanism were based on concrete strains directly measured at the midspan *cgp* and those predicted using Equation 4-5 were based on the measured material properties. Almost all measured losses were greater than predicted based on measured properties (by an average of 6%). However, SCC girders regularly exhibited more predictable losses using measured E_{ci} than did VC girders relative to measured E_{ci}—measured SCC losses were 101% of predicted losses, on average, versus 112% in the VC girders.

While SCC girders were predicted to experience 9–17% more losses than the companion VC girders based on measured properties (see "Predicted" in the table), they actually maintained

approximately as much effective prestress as directly measured in the VC girders (see "Measured" in the table). The difference in measured responses, an average of 0.3 ksi of effective prestress, is practically insignificant, representing a difference of less than 0.2% of f_{pbt}. From these observations, several conclusions are warranted:

- SCC-girder elastic prestress loss due to prestress transfer is at least as accurately predicted as in VC girders when using measured material properties, and
- Because SCC-girder elastic prestress responses to prestress transfer were consistently less than expected of VC girders of the same E_{ci}, SCC prestress-transfer behavior is acceptably similar to that of VC.

For context, the elastic prestress loss assumed during design was calculated according to Equation 4-5 in conjunction with the specified f'_{ci} and the E_{ci} calculated using Equation 3-4. Design initial losses equaled 18.3 and 18.6 ksi for BT-54s and BT-72s, respectively. These responses, which are also shown in Figure 4.16, are approximately 5.5 ksi greater in magnitude than the losses *measured* in either material and 5–7 ksi greater in magnitude than the losses *predicted* based on measured mechanical properties.

Two conclusions are drawn from these results: 1) the difference in the predictability of SCC behavior relative to that of VC behavior when using measured material properties is minor, and 2) design predictions can be conservative when calculated using design properties in place of expected material properties. The 5.5 ksi difference between measured-property and design initial elastic prestress loss calculations represents approximately 2.7% of f_{pbt}. However, the difference directly relates to the over-prediction of prestress losses discussed in Chapter 6 when using design properties, as time-dependent losses are calculated as an amplification of the elastic strain response (per the creep coefficient).

4.5 SUMMARY AND CONCLUSIONS

4.5.1 Summary

To better understand the prestress transfer behavior of SCC used in precast, prestressed applications, the bond of fully bonded and partially debonded strands were evaluated in twelve SCC and VC girders used to construct the Hillabee Creek Bridge, and elastic changes in prestress were measured in all twenty-eight girders for the bridge. Transfer length was calculated after measuring concrete surface strains at the bottom flange and applying the 95% AMS method of transfer length calculation described elsewhere (Dunham 2011); elastic prestress loss was calculated after measuring concrete strain changes at the midspan *cgp*. By testing multiple girders produced with essentially the same mixtures, valuable insights were gained regarding the

variability of measured results the dependence of l_t and Δf_{pES} on factors including mechanical properties, girder size, orientation in the prestressing plant, and SCC stability.

SCC transfer lengths normalized for $\sqrt{f_{ci}}$ or E_{ci}, prestress force, and strand diameter were evaluated both in relation to the companion VC girders used in the bridge and in relation to previous phases of this research conducted with smaller specimens. The full-scale girder values were also compared to current prediction models proposed by ACI 318 (2011) and AASHTO (2013) and to more refined estimates proposed by Barnes et al. (2003) and Levy (2007). Measured prestress losses were evaluated in relation to the companion VC girders as well as to the current model proposed by AASHTO (2013). The observations and conclusions made concerning the transfer behavior of the SCC and VC girders used in the Hillabee Creek Bridge are summarized in Section 4.5.2. That section includes conclusions regarding the effect of several variables and the applicability of the current prediction methods. The recommendations made based on this research are then given in Section 4.5.3.

4.5.2 Observations and Conclusions

4.5.2.1 Measured Transfer Length

- After normalizing for f_{pt}, d_b, and $\sqrt{f_{ci}}$, SCC transfer lengths were approximately 18% greater than those of the equivalent-strength companion VC girders in both fully bonded and partially debonded strands.
- Transfer lengths of partially debonded strands in both SCC and VC were less than those of fully bonded strands in directly adjacent fully bonded zones (approximately 90% of the associated fully bonded l_t).
- The increased transfer lengths of the SCC girders were likely related to the reduced stiffness of the utilized SCC.
- After normalizing transfer lengths for f_{pt}, d_b, and E_{ci} to remove the assumption of correlation to the square root of f_{ci}, SCC transfer lengths were approximately 5% longer than comparable VC transfer lengths. This suggests that differences in l_t are not uniquely associated with the use of SCC—the difference should occur in any two concretes whose E_{ci} differs relative to $\sqrt{f_{ci}}$.
- Normalization for E_{ci} accounted for the majority of the difference between SCC and VC l_t but normalization for f_{ct} did not appear to affect it. It is unclear whether the lack of correlation to f_{ct} is due to testing variability (of f_{ct} or l_t), a difference in tensile behavior of the concrete in response to confinement, or a greater bond dependence on elastic concrete stiffness (E_{ci}) than on tensile capacity (f_{ct}).

- By comparing normalized l_t between phases of AUHRC research in which very similar concrete mixtures were used, it was shown that specimen size has a distinct effect on l_t—transfer length decreased as specimen size increased. The observed size effect corroborates the conclusion of Russell and Burns (1993) that larger specimens exhibit shorter l_t because they are better able to absorb the kinetic energy of released strands.
- SCC was insignificantly different than VC in all associated AUHRC projects after accounting for E_{ci} directly—SCC values were approximately 0.85–1.10 of comparable VC values in these projects. Considering the size effect and effect of E_{ci}, recommendations for l_t that are based on tests of small specimens or less stiff concrete are likely to be conservative.
- The most significant factor affecting l_t appeared to be girder orientation in the prestressing bed—transfer zones adjacent to longer exposed lengths of strand (near the ends of the prestressing bed) produced approximately 30% longer transfer lengths than those adjacent to short exposed lengths of strand (between girders cast in the same production line) in both SCC and VC.
- Casting sequence had no greater effect on l_t in SCC than on l_t in VC girders—exterior ends exhibited longer transfer lengths than interior ends, regardless of which was cast first.
- The dosage of VMA incorporated in the SCC had no effect on transfer length—VMA dosage was doubled in BT-72 girders, but the BT-72s regularly exhibited shorter normalized l_t. This contradicts the claim of Girgis and Tuan (2005) that increasing the dosage of VMA leads to longer l_t.
- Neither age at transfer or concrete workability (slump or slump flow) correlated well with l_t, but SCC fresh stability did. However, these variables could not be evaluated independently, and all appeared to be insignificant relative to the effects of bed orientation and girder size.
- Improvements in fresh SCC stability are likely to lead to shorter l_t, but the effect was minor considering that all tested SCC exhibited acceptable stability.
- Similar to previous suggestions (Hamilton et al. 2005; Staton et al. 2009), the difference between SCC and VC appears to be less significant than the variation inherent to the full-scale construction process and transfer mechanism.

4.5.2.2 Prediction of Transfer Length

- All prediction methods assessed—two equations presented in ACI 318 (2011) and one presented in the *AASHTO LRFD* guidelines (2013)—were used to conservatively predict l_t in both materials.
- Although SCC l_t was slightly less over-predicted by the code-based models than VC l_t, no single SCC transfer length exceeded 0.82 of the value predicted using these codes.
- No VC transfer length was greater than 0.68 of any code-based prediction.
- Models proposed by Barnes et al. (2003) and Levy (2007) were more accurate and still conservative, on average, at predicting l_t than were the code-based models. However, one individual SCC transfer length exceeded the upper limit suggested by Barnes et al. (2003) by 12% (approximately 2 in.).
- No individual VC transfer length exceeded 93% of the upper limit suggested by Barnes et al. (2003).
- All of the least conservatively predicted transfer lengths were in exterior-end zones, and more BT-54 results approached the upper limits than did BT-72 results.

4.5.2.3 Initial Elastic Prestress Loss

- Almost all girders exhibited greater elastic deformation than predicted in response to the transfer mechanism (by an average of 6%). SCC-girder elastic deformations were approximately 1% greater than predicted when considering the SCC E_{ci}, while VC deformations were approximately 12% greater than predicted.
- SCC-girder elastic prestress losses at the time of prestress transfer were expected to be approximately 9–17% greater than in geometrically identical VC girders based on differences in measured material properties. Measured SCC losses at transfer were approximately 0.3 ksi greater in magnitude than in the companion VC girders, which was well within the precision of this testing.
- Considering these results, SCC-girder elastic prestress loss due to prestress transfer was at least as accurately predicted as that of VC girders when using measured material properties.
- Average measured losses due to prestress transfer (in both materials) were approximately 5 ksi less in magnitude than design estimates (indicating conservative behavior). Considering this, SCC-girder prestress-transfer behavior is acceptably similar to that of VC girders and is at least as conservatively predictable.

4.5.3 Recommendations

- Concerns about the full-scale bond behavior of SCC should not restrict the implementation of SCC in precast, prestressed applications. SCC transfer lengths measured in full-scale girders appear to be conservatively predictable and acceptably similar to those in companion, equivalent-strength VC girders.
- Based on these results and on the findings of Levy (2007) regarding moderate-strength Alabama concrete, no changes to the existing design predictions are recommended at this time. While the methodology recommended by Barnes et al. (2003) and Levy (2007) provided the best predictions *on average*, the variability of transfer lengths and their dependence on exposed strand length and girder size preclude any reduction in the existing predictions.
- Concerns about the elastic-response transfer behavior of SCC in full-scale precast, prestressed girders should not restrict the implementation of the material in that type of construction. Measured initial elastic prestress losses were essentially identical in companion SCC and VC girders and were conservatively predictable based on measured mechanical properties.
- The difference between predictions that incorporated measured properties and those based on design properties was larger than the difference between measured or expected SCC and VC responses. Further research concerning the discrepancy between measured transfer responses and the responses that would be predicted during design may be of value.

CHAPTER 5: TIME-DEPENDENT DEFORMABILITY OF PRECAST, PRESTRESSED CONCRETE

5.1 INTRODUCTION

Self-consolidating concrete can exhibit different time-dependent deformation tendencies than VC of the same compressive strength or intended use because it frequently incorporates different constituent proportions than VC. Time-dependent deformation of concrete is considered in two parts: creep, or the time-dependent increase in strain under a sustained compressive load, and shrinkage, or the time-dependent, load-independent contraction due to drying and hydration of concrete.

Drying shrinkage occurs as water escapes concrete due to a difference between its internal humidity and the surrounding relative humidity. Shrinkage due to the chemical hydration of portland cement, which can occur even in concrete exposed to 100% relative humidity, is referred to as autogenous shrinkage. It is impossible to distinguish between autogenous and drying shrinkage in a particular concrete without exposing matching specimens to both 100% relative humidity and ambient relative humidity conditions, so the two are frequently grouped together and termed “free shrinkage” (Neville 1996; Mindess et al. 2003). Furthermore, creep has been found to increase in concrete exposed to both sustained stress and drying at the same time. While creep can thus be classified as basic creep or drying creep, it is common practice to ignore the distinction and consider creep to equal the deformation under load in excess of the sum of the initial elastic strain and accumulated free shrinkage strain (Mehta and Monteiro 2006).

While the underlying mechanisms are complicated, the effects of creep and shrinkage are direct—they induce concrete length change. Depending on restraint and loading conditions, this can lead to stress development, cracking, and changes in deflections in concrete structures. In prestressed members, these length changes also result in a change in length of the prestressing tendons which directly relates to maintenance of prestress force—prestress force decreases as the strands and the surrounding concrete contract. Because of this dependence, accurate prediction of long-term time-dependent deformation is crucial in the design of prestressed structures (Khayat and Mitchell 2009).

Many of the deformation prediction models currently in use are based on outdated research and were formulated using assumptions that may no longer be valid in current practice. The applicability of these models to SCC behavior is especially questionable. To address this, the AUHRC team evaluated time-dependent deformability of the SCC and VC used to construct the Hillabee Creek Bridge. This evaluation was completed using specimens cast during production days SCC-B, SCC-C, SCC-E, VC-B, and VC-F, thus including batches of the same

mixtures that had been produced under varied exposure conditions. The primary objective of this work was to evaluate the acceptability and relative predictability of precast, prestressed SCC and VC time-dependent deformability.

5.2 LITERATURE REVIEW

Volumetric change of concrete over time is an inherent property of the material, and it is influenced by a variety of factors that are interdependent. From ACI 209 (1992), some of these influences include

- Concrete composition including paste content, *w/cm*, and aggregate type,
- Environmental conditions such as ambient humidity, in which less contraction is experienced when a higher relative humidity is maintained,
- Geometric member properties including volume-to-surface-area ratio (*V/S*), in which decreasing *V/S* leads to increasing deformation, and
- Stress state, in which stress concentrations or inelastic-level stresses cause less predictable deformation responses.

In this research, the primary differences between the studied SCC and VC involve only the first of these—changes in mixture materials and proportions incorporated to yield self-consolidating behavior. While the other factors are significant, they were approximately the same for both materials. Specimens of SCC and VC were always geometrically identical, they were each loaded proportionally to f_c, and they were all exposed to very similar ambient conditions in the field or in controlled environmental conditions maintained for standardized assessment.

Differences in volumetric-change behavior can be evaluated either by observing structural behaviors that are affected by the volumetric change or by measuring volumetric changes in representative samples. Literature concerning the time-dependent *material* behavior of concrete is reviewed in the following sections, and the effect of time-dependent deformation on structural performance of full-scale girders is discussed in Chapter 6.

5.2.1 Creep and Shrinkage of Self-Consolidating Concrete

In concrete, irreversible decreases in volume over time take place in the paste phase (cementitious material and water), while aggregate experiences almost no volumetric change and acts to restrain the contraction of the paste (Mehta and Monteiro 2006; Mindess et al. 2003; Neville 1996). Thus, greater time-dependent volumetric change is expected in concrete mixtures with greater paste volumes (Neville 1996; Mehta and Monteiro 2006). This dependence on paste

volume has been widely cited as the main reason that SCC may exhibit more time-dependent deformation than VC (EPG 2005; *fib* 2010; Koehler et al. 2008; Naito et al. 2005; Ziehl et al. 2009).

Results have been inconsistent concerning the influence of SCMs, such as fly ash and slag cement, on time-dependent deformability. Some researchers (Khayat 1999; Raghavan et al. 2002; Schindler et al. 2007) found deformability to be reduced through the use of SCMs, while others (Horta 2005; Khayat and Mitchell 2009) found that it was increased. The effects of SCMs at least partly relate to the delayed strength gain associated with their use (Mehta and Monteiro 2006; Mindess et al. 2003). Compliance (strain per unit of stress) has been found to be inversely proportional to the strength of concrete at the time of load application over a wide range of strengths. Because SCMs such as slag cement tend to delay strength gain, concrete made with SCMs may exhibit greater early-age deformability (Peirard et al. 2005; Ziehl et al. 2009). Pierard et al. (2005) further found that slag cement (which was utilized in this project) also affects the load-independent free shrinkage behavior of concrete by delaying and prolonging drying.

The effect of aggregate on time-dependent deformability is two-fold: increasing aggregate content coincides with a reduction in the paste volume of the concrete (thus indirectly reducing the potential for time-dependent deformation), and it directly relates to the stiffness of the material. Its contribution to E_c was discussed in detail in Chapter 3, and its effect on creep and shrinkage is similar—use of stiff aggregate restrains the volumetric deformation of the material (Mehta and Monteiro 2006). Therefore, SCC is expected to exhibit greater deformability when the volume of stiff coarse aggregate is reduced in the mixture (Khayat and Mitchell 2009; Koehler et al. 2007; Zia et al. 2005).

Similar to the effect of *s/agg* on E_c, Koehler et al. (2007) and Schindler et al. (2007) found that *s/agg* had essentially no effect on time-dependent deformability. Trejo et al. (2008), who worked with Koehler et al. (2007), hypothesize that the effect of *s/agg* on time-dependent deformability is minimized when elastic properties of the coarse and fine aggregates are similar. Ziehl et al. (2009) further found that SCC time-dependent properties were improved by the use of a larger *s/agg* because a weak coarse aggregate was incorporated in all mixtures tested during that research. Conflicting with these findings, Khayat and Mitchell found that increasing *s/agg* directly contributed to increased free shrinkage but had minimal effect on creep behavior.

Mehta and Monteiro (2006) and Neville (1996) conclude that f_c is strongly related to creep and shrinkage, both for direct and indirect reasons. Higher f_c may be achieved through the use of a lower *w/cm* or by other means, such as by increasing the content of high-quality aggregate. Reducing *w/cm* reduces water availability (which directly reduces creep and shrinkage), while the effects of increasing aggregate content have previously been discussed. Specifically regarding shrinkage, reducing *w/cm* increases autogenous shrinkage while reducing drying shrinkage. Thus, the effects of these changes on total free shrinkage depends upon the mixture.

Many underlying factors affect f_c (some of which are discussed in Chapter 3), and it is difficult to change one mixture variable without affecting others. For example, reducing the *w/cm* while keeping the cement content constant reduces the paste *volume* (because less water is used). This volumetric reduction (at a constant cement content) is offset by increasing the aggregate content.

Because mixture proportioning can be varied in many ways to produce concretes of similar mechanical properties (f_c or E_c), findings regarding SCC creep and shrinkage versus those of vibrated concrete have been inconsistent. The current European Model Code (*fib* 2010) notes in Sections 5.1.9.4.3 and 5.1.9.4.4 that SCC may exhibit 10–20% greater creep deformation and 20% greater shrinkage due to its increased paste content but that "deformations are within the scatter band for ordinary structural concrete, which is defined to be ±30%." This accepted level of precision is important when considering the accuracy of the prediction models described in Sections 5.2.2 and 5.2.3.

5.2.2 Creep Prediction Methods

Four current creep prediction models were selected for evaluation in this research. They include the model proposed by the ACI Committee for Creep and Shrinkage in Concrete (ACI 209 1992), the current model from Section 5.4.2.3.2 of *AASHTO LRFD* 6th Edition (AASHTO 2013), the SCC-specific adaptation of the AASHTO provisions developed by Khayat and Mitchell (2009), and the current model used in the European Model Code (*fib* 2010). These are referred to as the ACI 209, AASHTO 2013, NCHRP 628, and MC 2010 models, respectively, in the following subsections.

Several other creep prediction models, including older versions of the models used by AASHTO and *fib*, exist in the literature. These models were excluded from this report for several reasons:

1. They are outdated and are not regularly specified (especially among codes in which a more recent version of the same model has been implemented),
2. They are of little value to ALDOT, the chief sponsor of this research for whom these findings were prepared, due to the prevalence of the *AASHTO LRFD* specification, and
3. They were found to be no more accurate during other past studies of Alabama SCC creep conducted by Kavanaugh (2008) and Kamgang (2013).

5.2.2.1 ACI 209

The ACI Committee for Creep and Shrinkage of Concrete (ACI 209) has recommended the same creep prediction model since publishing its report on the topic in 1992 (*Prediction of Creep,*

Shrinkage, and Temperature Effects in Concrete Structures). The prediction method yields an ultimate creep coefficient, v_u, which is adjusted to account for mixture properties, loading age, specimen geometry, and environmental conditions. Defined as the ratio of creep strain to initial elastic strain resulting from the application of load, the ultimate creep coefficient is computed by the following equation:

$$v_u = 2.35(\gamma_{la}\,\gamma_\lambda\,\gamma_{vs}\,\gamma_\psi\,\gamma_s\,\gamma_a) \tag{5-1}$$

Where

γ_{la} is the loading age correction factor,
γ_λ is the relative humidity correction factor,
γ_{vs} is the volume-to-surface-area ratio correction factor,
γ_ψ is the fine aggregate percentage correction factor,
γ_s is the slump correction factor, and
γ_a is the air content correction factor.

The correction factors seen in Equation 5-1 are applied to the standard ultimate creep coefficient (2.35 in the equation) to account for conditions other than standard concrete composition and conditions. The derivations of these correction factors are given in ACI 209 (1992) and are discussed in relation to this project by Ellis (2012). Notable among them are γ_ψ and γ_s, which could have specific implications for SCC. Of the four creep prediction methods evaluated in this research, ACI 209 is the only method that specifically accounts for fine aggregate content or slump (water content).

Fine aggregate content was directly accounted for using the mixture proportions shown in Table 3.1. Meanwhile, the ACI 209 creep prediction method was developed before the introduction of HRWRA (and HRWRA-induced slumps or slump flows). Therefore, slump values had to be adjusted to account for the high admixture-induced slumps that occurred in these prestress-suitable mixtures. In past AUHRC research (Kamgang 2013; Kavanaugh 2008), an equivalent wet slump of 0.0 in. was chosen for SCC mixtures and a slump of 0.5 in. was chosen for prestress-suitable VC mixtures when determining the slump correction factor.

In addition to v_u, ACI 209 accounts for the growth in creep over time using a time-rate function. To ascertain the predicted creep coefficient for intermediate times of interest—such as at the time of girder erection—the ultimate creep coefficient is multiplied by a time parameter, v_t, that accounts for the time elapsed since the load was applied:

$$v_t = \frac{t^{0.6}}{10 + t^{0.6}} \tag{5-2}$$

In Equation 5-2, t is the length of time after loading (in days). After determining the creep coefficient at a given time, $v_u(t)$, the creep strain, ε_{cr}, for a constant load is predicted by multiplying $v_u(t)$ by the initial elastic strain due to that load.

5.2.2.2 AASHTO 2013

The current *AASHTO LRFD* creep prediction method (AASHTO 2013) was first implemented in the 2005 version of the *AASHTO LRFD Bridge Design Specifications*. This method may be used to determine the effects of creep on the loss of prestressing force in bridges that are not segmentally constructed, as discussed in Section 5.9.5.4 of the provisions and in Chapter 6 of this report. It is applicable for specified concrete strengths up to 15,000 psi, and the predicted creep is influenced by the magnitude and duration of the load applied, the maturity of the concrete at loading, and the relative humidity of the concrete. The *AASHTO LRFD* creep coefficient, $\psi(t,t_i)$, is computed using the following equation:

$$\psi(t,t_i) = 1.9(k_{hc}\, k_s\, k_f\, k_{td})t_i^{-0.118} \quad (5\text{-}3)$$

Where

k_{hc} is the relative humidity correction factor,
k_s is the volume-to-surface area ratio correction factor,
k_f is the concrete strength correction factor,
k_{td} is the time development correction factor, and
t_i is the age of the concrete at the time of load application (days).

The time development correction factor, k_{td}, can be used for both precast and cast-in-place concrete components and for accelerated and non-accelerated curing conditions because it is assumed that the load is applied after curing ends. This parameter is given by the following equation:

$$k_{td} = \frac{t}{61 - 4f'_{ci} + t} \quad (5\text{-}4)$$

In Equation 5-4, t is the amount of elapsed time (in days) since application of the sustained load. While the formulation of the above correction factors is different than those of the ACI 209 model, the principles are similar—they account for conditions other than the standard conditions in which the model was calibrated, and they include mixture and exposure conditions typically known by the engineer during design. After determining the creep coefficient, the predicted strain due to creep, ε_{cr}, is obtained by multiplying $\psi(t,t_i)$ by the elastic strain that would result from a given load.

5.2.2.3 NCHRP 628

The NCHRP 628 model was developed as part of the National Cooperative Highway Research Program (NCHRP) Project 18-12 (Khayat and Mitchell 2009). Objectives of the project were to develop guidelines for the use of SCC in precast, prestressed concrete bridge elements and to

recommend relevant changes to *AASHTO LRFD Bridge Design* and *Construction Specifications*. This model uses the AASHTO 2013 model format; however, it contains a specific modification for SCC, *A*, that depends upon cement type. Thus, the creep coefficient, $\psi(t,t_i)$, is computed according to the following equation:

$$\psi(t,t_i) = 1.9(k_{hc}\, k_s\, k_f\, k_{td})t_i^{-0.118}A \quad (5\text{-}5)$$

In Equation 5-5, *A* equals 1.19 for SCC incorporating Type I/II cement and 1.35 for SCC incorporating Type III cement with a 20% fly ash replacement (Class F fly ash was used during that project). All other factors are the same as those described following Equations 5-3 and 5-4.

While the *A* correction factor accounts for the use of SCC, it was only calibrated for two specific cementitious classes, neither of which was used in this project. Based on the proportions shown in Table 3.1, it was judged that the combination of cementitious materials used to make the SCC in this study is closer to the latter cementitious combination. This cementitious class was also chosen in past AUHRC research (Kamgang 2013) involving concrete mixtures similar to those used in this project.

5.2.2.4 MC 2010

MC 2010 is the latest version of the CEB-FIP Model Code (*fib* 2010), and it is applicable for concretes with f_c up to approximately 18,000 psi. Like the other methods, the MC 2010 method yields an ultimate creep coefficient, φ_o, that includes a coefficient to account for development of creep over time after loading, β_c. The creep coefficient at any intermediate time, $\varphi(t,t_o)$, is computed from

$$\varphi(t,t_o) = \varphi_o[\beta_c(t,t_o)] \quad (5\text{-}5)$$

In Equation 5-5, *t* is the age of concrete at the moment considered (in days) and t_o is the age of concrete at loading. Notably, t_o is based on the maturity-adjusted age at loading considering the curing history to which the concrete was exposed prior to loading. The creep development coefficient, β_c, is similar in nature to Equation 5-2, except that it is also a function of relative humidity. Both φ_o and β_c also incorporate factors to account for compressive strength, maturity-adjusted age at loading, and cement class, all of which are discussed in detail by Ellis (2012).

5.2.3 Shrinkage Prediction Methods

The four references described above also include unique shrinkage prediction models that were evaluated in this research. Like in the previous section, these are referred to as the ACI 209, AASHTO 2013, NCHRP 628, and MC 2010 shrinkage models, respectively, in the following

subsections. More specifically, the AASHTO 2013 provisions allow the use of any one of several methods to predict shrinkage behavior, but the "AASHTO 2013" model assessed comes from Section 5.4.2.3.3 of the provisions. In addition to these four, a fifth model was investigated that is based on a widely accepted European code—the *Eurocode 2: Design of Concrete Structures* (2004). The "Eurocode 2" method was convenient to investigate because the code incorporates the same creep prediction method as the MC 2010 but a slightly different shrinkage prediction method. It could thus produce a different prediction for total time-dependent strain.

Several other shrinkage prediction models, including older versions of the models used by AASHTO and *fib*, exist in the literature. These models were excluded from this report for several reasons:

1. They are outdated and are not regularly specified (especially among codes in which a more recent version of the same model has been implemented),
2. They are of little value to ALDOT, the chief sponsor of this research for whom these findings were prepared, due to the prevalence of the *AASHTO LRFD* specification, and
3. They were found to be no more accurate during other past studies of Alabama SCC conducted by Kavanaugh (2008).

5.2.3.1 ACI 209

Like the ACI 209 creep prediction method, the shrinkage prediction is based on determining an ultimate value, $(\varepsilon_{sh})_u$, that is modified for intermediate times by a time development factor. Thus, the ultimate shrinkage strain is computed by the following equation:

$$(\varepsilon_{sh})_u = 780(10)^{-6}(\gamma_\lambda\, \gamma_{vs}\, \gamma_\psi\, \gamma_s\, \gamma_a\, \gamma_c) \quad (5\text{-}6)$$

Where

γ_λ is the relative humidity correction factor,
γ_{vs} is the volume-to-surface-area ratio correction factor,
γ_ψ is the fine aggregate percentage correction factor,
γ_s is the slump correction factor,
γ_a is the air content correction factor, and
γ_c is the cement content correction factor.

The adjustment factors shown above, which are applied for the same purposes as those in Equation 5-1, are calculated using equations discussed further by Ellis (2012) and are applied to the standard ultimate shrinkage strain (-780 με in the equation). In addition to the slump (water content) correction and fine aggregate percentage correction factors, the cement content correction factor, γ_c, is of interest particularly for SCC. Among the five shrinkage prediction models evaluated in this research, the ACI 209 method is the only method that specifically

accounts for cement content; only some of the other methods even account for *type* of cementitious material. No guidance is given concerning the use of SCM, so the use of total powder content (portland cement plus SCMs) is feasible.

To ascertain the predicted shrinkage strain for intermediate times of interest such as at the time of girder erection, the ultimate shrinkage is multiplied by a time parameter, $(\varepsilon_{sh})_t$, that accounts for the time elapsed since the concrete was exposed to drying:

$$(\varepsilon_{sh})_t = \frac{t}{X + t} \tag{5-7}$$

In Equation 5-7, t is the length of time after initial curing (in days), and X depends on the type of curing (accelerated or non-accelerated). For concrete exposed to accelerated curing for 1–3 days, $X = 55$. No guidance is given for accelerated curing times less than 1 day. This was of importance to the evaluated data, as initial curing was frequently of a shorter duration (see Table 3.7 for ages in hours). After determining the time correction factor using Equation 5-7, the shrinkage strain at time t, $\varepsilon_{sh}(t)$, is predicted by multiplying the ultimate shrinkage strain by the time factor.

5.2.3.2 AASHTO 2013

The current *AASHTO LRFD* shrinkage prediction method may be used to determine the effects of shrinkage on the loss of prestressing force in bridges that are not segmentally constructed, as discussed in Section 5.9.5.4 of the provisions and in Chapter 6 of this report. Like the ACI 209 shrinkage model, the model involves calculation of an ultimate shrinkage strain, $(\varepsilon_{sh})_u$, that is modified for intermediate times by a time development factor. The ultimate strain is computed using the following equation:

$$\varepsilon_{sh} = 480(10)^{-6}(k_{hs}\, k_s\, k_f\, k_{td}) \tag{5-8}$$

Where

k_{hs} is the relative humidity correction factor,
k_s is the volume-to-surface area ratio correction factor,
k_f is the concrete strength correction factor, and
k_{td} is the time development correction factor.

Of the above factors, all except k_{hs} are calculated according to the same equations as used for the AASHTO 2013 creep prediction model. All are described further by Ellis (2012). After determining the ultimate shrinkage strain, the predicted shrinkage strain at intermediate times is calculated as in the AASHTO 2013 creep prediction method.

5.2.3.3 NCHRP 628

The NCHRP 628 shrinkage prediction model was developed by modifying the pre-2005 *AASHTO LRFD Bridge Design Specifications*. It is recommended specifically for shrinkage predictions of SCC for precast, prestressed applications. The strain due to shrinkage at any time, *t*, after drying exposure is calculated for accelerated-cured concrete according to Equation 5-9:

$$\varepsilon_{sh} = 560(10)^{-6}(k_s\, k_h)(\frac{t}{55+t})A \tag{5-9}$$

Where

k_s is the size factor,
k_h is the relative humidity factor,
t is the drying time (in days) after initial curing, and
A is the cement factor for SCC only, equaling 0.918 for Type I/II cement or 1.065 for Type III cement plus 20% fly ash replacement.

In the above correction factors, k_s is used to account for *V/S*. The time-adjustment factor shown in Equation 5-7 is integrated as would be necessary when computing shrinkage at intermediate times using the ACI 209 shrinkage model. All factors are discussed in detail by Ellis (2012).

5.2.3.4 MC 2010

The current *Model Code* shrinkage prediction model has been in use since 1999, when the *fib* revised the MC 90 shrinkage prediction method. The total shrinkage of concrete predicted using the MC 2010 method is given by

$$\varepsilon_{sh}(t, t_c) = \varepsilon_{cas}(t) + \varepsilon_{cds}(t, t_c) \tag{5-10}$$

Where

ε_{cas} is the autogenous shrinkage strain,
ε_{cds} is the drying shrinkage strain,
t is the age of concrete at the moment considered (days), and
t_c is the age of concrete at the beginning of drying (days).

The derivations of these components are given in the MC 2010 code (*fib* 2010) and are discussed in relation to this project by Ellis (2012). In the derivations, autogenous shrinkage is not dependent on the concrete maturity when initial curing ends, relative humidity, or *V/S*, but it is dependent on the concrete strength at twenty-eight days. Both it and the drying shrinkage

component are modified by the cement *type*, with distinction between slow-hardening cements, normal-to-rapid hardening cements, and rapid-hardening high-strength cements.

5.2.3.5 Eurocode 2

Like the MC 2010 model, the Eurocode 2 shrinkage prediction model distinguishes between autogenous shrinkage and drying shrinkage. The model is similar to the one employed by MC 2010, except with some different correction factors that are described by Ellis (2012). Distinctions described further in the referenced report include that

- Drying shrinkage is determined through direct application of *V/S* in the MC 2010 model but as a function of notional cross-sectional size (cross-sectional area divided by the length of perimeter exposed to drying) in the Eurocode 2,
- Numerical factors to account for cement type are slightly different between the models, although the same three cement classes are delineated—slow-hardening, normal-to-rapid hardening, or rapid-hardening high-strength cement, and
- Autogenous shrinkage calculated according to the Eurocode 2 model considers the compressive strength specified at any concrete age, *t*, but it is calculated using the mean 28-day f_c within the MC 2010 model.

5.3 EXPERIMENTAL PROGRAM

5.3.1 Measurement of Time-Dependent Strain in Cylindrical Specimens

Much of the experimental work pertaining to this research program has been described in Section 3.3.4 of this report and elsewhere by Ellis (2012). Important information from those sources is summarized by the following:

- Cylinders were produced for time-dependent deformation testing during five production days: SCC-B, SCC-C, SCC-E, VC-B, and VC-F, thus including concrete placed in all four spans of the completed bridge.
- All cylinders were tested for time-dependent deformation in accordance with ASTM C512 (2002) and were stored in a temperature- and humidity-controlled environment from the time of initial loading until when they were tested for late-age strength and elasticity (as described in Chapter 3).
- As with the strength and E_c assessments of Chapter 3, the exact placement location of the sampled batches within the girders could not be determined. Samples taken at the midpoint of each production day were assumed to be representative of the majority of concrete placed during that day.

- Three curing regimes were implemented: match curing based on the measured temperature at the center of the bottom bulb of the girders, steam-curing in the recesses of the formwork followed by temperature- and humidity-controlled storage, and steam-curing followed by approximately one year of ambient-exposure similar to that experienced by the girders.
- A single SCC and a single VC mixture were used throughout girder production and each set of cylinders (within and between production days) was exposed to a different curing and exposure history.
- In addition to concrete cylinders, free shrinkage prisms were produced for testing according to ASTM C157 (2008) from production groups SCC-E, VC-E, and VC-F. Additional free shrinkage prisms were produced during the placement of concrete in each span of the deck of the bridge over Hillabee Creek.

Assessment of time-dependent deformation according to ASTM C512 (2002) *Standard Test Method for Creep of Concrete in Compression* consists of two parts: measurement of the free shrinkage of unloaded cylindrical concrete specimens and measurement of the *total deformation* of companion cylinders exposed to the same drying conditions plus a known sustained compressive stress. Load-induced strain is then determined by subtracting the measured shrinkage strain in the unloaded cylinders from the measured total strain in the loaded cylinders. Finally, creep strain is then determined by subtracting the initial elastic strain from the calculated load-induced strain. These quantities are presented graphically in Figure 5.1.

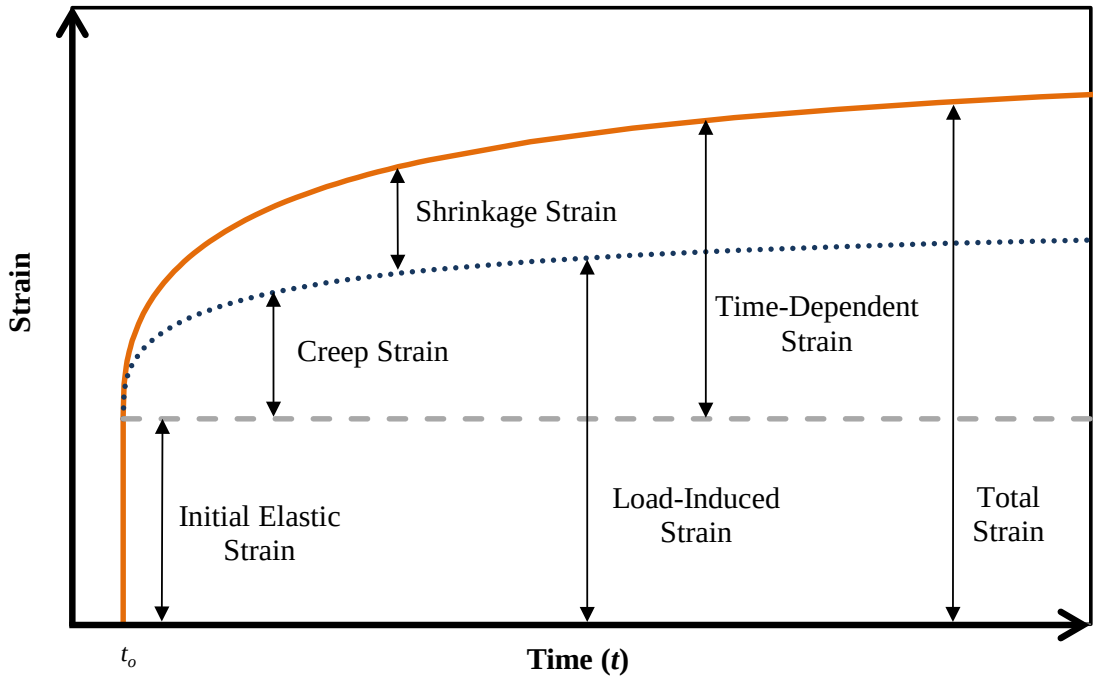

Figure 5.1: Components of strain in unrestrained concrete

During testing according to ASTM C512 (2002), it is difficult to precisely distinguish between instantaneous elastic strain and rapidly evolving creep strain at the beginning of testing because it may take several minutes to execute the cylinder loading process. For reference, notice that time-dependent strain evolves most rapidly at early ages in Figure 5.1. Therefore, the initial measurement of load-induced strain that is obtained once the total load is applied can include a creep component that is impossible to accurately quantify (ACI 209 2008).

5.3.1.1 Preparation of Test Specimens

In addition to the cylinders for evaluation of strength and E_c, cylinders were cast for measurement of time-dependent deformation according to ASTM C512 (2002), *Standard Test Method for Creep of Concrete in Compression*. These cylinders were always obtained during the second round of fresh concrete sampling to coincide with the majority of strength-cylinder production, and they were produced and stored alongside the other cylinders until approximately three hours before the girders were demolded and detensioned. At that time, all cylinders for time-dependent deformation testing were transported two hours to the laboratory in an insulated container which was used to allow a graduate temperature decrease from the elevated temperature in the bed to standard laboratory conditions. They were transported at this time so that some would be loaded to coincide with detensioning of the full-scale girders.

Approximately half of the cylinders that were used for time-dependent deformation testing were cured in the plant using a match-curing apparatus, as discussed further by Ellis (2012). The match-curing apparatus was temperature-controlled to match the internal temperature of the bottom bulb of a girder on the bed. The match-cured cylinders were frequently exposed to a different temperature history than steam-cured cylinders from the same production day. Two examples of the difference are shown in Figure 5.2 which illustrate that the difference was not consistent between production groups. In other words, match-cured cylinders were sometimes heated more and sometimes heated less than the companion tarp-cured cylinders.

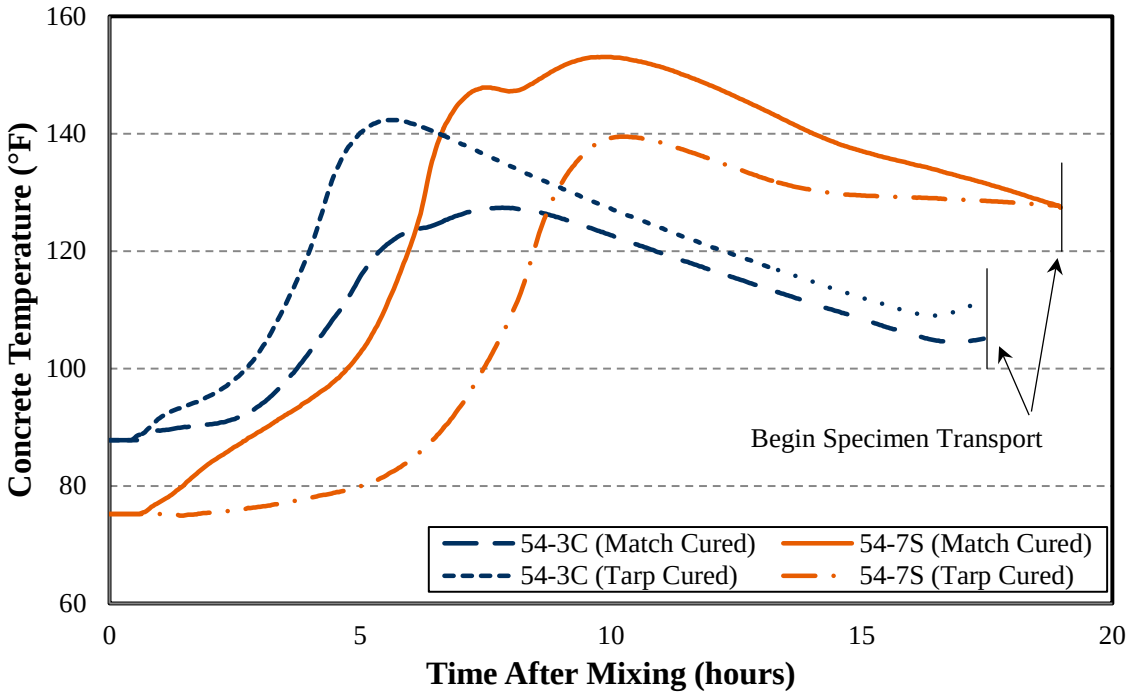

Figure 5.2: Measured temperature histories of cylindrical specimens used in time-dependent deformation testing

Once at the laboratory, the cylinders were demolded and prepared for creep loading and shrinkage testing. To ensure that the concrete cylinders were flat and smooth on their ends, a concrete grinder was used to achieve a smooth, level surface meeting the planeness requirements of ASTM C512. After both ends of each cylinder were ground, demountable, mechanical (DEMEC) strain-measurement points were attached to the specimens. After the DEMEC targets were installed, most of the specimens were placed into a climate-controlled room which maintains a humidity of 50% ± 10%. Here, the specimens were exposed to controlled drying and temperature conditions and, where applicable, sustained compressive loading until they all reached three years of age.

The appropriate sustained load (40% of f_c) was determined by testing two additional cylinders and calculating their average compressive strength. Match-cured sets of cylinders were loaded at the time of prestress transfer (to most closely match the behavior of the girders), and steam-cured sets were loaded at approximately twenty-six hours (always after the match-cured cylinders). An additional set of steam-cured cylinders were stored in ambient conditions until approximately when the deck was cast over the girders; mechanical-property results from these cylinders were reviewed in Chapter 3, but time-dependent behavior of these cylinders is included in a forthcoming report regarding in-place performance of the bridge (Keske et al. 2015).

In addition to cylinders, rectangular prisms measuring approximately 11.25 in. long with a 3 in. square cross section were prepared according to ASTM C157 (2008) during SCC production group E and during VC production groups E and F for unrestrained shrinkage evaluation. After being steam-cured alongside the girders until girder form removal, the prisms were taken to the laboratory to be air-cured in a climate-controlled room which maintains a humidity of 50% ± 10%. They were stored there and regularly measured until July of 2013, following completion of all in-field deformation measurements and live-load testing.

5.3.1.2 Reporting of Measured Time-Dependent Strain

Experimental determination of the creep coefficient, which is traditionally defined as the ratio of creep strain to initial elastic strain, is particularly sensitive to slight inaccuracies in the initial strain measurement (ACI 209 2008). Because of this, creep effects were assessed in this report primarily by considering the total load-induced deformation attributable to a sustained load. A standard measure of this phenomenon is the compliance, $J(t,t_i)$. Compliance represents the total load-induced strain (elastic strain *plus* creep strain) at age t per unit of uniaxial stress due to a load maintained since loading age, t_i. ACI 209 (1992) defines it as follows:

$$J(t,t_i) = \frac{Total\ Strain - Shrinkage\ Strain}{Applied\ Stress} \tag{5-11}$$

Compliance values allow for a more accurate comparison of creep results because they are normalized for applied load levels (ACI 209 1992), but the use of J implicitly emphasizes some concrete material properties and de-emphasizes others. Because it includes the initial elastic strain component, J is dependent upon E_{ci}—initial compliance *should* equal the inverse of E_{ci} since no time-dependent change would occur during theoretically instantaneous loading. Consequently, concrete with a higher E_{ci} exhibits less initial (elastic) compliance, regardless of the creep it may experience. In this way, J may de-emphasize the creep component—a material with high initial deformation but less creep deformation still exhibits a larger J than one with lower relative initial deformation, at least until later ages.

The reporting of *J* instead of measured creep strain also makes it impossible to compare the magnitude of creep strain to the magnitude of shrinkage strain. This is not of concern during this analysis, as it would be inappropriate to directly compare the measured creep strain, load-induced strain, or total strain in SCC and VC. Each set of cylinders exhibited a different f_{ci} and E_{ci} and was loaded to a different *force*, so compliance results are only comparable because they are normalized for stress.

5.3.1.3 Batch-Specific Considerations and Specimen Nomenclature

In addition to the basic nomenclature shown in Figure 3.8, identification suffixes were necessary for identification of the specimens produced for this testing. Cylinders were loaded at up to three different ages (at transfer, at approximately twenty-six hours, and at approximately one year), so the first identifier is based on the order of loading: -1, -2, or -3, respectively. Thus, two sets of cylinders were tested from SCC-B (SCC-B-1 and SCC-B-2), while three sets were tested from the other four referenced production groups. Additionally, free-shrinkage prisms are denoted with a "-P" suffix, as they were treated independently and were all tested using standardized practices.

Previously noted in Table 3.2, the match-curing apparatus used to cure some of the SCC-B-1 cylinders did not function correctly. The cylinders affected by this malfunction were not marked, so the maturity of the SCC-B-1 group is unclear. Consequently, this group is excluded from all prediction method analyses and calibrations discussed in Section 5.4. The second set of cylinders tested from production day SCC-B was unaffected by this malfunction, and they continue to be labeled SCC-B-2 through this report for continuity.

Additionally, two other sets of cylinders were not loaded to the intended target load, so these two sets are henceforth denoted as SCC-E-2U and VC-F-2U to indicate that they were under-loaded. These two sets are excluded from the analysis and calibration of load-dependent deformation predictions because the precision of the measurements would be disproportionately significant in these cylinders. Curing and drying of these sets was effectively controlled and free shrinkage measurement is load-independent, so the sets are still included in the analysis and calibration of shrinkage prediction models.

The aged-then-loaded cylinders (denoted "-3" where applicable) were exposed to uncontrolled ambient conditions for one year before being tested for time-dependent deformability. However, results from these cylinders are not included in this report, as they were loaded to coincide with the beginning of in-place bridge monitoring that is the subject of a forthcoming report regarding ALDOT project 930-799 (Keske et al. 2015).

5.3.2 Prediction of Time-Dependent Strains

5.3.2.1 Application of Prediction Methods

All of the referenced creep prediction models yield a creep coefficient based on the model-specific inputs reviewed in Section 5.2 (such as applied stress, f_c, relative humidity, age at the time of loading, etc.). This creep coefficient can then be applied to the elastic deformation corresponding to the applied stress to determine the creep strain. In light of the chosen reporting convention, conversion of these strains to predicted compliance values was necessary before they could be compared to the measured values obtained according to the testing method described earlier.

To most accurately evaluate the prediction models, it was necessary to base the predictions on measured concrete properties and exposure conditions whenever possible. The measured, utilized properties are shown in Table 5.1 at the end of this section. Thus, predictions of the time-dependent behavior of these full-scale cylinders were based on the following procedures:

- Elastic strain was calculated by dividing the actual applied stress by the measured E_{ci} of companion cylinders tested in accordance with ASTM C469 (2010).
- Creep strain was predicted by multiplying the predicted creep coefficient by the elastic strain calculated above.
- Compliance was predicted by dividing the sum of the creep strain (predicted by the model) and elastic strain (calculated using E_{ci}) by the actual applied stress as in Equation 5-11.
- Shrinkage predictions, which were compared directly to measured shrinkage strains, were based on the measured geometric, material, and exposure properties of the tested cylinders (V/S, relative humidity, etc.).
- Total-strain predictions consisted of the sum of the predicted creep strain (based on the predicted creep coefficient), elastic strain (based on measured E_{ci}), and predicted shrinkage; these total-strain predictions were compared directly to the total strain measured in the creep-loaded cylinders.

5.3.2.2 Testing and Model-Specific Considerations

Prediction of compliance required application of the predicted creep coefficient to the elastic response calculated using the E_{ci} tested in cylinders according to ASTM C469 (2010). However, to accelerate the initiation of time-dependent deformation testing, only f_{ci} was evaluated in the laboratory-tested group of specimens while f_{ci} and E_c were evaluated in cylinders at the plant as

part of the assessment presented in Chapter 3. Because E_c is widely considered to be proportional to the square root of f_c (see Chapter 3), E_{ci} of the specimens loaded for time-dependent deformation testing was estimated according to the following equation:

$$(E_{ci})_{lab} = (E_{ci})_{field} \frac{\sqrt{(f_{ci})_{lab}}}{\sqrt{(f_{ci})_{field}}} \quad (5\text{-}12)$$

In Equation 5-12, the properties of field-tested specimens (denoted with a "field" subscript) that were used to estimate E_{ci} of the laboratory-tested specimens are reported in Table 3.7. Laboratory- and field-tested cylinders were always produced from the same batch of concrete, and efforts were made to minimize differences in their temperature histories. Comparisons of field- and laboratory-tested compressive strengths can be made by comparing Table 3.7 and Table 5.1 at the end of this section.

Each creep and shrinkage prediction model incorporates correction factors to account for different nonstandard material and exposure conditions. Pertinent assumptions and choices are summarized below, and additional information is contained in the thesis prepared by Ellis (2012):

- Factors based on cement content were assumed to be based on total powder content, which included a replacement of Type III cement with slag cement during this research.
- Factors based on cement type in the NCHRP 628 models were chosen based on the "Type III + 20% Fly Ash" classification used in those models. Consequently, *A*-values of 1.35 and 1.065 were utilized when evaluating SCC creep and shrinkage according to these models.
- The "rapid-hardening high-strength cement" classification used in the MC 2010 and Eurocode 2 models was chosen based on the ACI 209 (2008) recommendation for its use when evaluating concrete proportioned with Type III cement.
- Slump correction factors were chosen based on the slump achievable without the use of HRWRA, which was approximated to equal 0.0 inches for the SCC and 0.5 inches for the VC used during this research.
- Concrete aging and curing were assumed to begin at the time at which the water and cementitious material were mixed at the plant, and the end of initial curing was assumed to occur when the cylinders were removed from their cylinder molds. Initiation of drying was assumed to coincide with the end of initial curing.

Notably, while ACI 209 (2008) recommends the use of the "rapid-hardening high-strength cement" factors in the European models when evaluating concrete proportioned with Type III cement, Section 5.1.9.4 of the MC 2010 provisions states that the use of SCMs (fly ash, specifically) may affect the applicability of the factors. SCMs may have contradictory effects: delayed hydration may directly increase early-age creep and reduce shrinkage, but overall creep

and shrinkage may also be affected as an indirect result of the relative reduction in portland cement content (*fib* 2010).

The European models incorporate ages that have been adjusted to reflect the actual maturity of accelerated-cured specimens, while the other models account for accelerated curing through the use of alternative factor derivations in conjunction with chronological ages. The methodology used to determine temperature-adjusted ages is discussed by Kamgang (2013) and Kavanaugh (2008), and considerations specific to this research are discussed by Ellis (2012). Chronological and temperature-adjusted ages are shown in Table 5.1 alongside the other measured and calculated inputs needed to apply the assessed prediction models. In the table, the inputs are as follows:

t_{cure} is the length of initial curing

t_i is the concrete age at which the load was applied, from the time of initial mixing

$t_i - t_{cure}$ is the length of time from initiation of drying to the application of load

$t_{i,T}$ is the temperature-adjusted age at loading

$t_{m,T}$ is the age at loading modified for temperature and cement class

f_{ci} is the compressive strength at prestress transfer

f_{c28} is the compressive strength at twenty-eight days

E_{ci} is the estimated elastic modulus at transfer based on Equation 5-12

C is the total cementitious content

S is the adjusted slump (in.), and

F is the applied and sustained compressive force.

Table 5.1: Inputs used in creep and shrinkage prediction calculations

Specimen ID	Measured Times			Adjusted Times		Mixture Properties			Measured Properties			
	t_{cure} (days)	t_i (days)	$t_i - t_{cure}$ (days)	$t_{i,T}$ (days)	$t_{m,T}$ (days)	*C* (lb/yd^3)	*Fines* (%)	*Air* (%)	f_{ci} (ksi)	f_{c28} (ksi)	E_{ci} (ksi)	*F* (kips)
SCC-B-2	0.99	1.15	0.15	4.55	9.57	892	48	3.0	8.93	10.8	6,450	102
SCC-C-1	0.89	0.99	0.10	3.86	8.78	892	48	4.2	7.88	10.18	6,050	88
SCC-C-2	0.91	1.12	0.21	3.10	7.84	892	48	4.2	7.49	10.18	5,900	86
SCC-E-1	0.75	0.84	0.09	3.26	8.04	895	47	4.3	7.06	10.77	5,550	84
SCC-E-2U	0.78	1.09	0.31	3.60	8.47	895	47	4.3	7.68	10.77	5,800	35
VC-B-1	0.81	0.90	0.09	2.41	6.86	820	38	4.5	7.11	9.67	6,350	81
VC-B-2	0.85	1.06	0.21	3.06	7.79	820	38	4.5	8.12	9.67	6,750	88
VC-F-1	0.77	0.86	0.10	2.39	6.83	833	38	3.1	7.98	11.05	6,650	91
VC-F-2U	0.79	1.14	0.35	2.83	7.48	833	38	3.1	8.88	11.05	7,050	34

5.4 PRESENTATION AND ANALYSIS OF RESULTS

In the following sections, time-dependent deformations of SCC and VC cylinders are compared at concrete ages up to one year. This was the approximate age at which composite action was achieved between the girders through the addition of a cast-in-place deck at the bridge site. The evaluation of the in-place behavior of the composite bridge is reported by Keske et al. (2015), and the long-term behaviors discussed in that report should complement and reinforce the findings presented below.

5.4.1 Comparison of Measured Time-Dependent Deformation

5.4.1.1 Compliance and Creep

In this section, the dependence of J on E_{ci} is especially important considering the SCC evaluated during this research. The evaluated SCC regularly exhibited a lower E_{ci} than that of the companion VC, which was expectable considering the changes required to induce self-consolidating behavior in the SCC (see Chapter 3 for further discussion). With this in mind, comparisons of J should be useful relative to precast, prestressed applications, as prestress losses are related to both the initial elastic shortening and time-dependent deformation of the surrounding concrete.

Compliance of the assessed mixtures is presented in Figure 5.3. Pertinent results from this data are then summarized in Table 5.2 below the figure. The data necessary to create this figure and table are presented by Keske (2014). In both the figure and table, only cylinders that were cured and tested according to ASTM C512 are presented; other, non-standard results are discussed in the next subsection.

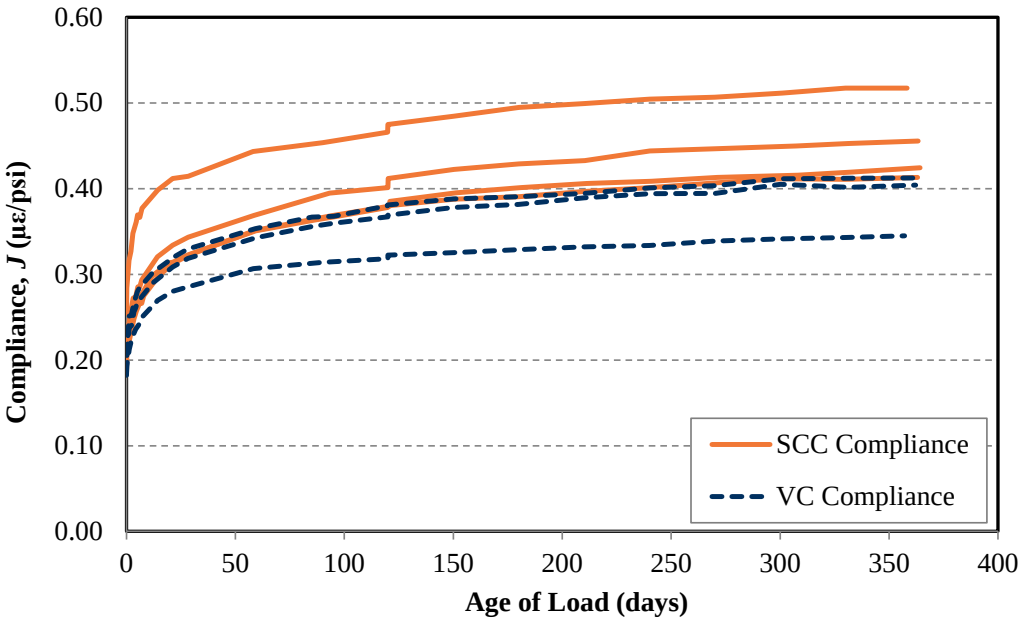

Figure 5.3: Measured compliance in specimens tested according to ASTM C512

Table 5.2: Compliance, *J*, of SCC and VC tested in accordance with ASTM C512

ID	Initial Compliance (με/psi)	56-Day Compliance (με/psi)	1-Year Compliance (με/psi)
SCC-B-2	0.20	0.35	0.41
SCC-C-1	0.21	0.37	0.46
SCC-C-2	0.19	0.35	0.42
SCC-E-1	0.25	0.44	0.52
SCC Avg.	*0.21*	*0.38*	*0.45*
VC-B-1	0.18	0.34	0.40
VC-B-2	0.18	0.35	0.41
VC-F-1	0.19	0.31	0.34
VC Avg.	*0.18*	*0.33*	*0.38*

In the table, *J* is presented for concrete ages at initial loading and fifty-six days, and one year. These three ages were chosen considering important ages in the life of the associated precast, prestressed girders:

1) Initial *J* should relate to the concrete behavior at prestress transfer,
2) Fifty-six days is a reasonable estimate of the time at which most precast, prestressed girders are erected, and
3) One-year is the approximate age at which the deck was cast in place over the girders.

The SCC cylinders exhibited *J* of approximately 15% more than in companion VC cylinders at all ages. This closely resembles the 10–15% reduction in E_{ci} discussed in Section 3.4.3.3, which could be expected between any two concretes that differ in mixture proportions. Thus, the difference in *J* should be expected of these evaluated mixtures. As noted previously, though, elastic effects could mask any differences in time-dependent deformation growth. Thus, isolation of time-dependent creep effects on *J* required consideration of the difficulties inherent to the testing process that were described in Section 5.3.1.

Considering that unmeasurable time-dependent effects resulting from creep testing would be approximately equal and random between all tests, creep compliance effects, *C*, were calculated according to Equation 5-13:

$$C = \frac{J(t, t_i) - J(t_i)}{J(t_i)} \tag{5-13}$$

Where

$J(t,t_i)$ is the measured compliance at time t due to a load sustained since time t_i, and

$J(t_i)$ is the measured initial compliance as shown in Table 5.2.

Importantly, *C* is presented in the same form as the creep coefficient determined according to each of the models described in Section 5.2.2 (such as v_u in ACI 209 or ψ in AASHTO 2013), but it is only used in this work for comparisons of *measured* results and not for comparisons of measured and predicted results. In other words, the *C* values reported below in Table 5.3 are not relatable to predicted creep coefficients because they all include an unknown amount of time-dependent effects. Measured *C* results at concrete ages of fifty-six days and one year are presented below, as are the average ratios of SCC results to VC results at these ages.

Table 5.3: Creep compliance effects, *C*, of SCC and VC cylinders

ID	56-Day Creep (Eq. 5-13)	1-Year Creep (Eq. 5-13)	SCC / VC	
			At 56 Days	At 1 Year
SCC-B-2	0.75	1.05	0.98	1.03
SCC-C-1	0.76	1.19		
SCC-C-2	0.84	1.21		
SCC-E-1	0.76	1.08		
SCC Avg.	*0.81*	1.14		
VC-B-1	0.89	1.22		
VC-B-2	0.94	1.28		
VC-F-1	0.63	0.79		
VC Avg.	*0.83*	1.11		

Based on the information presented in Table 5.3, the SCC cylinders appear to exhibit comparable creep as the VC cylinders (less than 5% different, on average). This difference is trivial considering the 30% variability of creep in "ordinary structural concrete" alluded to by the MC 2010 provisions (see Section 5.2.1). The individual-specimen results also highlight the between-batch variability inherent to this type of measurement. The variability between SCC specimens was no greater that the variability between VC specimens, thus further suggesting that the creep of the tested SCC and VC mixtures was practically the same.

In addition to the results obtained in accordance with ASTM C512, compliance was also measured in the under-loaded specimens. These results are included in Keske (2014). The compliance of the under-loaded specimens was very similar to those shown above (as expected because *J* is normalized for load), as were *C* (determined according to Equation 5-13) and the ratio of SCC creep to VC creep. However, only one set of SCC specimens (SCC-E-2U) and one set of VC specimens (VC-F-2U) were under-loaded, so these comparisons are limited.

5.4.1.2 Free Shrinkage

Free shrinkage results of the assessed mixtures are presented in Figure 5.4; the data necessary to create this figure are presented in Keske (2014). Pertinent results from this data are then summarized in Table 5.4 below the figure. Only results from cylinders that were cured and tested according to ASTM C512 are presented in the figure and table. As previously discussed, the shrinkage behavior of the under-loaded specimens was independent of their response to loads, so they are included in this section. Values are presented for concrete ages of fifty-six days and

one year because they should be representative of typical erection-age and the actual age at the time of deck addition. Values measured at a concrete age of seven days are included to compare rates of shrinkage growth.

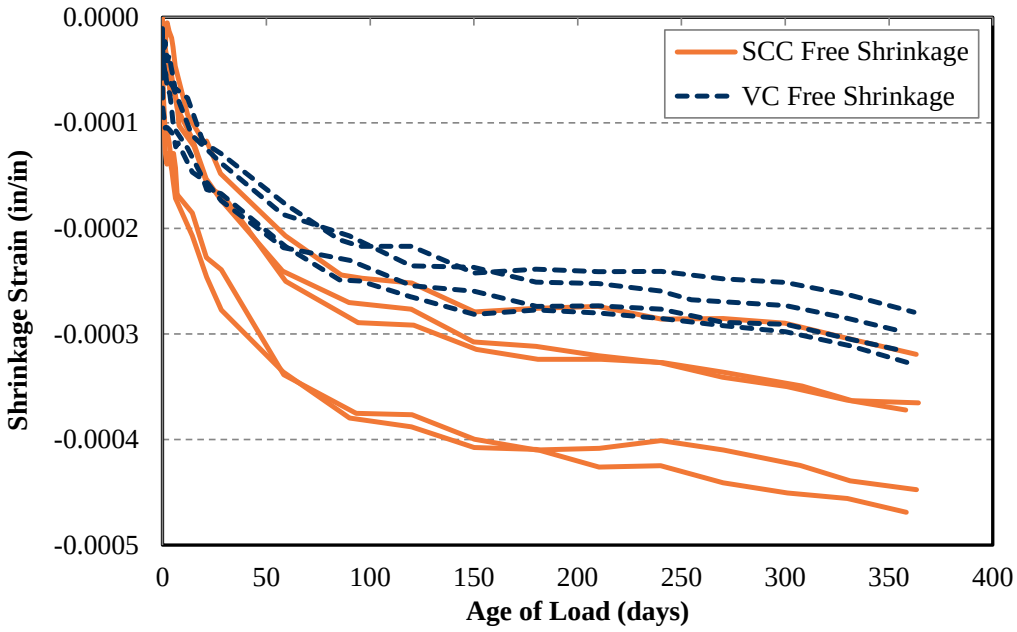

Figure 5.4: Measured shrinkage in specimens tested according to ASTM C512

Table 5.4: Shrinkage of SCC and VC tested in accordance with ASTM C512

ID	Measured Shrinkage (με)			Ratios		
	7-Day	56-Day	1-Year	56-Day/ 7-Day	1-Year/ 56-Day	1-Year/ 7-Day
SCC-B-2	-150	-210	-320	1.40	1.52	2.13
SCC-C-1	-170	-340	-450	2.00	1.32	2.65
SCC-C-2	-100	-250	-370	2.50	1.48	3.70
SCC-E-1	-180	-340	-470	1.89	1.38	2.61
SCC-E-2U	-90	-240	-370	2.67	1.54	4.11
SCC Avg.	*-140*	*-270*	*-400*	*2.09*	*1.48*	*2.90*
VC-B-1	-120	-220	-330	1.83	1.50	2.75
VC-B-2	-80	-180	-280	2.25	1.56	3.50
VC-F-1	-120	-220	-320	1.83	1.45	2.67
VC-F-2U	-80	-190	-300	2.38	1.58	3.75
VC Avg.	*-100*	*-200*	*-310*	*2.07*	*1.55*	*3.10*

The SCC cylinders exhibited approximately 30% more shrinkage than in companion VC cylinders at all ages shown in the table. While this difference is expectable due to the increase in paste content in the SCC and is in line with other findings (*fib* 2010; Khayat and Mitchell 2009), it is practically significant when considering that the two mixtures exhibited comparable f_c and E_c (see Chapter 3). Statistical significance was also confirmed: shrinkages at concrete ages of fifty-six days and one year were significantly different at a 90% CI and 95% CI, respectively.

The ratios presented in the table were given to compare shrinkage growth rates. Shrinkage growth is complicated because autogenous and drying shrinkage strains evolve at different rates over time, but the proportion of shrinkage that occurs before erection (assumed to occur at approximately fifty-six days) is of particular interest. Based on the ratios shown in Table 5.4 and the data shown in Figure 5.4, the SCC and VC appear to exhibit very similar shrinkage growth, with the most rapid changes occurring in the first fifty-six days. Shrinkage doubled between seven days and fifty-six days but only increased an additional 50% between fifty-six days and one year. This pattern was practically identical in the SCC and VC.

Rectangular prisms for unrestrained shrinkage evaluation were prepared according to ASTM C157 (2008) during SCC production day E and during VC production days E and F. Measured results are summarized in Table 5.5 in terms of length change—percentage length change is the recommended result format of the test, and it is directly comparable to the specifications set forth for this project.

Table 5.5: Length-change of SCC and VC prisms tested in accordance with ASTM C157

ID	28-Day (%)	56-Day (%)	1-Year (%)
SCC-E-P	-0.029	-0.034	-0.049
VC-E-P	-0.016	-0.021	-0.033
VC-F-P	-0.026	-0.035	-0.054

All girder-concrete prisms met the specifications set forth for this project (less than 0.04% length change at twenty-eight days). Variability between the girder-concrete prisms was high, so this data should be considered to compliment the free-shrinkage cylinder data presented earlier.

5.4.2 Comparisons of Measured Values to Predicted Values

While a direct comparison of the evaluated mixtures was warranted in the previous section because these two mixtures were produced to be direct companions in an in-service bridge, evaluation of the *predictability* of time-dependent deformation is of wider value in advancing the understanding of SCC. Within each model, each set of specimens would be expected to exhibit

different creep and shrinkage even if exposed to the same compressive stress and ambient conditions. Therefore, the ability of the various models to correctly identify measured differences is important.

5.4.2.1 Analysis Methodology

Results obtained from the assessment of time-dependent deformation according to ASTM C512 can be compared to predicted values in two general ways: by comparing the values at discrete, important ages (such as at girder erection or for ultimate long-term behavior) or by comparing every predicted and measured value over a particular region of measured behavior (such as only until deck addition or over the entire measured lifetime). Both methods of comparison are useful to this research, although for different reasons. Differences at discrete, important ages are evaluated because they are relevant for engineering purposes; differences between the trends are more relevant for understanding the behavior of the concrete over time.

Differences between predicted values ($Y_{Predicted}$) and measured values ($Y_{Measured}$) at discrete ages are evaluated according to Equation 5-14. By arranging the equation as shown, negative errors indicate that a given model under-predicts the magnitude of the result (compliance, shrinkage, or total strain) at a given time, while positive errors indicate that a given model over-predicts the magnitude of the measured result at that time.

$$Error\ (\%) = 100\left[\frac{Y_{Predicted} - Y_{Measured}}{Y_{Measured}}\right] \tag{5-14}$$

In comparisons of error percentages, the preferred range of error was selected as ±20% based on statements by Gardner and Lockman (2001) concerning creep and shrinkage prediction:

> A model that could predict the shrinkage within 15% would be excellent, and a prediction within 20% would be adequate. Obviously for compliance, the range of expected agreement would be worse because compliance is not measured but calculated by subtracting a large number (shrinkage) from another large number (total deformation).

In addition to error percentages at discrete ages, it was useful to utilize a single-parameter comparison tool to evaluate the overall accuracy of the prediction models. Results are collected on a nonlinear calendar according to the ASTM C512 guidelines (every day for the first week, then weekly for the first month, then monthly for the first year, and then quarterly or less frequently thereafter), which may bias common single-parameter forms of assessment such as the simple sum-of-squares error calculation. Several statistical indicators are presented in the ACI 209 (2008) *Guide for Modeling and Calculating Shrinkage and Creep in Hardened Concrete*

that can overcome this bias. In general, these indicators are calculated by dividing measured results into groups and weighting the groups statistically.

Of those presented in the ACI 209 (2008) guide, the model proposed by Bazant and Panula (1978) was selected for use during this assessment. The indicator from their model, the BP coefficient of variation, ω_{BP}, was developed by parsing measured data into logarithmic decades (0 to 9.9 days, 10 to 99.9 days, etc.) and weighting the measurements based on the number of measurements in each decade relative to the total number of measurements and decades. Calculation of ω_{BP} is described further in Appendix C.

5.4.2.2 Comparisons of Measured and Predicted Compliance

Errors between predicted and measured compliance for each reviewed prediction model are presented in Table 5.6. The data necessary to derive this table are presented elsewhere by Keske (2014). Per the discussion of the previous subsection, ω_{BP} gives the best indication of the overall accuracy of the various models, while error percentages are presented to indicate the margin of error in compliance at concrete ages of fifty-six days (an approximation of the age at erection) and one year (the approximate actual age at deck addition). ω_{BP} results are always positive, with results closer to zero indicating better accuracy; a positive average error percentage indicates an over-predicted compliance.

Table 5.6: Error comparisons for existing compliance prediction models

Compliance Prediction Model	ω_{BP}		Error % at 56 days		Error % at 1 year	
	SCC	VC	SCC	VC	SCC	VC
ACI 209	0.165	0.125	-7	-4	-5	3
AASHTO 2013	0.232	0.183	-9	-6	-9	-2
NCHRP 628	0.211	0.183	8	-6	11	-2
MC 2010[1]	0.153	0.077	-9	-3	-7	3

Note: Similar to model used in Eurocode 2

Several conclusions are warranted based on the results shown in Table 5.6. They include that

- All models were reasonably accurate for predicting compliance,
- While SCC compliance was slightly less predictable using the existing models, all average SCC and VC predictions were within 15% and 10% of actual results, respectively, at concrete ages of up to one year.

As previously discussed in Section 5.4.1.1, compliance is directly dependent upon E_{ci}, and the correlation may disguise differences in creep behavior. However, since measured E_{ci} was used to calculate the initial elastic strain to which predicted creep coefficients were applied in this analysis, the data presented in Table 5.6 directly indicate the predictability of the *creep* of the assessed SCC and VC. Therefore, it is concluded that, when using measured properties, all referenced creep predictions are reasonably accurate, on average, for evaluation of the pre-erection behavior of Alabama concrete for precast, prestressed applications as they are currently specified. The prediction of creep in the assessed SCC was slightly less accurate, but the error is insignificant considering the variability discussed in Section 5.4.1.1.

5.4.2.3 Comparisons of Measured and Predicted Shrinkage

Errors between predicted and measured shrinkage for each reviewed prediction model are presented in Table 5.7 using the same parameters as in the previous subsection (ω_{BP} and error percentages at fifty-six days and one year). Also like in the previous subsection, data used to derive this table are presented by Keske (2014).

Table 5.7: Error comparisons for existing shrinkage prediction models

Shrinkage Prediction Model	ω_{BP}		Error % at 56 days		Error % at 1 year	
	SCC	VC	SCC	VC	SCC	VC
ACI 209	0.615	0.683	24	42	42	54
AASHTO 2013	0.301	0.509	10	46	4	29
NCHRP 628	0.974	1.227	51	87	73	103
Eurocode 2	0.689	1.033	49	100	35	71
MC 2010	0.436	0.758	14	54	27	62

Several conclusions are warranted based on the results shown in Table 5.7:

- Prediction of the shrinkage of the assessed SCC and VC was far less accurate than prediction of their compliance,
- The AASHTO 2013 shrinkage model was markedly more accurate than the other models at predicting shrinkage in the assessed mixtures (in terms of ω_{BP} and percent error), especially in SCC,
- On average, the prediction models tended to over-predict shrinkage at all ages, especially in VC, and

- The only model that was reasonably accurate for SCC shrinkage prediction (AASHTO 2013) was also somewhat accurate for VC shrinkage prediction at later ages (within 30% at a concrete age of one year).

Notably, the time-dependent shrinkage deformation of Alabama concrete for precast, prestressed applications was also over-predicted in past AUHRC projects (Kavanaugh 2008; Levy et al. 2010), especially in mixtures proportioned with slag cement. Thus, the mixture proportions of the SCC and VC utilized in this project, which included a similar usage of slag cement, could partially explain the over-prediction of the shrinkage of the tested SCC and VC.

5.4.2.4 Comparisons of Measured and Predicted Total Strains

In the comparisons of measured SCC results to measured VC results, a direct comparison of total strain was not warranted because each specimen exhibited a different f_{ci} and E_{ci}. Note that, in this section, each specimen's total strain is only compared to the total strain predicted for that particular specimen. This could prove useful because an engineer is likely to use one reference's prediction models (AASHTO 2013 or MC 2010, for example) for both creep and shrinkage prediction.

Errors between predicted and measured total strain for each reviewed prediction model are presented in Table 5.8 using error percentages at fifty-six days and one year. The BP coefficient of variation was not accessed in this comparison, as the results are compared only to illustrate the relative magnitude of prediction errors that would occur under common engineering circumstances—during the use of a single reference's creep and shrinkage models.

Table 5.8: Error comparisons for total deformation predicted by existing references

Compliance Prediction Model	Error % at 56 days		Error % at 1 year	
	SCC	VC	SCC	VC
ACI 209	-3	3	5	13
AASHTO 2013	-7	2	-6	5
NCHRP 628	15	9	23	19
Eurocode 2	1	13	2	18
MC 2010	-5	6	0	15

Several conclusions are warranted based on the results shown in Table 5.8. They include that

- The total deformations of the tested SCC and VC were reasonably predictable using most of the referenced models (within 20% of measured results at concrete ages of fifty-six days and one year, on average, using all models except the NCHRP 628 model),
- Use of the AASHTO 2013 creep and shrinkage models led to the most under-predicted total strain predictions, while use the NCHRP 628 models led to the most over-predicted total strain predictions,
- Use of any model except the NCHRP 628 model (ACI 209, AASHTO 2013, Eurocode 2, or MC 2010 models) led to the accurate prediction of total SCC strain (within 10% of measured strains at concrete ages of fifty-six days and one year, on average), and
- Use of the AASHTO 2013 models led to the most accurate prediction of total VC strain (within 5% of measured strains at concrete ages of fifty-six days and one year, on average).

While use of any single reference's creep and shrinkage predictions led to accurate total strain prediction in both materials, the occurrence is only coincidental to these particular concretes. The references that most under-predicted compliance also tended to most over-predict shrinkage; only the current *AASHTO LRFD* models reasonably predicted both compliance and shrinkage. Still, the AASHTO 2013 (Section 5.4.2.3.2) model most under-predicted SCC compliance, and the AASHTO 2013 shrinkage model (Section 5.4.2.3.3) was only reasonably accurate (within 30% of measured results) concerning VC behavior at the late concrete age of one year. Therefore, mixture-specific corrections to all of the referenced models could be useful to provide more accurate prediction of each component of time-dependent strain.

5.5 SUMMARY AND CONCLUSIONS

5.5.1 Summary

To better understand the time-dependent deformability of SCC used in precast, prestressed applications, the SCC and VC used to construct the Hillabee Creek Bridge girders were tested for compliance, free shrinkage, and total strain deformation. This evaluation was completed using concrete from five production days (three SCC and two VC production days). By testing multiple batches of the same mixtures that had been produced under similar but varied exposure conditions, valuable insights were gained regarding the time-dependent deformability of prestressed-suitable SCC and VC made using materials and practices common in Alabama.

SCC time-dependent deformation was evaluated both in relation to the companion VC used in the bridge and in relation to various current prediction models proposed by ACI 209 (ACI 209 1992), AASHTO (AASHTO 2013), NCHRP (Khayat and Mitchell 2009), and *fib* (*fib* 2010).

The observations and conclusions made concerning the measured deformability of SCC and VC used in the Hillabee Creek Bridge girders are summarized in Section 5.5.2; the recommendations made based on this research are then given in Section 5.5.3.

5.5.2 Observations and Conclusions

5.5.2.1 Measured Compliance and Shrinkage

- Measured SCC compliance was approximately 15% greater than that of the equivalent-strength companion VC. The increased compliance of the SCC was likely related to its reduced stiffness (SCC E_{ci} was approximately 10-15% less than that of the companion VC).
- Compliance growth (creep) of SCC was comparable to that of VC; average measured SCC creep was approximately 5% greater than that of the companion VC. Any difference was expectable in response to the differences in mixture proportions and was considered practically insignificant considering the inherent variability of creep testing.
- Measured SCC free shrinkage was approximately 30% greater than that of the equivalent-strength companion VC. The increased shrinkage of the SCC was likely related to its increased paste volume and reduced aggregate content.
- Shrinkage growth of SCC was comparable to that of VC when compared over a range of time periods. In both concretes, the free shrinkage doubled between concrete ages of seven days and fifty-six days but grew by approximately an additional 50% between fifty-six days and one year.
- High variability was observed in the shrinkage measurements of SCC and VC prisms tested in accordance with ASTM C157, but all specimens satisfied the requirement of the project that length change be no greater than 0.04% after twenty-eight days of drying.

5.5.2.2 Prediction of Compliance, Shrinkage, and Total Strain

- All of the reviewed creep prediction models—ACI 209, AASHTO 2013, NCHRP 628, and MC 2010—were reasonably accurate at predicting the compliance of SCC and VC at concrete ages of fifty-six days and one year.
- While SCC *J* was slightly less predictable using the existing models, predictions of SCC *J* were within 15% of measured results, on average, and those of VC *J* were within 10%, on average, at concrete ages of up to one year.

- Prediction of the shrinkage of the tested concretes was less accurate than prediction of their time-dependent compliance. On average, the prediction models tended to over-predict shrinkage, especially in vibrated concrete.
- Only the AASHTO 2013 shrinkage model was reasonably accurate at predicting shrinkage in the assessed mixtures; it was more accurate at predicting shrinkage of the tested SCC, in which the predicted shrinkage was within 10% of the measured result, on average.
- While use of any single reference's creep and shrinkage predictions led to accurate total strain prediction in both SCC and VC, the occurrence is only coincidental to these particular concrete mixtures and circumstances—each reference compensated for under-predicting *J* by over-predicting shrinkage.

5.5.3 Recommendations

- Concerns about the increased pre-erection compliance or creep of SCC should not restrict the implementation of SCC in precast, prestressed applications because increases were minor and expectable in response to mixture changes commonly used to achieve self-consolidating behavior.
- While many current provisions for creep and shrinkage were used to accurately predict total time-dependent strain of SCC or VC cylinders tested according to ASTM C512, no single reference yielded accurate prediction of both time-dependent strain components of both materials. Therefore, adjustment of the models to accurately reflect the separate creep and shrinkage behaviors of Alabama concrete may be valuable. Such adjustments should incorporate long-term results (such as those measured during ALDOT project 930-799).
- In the absence of more refined analysis, use of the *AASHTO LRFD* (2013) models should allow for reasonable estimation of pre-erection time-dependent behavior of SCC of similar constituents and proportions as the mixture utilized during this research.
- On average, the concrete tested during this research exhibited less shrinkage than predicted by current design provisions, although SCC free shrinkage was approximately 30% greater than that of the companion VC. The sensitivity of full-scale structural behavior to this difference in unrestrained-shrinkage behavior is evaluated in the next chapter.

CHAPTER 6: TIME-DEPENDENT BEHAVIOR OF GIRDERS

6.1 INTRODUCTION

In Chapter 5 of this report, the difference in the time-dependent load-dependent behavior of SCC cylinders was shown to be minor and largely explainable by the differences in mixture proportions and hardened mechanical properties observed between the tested SCC and VC. The difference in load-independent free-shrinkage behavior of the tested SCC relative to that of the companion VC was also assessed. While increased paste content or other confounding variables (such as *s/agg*, coarse aggregate gradation, or chemical admixture use) led to approximately 30% greater unrestrained shrinkage in the SCC than in the vibrated concrete, the increase was expectable in response to such mixture changes, and both concretes exhibited less shrinkage than predicted using current models.

The primary time-dependent structural performance characteristics evaluated in the Hillabee Creek Bridge girders were their midspan camber and effective prestress in the prestressed strands. These behaviors directly relate to the creep and shrinkage properties evaluated in the previous chapter, as well as the mechanical properties evaluated in Chapter 3. Evaluation of full-scale behavior is critical because existing full-scale evaluations of SCC have been limited, and their implications for SCC girders of the scale used in this bridge and made using Alabama materials and methods are unclear. Furthermore, existing evaluations have been limited in duration, which is of clear significance since time-dependent deformations were found in Chapter 5 to continue to evolve through a concrete age of one year.

Prediction of full-scale time-dependent behavior is frequently based on empirical formulas derived from the evaluation of representative cylinders. For this project, these small-specimen tests were conducted on some batches of concrete placed in the girders, so the measured material properties were directly used in the predictions. In this way, the predictability of full-scale behavior of SCC girders was assessed while using the most accurate material properties determined from testing representative cylinders. This evaluation required consideration of both the companion VC girders used in the bridge and the time-dependent behavioral models discussed in Chapter 5.

To effectively evaluate full-scale time-dependent properties, measurements that reflect varying ambient conditions must be adjusted to account for differences in concrete temperature at the times of data collection. While variations due to ambient thermal conditions may be important, measurements obtained during this research were corrected relative to a standard reference temperature to isolate the gradual time-dependent changes due to creep and shrinkage from those due to transient thermal effects. Thus, it was useful to determine the coefficient of

thermal expansion (CTE) of each mixture. This analysis was valuable because CTE is a load-independent material property that, like unrestrained shrinkage behavior, is affected by concrete proportioning (Neville 1996).

6.2 LITERATURE REVIEW

6.2.1 Time-Dependent Behavior of Precast, Prestressed Girders

The two full-scale time-dependent behaviors most commonly assessed in precast, prestressed girders are camber and effective prestress. Incorrectly predicting the amount of prestress lost over the service life of a girder can have significant effects. Over-prediction of losses can result in the use of an unnecessarily large amount of prestressing in the girder, driving up the cost of that girder; under-prediction can lead to cracking and excessive deflections under service loads. Although under-prediction of prestress loss is not likely to affect flexural strength, it can lead to an over-estimation of concrete shear strength in the end regions of prestressed concrete beams. In a similar fashion, the significant over-prediction of camber can cause issues during the construction of the bridge and afterwards: the casting of a deck over girders with a smaller than expected camber requires an increased volume of deck concrete, which increases cost and superimposed dead loads. In extreme cases, low-camber girders may eventually sag under superimposed dead loads.

In light of the previous statements regarding over-prediction of camber, the property is most important at early ages prior to the time of deck construction. As long as the camber at the time of deck construction is adequately predicted, long-term cambers are not likely to be problematic. Only the minimum camber at shipment (greater than 0.5 in.) was specified in the special provision of this project. However, estimates of initial camber and camber at the time of deck construction were provided on the construction plans.

Results from the full-scale research projects regarding SCC girder behavior have been mixed. Naito et al. (2005) and Ziehl et al. (2009) found that SCC girders exhibited greater elastic shortening due to the reduced stiffness of the SCC, but that the SCC girders exhibited less growth over time. Trent (2007) also found that SCC girders exhibited less prestress loss despite being of the same strength and stiffness as the companion VC. Thus, these researchers suggested that SCC exhibited improved resistance to time-dependent deformation.

Other researchers (Hamilton et al. 2005; Schrantz 2012; Zia et al. 2005) have found no difference between SCC and VC camber or camber growth. Still others have found that SCC exhibits slightly greater (Erkmen et al. 2008; Ozyildirim 2008) or less (Khayat and Mitchell 2009) camber relative to companion VC girders. Many (Erkmen et al. 2008; Khayat and Mitchell 2009; Ozyildirim 2008) found that differences could be explained by differences in the material

properties measured in representative cylinders; Khayat and Mitchell (2009) specifically found that later-age SCC camber was reduced because of the increased volumetric shrinkage of the material.

Like the mixed conclusions discussed in previous chapters, it is difficult to directly compare structural properties of SCC and VC without accounting for differences in the tested materials. More importantly, Erkmen et al. (2008) and Trejo et al. (2008) concluded that representative-cylinder data could be used to predict measured in-place performance of SCC girders with as much accuracy as when predicting VC girder behavior. Storm et al. (2013) suggest that the variability inherent to the production process (including the use of many discrete batches of concrete, differences in curing and ambient temperature, and release method) greatly affects behavioral predictions in all precast, prestressed concrete.

Hamilton et al. (2005), Staton et al. (2009) and Trejo et al. (2008) state that such construction variations may be more important than the difference between SCC and VC. Furthermore, several researchers have indicated that the accuracy of full-scale behavioral predictions is most significantly improved by the use of measured engineering properties in place of design properties, whether considering VC (Stallings et al. 2003; Storm et al. 2013) or SCC (as discussed in this report).

Changes in concrete strain due to fluctuations in ambient temperatures are time-dependent because temperatures vary with time. However, after hydration-related early-age E_c evolution and thermal effects have stabilized, the effects of ambient temperature changes are transient—as long as restraint of thermal deformation does not lead to inelastic stresses, the change in strain corresponding to a particular change in temperature is reversed when the change in temperature is reversed. Meanwhile, time-dependent deformations due to creep and shrinkage are gradual and mostly irreversible; therefore, thermal deformation of concrete (see Section 6.2.3) is considered separately from these gradually occurring effects in this report.

6.2.2 Prediction of Camber and Prestress Losses using Incremental Time-Step Analysis

Time-dependent behavior of precast, prestressed girders involves many variables, many of which are interdependent or change with time. The most important variables include f_c, E_c, and time-dependent creep and shrinkage properties of the material (Stallings et al. 2003; Storm et al. 2013). Barr et al. (2008) concluded that errors in the prediction of full-scale behavior are predominantly due to errors in the material-behavior prediction models, which is why the time-dependent behavior of representative cylinders continues to be evaluated.

The compressive stress in full-scale precast, prestressed girders changes with time, both in response to changing external loads (such as the addition of a deck or diaphragms) and changing internal strains (due to creep, shrinkage, or thermal effects). Thus, an incremental time-

step method is typically needed to predict the full-scale behavior of these girders. In previous research at the AUHRC, Johnson (2012), Schrantz (2012), and Stallings et al. (2003) have used such a method based on compatibility, equilibrium, empirically defined material behaviors (elastic and time-dependent), and engineering beam theory. The method developed by Schrantz (2012) was used during this research, so topics related to it are discussed in Section 6.3.5.

6.2.3 Thermal Behavior of Concrete

Unrestrained concrete and steel each expand when heated and contract when cooled. The stress-free change in unit length per unit of temperature change is referred to as the coefficient of thermal expansion (CTE). It is used to describe the load-independent thermal strain (ε_T) response to a change in temperature (ΔT) according to Equation 6-1.

$$\varepsilon_T = CTE \times \Delta T \tag{6-1}$$

Concrete and steel exhibit different but very similar CTE: approximately 4.1–7.2 με/°F in concrete (average of 5.6 με/°F) and 6.1–6.7 με/°F in steel (FHWA 2011). Concrete and steel interact favorably because they exhibit similar CTE, but the disparity between the two can vary widely due to the heterogeneous nature of concrete. Each component of concrete—cement, SCM, sand, coarse aggregate, and water—exhibits a different CTE, so the CTE of the composite material varies widely and is based entirely on the mixture proportions and interactions between the components. In general, CTE of concrete is based on the paste volume, cementitious material type, and aggregate type, with aggregate type having the most significant influence because aggregate represents the largest portion of the material volume (Mindess et al. 2003).

An increasing understanding of the large stresses that can develop in integral concrete structures (especially bridge decks and concrete pavements) due to thermal expansion led the AUHRC research team to evaluate CTE in concrete made using typical Alabama materials and proportions. In that research, Sakyi-Bekoe (2008) determined that Alabama concrete made using siliceous river gravel exhibited a greater CTE than concrete made with crushed dolomitic limestone—6.9 με/°F versus 5.5 με/°F, respectively. The difference was attributed to the distinctly different CTE of the coarse aggregates. Mindess et al. (2003) state that quartz and similarly siliceous aggregates exhibit the highest aggregate CTE of approximately 6.9 με/°F, while dolomite may exhibit a CTE as low as 3.0 με/°F. Furthermore, the mineralogy of a particular aggregate type can vary between quarries, with direct implications on the CTE of the aggregate (Emanuel and Hulsey 1977).

The second largest effect observed in the AUHRC study by Sakyi-Bekoe (2008) was *s/agg*, at least when evaluating the dolomitic-limestone concrete. Because natural sand typically contains a high percentage of silica, it exhibits a CTE more similar to that of siliceous river gravel. Thus, increasing the coarse aggregate content or reducing the *s/agg* reduced the CTE of

concrete made with crushed dolomitic limestone (Sakyi-Bekoe 2008). Also, increasing total aggregate volume decreased CTE, but the effect of the variable was confounded in that work because *w/cm* was also increased, which would have the same effect on the concrete CTE.

CTE of hardened, saturated cement paste is approximately 10 με/°F, and it is affected by SCM replacement, *w/cm*, and (most importantly) degree of saturation (Mindess et al. 2003). The effects of SCMs and *w/cm* on paste CTE are generally considered to be minor except when comparing drastically different mixtures. In past AUHRC research, changing the *w/cm* from 0.32 to 0.44 typically decreased CTE by 3–10% (Sakyi-Bekoe 2008). Meanwhile, completely saturated concrete exhibits approximately the same CTE as oven-dried concrete, but concrete CTE increases by up to approximately 18% at partial saturation (maximum at approximately 70% relative humidity) (Neville 1996). More specifically, the CTE of the paste fraction has been observed to increase by 60–70% when exposed to approximately 50–70% relative humidity. This dependence is illustrated in Figure 6.1 from Neville (1996).

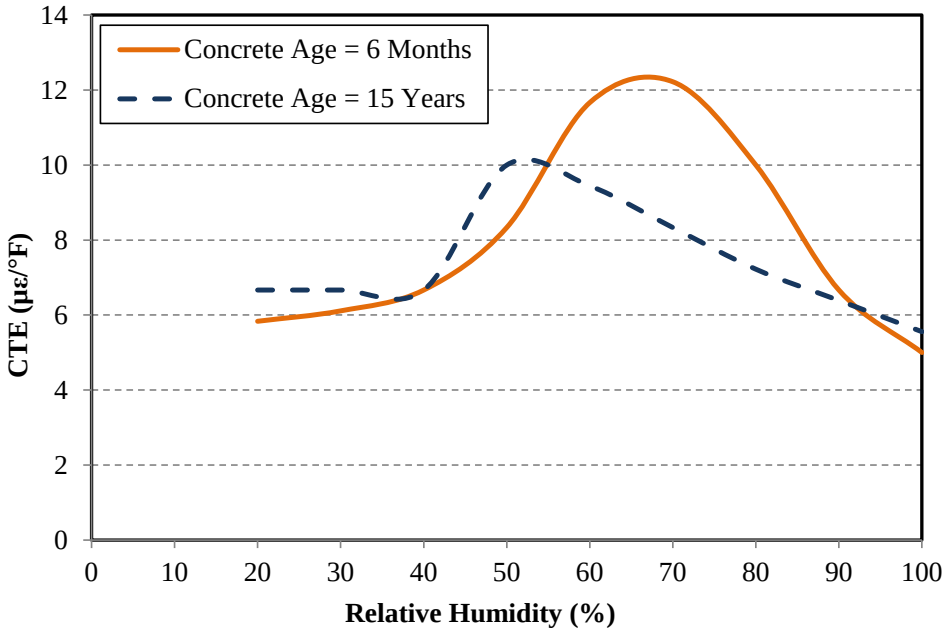

Figure 6.1: Variation of CTE of cement paste due to relative humidity (adapted from Neville 1996)

The effect of partial saturation on concrete CTE can also be interpreted from ACI 209 (1992) Equation 2-32, which is presented as Equation 6-2 below. In it, CTE (in με/°F) is estimated by an empirical formula with variables for concrete saturation (*x*) and coarse aggregate type (e_{agg}):

$$CTE = x + 1.72 + 0.72(e_{agg}) \quad (6\text{-}2)$$

In the equation, an e_{agg} value of 3.1 was recommended for limestone. The variable *x* was described as equaling 0.0 in saturated conditions and "0.83 to 1.11" in external beams exposed to

gradual drying. Based on this equation, CTE of limestone-aggregate concrete at a partially saturated relative humidity is as much as 17% greater than at full saturation. Furthermore, a Mississippi DOT report on the effect of relative humidity on CTE found that concrete made with Alabama limestone exhibited up to 26% greater CTE at 75% relative humidity than at saturation (Al-Ostaz 2007).

Emanuel and Hulsey (1977) first recommended a volumetrically weighted calculation of CTE for concrete. This concept was recommended by FHWA (2011) as being second in accuracy only to the physical measurement of CTE according to AASHTO T 336 (AASHTO 2012). Volumetric calculation of CTE was also used by Sakyi-Bekoe (2008) to estimate CTE in Alabama concrete. In a general form, this relationship is illustrated by Equation 6-3 (Emanuel and Hulsey 1977):

$$CTE_{Concrete} = CTE_{Paste}\left(\frac{V_{Paste}}{V_{Total}}\right) + CTE_{FA}\left(\frac{V_{FA}}{V_{Total}}\right) + CTE_{CA}\left(\frac{V_{CA}}{V_{Total}}\right) \quad (6\text{-}3)$$

Where

V_{Paste} is the volume of the cementitious paste,
V_{FA} is the volume of the fine aggregate,
V_{CA} is the volume of the coarse aggregate, and
V_{Total} is the total volume of concrete that includes air content.

Based on Equation 6-3, the CTE of SCC is expected to be different than that of VC if it contains a greater paste volume (which exhibits a relatively larger CTE) and sand volume (frequently siliceous, which exhibits a larger CTE than dolomitic limestone coarse aggregate). Notably, this difference would be expected between *any* two concretes with varying proportions or different types of aggregate.

While SCC may exhibit a larger CTE than comparable VC due to its different mixture proportions, documentation of thermal effects in full-scale SCC girders has been limited. Specifically, Zia et al. (2005) found that thermal fluctuations in internal strain were greater in SCC girders than in companion VC girders despite being of the same elastic stiffness. They stated that, "under seasonal temperature changes, the stiffness of the SCC girders appeared to decrease more than the stiffness of the regular concrete girders." What their results more likely indicate is a difference in CTE—E_c does not change seasonally, but load-independent strains would be different at a given temperature if two concretes exhibit different CTEs.

Elsewhere, varying values of concrete CTE were assumed during analyses of measured SCC and VC results. Khayat and Mitchell (2009) assumed a concrete CTE of 6.4. με/°F in both the SCC and VC they utilized because of the high paste content and low *w/cm* of those mixtures. Trejo et al. (2008) assumed an SCC CTE of 5.6 με/°F because it would be very similar to assumed steel and strain-gauge CTEs of 5.0 and 5.6 με/°F, respectively. Meanwhile, Erkmen et

al. (2008) assumed concrete and steel CTEs of 6.0 and 6.8 με/°F, respectively. All of these fell within the range published by the FHWA (2011) and described earlier, and none distinguished between the CTE of SCC and of VC.

6.3 EXPERIMENTAL PROGRAM

6.3.1 Concrete Coefficient of Thermal Expansion Evaluation

In addition to use for comparison of unrestrained shrinkage, the rectangular prisms discussed in Chapter 5 served a second purpose when the response of the bridge girders to diurnal heating was investigated by testing the apparent coefficient of thermal expansion (CTE) of the prisms. These rectangular prisms exhibited marginally different cross-sectional properties than specified for CTE measurement according to AASHTO T 336-09—they exhibit a square cross section with sides equaling 3 in., while the standard specifies the use of a cylindrical specimen with a diameter equaling four inches. Thus, the utilized specimens exhibited a smaller cross-sectional area and smaller *V/S*.

CTE was only tested in concrete from one girder-production group per material (SCC-E and VC-E). As the need for this testing only became apparent after the girders were cast, these were the only matching samples still available. Because of their similarity to the standard specimen used during testing according to AASHTO T 336-09, the testing of these prisms was deemed acceptable and necessary. All testing was conducted after the girder concrete reached an age of three years. At this age, deformations due to shrinkage that would occur during the testing interval were assumed to be minimal.

The prisms were tested using two methods. First, they were exposed to cycles of heating and cooling from 40–120°F using an environmental chamber to closely reflect the measured range of temperatures in the bridge. The apparatus used to measure the length change due to unrestrained shrinkage was then used to measure the length change due to thermal effects. After observing potentially significant differences between the materials, the specimens were then tested as described by AASHTO T 336-09. This required the ends to be sawn to shorten the prisms, as the test equipment requires a sample approximately 7.0 in. in length.

6.3.2 Girder Temperature Evaluation

To effectively compare measured time-dependent behaviors (maintenance of effective prestress and changes in camber), transient changes in these measures due to thermal effects must be isolated from those due to creep and shrinkage. Thermistors attached to the VWSGs used in this research (see Section 4.3.2) allowed development of a concrete temperature profile for use to

correct strain and camber measurements for thermal effects. By measuring both strain and temperature, the effects of concrete CTE on fluctuations in concrete strain and camber were also directly assessed.

As mentioned in Section 6.2, predictions of time-dependent camber, strain, and prestress losses are computed assuming a constant temperature throughout the girder cross section. However, the girders were stored outdoors and were exposed to varying environmental condition. The method described in the following subsections was developed by Johnson (2012) to isolate and account for these ambient effects.

6.3.2.1 Specimen Simplification for Thermal-Effect Analysis

The first step in the process of accounting for the thermal gradients in the instrumented cross sections was to simplify the standard sections for improved ease of analysis. The simplified BT-54 and BT-72 sections are shown below in Figure 6.2 and Figure 6.3. These idealized shapes were dimensioned in order to very closely resemble the BT-54 section and BT-72 section in such geometric properties as the location of the centroid, the area of the cross section, and the moment of inertia of the cross section.

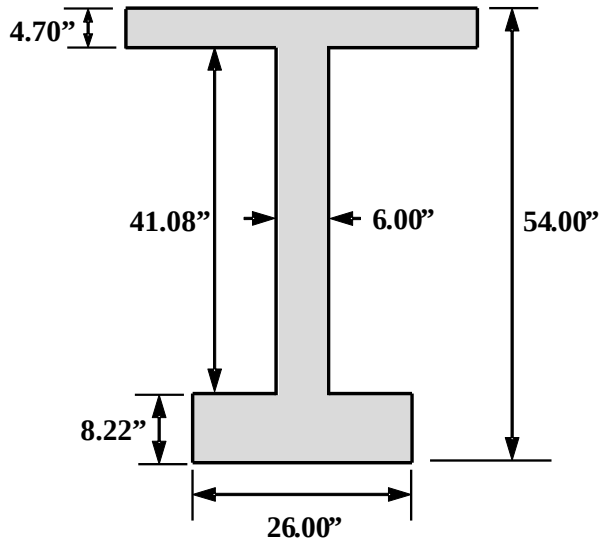

Figure 6.2: Simplified BT-54 composite section

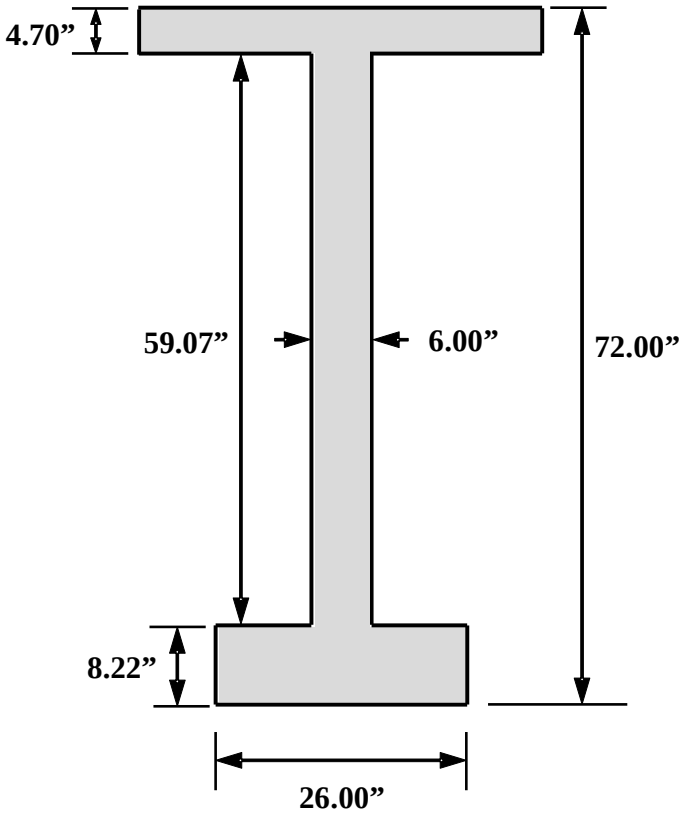

Figure 6.3: Simplified BT-72 composite section

With reference to the strain gauge locations shown in Figure 4.7 and Figure 4.8, it was necessary to assume a reasonable temperature profile between the discrete temperature measurements observed over the height of the girder. The assumed temperature profile is presented graphically in Figure 6.4 and is described by the following:

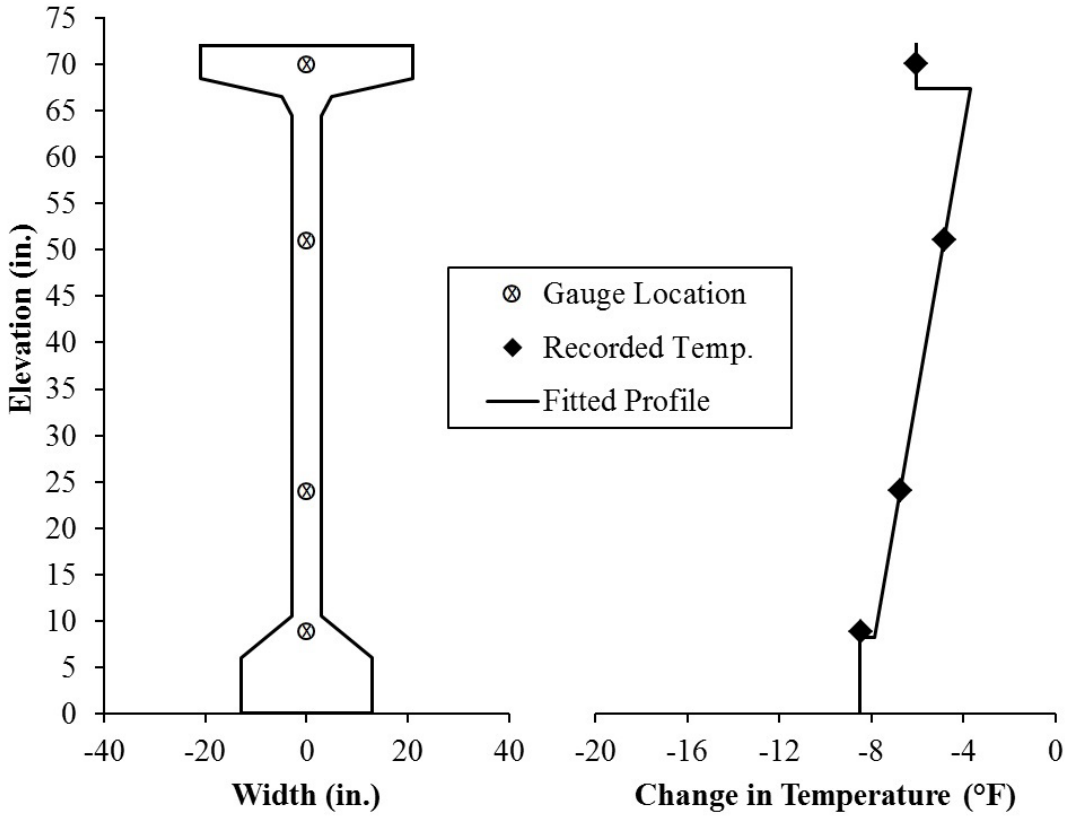

Figure 6.4: Example of idealized thermal gradient profile in BT-72

- The temperature was assumed to be uniform in each of the simplified bottom and top flanges. The utilized temperatures were those measured in the respective bottom- and top-flange thermistors; and
- A linear temperature gradient was assumed to occur through the simplified web of the girder which was created by passing a straight line through the two measured web-thermistor temperatures. This linear gradient was projected to the heights of the constant-temperature simplified flanges regardless of whether the projected temperatures matched those of the flanges.

Linear interpolation through the simplified web was understandable because two thermistors were installed in the web and were located well away from the flanges. It was also acceptable to disassociate the temperature of the web from those of the flanges because of the small *V/S* of the web. It is plausible that the temperatures actually measured in the web would not always relate to the temperatures measured in the self-insulated volumes of the top and bottom flanges. While a linear extrapolation of temperatures was imperfect compared to the actual thermal gradient in the web, it was a better approximation than to assume a constant temperature like in the simplified flanges. Trial analyses were also conducted by Johnson (2012)

assuming alternative gradients in the segments (flanges and web); results from those models did not differ significantly from the profile chosen.

6.3.2.2 Method of Isolation of Thermal Effects

To account for thermal effects, the CTEs of steel and concrete were assumed to be equal in this analysis, which was in line with the method employed elsewhere for thermal strain corrections (Erkmen et al. 2008; Trejo et al. 2008). While there may have been a slight discrepancy between the two materials, the area of steel is small relative to the area of the concrete. It would also be difficult to isolate the differential restraint experienced due only to the difference in CTEs. Considering the piecewise approximation of thermal gradients employed and that lateral temperature gradients could also exist (such as where sunlight warms only one side of the girder), this assumption is within the precision of the process.

In order to make accurate comparisons to predicted time-dependent behavior, the measured strains needed to be adjusted so that they would represent what the measured strain would have been if the girder exhibited a constant reference temperature. This reference was chosen arbitrarily to equal 68°F.

The process through which nonlinear thermal effects were calculated in this research was outlined by Johnson (2012). In summary, the strains expected to result from a nonlinear temperature distribution consist of an axial component of strain change ($\Delta\varepsilon_{cen,t}$) and a change in curvature ($\Delta\phi_t$). These components, which are derived by assuming plane sections remain plane and enforcing cross-section equilibrium, are described by Equations 6-4 and 6-5, respectively. To compensate for these nonlinear thermal effects, $\Delta\varepsilon_{cen,t}$ and $\Delta\phi_t$ are then subtracted from all measured strain readings.

$$\Delta\varepsilon_{cen,t} = \frac{CTE \int \Delta T dA'}{A'} \tag{6-4}$$

Where

CTE is the coefficient of thermal expansion of concrete,

ΔT is the difference in the temperature gradient of the cross section from 68°F, which is determined from a piecewise linear approximation in this research, and

A' is the simplified cross-sectional area

And

$$\Delta\phi_t = \frac{CTE \int \Delta T y dA'}{I} \tag{6-5}$$

Where

y is the vertical distance from the simplified centroid, and

I is the simplified cross-sectional moment of inertia.

While these equations are the same as previously employed by Johnson (2012), there were some differences in their application. First, an error was discovered in the application of these equations to the data—the slope of the temperature gradient through the web was accidentally reversed, which had varying effects on the corrections depending on the measured temperature data. Second, the corrections were improved (smoothed) by replacing the CTE value assumed by Johnson (2012) with more-representative *apparent* CTE values.

Finally, the way in which missing temperature information was replaced during this research was different than that employed by Johnson (2012). Recall that some of the girders had only one VWSG, which meant that the internal temperature could only be measured at this single location (the *cgp*). A full-depth profile is necessary to completely account for the changes in axial strain and curvature due to thermal effects. Therefore, in the previous work for this project, curvature changes were accounted for (when needed) by substituting curvatures from companion girders from the same casting group at each time step. This essentially assumed that all girders cast on the same day experienced the same thermal gradient and temperature-induced curvature.

Substitution of curvatures between companion girders in the constructed bridge would be difficult to accomplish considering the composite action of the group of girders once joined by intermediate diaphragms and a deck. Since analysis of this behavior was to be continued during a subsequent, related project (ALDOT project 930-799), an alternative method was used: temperatures from nearby girders were directly substituted prior to the integration. Similar to the previous work, this assumes that the temperatures in adjacent girders are approximately the same.

6.3.3 Prestress Loss Measurement

As previously discussed in Section 4.3.2, prestress losses were indirectly observed through the measurement of concrete strain using VWSGs installed in every girder in the bridge at midspan. The VWSGs were installed at various locations over the height of the girders (locations and girder geometries were identical in companion SCC and VC girders), which allowed for the direct comparison of measured concrete-strains and temperatures. Concrete strains were converted to changes in effective prestress through the use of linear-elastic stress-strain compatibility, and thermal effects were normalized prior to comparisons of f_{pe} according to the method described above. Isolation of thermal effects was necessary for comparison to the prestress-estimation methods described in Sections 6.3.5.

6.3.4 Camber Measurement

The camber measurement instrumentation and methodology utilized prior to girder erection at Hillabee Creek was described in detail by Johnson (2012). In summary, the method involved the measurement of girder-end and midspan elevations using a prism rod and a total station. An imaginary line was then drawn through the end-points prior to release and a permanent offset at midspan (due to variations in top-flange thickness) was determined. Offsets of the midspan reading in all subsequent measurements were then interpreted as camber.

To provide a specific and consistent location for the prism rod placement, a hex-headed lag bolt was embedded in the top surface of the girders at each location for use as a surveying target. One of these targets is shown in Figure 6.5.

Figure 6.5: Surveying target embedded in top surface of girder

6.3.5 Prediction of Camber and Prestress Losses Using Incremental Time-Step Analysis

6.3.5.1 Principles of Structural Deformation

One of the most important assumptions throughout these deformation predictions is that plane sections remain plane. This means that the change in strain at any level can be determined if the change in strain at the centroid and the change in curvature of the cross section are known, as shown in Equation 6-6 and Equation 6-7. In these equations, strain compatibility between

materials is maintained, meaning that the change in strain in prestressing steel is equal to that of the concrete surrounding it after bond is achieved.

$$\Delta\varepsilon_c = \Delta\varepsilon_{cen} + (\Delta\phi)y \tag{6-6}$$

$$\Delta\varepsilon_p = \Delta\varepsilon_{cen} + (\Delta\phi)y_p + \Delta\varepsilon_{p,i} \tag{6-7}$$

Where

$\Delta\varepsilon_c$ is the change in strain in the concrete,

$\Delta\varepsilon_{cen}$ is the change in strain at the centroid of the cross section,

$\Delta\phi$ is the change in curvature of the cross section,

y is the distance from the centroid (positive down) to the concrete depth being considered,

$\Delta\varepsilon_p$ is the change in strain in the prestressing steel,

y_p is the distance from the centroid of the cross section to the prestressing steel (positive down) being considered,

$\Delta\varepsilon_{p,i}$ is the initial difference in prestressing steel strain and strain in adjacent bonded concrete.

Because prestressing is applied eccentrically and external loads cause flexural stresses, prediction of girder deformation required calculation of an axial strain component (at the centroid of the cross section) and curvature-based strain component. Linear-elastic stress-strain material behavior requires that the strain and its accompanying stress at a location are related through a constant of proportionality, *E*. The integral of all of the changes in normal *stress* integrated over the cross-sectional area must be equal to the change in axial force, as indicated in Equation 6-8. The girders investigated in this research were all statically determinate, simply supported beams. There were no externally applied axial loads, so the net cross-sectional axial force, *N*, remained zero throughout the analysis.

$$\int_{A_c} \Delta f_c dA_c + \sum \left(\Delta f_p A_p\right) = \Delta N \tag{6-8}$$

Where

Δf_c is the change in stress in the concrete,

A_c is the cross-sectional area,

Δf_p is the change in stress in a layer of prestressing steel,

A_p is the cross-sectional area of the prestressing steel layer, and

ΔN is the change in applied axial load.

Equilibrium also requires that the integral of the changes in stress integrated over the cross section and multiplied by the distance from the centroid must equal the applied moment, *M*,

at the cross section, as indicated in Equation 6-9. The externally applied moment, which is caused only by the girder's self-weight in this program, does not change, so the change is set to zero after the initial prestress is applied.

$$\int_{A_c} \Delta f_c y dA_c + \sum \left(\Delta f_p y_p A_p\right) = \Delta M \tag{6-9}$$

Where

y is the distance from the centroidal axis (downward positive),
y_p is the distance from the centroidal axis to the prestressing steel, and
Δ*M* is the change in externally applied moment.

The changes in strain at the centroid of a cross section and cross-sectional curvature can be attributed to two different types of strain changes. The first type of strain is stress-dependent strain. These strain changes (elastic and time-dependent) result directly from the linear-elastic girder response to changes in the state of stress on the material. The second type of strain includes the strain components that occur independently of stress changes, including thermal, and shrinkage strains. Both types of strain (load-dependent and load-independent) can be described by various empirical material models, several of which were described in Chapter 5.

In this analysis, shrinkage strains are considered constant over the depth of the cross section when unrestrained (appropriate considering that these girders are simply supported). The creep strain, however, varies with depth because load-induced stress varies linearly over the depth of the cross section. Therefore, the creep strains are described by an axial component combined with as an associated curvature component that describes their variation through the depth. The total strain change in the concrete is the sum of the stress-dependent strain and the stress-independent strains as shown in Equation 6-10.

$$\Delta\varepsilon_c = \frac{\Delta f_c}{E_c} + \Delta\varepsilon_{c,cr} + \Delta\varepsilon_{c,sh} + \Delta\varepsilon_{c,T} \tag{6-10}$$

Where

$\Delta\varepsilon_c$ is the total change in strain in the concrete,
$\Delta\varepsilon_{c,cr}$ is the change in concrete strain due to creep,
$\Delta\varepsilon_{c,sh}$ is the change in concrete strain due to shrinkage, and
$\Delta\varepsilon_{c,T}$ is the change in concrete strain due to temperature.

Because temperature changes are transient, they were neglected in the prediction models used for this research. Experimental results were later corrected to address thermal changes, as described in Section 6.3. Rearrangement of Equation 6-10 to solve for the change in concrete stress yields Equation 6-11. Using the time-step program developed by Schrantz, this

change in concrete stress is then considered during the calculation of stress-dependent creep in all subsequent time steps.

$$\Delta f_c = E_c\left[\Delta\varepsilon_c - \left(\Delta\varepsilon_{c,cr} + \Delta\varepsilon_{c,sh}\right)\right] \quad (6\text{-}11)$$

Because the prestressing reinforcement does not shrink and its viscoelastic response is usually described as stress relaxation rather than creep strain, an additional term for relaxation losses must be added to the stress-strain response to $\Delta\varepsilon_p$ (from Equation 6-7). The change in stress in the reinforcement is thus computed according to Equation 6-12:

$$\Delta f_p = E_p\left(\Delta\varepsilon_p\right) + \Delta f_{p,R} \quad (6\text{-}12)$$

Where

$\Delta f_{p,R}$ is the change in prestress due to relaxation.

6.3.5.2 Calculation of Initial Strain, Prestress Losses, and Camber

To evaluate the time-dependent deformability of full-scale girders, the initial elastic response to the transfer mechanism must be calculated first. Calculation of the prestress loss due to the elastic shortening of the concrete, Δf_{pES}, was described in Section 4.2.2. Camber at midspan, δ, is calculated using the general equation shown below. During this research, the beams are simply-supported and symmetrical with a uniformly distributed self-weight, meaning that camber at midspan equals the change in deflection over half of the length of the beam. Also, pre-release curvature is assumed to equal zero, so camber at release is calculated by integrating the change in cross-sectional curvature due to the transfer mechanism, $(\Delta\phi)_{ES}$ from Equation 4-5:

$$\delta = \int_0^{0.5L} (\Delta\phi)_{ES} x \, dx \quad (6\text{-}13)$$

In this research, curvatures are determined at a user-specified number of cross sections along the girder length, and these curvatures are used to compute the midspan deflection using the moment-area method described in detail by Schrantz (2012). That method assumed linear changes in curvature between the analyzed cross sections, so an increase in the number of cross sections analyzed corresponds to an increase in the accuracy of the camber prediction.

6.3.5.3 Determination of Incremental Material Properties

In addition to the initial elastic responses discussed and analyzed previously, calculation of time-dependent responses also requires the use of several empirically defined material behaviors:

- Elastic mechanical properties of concrete and prestressing steel (defined by *E*)
- Time-dependent, stress-dependent properties of concrete (creep) and steel (relaxation), and

- Time-dependent, stress-independent properties of concrete (shrinkage).

In all analyses discussed in this report, the modulus of elasticity of prestressed strand (E_p) was assumed to equal a constant 28,600 ksi. Meanwhile, E_c is generally assumed to vary proportionally to the square root of compressive strength (see Chapter 3); like f_c, E_c therefore increases over time. The software program developed by Schrantz (2012) and used for this project allows for different ways to account for the change in E_c during the time-step computation of camber. The user can select a constant E_c or select a two-point method in which measured or assumed modulus values at transfer (E_{ci}) and at 28 days ($E_{c,28}$) are used to establish a growth curve over time.

Equations 6-14 and 6-15 shown below were developed based on the time-dependent coefficient $\beta_{cc}(t)$ found in the MC 90 equation for development of concrete strength with time (CEB 1990). The modulus of elasticity of the concrete is a function of the concrete age at the beginning of each interval, 28-day $E_{c,28}$, and a growth rate function, s. The two-point system described below was used for all of the incremental-analysis predictions developed in this study.

$$E_{c,t} = E_{c,28} exp\left\{ s\left[1 - \left(\frac{28}{age_{t1}} \right)^{0.5} \right] \right\} \tag{6-14}$$

In which

$$s = \frac{ln\left(\frac{E_{ci}}{E_{c,28}} \right)}{1 - \left(\frac{28}{age_{ti}} \right)^{0.5}} \tag{6-15}$$

And where

$E_{c,t}$ is the modulus of elasticity of concrete at the beginning of given time step,
age_{t1} is the concrete age at the beginning of the interval (days), and
age_{ti} is the concrete age at transfer (days).

A typical growth curve for E_c developed using Equations 6-14 and 6-15 is shown in Figure 6.6. In it, a release age of 20 hours and initial and 28-day E_c values of 6,000 ksi and 6,600 ksi, respectively, are utilized because these values are similar to the average values observed during this research.

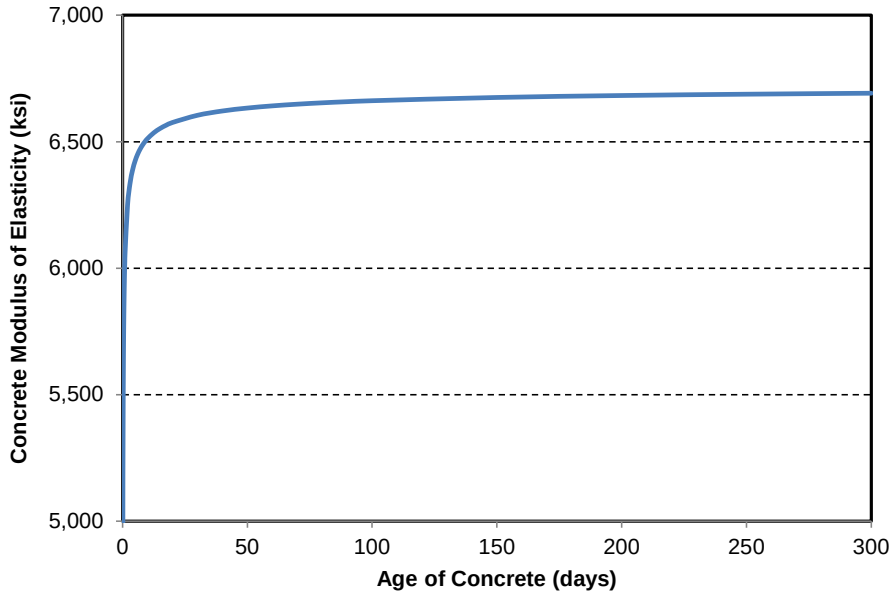

Figure 6.6: Concrete modulus of elasticity development using the two-point method

Several methods are available to estimate the strain-independent prestress loss due to steel relaxation. In this incremental analysis, this loss was estimated according to Equation 6-16, which is similar to Equation 4-6 regarding pre-release relaxation losses:

$$\Delta f_{p,R} = f_{pi}\left[\frac{\log(t_2) - log(t_1)}{45}\right]\left[\left(\frac{f_{pi}}{f_{py}}\right) - 0.55\right] \quad (6\text{-}16)$$

Where

$\Delta f_{p,R}$ is the change in prestress force due to stress relaxation (ksi),
f_{pi} is the jacking stress at the beginning of the time step (ksi),
t_1 is the time at the beginning of the time step (hours),
t_2 is the time at the end of the time step interval (hours), and
f_{py} is the yield strength of the prestressing reinforcement (ksi).

In addition to these assumed models of concrete stiffness and steel relaxation, time-dependent creep and shrinkage behaviors are of primary significance in this research. Several empirical methods for estimating these behaviors are outlined in Chapter 5. The *AASHTO LRFD Bridge Design Specification* (2013) Section 5.4.2.3.1 allows for the use of a variety of creep and shrinkage prediction models to estimate the time-dependent behavior of concrete bridge components. In this incremental analysis, the three most common and current deformation models from Chapter 5 were assessed: ACI 209 (1992), *AASHTO LRFD* (2013) Section 5.9.5.4, and MC 2010.

6.3.5.4 Calculation of Incremental Time-Dependent Deformation

Using the referenced material models, time-dependent deformations were computed by incrementally evaluating the changes in strain over all of the time steps leading up to the time of interest—at midspan to determine effective prestress, f_{pe}, and over a user-defined number of cross sections to determine camber. To determine incremental strain changes, the relationships defined above in Equation 6-11 and Equation 6-12 are combined and substituted into the equilibrium relationship of Equation 6-8. The strain change resulting from temperature is ignored in this program, so that term from Equation 6-10 is not needed. The resulting equation is solved for the change in strain at the centroid of the cross section and is shown as Equation 6-17:

$$\Delta\varepsilon_{cen} = \frac{E_c A_c\left(\Delta\varepsilon_{cen,cr} + \Delta\varepsilon_{c,sh}\right) + E_c \Delta\phi_{cr} \int_{A_c} y dA_c - \sum\left(A_p \Delta f_{p,R}\right)}{E_c A_c + E_p \sum A_p} \tag{6-17}$$

Applying the principles of transformed-section analysis and combining like terms, Equation 6-17 can be rewritten as Equation 6-18 for determining the incremental strain at the centroid of the cross section:

$$\Delta\varepsilon_{cen} = \frac{A_c}{A_{tr}}\left(\Delta\varepsilon_{cen,cr} + \Delta\varepsilon_{c,sh}\right) - \left[\frac{\Delta\phi_{cr}\left\{\Sigma\left(n_p y_p A_p\right)\right\} + \frac{1}{E_c}\Sigma\left(A_p \Delta f_{p,R}\right)}{A_{tr}}\right] \tag{6-18}$$

Where

A_{tr} is the transformed cross-sectional area,
$\Delta\varepsilon_{cen,cr}$ is the change in strain at the cross-sectional centroid due to creep,
$\Delta\phi_{cr}$ is the change in curvature of the cross section due to creep, and
n_p is the modular ratio for the prestressing steel and concrete (E_p/E_c).

Careful examination of this equation reveals that the centroidal strain change is primarily a result of the shrinkage strain and the axial component of the creep strain. However, the change in curvature due to creep and the steel relaxation also contribute slightly if the section is eccentrically reinforced. The change in curvature for each time step is found in a similar fashion as illustrated above. The same relationships from Equations 6-11 and 6-12 are substituted into Equation 6-9, and then the equation is solved for the change in curvature using transformed-section analysis:

$$\Delta\phi = \Delta\phi_{cr}\left[1 - \frac{\Sigma\left(n_p {y_p}^2 A_p\right)}{A_{tr}}\right] - \left[\frac{\left\{\left(\Delta\varepsilon_{cen,cr} + \Delta\varepsilon_{c,sh}\right)\left(n_p y_p A_p\right) + \left(\Sigma n_p\left(\frac{\Delta f_{p,R}}{E_p}\right) y_p A_p\right)\right\}}{I_{tr}}\right] \tag{6-19}$$

In the above equation, I_{tr} is the area moment of inertia of the transformed cross section. Careful examination of this equation reveals that the curvature change is primarily a result of the

bending (curvature) component of the creep strain. However, the shrinkage, steel relaxation, and axial component of the creep also contribute slightly to the curvature change if the section is eccentrically reinforced.

6.3.6 Nomenclature and Additional Considerations

6.3.6.1 Nomenclature and Use of Data

Only the basic nomenclature shown in Figure 3.7 was necessary to identify the girders during this full-scale analysis. As with the assessments of the other chapters, the exact placement location of the batches sampled for laboratory testing could not be isolated within the girders. Samples taken at the midpoint of each girder-production day were assumed to be representative of the majority of concrete placed during those days.

The use of production-group hardened mechanical properties (see Section 3.4.3) is of imperfect accuracy for the prediction of individual-girder behavior. However, it would be less accurate to incorporate measured results any differently. Essentially only two mixtures (for SCC girders and for VC girders) were used throughout production, but every element could have been subjected to different curing and ambient exposure histories. The precision of all comparisons should be considered in light of the inherent variability of concrete material testing and full-scale property measurement.

6.3.6.2 Prediction Application Considerations

Based on the literature reviewed in Section 6.2 and the discussions of Section 6.3, inputs had to be selected for implementation in the various equations required for this work. Many of the material-specific considerations were already discussed in Chapter 5, as the work of that chapter involved the concrete and material models analyzed in this chapter. Pertinent assumptions and choices are summarized below, and further explanations of these selections are reported by Ellis (2012), and Johnson (2012):

- Gross section properties (V/S, A_g, I_g, etc.) were those specified in the *AASHTO LRFD* provisions (AASHTO 2013).
- A constant relative humidity of 70% was used during the modeling of time-dependent behavior of these girders based on Figure 5.4.2.3.3-1 of the *AASHTO LRFD* provisions (AASHTO 2013).
- Measured values of f_c and E_c that were used for time-dependent creep modeling were discussed in Sections 6.3.5.3 (regarding incremental analysis) and 3.4.3 (regarding measured mechanical properties).

- Measured values of f_c for time-dependent shrinkage modeling were those measured at the earliest age after the end of curing (f_{ci}).
- The modulus of elasticity of prestressed strand (E_p) was assumed to equal 28,600 ksi to match the work of Johnson (2012).

During this project, strands were always stressed the day before placing the concrete; thus, the strands were stressed for approximately two days between jacking and release. Using Equation 6-5, the prestress loss due to pre-release steel relaxation was estimated to equal approximately 2.1 ksi. This estimate agrees well with measured pre-release stress relaxation losses measured during previous AUHRC work (Boehm et al. 2010). Therefore, (f_{pbt}) was assumed to equal f_{pj} (202.5 ksi) minus the estimated relaxation loss. This f_{pbt}, 200.4 ksi, was used during all calculations of the f_{pe} of the girders.

6.4 PRESENTATION AND ANALYSIS OF RESULTS

Results and discussion relevant to the assessment of full-scale time-dependent girder behavior are presented in this section, including evaluations of full-scale changes due to transient thermal conditions and due to time-dependent creep and shrinkage. Strength and stiffness measurements were also necessary to compute the predictions of time-dependent behavior. The evaluation of these mechanical properties and their predictability (Chapter 3) are more relevant to the evaluation of the elastic responses to transfer, which were reviewed in Chapter 4.

6.4.1 Coefficient of Thermal Expansion

Results from CTE testing are presented below in Table 6.1. In the table, “Dry” and “Saturated” measurements reflect the two methods of measurement discussed in Section 6.3.1—using the apparatus usually used to measure unrestrained drying shrinkage (from ASTM C157) and tested in accordance with AASHTO T 336, respectively. The calculated values were determined by proportional weighting of constituents using Equation 6-3.

Table 6.1: Comparison of coefficients of thermal expansion

Concrete	CTE (με/°F)				
	Measured		Calculated (Eq. 6-3)	Comparison	
	Dry	Saturated		*Dry/Calc.*	*Sat./Calc.*
SCC Girder	7.4	5.2	6.4	*1.15*	*0.81*
VC Girder	6.8	5.1	6.1	*1.12*	*0.83*
SCC/VC Girder	*1.08*	*1.03*	*1.05*	-	-

The CTE of concrete can be as much as 30% greater at a relative humidity of approximately 50–70% than at 100% saturation, so the relatively higher dry-tested CTE results are expected. The humidity was not well controlled in the environmental chamber used for dry testing though, so dry-tested results should be considered mainly as an upper bound. Because AASHTO T 336 involves the testing of completely saturated concrete, the results determined from saturated testing should be considered as a lower bound of the ambient-humidity thermal behavior of the in-place girder concrete. The CTE of concrete is generally considered to be lowest at 100% relative humidity (Neville 1996). Meanwhile, estimates of the CTE values expected at ambient conditions were needed during this research to accurately account for thermal effects that occurred in the girders. The estimated, "apparent CTE" values selected to account for in-place thermal effects in the girders are discussed in Section 6.4.2.

The calculated results in the table were based on the mixture proportions described in Table 3.1 and constituent-CTE values described by Sakyi-Bekoe (2008) and others (FHWA 2011; Mindess et al. 2003). The CTE values of constituent materials were as follows: 10.0 με/°F for hardened cement paste, 6.8 με/°F for siliceous natural-sand fine aggregate, and 3.3 με/°F for dolomitic limestone coarse aggregate. Because references to the effect of SCMs on paste CTE are limited and conclusions were mixed, only total cementitious content was considered in these calculated values. Also, calculations were volumetrically weighted while using measured air contents—4.0% and 3.7% for SCC-girder and VC-girder mixtures, respectively, per the referenced tables of proportions.

As presented in Table 6.1, SCC appeared to exhibit a marginally higher CTE than its companion VC mixture (approximately 5%). This trend is expected in response to the differences in mixture proportioning recurrently discussed in this report. The SCC was proportioned with a higher paste content and *s/agg*, both of which would lead to the observed 3–8% difference. The difference is also confirmed by comparison to the calculated ratio of SCC-to-VC-girder CTE—in both upper- and lower-bound testing, measured differences were completely identifiable when calculated using actual proportions.

Considering these results and the range of the measured and recommended CTEs presented earlier, the CTE of the SCC-girder mixture is considered acceptably similar to that of the companion VC-girder mixture. Additional insights may be gained by comparison to the concrete mixture used to cast the bridge deck, but that comparison is addressed in a separate report regarding the in-place behavior of the composite bridge (Keske et al. 2015).

6.4.2 Measured Time-Dependent Responses

The primary time-dependent full-scale girder properties assessed in this report are the associated properties of camber, internal concrete strain, and effective prestress (f_{pe}). As previously discussed, changes in concrete strain since immediately prior to transfer are directly measured using VWSGs cast into the concrete at the *cgp*, and these strains are converted to effective prestress according to Equation 4-8. However, thermal effects also cause apparent camber strain changes, but such apparent changes do not necessarily correspond to a change in effective prestress because the steel and concrete both deform in response to changes in temperature. Therefore, to effectively compare measured responses, it is necessary to isolate transient thermal effects due to ambient conditions from gradually occurring time-dependent changes due to creep and shrinkage.

In addition to isolating these effects, time-dependent transient thermal effects were considered to better understand the changes in girder behavior corresponding to diurnal and seasonal thermal strain variation. To that effect, measured thermal strains were evaluated, and adjustments to account for them were applied to the measured $\Delta\varepsilon_{cgp}$ results prior to the evaluation of creep and shrinkage behavior. These thermal-effect considerations are discussed in Section 6.4.2.1. Temperature-adjusted measured responses are then discussed in Sections 6.4.2.2 (prestress loss) and 6.4.2.3 (camber).

6.4.2.1 Thermal Effects in Full-Scale Girders

Measured changes in concrete strain due to transient thermal effects (corrected for gauge temperature but not concrete temperature) are illustrated in Figure 6.7, in which concrete strains noticeably fluctuate daily and seasonally. Also, using the simplified cross-sectional representations shown in Figure 6.2 and Figure 6.3 and the method summarized in Section 6.3.2.2, changes in girder strain due to transient thermal effects were isolated from those due to gradually changing creep and shrinkage deformations in the concrete material. This process, the effect of which can be evaluated by comparing “Measured Strain” and “Corrected Strain” results in the figure, is discussed in the next section.

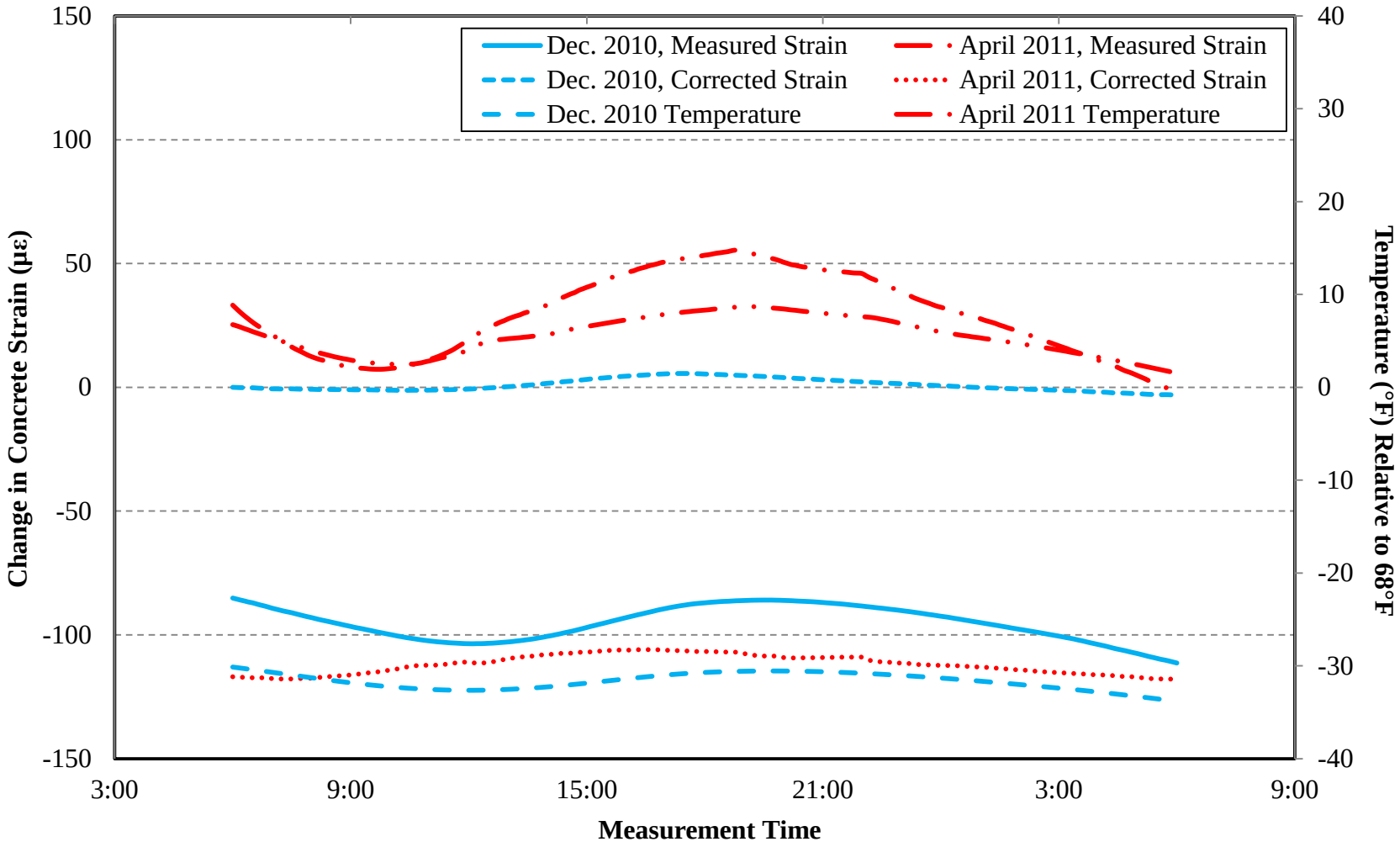

Figure 6.7: Concrete strains and temperatures at the center of gravity of prestress

From Figure 6.7, the temperature of the concrete has a distinct effect on the measured concrete strain. Measured concrete strains (corrected for gauge temperature but not for concrete temperature) changed by an average of 150 με between the first winter after girder production and the following summer. While smaller in magnitude, diurnal strain changes also approached 50 με. While attempts were made to account for these variations prior to evaluation of time-dependent behavior, the magnitude of these diurnal and seasonal changes is noteworthy. Based on the relationship described by Equation 4-8, these measured concrete strain changes would equate to diurnal and seasonal changes in effective prestress of approximately 1.5 and 4.5 ksi. Since both the concrete and encapsulated steel can experience stress-independent deformations due to thermal effects, these apparent strain changes do not necessarily correspond to a change in effective prestress. Furthermore, uncorrected strains would indicate that effective prestress *increased* over time. Therefore, it is crucial to account for thermal effects before comparing time-dependent results to each other and to those predicted by the referenced empirical models.

Ideally, the "Corrected" strains in Figure 6.7 would not vary at all diurnally. The slight gradients shown are acceptable when considering the errors relative to the actual differences in measured strain. From measured diurnal changes of up to approximately 50 με, the average diurnal difference in the corrected values shown in Figure 6.7 was 4 με. Other sources of the slight errors have been discussed previously in Section 6.3:

- The idealized thermal gradient shown in Figure 6.4 may only coarsely model the actual thermal gradient present, as the actual gradient could be very complex and dependent upon the sunlight, precipitation, wind, or other environmental conditions present,
- Differences between the temperature at the external girder surface and that measured at the *cgp* would vary depending upon the same environmental conditions,
- Changes in relative humidity due to moisture fluctuation would affect the CTE of the concrete material (as discussed previously in Section 6.4.1), and
- The simplified cross-sectional properties are only an approximation of the actual girder dimensions.

Not only is the diurnal fluctuation smaller than in the measured results, but it is of a much smaller magnitude than the difference between corrected results obtained five months apart (approximately 100 με). Errors were also minimized during this work by regularly utilizing readings obtained at around dawn. At this time of day, the temperature gradient across the girder is usually the most constant, meaning that the entire cross section should be close to the same temperature. This is confirmed by viewing Figure 6.7—corrected values appeared to be changing the least from approximately 3:00–6:00 AM each day.

The appropriate *apparent* CTE values to implement in the thermal-adjustment calculations were chosen by evaluating the apparent change in f_{pe} and concrete strain of the

temperature-corrected results. Preliminary analysis indicated that girder-CTE values of approximately 6.1–6.9 με/°F would be acceptable, with consistent improvement by differentiating between SCC and VC-girder values by approximately 0.5 με/°F. While this difference does not precisely match the difference in measured SCC and VC-girder CTEs shown in Table 6.1 (approximately 0.3 με/°F), it was acceptable considering the precision of these corrections and the potential sources of errors in the correction method. Further analysis of these CTE results is included in a forthcoming report by Keske et al. (2015) regarding in-place behavior, when time-dependent deformations were expected to plateau.

6.4.2.2 Time-Dependent Prestress Losses

After correcting for thermal effects as discussed in the previous section, measured concrete strains were converted to values of effective prestress, f_{pe}, by Equation 4-8. Total measured prestress losses were determined by subtracting f_{pe} from f_{pbt}. Measured total losses from the assessed girders are presented graphically in Figure 6.8 and Figure 6.9.

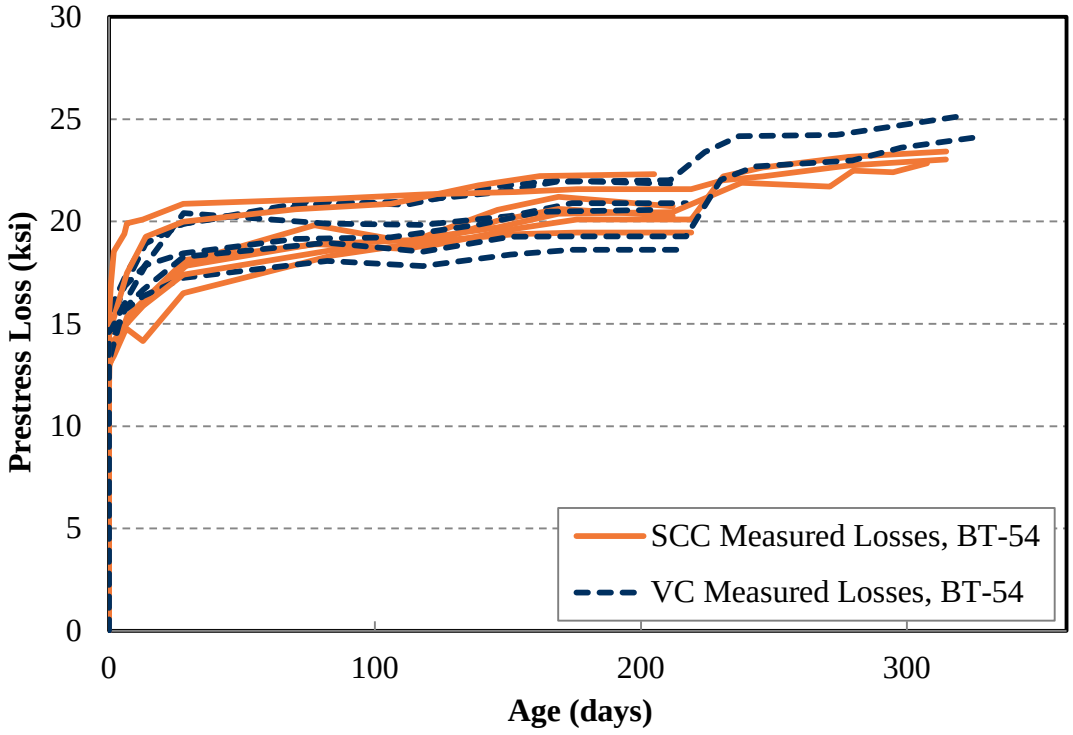

Figure 6.8: Total measured prestress losses in BT-54s

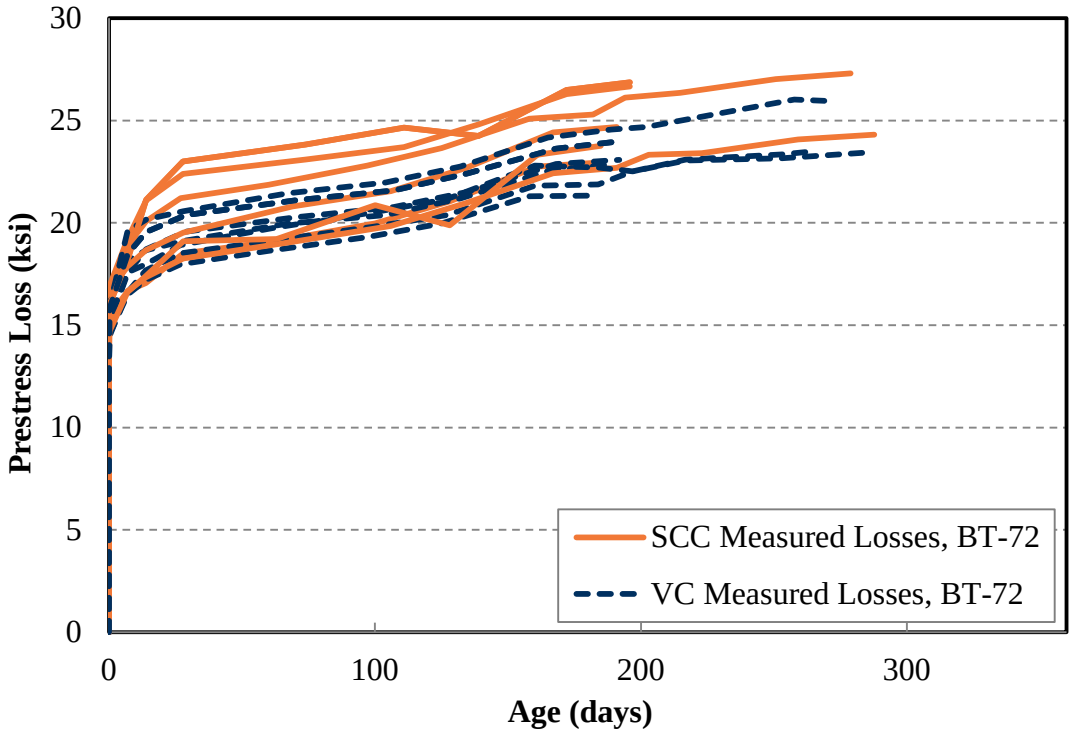

Figure 6.9: Total measured prestress losses in BT-72s

Several conclusions are warranted from the above figures, first among which is that the SCC girders appear to have accumulated similar total measured prestress losses of approximately 20–25 ksi, or 10–12% of f_{pbt}, prior to achieving composite action at the bridge site. They also appear to have accumulated those losses in the same manner over time. To further confirm the time-dependent results presented in Figure 6.8 and Figure 6.9, total prestress losses are also tabulated below in Table 6.2. Losses were evaluated at two critical ages: at approximately fifty-six days and immediately prior to deck addition.

Table 6.2: Total measured time-dependent prestress losses

Girder	Losses at 56 Days		Losses at Deck Add.		*SCC/VC*	
	(ksi)	(%f_{pbt})	(ksi)	(%f_{pbt})	*At 56d*	*At Deck*
54-S Average	18.9	9.4%	20.7	10.4%	*0.98*	*1.01*
54-V Average	19.3	9.7%	20.5	10.3%		
72-S Average	21.1	10.5%	25.0	12.5%	*1.07*	*1.09*
72-V Average	19.7	9.8%	22.9	11.5%		

The results shown above confirm the graphical results—SCC girders have experienced practically no different time-dependent behavior prior to the time of deck construction. While

these total losses include elastic losses that were reviewed in Chapter 4, these results suggest that the SCC girders are behaving very similarly to their companion VC girders over time. The most important practical consideration may be the difference between SCC and VC losses as a percent of f_{pbt}: total differences at either reported age would equate to less than 1% of f_{pbt}, indicating that the SCC and vibrated concrete are indistinguishable to within the precision of the application of this data.

Interestingly, this contradicts the findings presented in Chapter 5, in which SCC cylinders were found to exhibit approximately 15% greater compliance and up to 30% greater shrinkage than the companion VC cylinders at all concrete ages up to approximately one year. While further conclusions are drawn by comparing these results to those predicted by the *AASHTO LRFD* provisions, these results alone are sufficient to conclude that the full-scale early-age time-dependent behavior of these SCC girders is acceptably similar to that of the companion VC girders.

6.4.2.3 Camber

Measured cambers from all girders, after correcting for thermal effects, are presented graphically in Figure 6.8 and Figure 6.9. In the figures, the duration of camber data does not match that of the prestress loss data presented earlier—camber measurement was ceased during preparation of the girders for deck addition at the bridge site. Still, with an average final reading age of 200 days, valuable insight can be gained from comparison of these pre-erection measurements.

Very early age camber measurements shown in the figures are somewhat erratic, likely because of conditions on the casting bed. While a correction was applied to the camber readings to account for the temperature gradient, this correction is approximate, and it did not account for any cracking that might have occurred due to these temperature gradients (documented in Chapter 3). Also, the specific girders that were affected by the release of the prestressing hold-down points were not documented, and this may also have affected early-age readings.

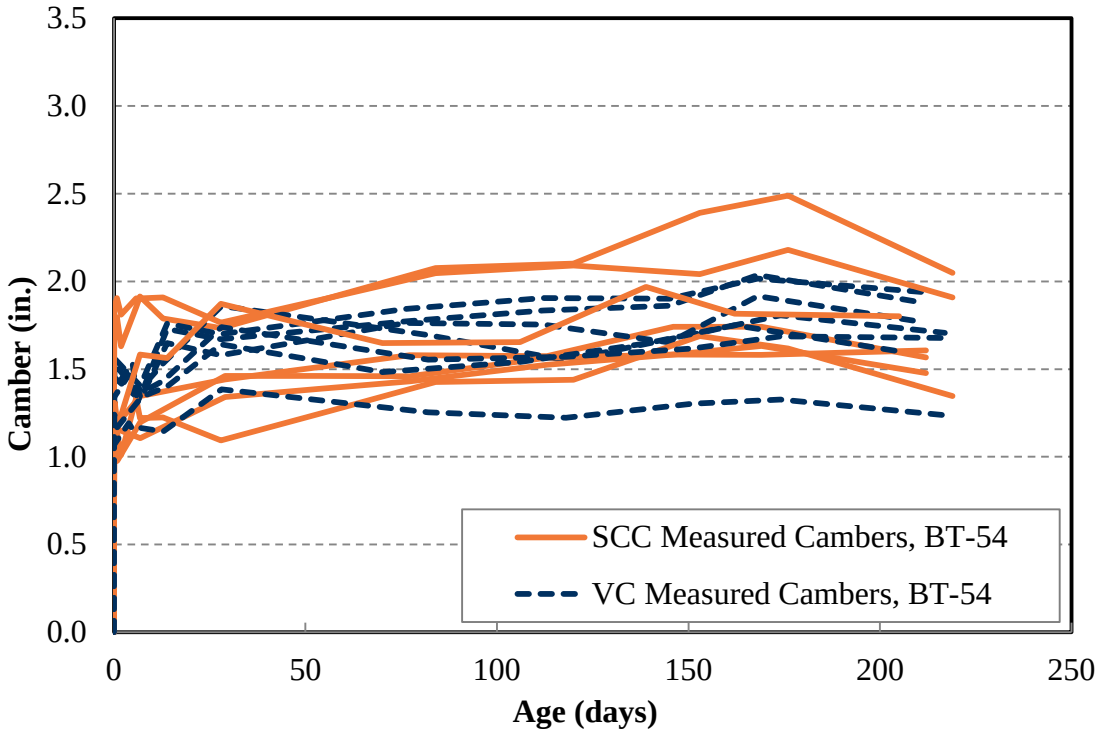

Figure 6.10: Measured camber in BT-54s

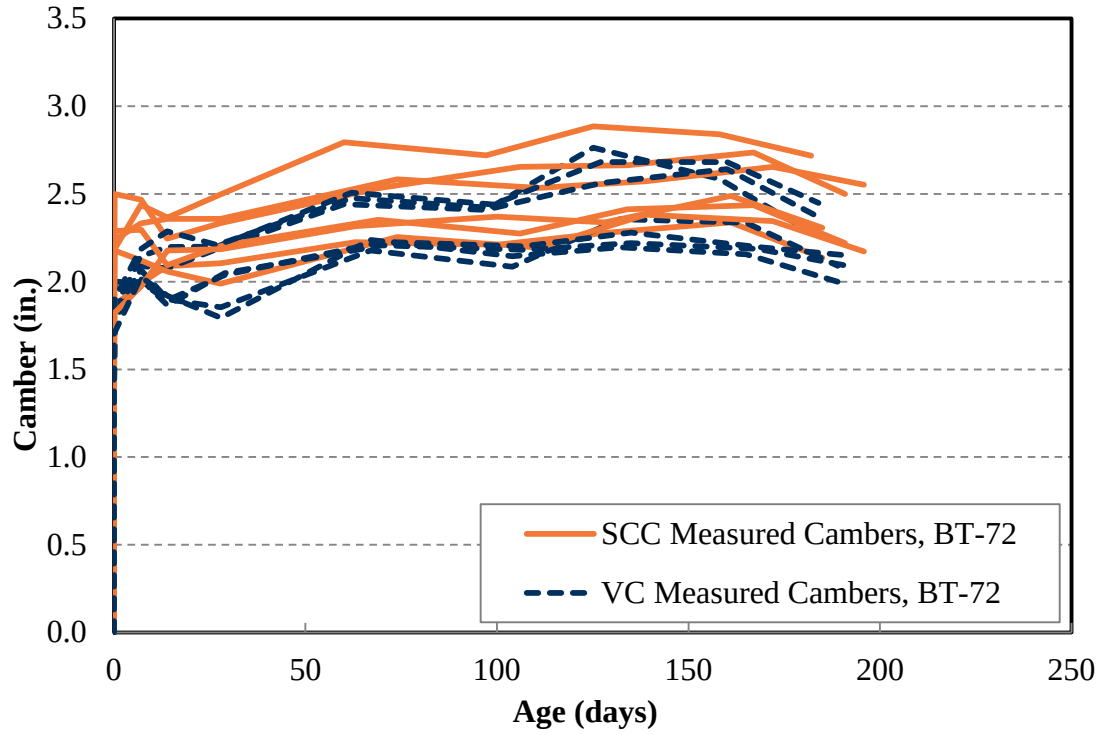

Figure 6.11: Measured camber in BT-72s

The results presented graphically above correspond well with the prestress-loss results presented earlier—SCC and VC girders appear to have exhibited essentially the same initial camber and time-dependent camber growth prior to achieving composite action at the bridge site. To further confirm the results presented in Figure 6.10 and Figure 6.11, average cambers are also tabulated below in Table 6.3. Temperature-corrected cambers were evaluated at three critical ages: at release, approximately fifty-six days, and immediately prior to deck addition. To compensate for the erratic nature of the camber measurements obtained while the girders were still on the prestressing bed, the "Transfer" values reported below were obtained after the girders were moved from the bed for storage, approximately four hours after release.

Table 6.3: Total measured pre-erection cambers

Girder	Camber (in.)			*SCC/VC*		
	Transfer	**56 Days**	**Deck Add.**	***Transfer***	***56 Days***	***Deck Add.***
54-S Average	1.4	1.6	1.7	*1.02*	*0.98*	*1.00*
54-V Average	1.4	1.6	1.7			
72-S Average	2.1	2.3	2.4	*1.16*	*1.06*	*1.08*
72-V Average	1.8	2.2	2.2			

The results shown above confirm the graphical results—SCC girders have experienced essentially no different elastic or time-dependent camber behavior prior to the time of deck construction. The results also parallel the prestress-loss results presented earlier: BT-54s are more similar than BT-72s, but even the difference between SCC and VC BT-72s was minor at all ages (no greater than 0.3 in., with decreasing differences over time). The most important practical consideration may be the difference between SCC and VC cambers relative to the length of the girders: total differences at any of the three reported ages would equate to less than *L/5,000*, indicating that the SCC and vibrated concrete are identical to within the precision of the application of this data.

While further conclusions are drawn by comparing these results to those predicted using the time-step analysis described in Section 6.3, these results alone are sufficient to confirm that the full-scale early-age time-dependent behavior of these SCC girders is acceptably similar to that of the companion VC girders.

6.4.3 Comparisons of Measured Responses to Predicted Responses

While it was instructive to compare the measured responses of the SCC and VC girders because they were to be placed in matching spans of an in-service bridge, it is equally or more important

to evaluate the predictability of the measured girder responses after accounting for their unique material properties. In the following sections, measured responses are compared to those predicted using the time-step analysis created by Schrantz (2012) in conjunction with the reviewed material models.

To make equitable comparisons of measured and predicted results, the way in which measured data are collected must be considered: as previously discussed, only changes in concrete strain are measured by embedded VWSGs, and these strains are converted to prestress losses or effective prestress according to Equation 4-8. Therefore, *strain-independent* prestress losses due to stress relaxation occurred in the girders but were not measured. It was appropriate to *subtract* the predicted relaxation losses after release (Δf_{pR}) to account for this during comparisons of predicted prestress losses—in all comparisons, measured results are compared to predicted results minus predicted relaxation losses. Note that this does not affect the choice of f_{pbt}: pre-release relaxation losses are measurable in the prestressing bed prior to concrete placement (Boehm et al. 2010), and their inclusion is necessary to accurately assess elastic and time-dependent responses (Stallings et al. 2003).

6.4.3.1 Prestress Loss

The time-step program created by Schrantz (2012) was capable of calculating strain at midspan at any depth within a girder cross section. In this research, it was convenient to determine predicted strains at the location of the bottom-bulb VWSG that approximately coincided with the center of gravity of prestressing (*cgp*). As with the measured responses compared earlier, this allowed for conversion of predicted strains to predicted prestress losses by Equation 4-8. A sample of these predicted losses is shown in Figure 6.12. In the figure, the same prediction is applicable to all measured responses from the given production group (SCC-B) because all girders cast at the same time were modeled using the same time-dependent material estimates.

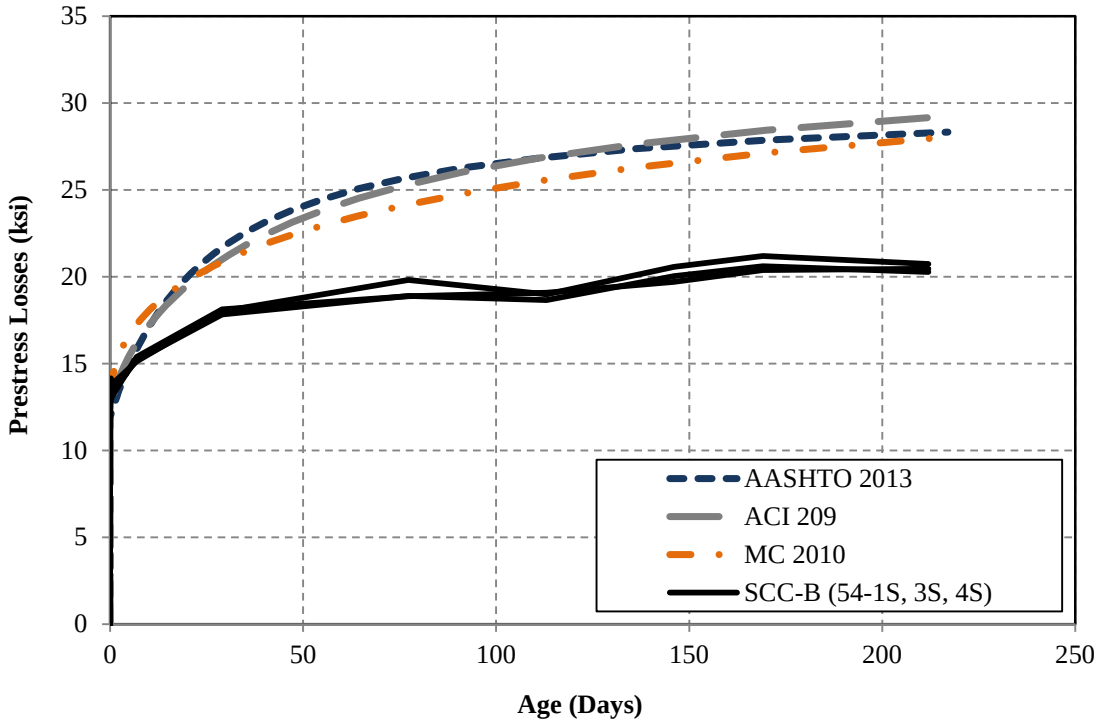

Figure 6.12: Sample comparison of predicted prestress losses in SCC BT-54s

As illustrated in the above figure, measured time-dependent losses appear to be less than predicted using any of the assessed material models. All predictions also appear to be approximately equal, with slightly variation of development. To confirm these results, each girder's measured prestress losses were compared to those predicted using the time-step program previously developed by Schrantz (2012). Values were evaluated at two critical girder ages: at approximately fifty-six days and immediately prior to deck addition. These comparisons are given in Figure 6.13 and Figure 6.14.

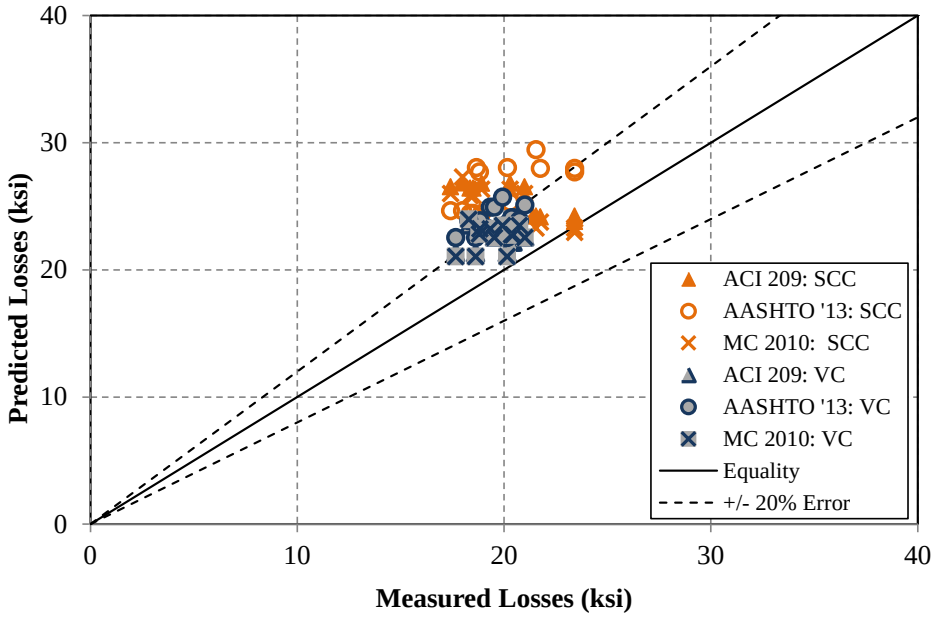

Figure 6.13: Comparison of measured and predicted prestress losses at fifty-six days

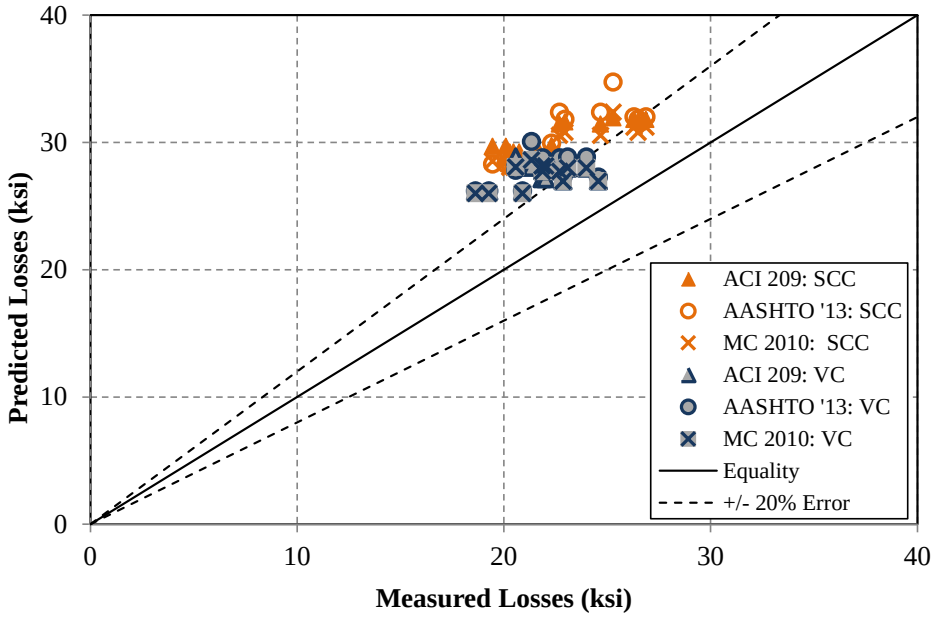

Figure 6.14: Comparison of measured and predicted prestress losses prior to deck addition

Several conclusions are warranted from the above figures, first among which is that all girders appear to have experienced less prestress loss prior to achieving composite action at the bridge site than predicted. Second, the predictability of SCC behavior appears to be practically similar to that of VC behavior. Third, in both materials, losses were more over-predicted at the

later evaluated age (just prior to deck addition), indicating that the girders exhibited less *time-dependent* deformation than predicted.

Recall from Chapter 4 that both materials exhibited approximately equal and highly predictable elastic losses due to the transfer mechanism—measured and predicted elastic losses equaled approximately 12 ksi. Measured losses immediately prior to deck addition were distinctly larger (approximately 22 ksi) but were approximately 6–9 ksi (3.0–4.5% of f_{pbt}) *less* than predicted. This reinforces the conclusion that the girders are experiencing less time-dependent deformation than predicted. From the data presented in this section, it is concluded that pre-erection time-dependent behavior of SCC girders is

- Acceptably similar to that of the companion VC girders, and
- Conservatively predictable using the assessed time-step program in conjunction with any of the three assessed material models.

6.4.3.2 Camber

The time-step program created by Schrantz (2012) was also used to computer midspan camber. Temperature-corrected cambers and time-step estimated cambers were compared at three critical ages: at release, approximately fifty-six days, and immediately prior to deck addition. As in the comparison of measured SCC and VC results, the erratic nature of the earliest camber measurements was avoided by comparing cambers that were obtained after the girders were moved from the bed for storage, approximately four hours after release. These comparisons are given in Figure 6.15 through Figure 6.17, and the data used to create them is presented in Appendix D.

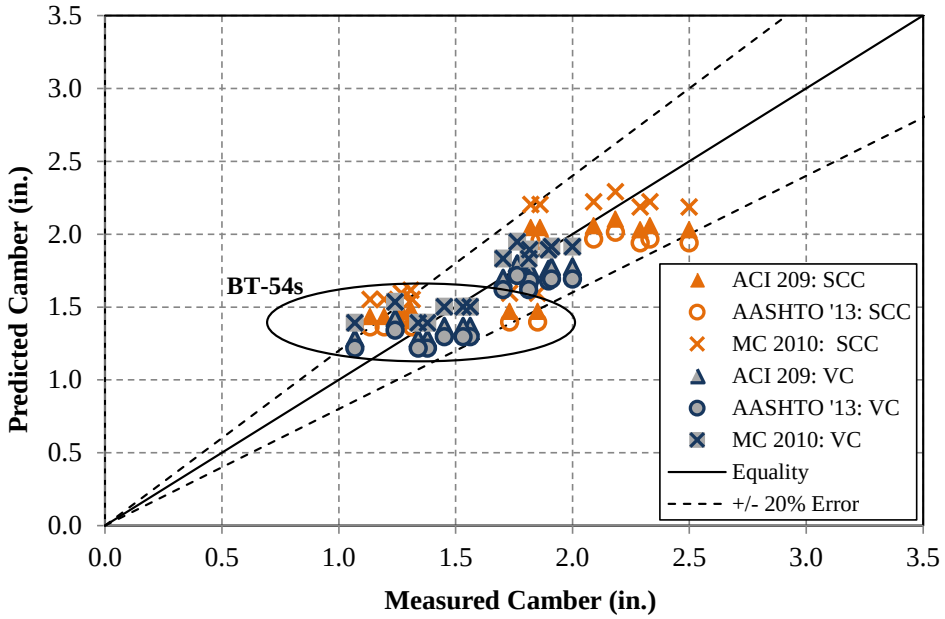

Figure 6.15: Comparison of measured and predicted cambers after release

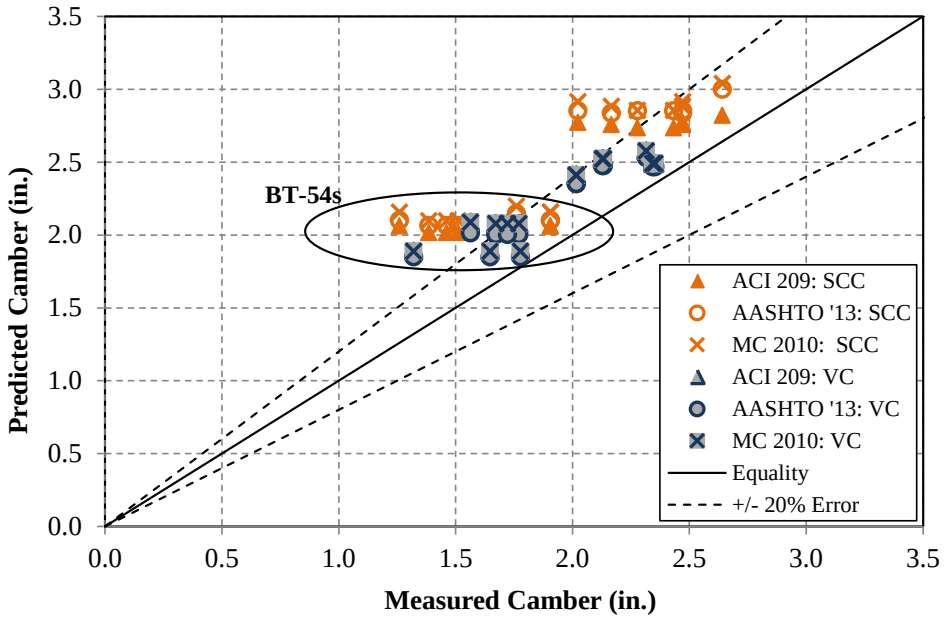

Figure 6.16: Comparison of measured and predicted cambers at fifty-six days

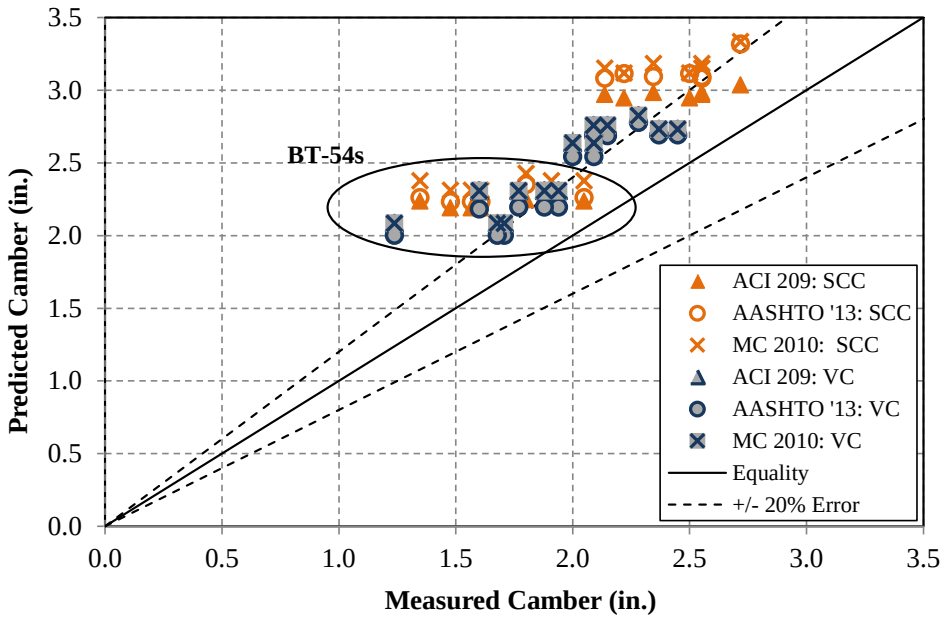

Figure 6.17: Comparison of measured and predicted cambers prior to deck addition

Several conclusions are warranted from the above figures:

- The predictability of SCC camber behavior appears to be practically similar to that of VC camber behavior,
- Temperature-corrected cambers shortly after release are predictable in both materials, although variance between girders was somewhat high (up to 1 in. or ± 20% difference between geometrically identical girders), and
- Cambers in both materials grew less than predicted over time, indicating that the girders exhibited less time-dependent deformation than predicted.

The accuracy of the time-step procedure in calculating camber based on curvatures at a user-specified number of cross sections is confirmed in Figure 6.15, as very little time-dependent deformation should have occurred within the first few hours after release. At this age, SCC cambers were, on average, approximately 5% (0.10 in.) greater than predicted, and VC cambers were approximately 9% (0.13 in.) greater than predicted. Considering the precision of the camber measurement technique, the variability of the measured results, and the approximations involved in the camber-prediction and thermal-effect models, these results indicate that SCC and VC initial camber responses are reasonably predictable when using measured mechanical properties.

Since cambers gradually became over-predicted (more so at later ages), it is likely that the time-dependent material models implemented in the time-step procedure over-estimate time-dependent deformation. These findings disagree with the findings of Chapter 5, since the time-dependent behavior of SCC cylinders was shown to exceed that of the companion VC cylinders, and total deformation of both materials was found to be reasonably predictable in that chapter.

However, the above data confirms the conclusions of the previous subsection: pre-erection time-dependent behavior of SCC girders is acceptably similar and equally predictable to that of the companion VC girders using the assessed time-step program in conjunction with any of the three assessed material models.

6.4.4 Comparisons of Measured Responses to Design Predictions

In Section 6.4.2, measured full-scale SCC time-dependent responses were found to be reasonably similar to those measured in comparable VC girders. In Section 6.4.3, the behavior of SCC and VC girders was found to be conservatively predictable using a previously developed time-step analysis, at least when considering measured material properties. In previous AUHRC research, Stallings et al. (2003) concluded that the use of design properties (such as f'_c) could lead to gross errors in the predictions, so a further analysis of this occurrence was warranted in this evaluation of full-scale behavior. In this way, differences in the measured SCC and VC responses, and differences in their predictability, are evaluated relative to the level of accuracy expectable in a typical design environment.

A number of assumptions were required to calculate the time-step estimates of design effective prestress and camber. Specified f'_{ci} was used, as was an assumed relative humidity of 70%; similarly, all values of E_c were calculated using Equation 3-4 ($57{,}000\sqrt{f'_c}$). Other assumed values were based on the average exposure conditions experienced by the girders such that differences between the design estimates and the measured-property predictions mainly illuminate differences between the *concrete material* properties. Primarily, this involved implementing average release times, t_i, of 0.99 days and 0.88 days for BT-54s and BT-72s, respectively, based on the information presented in Table 3.7. Additional information can be found in Appendix B of the thesis prepared by Johnson (2012).

For this exercise, only the AASHTO 2013 material models were assessed—all predictions appeared to be approximately equal when utilizing measured mechanical properties, and the current *AASHTO LRFD* (2013) models are the models most commonly used by ALDOT during design. Design camber and effective prestress are illustrated in Figure 6.18 and Figure 6.19, respectively. In both figures, the measured response of girder 72-1V and the response predicted for that girder using measured f_c and E_c are given for reference.

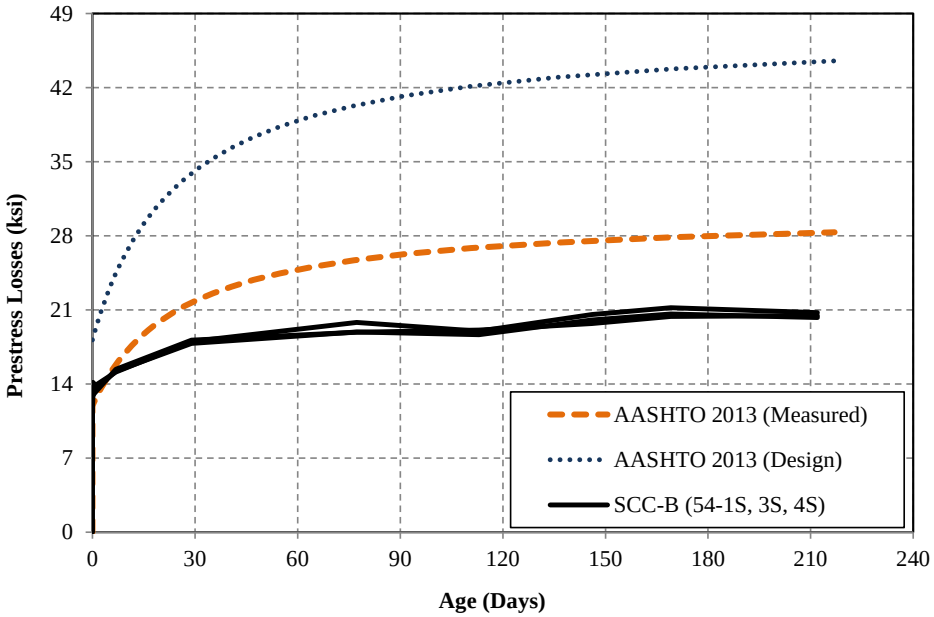

Figure 6.18: Comparison of measured, predicted, and design prestress losses

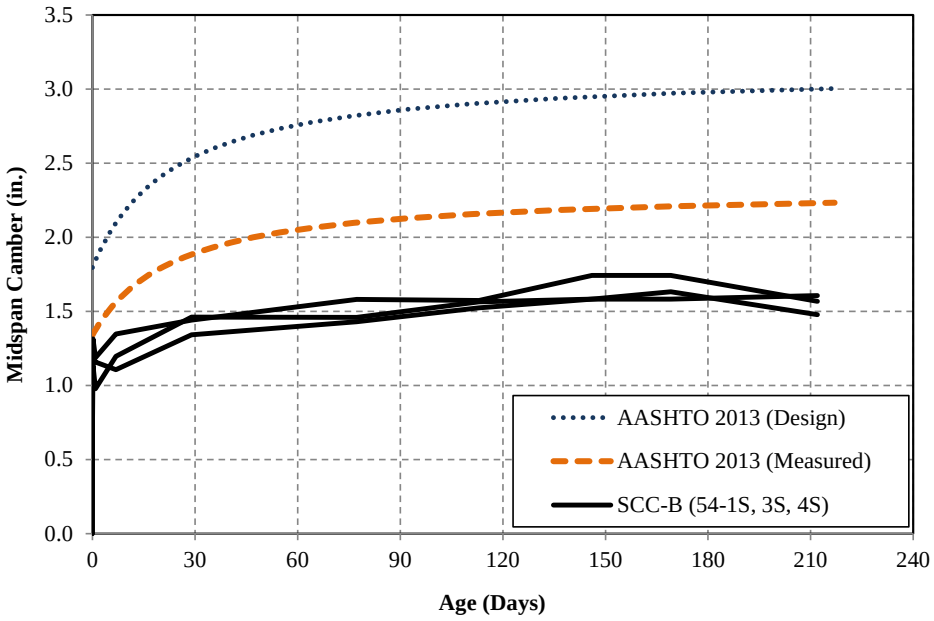

Figure 6.19: Comparison of measured, predicted, and design midspan camber

In the above figures, differences are apparent between measured time-dependent behavior, predicted behavior based on measured mechanical properties, and design behavior based on specified properties. Especially among BT-54s, the design predictions appear to grossly over-predict prestress losses—versus the 6–9 ksi difference at deck construction between measured results and those predicted based on measured mechanical properties (discussed

previously in Section 6.4.3.1), design losses at this time were approximately 25 ksi (12.5% of f_{pbt}) greater than measured losses and 18 ksi (9% of f_{pbt}) greater than measured-property predictions. Similar was true when comparing BT-72 design results, as previously reported by Johnson (2012): design BT-72 losses were approximately 16 ksi greater than equivalent predictions based on measured mechanical properties. Thus, the use of measured or expected properties in place of design properties may be significant.

Errors between measured and design camber predictions were similarly large. The shop drawings provided by the girder manufacturer list a theoretical BT-54 camber of 2.75 in. before placement of the bridge deck. The deck-placement result would seem to agree with the prediction based on the design strength and modulus of elasticity values at an age of 30 to 60 days (usually assumed for an erection age). However, these results are noticeably larger than measured or predicted using measured mechanical properties (0.25 in. and up to 1.0 in. at transfer and deck addition, respectively). At the later ages (30–60 days and at the actual time of deck construction), the difference between measured and design cambers was approximately twice the difference between measured results and those predicted using measured mechanical properties. This further suggests that the use of measured or expected properties in place of design properties could be significant during design.

In conjunction with the elastic-response data analyzed in Chapter 4, the error between these design and measured values is due largely to two sources: error in the estimation of the elastic stiffness (E_c) when using specified design strength (f'_c), and error in the prediction of time-dependent deformation growth. Since the measured-property elastic-response predictions (initial camber and prestress loss) were fairly accurate when utilizing measured E_c, the error between measured responses and measured-property predictions arises largely from the uncertainty of the time-dependent material behavior of the girders. These errors were discussed in previous sections and have to do with the accuracy of the creep and shrinkage models with respect to these two concrete mixtures.

The error in time-dependent response prediction is compounded when also utilizing an elastic stiffness based on specified design strength. Since time-dependent girder behavior is predicted by amplifying the calculated elastic response, errors in design initial losses and camber—approximately 5 ksi and 0.25 in. for the evaluated BT-54s—are magnified greatly by the time of deck addition. This suggests that errors due to poor estimation of elastic stiffness during design can be at least as severe as those due to poor prediction of time-dependent behavior. This also confirms the conclusion of Stallings et al. (2003): predictions can be highly conservative when using design properties in place of measured or expected material properties. Further research concerning the discrepancy between measured time-dependent behavior and the values that would be predicted during design should be investigated.

6.5 SUMMARY AND CONCLUSIONS

6.5.1 Summary

The work documented in this chapter was conducted to evaluate the full-scale time-dependent structural performance of the SCC girders used to construct the bridge over Hillabee Creek, both in relation to the companion VC girders used in the bridge and in relation to currently employed predictions. The primary full-scale structural properties evaluated were the camber and pre-erection effective prestress in the prestressed strands. Additionally, to isolate transient thermal effects from gradually occurring time-dependent effects, the CTE of the utilized concrete mixtures was evaluated. Measured material properties (CTE, f_c, E_c, etc.) were then implemented in the models used to predict the full-scale responses.

By incorporating the measured material properties in this evaluation, the acceptability of the SCC-girder behavior, and ways in which it may be affected differently than that of VC girders by material properties, was thoroughly evaluated. Not only are such full-scale evaluations of SCC girders limited or nonexistent, but their implications for SCC girders of the scale used in this bridge and made using Alabama materials and methods are unclear. The observations and conclusions made concerning this evaluation are summarized in Section 6.5.2. The recommendations made based on this research are then given in Section 6.5.3.

6.5.2 Observations and Conclusions

6.5.2.1 Coefficient of Thermal Expansion and Thermal Responses of Girders

- In standardized testing and in testing conducted in ambient-humidity conditions, the studied SCC exhibited a marginally higher CTE than that of the comparable VC-girder mixture (approximately 5% higher). The difference was explainable by the difference in mixture proportions of the two and would be expected between any two concretes with different proportions.
- Diurnal and, more significantly, seasonal thermal effects affected the apparent concrete strains and cambers measured in these girders (but would not affect effective prestress because steel responds similarly to thermal effects); it was, therefore, crucial to account for these thermal effects before evaluating time-dependent changes in behavior due to creep and shrinkage.

6.5.2.2 Measured Time-Dependent Behavior of Full-Scale Girders

- After accounting for thermal effects, SCC girders exhibited practically identical effective prestress and camber as the companion VC girders throughout the first year after casting. Differences in total losses between the materials equated to no greater than 1% of f_{pbt} at the time of deck construction. Differences in camber were less than 0.2 in., or *L/5,000*, at this time.
- The time-dependent structural behavior of the SCC girders contradicts the findings presented in Chapter 5—cylinders of SCC were found to exhibit up to 15% greater compliance and 30% greater unrestrained shrinkage at all concrete ages, but full-scale time-dependent behavior of SCC girders was essentially identical to that of the companion VC girders.

6.5.2.3 Prediction of Time-Dependent Behavior of Full-Scale Girders

- All of the creep and shrinkage models investigated—ACI 209, AASHTO 2013, and MC 2010—were reasonably accurate in predicting full-scale prestress losses, at least when incorporating measured mechanical properties.
- Temperature-corrected cambers were predictable at release, although camber growth was less than predicted. The discrepancy was due more to error in the estimation of time-dependent material behavior than error in the calculation of the initial elastic response, at least when incorporating measured mechanical properties.
- Use of *design* material properties (f'_{ci} and others) led to very conservative and less accurate predictions of time-dependent camber and prestress loss. The resulting prediction errors were at least as large as the error associated with the creep and shrinkage material models because the material models magnify the error in calculated elastic responses.
- In light of these findings, the pre-erection time-dependent behavior of full-scale SCC girders was considered to be conservatively predictable and acceptably similar to that of the companion VC girders.

6.5.3 Recommendations

- Concerns about the early-age time-dependent structural behavior of SCC in full-scale precast, prestressed girders should not restrict the implementation of the material in that type of construction. Measured full-scale time-dependent structural responses were

essentially identical in companion SCC and VC girders and all behaviors were conservatively predictable based on measured material properties.

- Further research concerning the time-dependent behavior of the Hillabee Creek Bridge girders should be conducted on the in-place girders to confirm that the long-term in-place behavior of the girders is also acceptable.
- The difference between predictions that incorporated measured properties and those based on design properties was distinctly larger than the difference between SCC and VC. Further research concerning the discrepancy between measured time-dependent behavior and the values that would be predicted during design should be investigated.

CHAPTER 7: RESEARCH CONCLUSIONS AND RECOMMENDATIONS

7.1 SUMMARY OF WORK

Because of its fluid nature, SCC can efficiently fill congested or irregularly shaped members more easily than vibrated concrete while also providing an improved uniformity and surface finish. Therefore, one of the most advantageous uses of SCC is in the production of precast, prestressed bridge girders, where reinforcement congestion and member shape make filling and consolidation of VC difficult. SCC achieves its unique fresh characteristics through the use of differences in mixture proportions. However, research concerning the effects of these mixture changes has been limited, both with regard to fresh behavior and hardened-material and structural behavior.

Understanding these effects is critical in the especially demanding implementation of the material in the production of precast, prestressed girders. Consequently, prior to statewide acceptance of SCC in precast, prestressed bridge member production, ALDOT sponsored an investigation of the material to be performed by the AUHRC. The work presented in this report continued this investigation and included a performance evaluation of precast, prestressed SCC girders produced for Alabama's first full-scale implementation of SCC in an in-service bridge.

The final phase of laboratory work for the AUHRC investigation focused on quantification of SCC stability, a unique property of the material that has been difficult to assess previously. In the investigation, five fresh concrete stability tests were conducted on nine SCC mixtures each placed in walls of heights equaling 54, 72, and 94 inches. The same walls were also constructed with two VC mixtures, and the in-place hardened concrete uniformity of each of the eleven groups of walls was evaluated. Fresh SCC stability test results were then compared to the results of the hardened concrete uniformity testing. Based on those results, suitable fresh SCC test methods and acceptance criteria are recommended for ALDOT use during the implementation of SCC in the statewide production of precast, prestressed elements.

During the evaluation of full-scale SCC-girder behavior, fresh and hardened mechanical properties, prestress transfer bond length, elastic responses to the transfer mechanism, and early-age time-dependent properties were assessed until immediately before the girders achieved composite action at the Hillabee Creek Bridge. Measured SCC and VC responses were compared to each other, as well as to current estimates and design provisions.

While some concrete material properties and isolated structural behaviors appeared to be less conservative in the SCC, the differences were within expectations considering the differences between its mixture proportions and those of the companion VC. In other words, the

observed differences were not unique to the use of SCC because any two concretes proportioned differently would exhibit such differences. All predictions were conservative based on measured material properties and more so based on design properties. The differences between the as-produced SCC and VC were frequently within the precision of the testing or were less significant than the observed variability that resulted from typical construction practices.

Analyses of several important full-scale structural behaviors suggest that the SCC girders are behaving practically identically to the companion VC girders. This slightly disagrees with the findings of complimentary small-scale testing but indicates that SCC behavior can be at least as conservatively predicted when using measured material properties. Based on these results, acceptance of SCC as an alternative to vibrated concrete in the construction of precast, prestressed bridge girders is recommended.

7.2 RESEARCH CONCLUSIONS AND RECOMMENDATIONS

The work documented in this report was conducted in two parts. The first involved the evaluation of fresh stability test methods during the production of nine different SCC mixtures and the second involved the evaluation of a variety of fresh material, hardened material, and structural behaviors in a one-to-one comparison of an plant-produced SCC and VC. The conclusions and recommendations summarized in Section 7.2.1 are supported by the work of the first part, and the conclusions and recommendations summarized in Sections 7.2.2–7.2.7 are supported by the second part.

7.2.1 Concrete Stability, Hardened Uniformity, and Fresh Test Methods

Conclusions and recommendations are supported by the research presented in Chapter 2:

- Embedded-reinforcement pullout tests and ultrasonic pulse velocity (UPV) measurements indicate that acceptable hardened concrete uniformity is achievable in a variety of SCC mixtures relative to that of high-quality VC and to code-accepted behavior.
- Among five evaluated fresh SCC stability test methods, the VSI, sieve stability, and surface settlement tests were found to most strongly correlate to several measures of in-situ hardened concrete uniformity in full-scale specimens. Strong preference for these tests is therefore recommended during the assessment of fresh stability in SCC.
- The column segregation test (ASM C1610) and rapid penetration test (ASTM C1712) were found to poorly correlate to other measures of fresh stability and in-situ uniformity of concrete, so their use is of little value relative to use of the three fresh concrete stability tests recommended above.

- The VSI correlated well with quantitative measures of concrete stability and in-situ uniformity. When conducted by trained personnel, it can be valuable in determining SCC stability despite its subjective nature.

Based on these results, a stability testing protocol is recommended for use during ALDOT implementation of SCC in precast, prestressed girder production. If initial testing according to the VSI indicates questionable stability (VSI result greater than 1.0), then the use of the sieve stability test should provide an objective, quantitative means of determining final batch acceptance. Acceptance criteria for the sieve stability test are presented in Chapter 2. If the VSI result is less than or equal to 1.0, then the sieve stability test may be ceased. The prolonged testing time required of the sieve stability test is a potential hindrance of the method, and the use of an abbreviated testing time is further evaluated in the Phase II report by Keske et al. (2015).

7.2.2 Production of Full-Scale Precast, Prestressed Girders

Conclusions and recommendations are supported by the work presented in Chapter 3:

- Improved placement efficiency was observed during the implementation of SCC in full-scale precast, prestressed girders, but the most significant improvement observed during the implementation may be the improvement of surface finish.
- SCC slump flows were regularly less than specified for this project, while VC slumps were occasionally greater than specified. SCC girders were still more easily constructed and exhibited a much better surface finish than VC girders despite the observed tendencies in workability. Consequently, specification of a relatively high SCC slump flow may not be necessary during this type of production.
- A longer delay was required before texturing the top surface of the SCC girders to ensure that the concrete would hold the desired surface texture. While this did not seem to affect construction times because a delay was always observed prior to covering the girders for steam curing, special attention may be necessary to assure that the desired top-surface texture is maintained in SCC girders prior to covering.

Considering the results presented in Chapter 3, SCC girders can be produced using the same level of quality assurance and quality control as already employed during the production of VC girders. Also, existing construction procedures should allow production of SCC girders of an equal in-situ hardened uniformity and quality as VC girders. The variation in behavior due only to typical construction practices should be no different during the use of SCC in the production of precast, prestressed girders.

7.2.3 Mechanical Properties of Plant-Produced Concrete

The work of Chapter 3 also supports the following conclusions and recommendations:

- The prestress-transfer compressive strength, f_{ci}, of both materials exhibited a significant dependence on the age of the concrete at transfer—release ages varied from 18–25 hours, which corresponded with up to a 2,000 psi difference in f_{ci} between days of production. The dependence was statistically indistinguishable between the two materials, but the predictability of hardened-material and structural responses should be considered in light of this observed construction variability.
- The 28-day f_c of concrete batches produced within the same production day varied by as much as 860 psi (averaging 2.6% COV) in SCC and 1,170 psi (averaging 4.1% COV) in VC. Therefore, the uniformity of f_c in SCC batches can be at least as consistent as that of batches of VC.
- Compressive strength in both materials greatly exceeded specified f'_c values: 30–64% greater at release and 31–73% greater at twenty-eight days. Because the same mixture was utilized in both girder sizes while different values of f'_c were specified for each, BT-54 f_c values exceeded specified values by a larger margin than did BT-72 f_c values. The conservatism of measured compressive strength in relation to specified f'_c may be important during design.
- SCC achieved a practically identical compressive strength at every age tested despite being proportioned with a higher *s/agg* (0.47 versus 0.39 in VC), smaller coarse aggregate (½ in. versus ¾ in. in VC), and lower total aggregate content (63% versus 67% in VC). Therefore, differences in f_c of SCC resulting from its mixture proportions should not be of concern during its implementation.
- SCC achieved a practically identical f_{ct} despite the differences in proportioning outlined above. Predictions of f_{ct} ranged from 6% over to 17% less than measured results, relative to $\sqrt{f_c}$, at various ages and using various models. Measured properties exceeded design values predicted using $\sqrt{f'_c}$, but to a lesser extent than measured f_c exceeded f'_c. Thus, f_{ct} of SCC can be acceptably similar and as conservatively predicted as that of VC.
- E_c of the tested SCC was 10–15% less than that of the VC at transfer and twenty-eight days. Because the mixtures exhibited practically identical f_c, SCC E_c was reduced relative to $\sqrt{f_c}$ compared to that of VC. The reduction was expectable in response to the changes in its proportions described earlier, which indicates that the reduction is not unique to the SCC.
- SCC E_c was at least as accurately predicted as that of VC when considering measured w_c and f_c. Unless more accurate mixture proportioning or trial batch data are available, an *unreinforced* concrete unit weight, w_c, of 150 lb/ft^3 should be used during the design of

precast, prestressed girders constructed with proportions similar to those utilized in this research.

- The E_c of both materials was more accurately predicted according to the equation presented in the *AASHTO LRFD* (2013) provisions than using the ACI 363 (1992) equation developed for high-strength concrete, even though the SCC and VC exhibited compressive strengths of up to approximately 11,000 psi. Use of *LRFD* (2013) Equation 5.4.2.4-1 is recommended.
- Long-term, three-year E_c was evaluated in twenty-eight sets of cylinders. Results suggest that long-term E_c of the tested SCC and VC are expectably similar (SCC E_c was 6% less). Therefore, the long-term elastic stiffness of SCC should be similar to that of VC proportioned with similar aggregates and cementitious materials.

Considering these results, hardened mechanical properties of plant-produced SCC are considered acceptably similar to those of equivalent-use VC, and minor differences should be no different than those present between any two differently proportioned concretes. Variability due to typical construction practices (particularly variation in age at release) was more significant than any difference between the tested SCC and VC. Measured properties are conservatively predictable and can be distinctly conservative relative to design values.

7.2.4 Transfer Length of Full-Scale Girders

Conclusions and recommendations are supported by the work presented in Chapter 4:

- After normalizing for f_{pt}, d_b, and $\sqrt{f_{ci}}$, SCC transfer lengths were approximately 18% greater than those of the companion VC girders. The increase was likely related to the reduced E_{ci} of the utilized SCC. After normalizing for E_{ci} to remove the assumption of correlation to the square root of f_{ci}, SCC transfer lengths were insignificantly different than those of VC girders. This suggests that differences in l_t are not uniquely associated with the use of SCC—the difference should occur between any two concretes whose E_{ci} differ.
- Comparing E_{ci}-normalized l_t between phases of AUHRC research, l_t consistently decreased as specimen size increased, and SCC l_t was insignificantly different than VC l_t in all phases. The observed size effect corroborates previous hypotheses that larger specimens exhibit shorter l_t, and all results indicate that SCC l_t behavior is acceptably similar to that of VC after accounting for E_{ci}.
- The most significant factor affecting l_t appeared to be girder orientation in the prestressing bed—transfer zones adjacent to longer exposed lengths of strand near the ends of the prestressing bed produced approximately 30% longer transfer lengths than

those adjacent to short exposed lengths of strand in both SCC and VC. Thus, high variability due to construction practices should be expected.

- The combined effects of age at transfer, VMA use, and SCC fresh stability could not be evaluated independently; transfer age was similar between materials, all SCC included VMA while vibrated concrete did not, and all SCC was acceptably stable. While not intentionally varied, all appear to be insignificant variables on l_t relative to the effects of bed orientation and girder size.
- Two predictive equations presented in ACI 318 (2011) and one presented in the *AASHTO LRFD* guidelines (2013) were used to conservatively predict l_t in both materials. Although these models do not consider E_{ci}, they appear to be acceptable for use with either material.

Based on these results, SCC transfer lengths measured in full-scale girders appear to be conservatively predictable and acceptably similar to those in companion VC girders. Considering the variability of transfer lengths and their dependence on exposed strand length and girder size, no changes to the existing predictions are recommended at this time.

7.2.5 Camber and Prestress Response to Transfer

The work of Chapter 4, as well as of Chapter 6 regarding camber, supports the following conclusions and recommendations:

- SCC-girder elastic strains due to prestress transfer were predicted to be approximately 9–17% greater than in geometrically identical VC girders because of the difference in measured E_{ci}. Measured SCC-girder elastic strains were no more than 2% greater than measured VC-girder elastic strains, which would correspond to 0.1% of f_{pbt} in the strands. Thus, the elastic response of SCC girders to the transfer mechanism is acceptably similar to that of VC girders.
- Almost all girders exhibited greater elastic prestress loss than predicted in response to the transfer of prestress (by an average of 6%) when using measured properties; SCC-girder elastic losses were approximately 1% greater than predicted based on measured E_{ci}, while VC-girder losses were approximately 13% greater than predicted. This indicates that the elastic response of SCC girders to the prestress transfer mechanism is conservatively predictable.
- Temperature-corrected SCC-girder elastic camber gains in response to prestress transfer were predicted to be similar to those of VC girders. Measured SCC-girder cambers were practically similar to VC-girder cambers, and all were approximately 5–9% (0.1 in.) greater than predicted using measured mechanical properties. The difference between

measured and predicted results was practically insignificant, indicating that the elastic camber response of SCC girders to the transfer mechanism is acceptably similar and as predictable as that of VC girders.

- All full-scale elastic responses to prestress transfer were highly conservative relative to design predictions (in both materials). Therefore, SCC-girder transfer behavior can be acceptably similar and as conservatively predicted as that of VC girders, and the use of expected mechanical properties in place of design properties may be significant.

7.2.6 Time-Dependent Deformation of Concrete Cylinders

Conclusions and recommendations are supported by the work presented in Chapter 5:

- Measured SCC compliance was approximately 15% greater than that of the companion VC through a concrete age of one year. On average, creep of the SCC was no more than 10% greater than that of the equivalent-strength VC.
- The increased J of the SCC cylinders was in line with its reduced E_{ci}, and any increased creep was minor and expectable considering its mixture proportions. These differences suggest that differences in J and creep are not uniquely associated with the use of SCC—the difference should occur in any two concretes whose proportions differ.
- Measured SCC unrestrained shrinkage was approximately 30% greater than that of the equivalent-strength companion VC cylinders. The increased shrinkage of the SCC was expectable in response to the differences in its proportions but was more severe than the difference between SCC and VC J or creep.
- Shrinkage growth of SCC was comparable to that of VC; free shrinkage approximately doubled between seven days and fifty-six days but only grew an additional 50% through one year, in both materials.
- In both materials, time-dependent creep was approximately equal to that predicted by several models while shrinkage was less than predicted, when using measured properties and testing times. Because the models that over-predicted shrinkage also under-predicted creep, all evaluated models were reasonably accurate at predicting total time-dependent deformation. Prediction of the separate components of time-dependent behavior may be improved through the use of mixture-specific adjustment factors.

7.2.7 Time-Dependent Behavior of Full-Scale Girders

Conclusions and recommendations are supported by the work presented in Chapter 6:

- Small-scale testing revealed that the studied SCC exhibited a CTE approximately 5% greater than that of the companion VC-girder mixture. The difference was explained by the difference in mixture proportions and is therefore not a unique concern of SCC—the difference should occur between any two concretes exhibiting differences in proportions or materials. The significance of the difference between the girder CTEs should be minimal in this type of application (simply supported girders not restrained against thermal deformation).
- Thermal effects distinctly affected the apparent internal-strain measurements obtained in the girders. These changes in apparent strain (up to 150 με at the *cgp* between seasons when accounting for gauge temperature but not concrete temperature) do not necessarily correspond to changes in f_{pe} because both steel and concrete deform in response to thermal effects. Therefore, thermal effects must be accounted for to effectively study the time-dependent creep and shrinkage behavior of full-scale girders.
- Transient thermal effects were accurately isolated in this work using simplified representations of the measured thermal gradients and cross sections. By determining the axial deformation and curvature caused by nonlinear thermal effects, thermal-strain effects were isolated from the effects of long-term time-dependent material deformation. The implemented correction method should be applicable in other situations, and its use is recommended in this type of testing.
- After accounting for thermal effects, SCC girders exhibited practically the same prestress losses as the companion VC girders at all concrete ages prior to deck addition. Differences in total measured losses between the materials at the latest time assessed equated to no greater than 1% of the pre-release strand stress, f_{pbt}. This indicates that the pre-erection prestress maintenance behavior of SCC girders can be acceptably similar to that of VC girders.
- Use of the time-step program created by Schrantz (2012) in conjunction with any of the three assessed time-dependent material models (ACI 209, AASHTO 2013, or MC 2010) led to reasonably conservative over-estimation of prestress losses over time, at least when using measured mechanical properties. The difference between measured losses and those predicted using measured mechanical properties was approximately 6–9 ksi (3–4.5% of f_{pbt}), indicating that SCC and VC time-dependent behavior is slightly over-predicted using the assessed models.
- Use of the time-step program created by Schrantz (2012) in conjunction with any of the three assessed time-dependent material models (ACI 209, AASHTO 2013, or MC 2010) led to reasonably conservative over-estimation of prestress losses over time when using measured mechanical properties. The difference between measured losses and those predicted using measured mechanical properties was approximately 6–9 ksi (3–4.5% of

f_{pbt}), indicating that SCC time-dependent prestress maintenance is at least as conservatively predicted using the assessed models.

- Use of the time-step program created by Schrantz (2012) in conjunction with any of the three assessed time-dependent material models (ACI 209, AASHTO 2013, or MC 2010) led to over-estimation of camber development over time when using measured mechanical properties. Cambers at the time of deck addition were over-predicted by approximately 0.5–1.0 inches (recall that initial cambers were under-predicted by approximately 0.1 in.). This further indicates that SCC and VC time-dependent behavior is over-predicted using the assessed models.
- Use of the time-step method with *design* material properties (such as f'_{ci}) led to very conservative predictions. Pre-erection design predictions under-predicted measured f_{pe} by up to 25 ksi (12.5% of f_{pbt}) and under-predicted equivalent predictions of f_{pe} that incorporated measured properties by up to 19 ksi (10% of f_{pbt}).
- In light of these findings, the pre-erection time-dependent behavior of full-scale SCC girders is considered to be conservatively predictable and acceptably similar to that of the companion VC girders.

7.3 RECOMMENDATIONS FOR FUTURE RESEARCH

Based on the research presented in this report, the following recommendations are given for potential areas of future research:

1. Transfer lengths were conservatively predicted on average, but high variability was observed as a result of common construction practices. The tested girders were made with concrete that met or exceeded ALDOT specifications, and they also appeared to benefit from a size effect. Since these conditions are not universal, the acceptability of transfer-length behavior in smaller prestressed elements with less stiff concrete may need to be investigated further.
2. Predictions of time-dependent prestress losses and cambers based on measured material properties were compared to those predicted using design properties. Design predictions of elastic losses and cambers were up to 5 ksi and 0.25 in. different than equivalent predictions that incorporated measured properties. Design predictions of time-dependent losses and cambers compounded the error and over-predicted equivalent deformation predictions that incorporated measured properties by up to 19 ksi (10% of f_{pbt}) and 1.0 in. at the time of deck addition. Since measured-property predictions were still conservative, the use of expected material properties, instead of design material properties, during the prediction of prestress losses and camber may be significant. This should be investigated further.

REFERENCES

AASHTO. 2010. *AASHTO Bridge Construction Specifications.* 3rd ed. Washington, DC: American Association of State Highway and Transportation Officials.

AASHTO. 2013. *AASHTO LRFD Bridge Design Specifications: Customary U.S. Units.* 6th ed. Washington, DC: American Association of State Highway and Transportation Officials.

AASHTO. 2012. *Standard Specification for Transportation Materials and Methods of Sampling and Testing*. 28th ed. Washington, DC: American Association of State Highway and Transportation Officials.

Abo-Qudais, S.A. 2005. Effect of Concrete Mixing Parameters on Propagation of Ultrasonic Waves. *Construction and Building Materials* 19 (4): 257–263.

ACI 209. 1992. Prediction of Creep, Shrinkage, and Temperature Effects in Concrete Structures (ACI 209R-92). (Reapproved 1997). Farmington Hills, MI: American Concrete Institute.

ACI 209. 2008. Guide for Modeling and Calculating Shrinkage and Creep in Hardened Concrete (ACI 209.2R-08). Farmington Hills, MI: American Concrete Institute.

ACI 237. 2007. Self-Consolidating Concrete (ACI 237R-07). Farmington Hills, MI: American Concrete Institute.

ACI 318. 2011. Building Code Requirements for Structural Concrete (ACI 318-11) and Commentary. Farmington Hills, MI: American Concrete Institute.

ACI 363. 1992. State-of-the-Art Report on High-Strength Concrete (ACI 363R-92). Farmington Hills, MI: American Concrete Institute.

ACI 408. 2003. Bond and Development of Straight Reinforcing Bars in Tension (ACI 408R-03). Farmington Hills, MI: American Concrete Institute.

Alabama Department of Transportation. 2010a. Procedure ALDOT-367: Production and Inspection of Precast Non-Prestressed and Prestressed Concrete. *ALDOT Testing Manual*. Montgomery, AL: Alabama Department of Transportation.

Alabama Department of Transportation. 2010b. Section 513: Prestressed Concrete Bridge Members. *ALDOT Testing Manual*. Montgomery, AL: Alabama Department of Transportation.

Alabama Department of Transportation. 2014. Alabama Traffic Database, Counter ID AL-62-572. *ALDOT Transportation Planning Bureau*. Accessed May 19, 2014. http://aldotgis.dot.state.al.us/atd/default.aspx.

Alavi-Fard, M., and H. Marzouk. 2004. Bond of High-Strength Concrete Under Monotonic Pull-Out Loading. *Magazine of Concrete Research* 56 (9): 545–557.

Almeida Filho, F.M., B.E. Barragan, J.R. Casas, and A.L.H.C. El Debs. 2010. Hardened Properties of Self-Compacting Concrete – A Statistical Approach. *Construction and Building Materials* 24 (9): 1608–1615.

Almeida Filho, F.M., M.K. El Debs, and A.L.H.C. El Debs. 2008. Bond-Slip Behavior of Fresh Self-Compacting Concrete and Vibrated Concrete Using Pull-Out and Beam Tests. *Materials and Structures* 41 (6): 1073–1089.

Al-Omaishi, N. 2001. Prestress Losses in High Strength Pretensioned Concrete Bridge Girders. Report, University of Nebraska-Lincoln.

Al-Omaishi, N., M.K. Tadros, and S.J. Seguirant. 2009. Elasticity Modulus, Shrinkage, and Creep of High-Strength Concrete as Adopted by AASHTO. *PCI Journal* 54 (4): 44–63.

Al-Ostaz, A. 2007. *Effect of Moisture Content on the Coefficient of Thermal Expansion of Concrete*. Report FHWA/MS-DOT-RD-07-187. Oxford, MS: University of Mississippi.

Assaad, J., K.H. Khayat, and J.A. Daczko. 2004. Evaluation of Static Stability of Self-Consolidating Concrete. *ACI Materials Journal* 101 (3): 207–215.

ASTM C39. 2010. Standard Test Method for Compressive Strength of Cylindrical Concrete Specimens. *ASTM International*. West Conshohocken, PA.

ASTM C94. 2011. Standard Specification for Ready-Mixed Concrete. *ASTM International*. West Conshohocken, PA.

ASTM C157. 2008. Standard Test Method for Length Change of Hardened Hydraulic-Cement Mortar and Concrete. *ASTM International*. West Conshohocken, PA.

ASTM C469. 2010. Standard Test Method for Static Modulus of Elasticity and Poisson's Ratio of Concrete in Compression. *ASTM International*. West Conshohocken, PA.

ASTM C496. 2011. Standard Test Method for Splitting Tensile Strength of Cylindrical Concrete Specimens. *ASTM International*. West Conshohocken, PA.

ASTM C512. 2002. Standard Test Method for Creep of Concrete in Compression. *ASTM International*. West Conshohocken, PA.

ASTM C597. 2002. Standard Test Method for Pulse Velocity Through Concrete. *ASTM International*. West Conshohocken, PA.

ASTM C1610. 2006. Standard Test Method for Static Segregation of Self-Consolidating Concrete Using Column Technique. *ASTM International*. West Conshohocken, PA.

ASTM C1611. 2005. Standard Test Method for Slump Flow of Self-Consolidating Concrete. *ASTM International*. West Conshohocken, PA.

ASTM C1712. 2009. Standard Test Method for Rapid Assessment of Static Segregation Resistance of Self-Consolidating Concrete Using Penetration Test. *ASTM International*. West Conshohocken, PA.

Baran, E., C. French, and C. Shield. 2003. *Effects of Vertical Pre-Release Cracks on Prestressed Bridge Girders*. University of Minnesota Report MN/RC 2003-33. Minneapolis, MN: University of Minnesota.

Barnes, R..W., N.H. Burns, and M.E. Kreger. 2000. *Development Length of 0.6-Inch Prestressing Strand in Standard I-Shaped Pretensioned Concrete Beams*. CTR Research Report

1388-1. Austin, TX: Center for Transportation Research, The University of Texas at Austin.

Barnes, R.W., J.W. Grove, and N.H. Burns. 2003. Experimental Assessment of Factors Affecting Transfer Length. *ACI Structural Journal* 100 (6): 740–748.

Barr, P.J., B.M. Kukay, and M.W. Halling. 2008. Comparison of Prestress Losses for a Prestress Concrete Bridge Made with High-Performance Concrete. *Journal of Bridge Engineering*, ASCE. (September/October): 468–475.

Bartos, P.J.M. 2005. Assessment of Key Characteristics of Fresh Self-Compacting Concrete: A European Approach to Standardisation of Tests. In *Second North American Conference On The Design And Use Of Self-Consolidating Concrete And The Fourth International RILEM Symposium On Self-Compacting Concrete*. Edited by S.P. Shah. pp. 807–829. Addison, IL: Hanley-Wood.

Bazant, Z.P. and L. Panula. 1978. Practical Prediction of Time Dependent Deformations of Concrete, Parts I–IV. *Materials and Structures* 11: 307–378, 425–343, and 12: 169–183.

Boehm, K.M., R.W. Barnes, and A.K. Schindler. 2010. *Performance of Self-Consolidating Concrete in Prestressed Girders.* Auburn, AL: Auburn University Highway Research Center.

Bonen, D., and S.P. Shah. 2004. The Effects of Formulation on the Properties of Self-Consolidating Concrete. In *Concrete Science And Engineering: A Tribute To Arnon Bentur.* Edited by K. Kovler, J. Marchand, S. Mindess, and J. Weiss. pp. 43–56. Cachan Cedex, France: RILEM Publications s.a.r.l.

Bonen, D., and S.P. Shah. 2005. Fresh and Hardened Properties of Self-Consolidating Concrete. *Progress in Structural Engineering and Materials* 7 (1): 14–26.

Bui, V.K., E.K. Attiogbe, D. Vojtko, S. Schaef, and H.T. See. 2007. A Rapid Test for Segregation Resistance of Self-Consolidating Concrete. In *2007 Concrete Technology Forum: Focus On High Performance Concrete*. Dallas: National Ready Mixed Concrete Association.

Buettner, D.R. and R.L. Hollrah. 1968. Creep Recovery of Plain Concrete. *ACI Materials Journal* 65 (6): 452–461.

Castel, A., T. Vidal, K. Viriyametanont, and R. Francois. 2006. Effect of Reinforcing Bar Orientation and Location on Bond with Self-Consolidating Concrete. *ACI Structural Journal* 103 (4): 559–567.

Cattaneo, S., G. Muciaccia, and G. Rosati. 2008. Bond Strength in Limestone Self-Compacting Concrete. In *3rd North American Conference On The Design And Use Of Self-Consolidating Concrete: Challenges And Barriers To Application*. Evanston, Illinois: Center for Advanced Cement Based Materials (ACBM). CD-ROM.

CEB (Comite Euro-International du Beton). 1990. Creep and Shrinkage. In *CEB-FIP Model Code 1990*. Lausanne, Switzerland: CEB.

Chan, Y., Y. Chen, and Y. Liu. 2003. Development of Bond Strength of Reinforcement Steel in Self-Consolidating Concrete. *ACI Structural Journal* 100 (4): 490–498.

Cussigh, F. 1999. Self-Compacting Concrete Stability Control. In *First International RILEM Symposium On Self-Compacting Concrete*. Edited by A. Skarendahl and O. Petersson. pp. 153–167. Cachan Cedex, France: RILEM Publications s.a.r.l.

Daczko, J.A. 2003. Stability of Self-Consolidating Concrete, Assumed or Ensured?. In *First North American Conference On The Design And Use Of Self-Consolidating Concrete*. Edited by S. Shah, J. Daczko, and J. Lingscheit. pp. 245–251. Addison, IL: Hanley-Wood.

Dunham, E.L. 2011. Transfer Length in Bulb-Tee Girders Constructed with Self-Consolidating Concrete. M.S. Thesis, Auburn University.

El-Chabib, H., and M. Nehdi. 2006. Effect of Mixture Design Parameters on Segregation of Self-Consolidating Concrete. *ACI Materials Journal* 103 (5): 374–383.

Ellis, M.A. 2012. Time-Dependent Deformations of Concrete for Precast/Prestressed Bridge Components. M.S. Thesis, Auburn University.

Emanuel, J.H. and J.L. Hulsey. 1977. Prediction of the Thermal Coefficient of Expansion of Concrete. *ACI Journal* 74 (4): 149–155.

EPG (Self-Compacting Concrete European Project Group). 2005. *The European guidelines for self-compacting concrete*. Farnham, UK: EFNARC.

Erkmen, B., C.K. Shield, and C.E. French. 2008. *Self-Compacting Concrete (SCC) for Prestressed Bridge Girders*. MnDOT Report 2008-51. Minneapolis, MN: University of Minnesota.

Esfahani, M.R., M. Lachemi, and M.R. Kianoush. 2008. Top-Bar Effect of Steel Bars in Self-Consolidating Concrete (SCC). *Cement and Concrete Composites* 30 (1): 52–60.

Fang, W., C. Jianxiong, and Y. Changhui. 1999. Studies on Self-Compacting High Performance Concrete with High Volume Mineral Additives. In *First International RILEM Symposium On Self-Compacting Concrete*. Edited by A. Skarendahl and O. Petersson. pp. 569–578. Cachan Cedex, France: RILEM Publications s.a.r.l.

Fang, C.F. and S. Labi. 2006. Evaluating the Static Segregation Resistance of Hardened Self-Consolidating Concrete Using Image Processing Technology. In *Proceedings of the 86th Annual Meeting of the Transportation Research Board*. Washington, DC: Transportation Research Board.

fib. 2010. Creep and Shrinkage. In *fib Model Code for Concrete Structures 2010*. Lausanne, Switzerland: International Federation for Structural Concrete (*fib*).

FHWA. 2011. Coefficient of Thermal Expansion in Concrete Pavement Design. *ACPT TechBrief* FHWA-HIF-09-015.Springfield, VA: ACPT.

Gardner, N.J. and M.J. Lockman. 2001. Design Provisions for Drying Shrinkage and Creep of Normal-Strength Concrete. *ACI Materials Journal* 98 (2): 159–167.

Gardner, N.J. and H. Tsuruta. 2004. Is Superposition of Creep Strains Valid for Concrete Subjected to Drying Creep? *ACI Materials Journal* 101 (5): 409–415.

Gaydecki, P.A., F.M. Burdekin, W. Damaj, D.G. John, and P.A. Payne. 1992. The Propagation and Attenuation of Medium-Frequency Ultrasonic Waves in Concrete: A Signal Analytical Approach. *Measurement Science And Technology* 3 (1): 126–134.

Geokon. 2010. Model 4200/4204/4210 Vibrating Wire Strain Gauge Instruction Manual. Rev. N, 8/10.

Girgis, A.F.M., and C.Y. Tuan. 2005. Bond Strength and Transfer Length of Pretensioned Bridge Girders Cast with Self-Consolidating Concrete. *PCI Journal* 50 (6): 72–87.

Hamilton, H.R., T. Labonte, and M.H. Ansley. 2005. *Self-Consolidating Concrete (SCC) Structural Evaluation*. University of Florida Report BD545, RPWO#21. Gainesville, FL: University of Florida.

Hassan, A.A.A., K.M.A. Hossain, and M. Lachemi. 2010. Bond Strength of Deformed Bars in Large Reinforced Concrete Members Cast with Industrial Self-Consolidating Concrete Mixture. 2010. *Construction and Building Materials* 24, (4): 520–530.

Horta, A. 2005. Evaluation of Self-Consolidating Concrete for Bridge Structure Applications. M.S. thesis, Georgia Institute of Technology.

Hossain, K.M.A., and M. Lachemi. 2008. Bond Behavior of Self-Consolidating Concrete with Mineral and Chemical Admixtures. *Journal of Materials in Civil Engineering* 20 (9): 608–616.

Hwang, S., K.H. Khayat, and O. Bonneau. 2006. Performance-Based Specifications of Self-Consolidating Concrete Used in Structural Applications. *ACI Materials Journal* 103 (2): 121–129.

Jeanty, P.R., D. Mitchel, and M.S. Mirza. 1988. Investigation of “Top-Bar” Effects in Beams. *ACI Structural Journal* 85 (3): 251–257.

Johnson, B.R. 2012. Time-Dependent Deformations in Precast, Prestressed Bridge Girders. M.S. Thesis, Auburn University.

Johnson, D., G. Johnson, and I.N. Robertson. 2010. *Qualifying Segregation in Self-Consolidating Concrete Through Image Analysis*. Research report UHM/CEE/10-04. Manoa, HI: Department of Civil and Environmental Engineering.

Kamgang, J. 2013. Compliance of Self-Consolidating Concrete for Prestressed Applications. M.C.E. report, Auburn University.

Kavanaugh, B. 2008. Creep Behavior of Self-Consolidating Concrete. M.S. thesis, Auburn University.

Keske, S.D. 2011. Assessment of Stability Test Methods for Self-Consolidating Concrete. M.S. thesis, Auburn University.

Keske, S.D. 2014. Use of Self-Consolidating Concrete in Precast, Prestressed Girders. Ph.D. dissertation, Auburn University.

Keske, S.D., R.W. Barnes, A.K. Schindler, E.L. Dunham, M.A. Ellis, B.R. Johnson, and W.O. Bullock. 2013. SCC Precast, Prestressed Girders in the Hillabee Creek Bridge. In *Proceedings of the 5th North American Conference on the Design and Use of Self-Consolidating Concrete*. Chicago, May 12–15, 2013. Center for Advanced Cement-Based Materials, Chicago.

Keske, S.D., R.W. Barnes, A.K. Schindler, B.R. Johnson, M.A. Ellis, D.E. Miller, and T.L. Neal. 2015. *Self-Consolidating Concrete for Prestressed Applications—Phase II: Bridge Construction and In-Place Performance.* Auburn, AL: Auburn University Highway Research Center.

Khan, L.F. and K.E. Kurtis. 2010. Self-Consolidating Concrete in Congested Sections: Mixture Characteristics and Assessment of Performance. *PCI Journal* 55 (5): 79–96.

Khayat, K.H., 1998. Use of Viscosity-Modifying Admixtures to Reduce Top-Bar Effect of Anchored Bars Cast with Fluid Concrete. *ACI Materials Journal* 95 (2): 158–167.

Khayat, K.H. 1999. Workability, Testing, and Performance of Self-Consolidating Concrete. *ACI Materials Journal* 96 (3): 346–353.

Khayat, K.H., and J. Assaad. 2002. Air-Void Stability in Self-Consolidating Concrete. *ACI Materials Journal* 99 (4): 408–416.

Khayat, K.H., E.K. Attiogbe, and H.T. See. 2007. Effect of Admixture Combination on Top-Bar Effect of Highly Flowable And Self-Consolidating Concrete Mixtures. In *Special Publication SP-247: Self-Consolidating Concrete for Precast Prestressed Applications*, ed. A.K. Schindler, D. Trejo, and R.W. Barnes. Farmington Hills, MI: American Concrete Institute. CD-ROM.

Khayat, K.H., A. Ghezal, and M.S. Hadriche. 2000. Utility of Statistical Models in Proportioning Self-Consolidating Concrete. *Materials and Structures* 33 (5): 338–344.

Khayat, K.H., S.D. Hwang, and K. Belaid. 2010. Performance of Cast-In-Place Self-Consolidating Concrete Made With Various Types of Viscosity-Enhancing Admixtures. *ACI Materials Journal* 107 (4): 403–412.

Khayat, K.H., K. Manai, and A. Trudel. 1997. In Situ Mechanical Properties of Wall Elements Cast Using Self-Consolidating Concrete. *ACI Materials Journal* 94 (6): 491–500.

Khayat, K.H., and D. Mitchell. 2009. *National Cooperative Highway Research Program (NCHRP) Report 628: Self-Consolidating Concrete for Precast, Prestressed Concrete Bridge Elements*. Washington, DC: Transportation Research Board.

Khayat, K.H., N. Petrov, E.K. Attiogbe, and H.T. See. 2003. Conventional Flowable and Self-Consolidating Concrete Mixtures. In *Third International Symposium on Self-Compacting Concrete*. Edited by O. Wallevik and I. Nielsson. pp. 703–712. Bagneux, France: RILEM Publications S.A.R.L.

Kim, Y.H., D. Trejo, H.N. Atahan, and M.B.D. Hueste. 2012. Mechanical Property Prediction for High Early Strength Self-Consolidating Concrete. *Journal of Materials in Civil Engineering* 24 (12): 1501–1512.

Koehler, E.P., and D.W. Fowler. 2008. Static and Dynamic Yield Stress Measurements of SCC. *Third North American Conference on the Design and Use of Self-Consolidating Concrete*, Chicago, IL. CD-ROM.

Koehler, E.P., and D.W. Fowler. 2010. Comparison of Workability Test Methods for Self-Consolidating Concrete. *Journal of ASTM International* 7 (2).

Koehler, E.P., D.W. Fowler, E.H. Foley, G.J. Rogers, S. Watanachet, and M.J. Jung. 2007. *Self-Consolidating Concrete for Precast Structural Applications: Mixture Proportions, Workability, and Early-Age Hardened Properties*. CTR Technical Report 0-5134-1. Austin, TX: Center for Transportation Research, The University of Texas at Austin.

Komlos, K., S. Popovics, T. Nurnbergerova, B. Babal, and J.S. Popovics. 1996. Ultrasonic Pulse Velocity Test of Concrete Properties as Specified in Various Standards. *Cement and Concrete Composites* 18 (5): 357–364.

Kwan, A.K.H., and I.Y.T. Ng. 2009. Optimum Superplasticizer Dosage and Aggregate Proportions for SCC. *Magazine of Concrete Research* 61 (4): 281–292.

Lange, D.A., L.J. Struble, M.D. D'Ambrosia, L. Shen, F.Tejeda-Dominguez, B.F. Birch, and A.J. Brinks. 2008. *Performance and Acceptance of Self-Consolidating Concrete: Final Report*. Illinois Center for Transportation Report FHWA-ICT-08-120. Urbana, IL: Illinois Center for Transportation.

Lemieux, G., S.D. Hwang, and K.H. Khayat. 2010. Effect of Material Constituents and Mix Design on Performance of SCC for Precast, Prestressed Girders. In *Design, Production, and Placement of Self-Consolidating Concrete*. Edited by K.H. Khayat and D. Feys. pp. 25–35. New York, NY: Springer.

Levy, K.R. 2007. Bond Behavior of Prestressed Reinforcement in Beams Constructed with Self-Consolidating Concrete. M.S. Thesis, Auburn University.

Levy, K.R., R.W. Barnes, and A.K. Schindler. 2010. Time-Dependent Deformations of Pretensioned, Self-Consolidating Concrete. In *Think Globally, Build Locally: Proceedings of the Third International fib Congress and Exhibition in Washington, D.C*. 29 May-2 June 2010, Chicago: Precast/Prestressed Concrete Institute.

Lin, Y., S. Kuo, C. Hsiao, and C. Lai. 2007. Investigation of Pulse Velocity-Strength Relationship of Hardened Concrete. *ACI Materials Journal* 104 (4): 344–350.

Lin, Y., C. Lai, and T. Yen. 2003. Prediction of Ultrasonic Pulse Velocity (UPV) in Concrete. *ACI Structural Journal* 100 (1): 21–28.

Malhotra, V.M. and V. Sivasundaram. 2004. Resonant Frequency Methods. In *Handbook on Nondestructive Testing of Concrete,* 2nd ed. Edited by V.M. Malhotra and N.J. Carino. Boca Raton, FL: CRC Press LLC.

Mehta, P.K., and P.J.M. Monteiro. 2006. *Concrete: Microstructure, Properties, and Materials*. 3rd ed. New York, NY: The McGraw Hill Companies.

Mindess, S., J.F. Young, and D. Darwin. 2003. *Concrete*. 2nd ed. Upper Saddle River, NJ: Pearson Education.

Mitchell, D., W.D. Cook, A.A. Kahn, and T. Tham. 1993. Influence of High-Strength Concrete on Transfer and Development Length of Pretensioning Strand. *PCI Journal* 38 (3): 52–66.

Mouret, M., G. Escadeillas, and A. Bascoul. 2008. Metrological Significance of the Column Test in Assessment of the Static Segregation of Self-Compacting Concrete in the Fresh State. *Materials and Structures* 41 (4): 663–679.

Myers, J.J. 2008. The Use Of High Strength/High Performance Concrete In America: A Code and Application Perspective. In *Proceedings of the 8th International Symposium on Utilization of High-Strength Concrete and High-Performance Concrete*. 27-29 October 2008, Tokyo: International Federation for Structural Concrete (*fib*).

Naito, C., G. Brunn, G. Parent, and T. Tate. 2005. *Comparative Performance of High Early Strength and Self-Consolidating Concrete for Use in Precast Bridge Beam Construction: Final Report*. ATLSS Report 05-03. Lehigh, PA: Advanced Technology for Large Structural Systems.

Naik, T.R., V.M. Malhotra, and J.S. Popovics. 2004. The Ultrasonic Pulse Velocity Method. In *Handbook on Nondestructive Testing of Concrete,* 2nd ed. Edited by V.M. Malhotra and N.J. Carino. Boca Raton, FL: CRC Press LLC.

Neville, A.M. 1996. *Properties of Concrete,* Fourth Edition. New York: John Wiley & Sons, Inc.

Nilson, A.H. 1987. *Design of Prestressed Concrete*, Second Edition. New York: John Wiley & Sons, Inc.

Ng, I.Y.T., H.H.C. Wong, and A.K.H. Kwan. 2006. Passing Ability and Segregation Stability of Self-Consolidating Concrete with Different Aggregate Proportions. *Magazine of Concrete Research* 58 (7): 447–457.

Ozyildirim, C. 2008. *Bulb-T Beams with Self-Consolidating Concrete on the Route 33 Bridge Over the Pamunkey River in Virginia.* FHWA/VTRC Report 09-R5. Charlottesville, VA: VTRC.

Ozyildirim, C., and D.S. Lane. 2003. *Virginia Transportation Research Council (VTRC) Report: Evaluation of Self-Consolidating Concrete.* Charlottesville, VA: VTRC.

Panesar, D.K. and B. Shindman. 2011. Elastic Properties of Self-Consolidating Concrete. *Construction and Building Materials* 25 (8): 3334–3344.

Parra, C., M. Valcuende, and F. Gomez. 2011. Splitting Tensile Strength and Modulus of Elasticity of Self-Compacting Concrete. *Construction and Building Materials* 25 (1): 201–207.

PCI (Precast/Prestressed Concrete Institute). 2004. *Interim Guidelines for the Use of Self-Consolidating Concrete in Precast/Prestressed Concrete Institute Member Plants*, 1st ed. Chicago: Precast/Prestressed Concrete Institute.

Peterman, R.J. 2007. The Effects of As-Cast Depth and Concrete Fluidity on Strand Bond. *PCI Journal* 52 (3): 72–101.

Peterson, K., L. Sutter, and T. VanDam. 2002. Air Void Analysis of Hardened Concrete with a High-Resolution Flatbed Scanner. In *Proceedings of the 24th International Conference on Cement Microscopy*. pp. 611–617. San Diego, CA: International Cement Microscopy Association.

Pierard, J., V. Dieryck, and J. Desmyter. 2005. Autogeneous Shrinkage of Self-Compacting Concrete. In *Second North American Conference on the Design and Use of Self-Consolidating Concrete and the Fourth International RILEM Symposium on Self-Compacting Concrete*. pp. 1013–1022. Addison, Illinois: Hanley-Wood.

Pozolo, A.M. and B. Andrawes. 2011. Transfer Length in Prestressed Self-Consolidating Concrete Box and I-Girders. *ACI Structural Journal* 108 (3): 341–349.

Raghavan, K.P., Sarma, B.S., Chattopadhyay, D. 2003. Creep, Shrinkage and Chloride Permeability Properties of Self-Consolidating Concrete. In *First North American Conference on the Design and Use of Self-Consolidating Concrete.* Edited by S. Shah, J. Daczko, and J. Lingsheit. pp. 307–317. Evanston, Illinois: Hanley-Wood.

Ramge, P., T. Proske, and H.C. Kuhn. 2010. Segregation of Coarse Aggregates in Self-Compacting Concrete. In *Design, Production, And Placement Of Self-Consolidating Concrete*. Edited by K.H. Khayat and D. Feys. pp. 113–126. New York, NY: Springer.

Russell, B.W. and N.H. Burns. 1993. *Design Guidelines for Transfer, Development and Debonding of Large Diameter Seven Wire Strands in Pretensioned Concrete Girders*. CTR Research Report 1210-5F. Austin, TX: Center for Transportation Research, The University of Texas at Austin.

Saak, A.W., H.M. Jennings, and S.P. Shah. 2001. New Methodology for Designing Self-Compacting Concrete. *ACI Materials Journal* 98 (6): 429–439.

Sahmaran, M., O. Yaman, and M. Tokyay. 2007. Development of High-Volume Low-Lime and High-Lime Fly-Ash-Incorporated Self-Consolidating Concrete. *Magazine of Concrete Research* 59 (2): 97–106.

Sakyi-Bekoe, K.O. 2008. Assessment of the Coefficient of Thermal Expansion of Alabama Concrete. M.S. Thesis, Auburn University.

Schindler, A.K., R.W. Barnes, J.B. Roberts, and S. Rodriguez. 2007. Properties of Self-Consolidating Concrete for Prestressed Members. *ACI Materials Journal* 104 (1): 53–61.

Schrantz, C.E. 2012. Development of a User-Guided Program for Predicting Time-Dependent Deformations in Prestressed Bridge Girders. M.S. Thesis, Auburn University.

Schwartzentruber, L.D., and G.V.M. Broutin. 2005. Quantifying the Segregation Risk of Self-Compacting Concrete by Gammadensitometry. In *Second North American Conference on The Design and Use of Self-Consolidating Concrete and the Fourth International RILEM Symposium on Self-Compacting Concrete*. Edited by S.P. Shah. pp. 713–720. Addison, IL: Hanley-Wood.

Shen, L. 2007. Role of Aggregate Packing in Segregation Resistance and Flow Behavior of Self-Consolidating Concrete. Report, University of Illinois.

Shen, L., L. Struble, and D. Lange. 2007. New Method for Measuring Static Segregation of Self-Compacting Concrete. *Journal of Testing and Evaluation* 35 (3).

Solis-Carcano, R., and E.I. Moreno. 2008. Evaluation of Concrete Made with Crushed Limestone Aggregate Based on Ultrasonic Pulse Velocity. *Construction and Building Materials* 22 (6): 1225–1231.

Sonebi, M., and P.J.M. Bartos. 1999. Hardened SCC and Its Bond with Reinforcement. In *First International RILEM Symposium on Self-Compacting Concrete*. Edited by A. Skarendahl and O. Petersson. pp. 275–284. Cachan Cedex, France: RILEM Publications s.a.r.l.

Sonebi, M., and P.J.M. Bartos. 2002. Filling Ability and Plastic Settlement of Self-Compacting Concrete. *Materials and Structures* 35 (8): 462–469.

Soshiroda, T., K. Voraputhaporn, and Y. Nozaki. 2006. Early-Age Inspection of Concrete Quality in Structures by Combined Nondestructive Method. *Materials and Structures* 39 (2): 149–160.

Soylev, T.A., and R. Francois. 2003. Quality of Steel-Concrete Interface and Corrosion of Reinforcing Steel. *Cement and Concrete Research* 33 (9): 1407–1415.

Stallings, J.M., R.W. Barnes, and S. Eskildsen. 2003. Camber and Prestress Losses in Alabama HPC Bridge Girders. *PCI Journal* 48 (5): 90–104.

Staton, B.W., N.H. Do, E.D. Ruiz, and W.M. Hale. 2009. Transfer Lengths of Prestressed Beams Cast with Self-Consolidating Concrete. *PCI Journal* 54 (2): 64–83.

Stocker, M.F., and M.A. Sozen. 1970. *Engineering Experiment Station Bulletin 503: Investigation of Prestressed Reinforced Concrete For Highway Bridges, Part Five: Bond Characteristics of Prestressing Strand*. Edited by V. Griffin. Urbana, IL: University of Illinois

Storm, T.K., S.H. Rizkalla, and P.Z. Zia. 2013. Effects of Production Practices on Camber of Prestressed Concrete Bridge Girders. *PCI Journal* 58 (2): 96–111.

Su, J. K., S.W. Cho, C.C. Yang, and R. Huang. 2002. Effect of Sand Ratio on the Elastic Modulus of Self-Compacting Concrete. *Journal of Marine Science and Technology* 10 (1): 8–13.

Swords, J.S. 2005. Transfer Length in Prestressed Self-Consolidating Concrete. M.S. thesis, Auburn University.

Tadros, M.K., N. Al-Omaishi, S.J. Seguirant, and J.T. Gallt. 2003. *NCHRP Report 496: Prestress Losses in Pretensioned High-Strength Concrete Bridge Girders*., National Cooperative Highway Research Program (NCHRP). Washington, DC: Transportation Research Board.

Tregger, N., L. Ferrara, and S.P. Shah. 2010. Predicting Dynamic Segregation of Self-Consolidating Concrete from the Slump-Flow Test. *Journal of ASTM International* 7 (1).

Trejo, D., M.B. Hueste, Y.H. Kim, and H. Atahan. 2008.*Characterization of Self-Consolidating Concrete for Design of Precast, Prestressed Bridge Girders*. College Station, Texas: Texas Transportation Institute.

Trent, J.D. 2007. Transfer Length, Development Length, Flexural Strength, and Prestress Loss Evaluation in Pretensioned Self-Consolidating Concrete Members. M.S. thesis, Virginia Polytechnic Institute and State University.

Ye, Y., D. Bonen, and S.P. Shah. 2005. Fresh Properties and Segregation Resistance of Self-Compacting Concrete. In *Second North American Conference on the Design and Use of Self-Consolidating Concrete and the Fourth International RILEM Symposium on Self-Compacting Concrete*. Edited by S.P. Shah. pp. 621–627. Addison, IL: Hanley Wood.

Yue, L.L. and L. Taerwe. 1993. Two-Function Method for the Prediction of Concrete Creep Under Decreasing Stress. *Materials and Structures* 26 (159): 268–273.

Zhu, W., J.C. Gibbs, and P.J.M. Bartos. 2001. Uniformity of In Situ Properties of Self-Compacting Concrete in Full-Scale Structural Elements. *Cement and Concrete Composites* 23 (1): 57–64.

Zia, P., R.A. Nunez, and L.A. Mata. 2005. *Implementation of Self-Consolidating Concrete for Prestressed Concrete Girders*. Raleigh, NC: North Carolina Department of Transportation.

Ziehl, P.H., D.C. Rizos, J.M. Caicedo, F. Barrios, R.B. Howard, and A.S. Colmorgan. 2009. *Investigation of the Performance and Benefits of Lightweight SCC Prestressed Concrete Bridge Girders and SCC Materials*. Report No. FHWA-SC-09-02. Columbia, South Carolina: University of South Carolina.

APPENDICES

Laboratory Phase (work related to Chapter 2)

Appendix A: Laboratory-Phase Test Results

Appendix B: Fresh Concrete Stability Test Methods

Field Phase (work related to Chapters 3–6)

Appendix C: BP Coefficient of Determination (ω_{BP})

Appendix D: Thermal Effects and Full-Scale Girder Responses

APPENDIX A: LABORATORY-PHASE TEST RESULTS

Table A.1–Table A.3: Fresh Concrete Stability Results

Table A.4–Table A.10: Hardened Concrete Uniformity Results

Table A.1: Individual fresh concrete stability test results

Mixture ID	VSI	Seg. Index (%)	Rapid Penetration (in.)	Sieve Fraction (%)	Rate of Settlement (%/hr)	Maximum Settlement (%)
SCC-1A	1.5, 2.5	3.2, 8.0	0.20, 0.31	*	0.16	0.60
SCC-1B	0.5, 1	0.0, 0.0	0.08, 0.31	5.6, 7.3	0.12, 0.21	0.31, 0.41
SCC-1C	1, 1.5	8.0, 8.7	0.12, 0.12	7.4, 9.0	0.06, 0.15	0.03, 0.04
SCC-1D	1, 1.5	20.7, 14.3	0.28, 0.39	13.8, 17.7	0.01, 0.02	0.01, 0.01
SCC-2A	1.5, 2	7.4, 8.6	0.24, 0.47	13.6, 13.9	0.02, 0.06	0.02, 0.03
SCC-2B	3, 3	18.1, 21.9	0.24, 0.43	24.4, 36.6	0.18, 0.33	0.13, 0.15
SCC-2C	1.5, 2	0.8, 5.2	0.08, 0.20	8.7, 9.2	0.09, 0.15	0.07, 0.10
SCC-2D	1, 1.5	6.4, 15.7	0.08, 0.12	4.9, 5.4	0.23, 0.27	0.09, 0.17
SCC-2E	1.5, 2	14.7, 18.4	0.12, 0.16	13.3, 15.2	0.15, 0.19	0.12, 0.23

*Note: * = sieve fraction result recorded incorrectly by operator*

Table A.2: Surface settlement results—additional information

Mixture ID	Rate of Settlement (%/hr)	Maximum Settlement (%)	Settlement at 10 min. (%)	Settlement at 15 min. (%)	Time at Ultimate Settlement (min.)
SCC-1A	0.15	0.60	0.35	0.37	105
SCC-1B	0.15	0.35	0.31	0.32	30
SCC-1C	0.11	0.03	0.02	0.03	60
SCC-1D	0.02	0.01	0.00	0.01	60
SCC-2A	0.05	0.02	0.01	0.02	60
SCC-2B	0.25	0.14	0.08	0.10	60
SCC-2C	0.12	0.09	0.03	0.04	105
SCC-2D	0.25	0.13	0.08	0.10	30
SCC-2E	0.17	0.18	0.11	0.13	60

Table A.3: Fresh concrete stability test result nonlinear R^2 values

Test Result	VSI	Seg. Index	Rapid Pen.	Sieved Fraction	Rate of Settlement	Max. Settlement
Maximum Settlement	0.03	0.00	0.00	0.00	0.47	-
Rate of Settlement	0.09	0.00	0.00	0.00	-	
Sieved Fraction	0.66	0.53	0.46	-		
Rapid Penetration	0.13	0.05	-			
Segregation Index	0.29	-				
VSI	-					

Table A.4: Horizontal row average measurements from UPV testing—94 in. walls

Norm. Ht of 94 in.	Average Measured Ultrasonic Pulse Velocity (10^3 ft/s)										
	VC-1	SCC-1A	SCC-1B	SCC-1C	SCC-1D	VC-2	SCC-2A	SCC-2B	SCC-2C	SCC-2D	SCC-2E
0.95	14.61	13.93	14.53	13.99	13.19	14.21	13.57	13.06	14.54	12.64	14.11
0.87	14.72	14.11	14.55	13.84	13.09	14.77	13.53	14.13	14.42	12.90	13.87
0.78	14.66	13.97	14.53	13.62	13.02	14.58	13.68	14.50	14.40	13.09	13.84
0.70	14.57	13.88	14.45	13.76	13.16	14.53	13.65	14.38	14.55	13.11	13.77
0.61	14.50	14.03	14.73	13.68	13.26	14.85	13.73	14.28	14.58	13.14	14.09
0.53	14.34	14.05	14.35	13.63	13.47	14.88	13.80	14.33	14.40	13.20	14.18
0.44	14.42	13.91	14.62	13.66	13.30	14.77	13.71	14.40	14.65	13.17	13.99
0.37	14.39	13.76	14.36	13.79	13.14	14.98	13.60	14.25	14.31	13.17	14.06
0.30	14.20	13.80	14.37	13.53	13.20	14.77	13.76	14.45	14.37	13.24	14.24
0.21	14.40	14.56	14.44	13.76	13.39	14.60	13.74	14.41	14.33	13.12	14.11
0.13	14.30	13.85	14.30	13.74	13.29	14.72	13.71	14.33	14.23	13.11	14.01
0.04	14.48	14.76	14.75	13.78	13.51	14.54	13.88	14.55	14.39	13.34	14.22

Table A.5: Horizontal row average measurements from UPV testing—72 in. walls

Norm. Ht of 72 in.	Average Measured Ultrasonic Pulse Velocity (10^3 ft/s)										
	VC-1	SCC-1A	SCC-1B	SCC-1C	SCC-1D	VC-2	SCC-2A	SCC-2B	SCC-2C	SCC-2D	SCC-2E
0.94	14.29	14.00	14.34	13.93	13.17	13.75	13.25	14.03	14.40	12.69	13.89
0.83	14.69	14.20	14.52	13.95	13.11	14.26	13.44	14.32	14.37	13.07	13.81
0.74	14.66	14.28	14.56	14.04	13.22	14.36	13.45	14.36	14.52	13.22	13.76
0.63	14.68	14.16	14.57	13.90	13.05	14.59	13.63	14.21	14.50	13.12	13.84
0.53	14.51	14.36	14.74	13.87	13.02	14.65	13.65	14.10	14.31	13.25	13.77
0.42	14.47	14.39	14.82	13.92	13.40	14.47	13.65	14.12	14.30	12.95	13.90
0.33	14.29	14.33	14.71	13.80	13.28	14.53	13.63	13.99	14.34	13.01	13.93
0.25	14.35	14.39	14.55	13.89	13.27	14.47	13.55	13.92	14.27	12.97	13.93
0.17	14.46	14.24	14.53	13.99	13.45	14.36	13.48	14.09	14.33	13.19	14.05
0.06	14.59	14.46	14.90	14.20	13.50	14.22	13.80	14.34	14.45	13.31	14.12

Table A.6: Horizontal row average measurements from UPV testing—54 in. walls

Norm. Ht of 54 in.	Average Measured Ultrasonic Pulse Velocity (10^3 ft/s)										
	VC-1	SCC-1A	SCC-1B	SCC-1C	SCC-1D	VC-2	SCC-2A	SCC-2B	SCC-2C	SCC-2D	SCC-2E
0.93	14.41	-	14.29	13.82	12.83	13.90	13.53	14.26	14.19	12.72	14.01
0.78	14.64	14.46	14.36	13.83	12.98	14.22	13.53	14.16	14.15	12.98	13.88
0.65	14.52	14.78	14.44	13.92	13.00	14.28	13.56	14.14	14.19	13.06	13.76
0.54	14.52	14.47	14.51	14.01	13.12	14.27	13.60	14.44	14.15	12.92	13.68
0.41	14.31	14.14	14.44	13.74	13.07	14.39	13.52	14.09	14.05	13.08	13.73
0.31	14.34	14.13	14.51	13.91	13.05	14.35	13.58	14.10	14.26	13.10	13.72
0.22	14.44	14.22	14.46	13.92	13.21	14.33	13.53	14.09	14.24	12.98	13.84
0.07	14.46	14.18	14.53	13.86	13.22	14.23	13.53	14.26	14.35	13.25	13.97

Note: - = Result not obtained

Table A.7: Maximum and minimum horizontal row average measurements from UPV testing, and calculated UPV segregation indices

Mixture ID	94 in. Wall		72 in. Wall		54 in. Wall	
	Max, Min (10^3 ft/s)	UPV Unif.	Max, Min (10^3 ft/s)	UPV Unif.	Max, Min (10^3 ft/s)	UPV Unif.
CTRL-1	14.72 14.20	1.036	14.69 14.29	1.028	14.64 14.31	1.023
SCC-1A	14.76 13.76	1.073	14.46 14.00	1.033	14.78 14.13	1.046
SCC-1B	14.75 14.30	1.031	14.90 14.34	1.039	14.53 14.36	1.012
SCC-1C	13.99 13.53	1.034	14.20 13.80	1.029	14.01 13.74	1.019
SCC-1D	13.51 13.02	1.038	13.50 13.02	1.036	13.22 12.98	1.019
CTRL-2	14.98 14.21	1.054	14.65 13.75	1.066	14.39 14.22	1.011
SCC-2A	13.88 13.53	1.026	13.80 13.25	1.042	13.60 13.52	1.006
SCC-2B	14.55 13.06	1.114	14.36 13.92	1.032	14.44 14.09	1.025
SCC-2C	14.65 14.23	1.030	14.52 14.27	1.017	14.35 14.05	1.021
SCC-2D	13.34 12.64	1.056	13.31 12.69	1.049	13.25 12.92	1.026
SCC-2E	14.24 13.77	1.034	14.12 13.76	1.026	13.97 13.68	1.021

Table A.8: Eight-bar-group average pullout strength and top-bar factor—94 in. walls

Norm. Ht of 94 in.	Average Measured Pullout Strength (lb)										
	VC-1	SCC-1A	SCC-1B	SCC-1C	SCC-1D	VC-2	SCC-2A	SCC-2B	SCC-2C	SCC-2D	SCC-2E
0.91	8,324	6,230	8,779	5,507	3,724	4,364	4,905	3,646	7,003	3,050	3,490
0.08	8,294	7,106	10,212	6,381	4,058	7,625	5,701	7,091	7,908	4,004	5,454
Top-Bar	1.00	1.14	1.16	1.16	1.09	1.75	1.16	1.94	1.13	1.31	1.56

Table A.9: Eight-bar-group average pullout strength measurement—72 in. walls

Norm. Ht of 72 in.	Average Measured Pullout Strength (lb)										
	VC-1	SCC-1A	SCC-1B	SCC-1C	SCC-1D	VC-2	SCC-2A	SCC-2B	SCC-2C	SCC-2D	SCC-2E
0.89	8,341	7,669	7,031	6,071	4,295	4,204	4,062	3,844	6,470	2,321	4,617
0.11	9,078	8,355	9,443	6,860	4,223	6,899	5,157	7,245	7,614	3,884	5,156
Top-Bar	1.09	1.09	1.34	1.13	1.00	1.64	1.27	1.88	1.18	1.67	1.12

Table A.10: Eight-bar-group average pullout strength measurement—54 in. walls

Norm. Ht of 54 in.	Average Measured Pullout Strength (lb)										
	VC-1	SCC-1A	SCC-1B	SCC-1C	SCC-1D	VC-2	SCC-2A	SCC-2B	SCC-2C	SCC-2D	SCC-2E
0.85	8,749	6,157*	5,653	5,913	4,144	3,923	4,986	2,312	6,076	1,778	3,495
0.15	8,918	7,634	8,794	6,456	4,495	6,500	5,761	6,467	7,920	3,651	5,110
Top-Bar	1.02	1.24	1.56	1.09	1.08	1.66	1.16	2.80	1.30	2.05	1.46

*Note: * = The recorded pullout strength was the average of four pullout specimens located at a normalized height of 0.78h (42 in.)*

APPENDIX B: FRESH CONCRETE STABILITY TEST METHODS

Appendix B.1: Sieve Stability Test Method

Appendix B.2: Surface Settlement Test Method

Appendix B.1: Sieve Stability Test Method

1. Scope

1.1. This procedure provides a method for quantitatively measuring the stability of fresh self-consolidating concrete (SCC). This test method is used to monitor the ability of the freshly mixed SCC to resist segregation, or separation of its constituent materials, during or after placement.

2. General

2.1. This test method is intended for laboratory or field use.

2.2. This test shall be conducted near concurrent fresh-property testing but shall be positioned to avoid disturbance from vibration or impact during testing.

2.3. The use of at least one apparatus to obtain the result is required. The simultaneous use of two apparatuses to obtain an average result is recommended. When using two apparatuses to obtain an average result, filling of the apparatuses shall be conducted consecutively within a single 60-second period.

2.4. The Contractor shall supply all equipment necessary to execute this procedure. The equipment shall be approved by the Materials and Tests Engineer prior to use.

3. Equipment

3.1. 12 in. {305 mm} diameter No. 4 sieve, at least 2 in. {50 mm} tall from upper surface of wire mesh to upper lip of sieve.

3.2. Sieve pan, from which the sieve can be easily removed by lifting vertically.

3.3. Scale, having a flat platform to firmly support the sieve and pan, a capacity of at least 22 lb {10 kg}, and calibrated increments of ≤ 0.02 lb {10 g}.

3.4. Cylindrical sample container, either plastic or metal, with an internal diameter of 12 in. ± 3/8 in. {300 mm ± 10 mm} and a capacity of 3 gal. ± 0.1 gal. {11.4 L ± 0.4 L}. The sample container shall be clearly marked to indicate a volume of 2.6 gal. {10 L} for use when obtaining the concrete sample. An example of this marking is illustrated in Figure B.2.

3.5. Pouring apparatus, which shall be used to support the sample container and ensure a constant pouring height of 20 in. ± 2 in. {510 mm ± 51 mm}. Example pouring apparatuses are shown in Figure B.1 and Figure B.2.

4. Testing Procedure

4.1. Weigh the pan while empty, and record the mass (pan). Then add the sieve, weigh the empty sieve and pan, and record the mass (sieve + pan).

4.2. Place 2.6 gal. ± 0.1 gal. {10 L ± 0.5 L} of concrete in the sample container and allow it to stand in a level position undisturbed for {15 min. ± 30 s}*. While the sieve and pan are still on the scale, and after the {15 min.}* standing period, pour 10.5 lb ± 0.5 lb {4.8 kg ± 0.2 kg}, of concrete (including bleed water) onto the center region of the sieve from a height of 20 in. ± 2 in. {510 mm ± 51 mm} above the sieve mesh. Record the total weight on the scale (sieve + pan + SCC total). *Note: * = Testing according to the sieve stability test has been updated per Keske et al. (2015) report to include a standing period of 80 s ± 5 s.*

4.2.1. The 20 in. {510 mm} height is measured from the lowest point of the rim of the cylindrical sample container to the upper surface of the sieve mesh, as illustrated in Figure B.1.

4.2.2. An example of a pouring apparatus is illustrated in Figure B.1. The hinge for the pouring apparatus is positioned such that the lowest point of the rim of the cylindrical sample container remains at a constant height as the concrete is poured. Note: To maintain a constant pouring height of 20 in. ± 2 in. {510 mm ± 51 mm} above the sieve mesh, the distance from the ground to the hinge will depend on the combined height of the scale, pan, and sieve utilized, as shown in Figure B.1.

4.2.3. A scale with instantaneous reading display is recommended for use when pouring 10.5 lb ± 0.5 lb {4.8 kg ± 0.2 kg} of concrete (including bleed water) onto the center of the sieve.

4.3. Allow the concrete to rest on the sieve for 120 s ± 5 s, and then remove the sieve vertically from the pan while avoiding any agitation. Record the mass of the pan and concrete that has passed into it from the sieve (pan + SCC sieved fraction).

5. Result

5.1. The sieved fraction (S) is calculated by dividing the weight of SCC passing into the pan by the total weight of SCC tested. It is calculated according to the following equation:

$$S = \frac{[(pan + SCC\ sieved\ fraction) - (pan)]}{[(sieve + pan + SCC\ total) - (sieve + pan)]} \times 100$$

5.2. Record S to the nearest half of a percent.

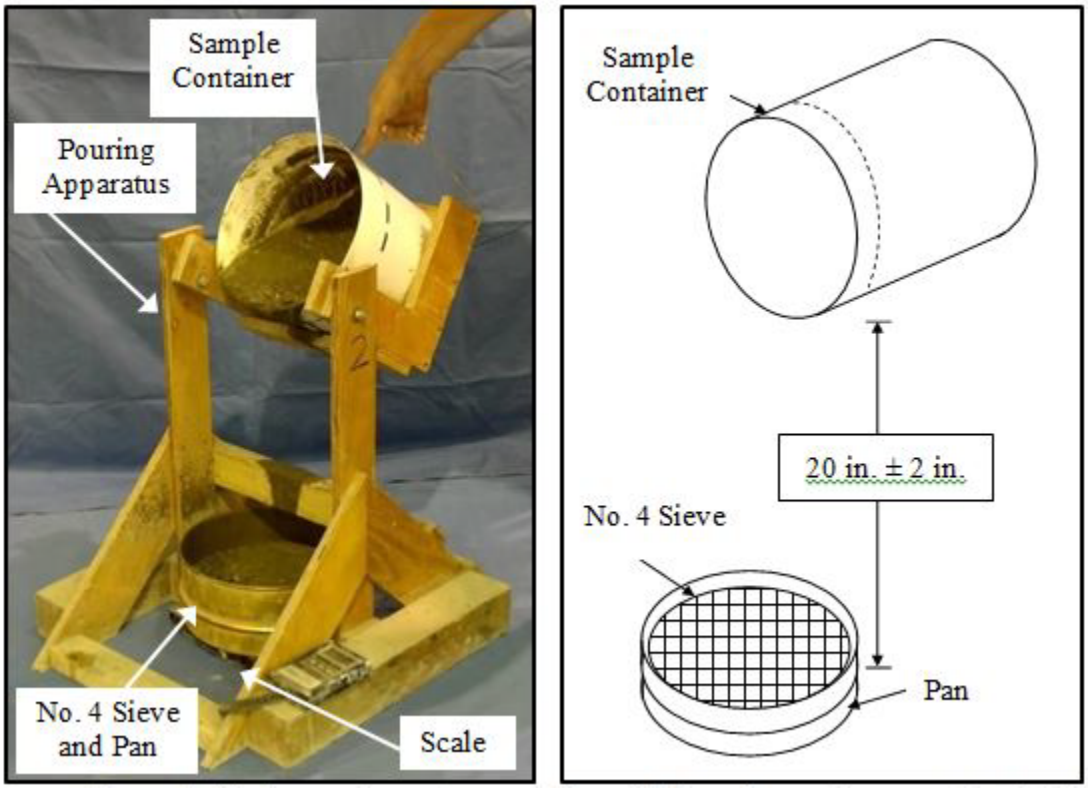

Figure B.1: Sieve stability test (*left*) equipment and (*right*) pouring height of sample

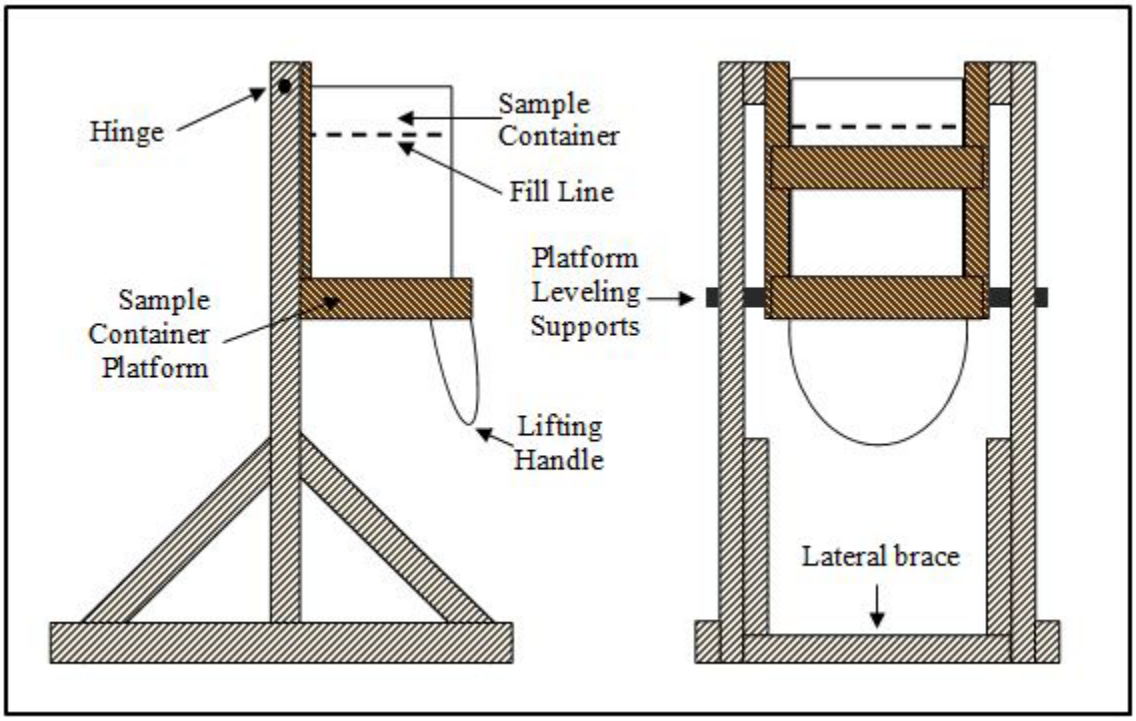

Figure B.2: Pouring apparatus (side and front elevations)

Appendix B.2: Surface Settlement Test Method

1. Scope

1.1. This procedure provides a method for quantitatively measuring the stability of fresh self-consolidating concrete (SCC). This test method is used to monitor the ability of the freshly mixed SCC to resist segregation, or separation of its constituent materials, during or after placement.

2. General

2.1. This test method is intended for laboratory use only.

2.2. This test shall be conducted near concurrent fresh-property testing but shall be positioned to avoid disturbance from vibration or impact during testing.

2.3. The use of at least one apparatus to obtain the result is required. The simultaneous use of two apparatuses to obtain an average result is recommended. When using two apparatuses to obtain an average result, filling of the apparatuses shall be conducted consecutively within a single 4-minute period.

2.4. The Contractor shall supply all equipment necessary to execute this procedure. The equipment shall be approved by the Materials and Tests Engineer prior to use.

3. Equipment

3.1. Column mold, as shown in Figure B.3. Made of Schedule 40 PVC, the column shall be 8 in. {200 mm} in diameter and 26 in. {660 mm} tall and shall be securely attached to the rigid, nonabsorbent base plate.

3.2. Dial indicator, with a 0.0004 in. {0.01 mm} precision and minimum travel length of 2 in. {50 mm}, or linear variable differential transformer (LVDT), with a minimum travel length of 2 inches {50 mm}.

3.3. Acrylic plate, as shown in Figure B.3. The plate shall be 6 in. {150 mm} in diameter and 0.15 in. {4 mm} in thickness. It shall have four ½ in. {13 mm} holes and four 1.4 in. {35 mm} screws that penetrate downward into the sample. The configuration of holes and screws is shown in the figure.

3.4. Sample container, of sufficient capacity to allow sufficient remixing of the entire sample and rapid filling of the column mold apparatus.

4. Testing Procedure

4.1. Fill the column mold with concrete to a level of 19.7 in. {500 mm} within 2 minutes.

4.2. Install the acrylic plate, with screws facing downward into the concrete, directly over the center of the column mold. Then, install the dial indicator or LVDT over the center of the acrylic plate.

4.3. Record an initial reading of the dial indicator or LVDT 60 sec. after its installation. Then, record readings at 5 min. intervals through the first 15 minutes.

4.4. Optionally (not recommended), continue to record readings every 5 minutes until total elapsed time since initial reading equals 30 minutes, then record readings every 30 min. until concrete reaches initial set.

5. Result

5.1. The rate of settlement is calculated using the readings recorded at 10 min. (S_{10}) and 15 min. (S_{15}) after the initial reading, using the equation shown below:

$$rate\ of\ \ settlement\ (\%/hr) = \frac{\left[\frac{(S_{15} - S_{10})}{19.7\ in.}\right]}{5\ \text{min}} \times \frac{60\ \text{min}}{1\ hr} \times 100$$

5.2. The maximum settlement (S_{max}) is calculated using the initial ($S_{initial}$) and final (S_{final}) readings, using the equation shown below:

$$S_{\max}(\%) = \frac{(S_{final} - S_{initial})}{19.7\ in} \times 100$$

5.3. In the above equations, uniformity of notation is required—if surface settlement readings are measured in millimeters, then the difference between measurements must be divided by 500 mm instead of 19.7 inches.

5.4. Record the rate of settlement per hour as a percentage of the sample height. Optionally (not recommended), record the maximum settlement as a percentage of the sample height.

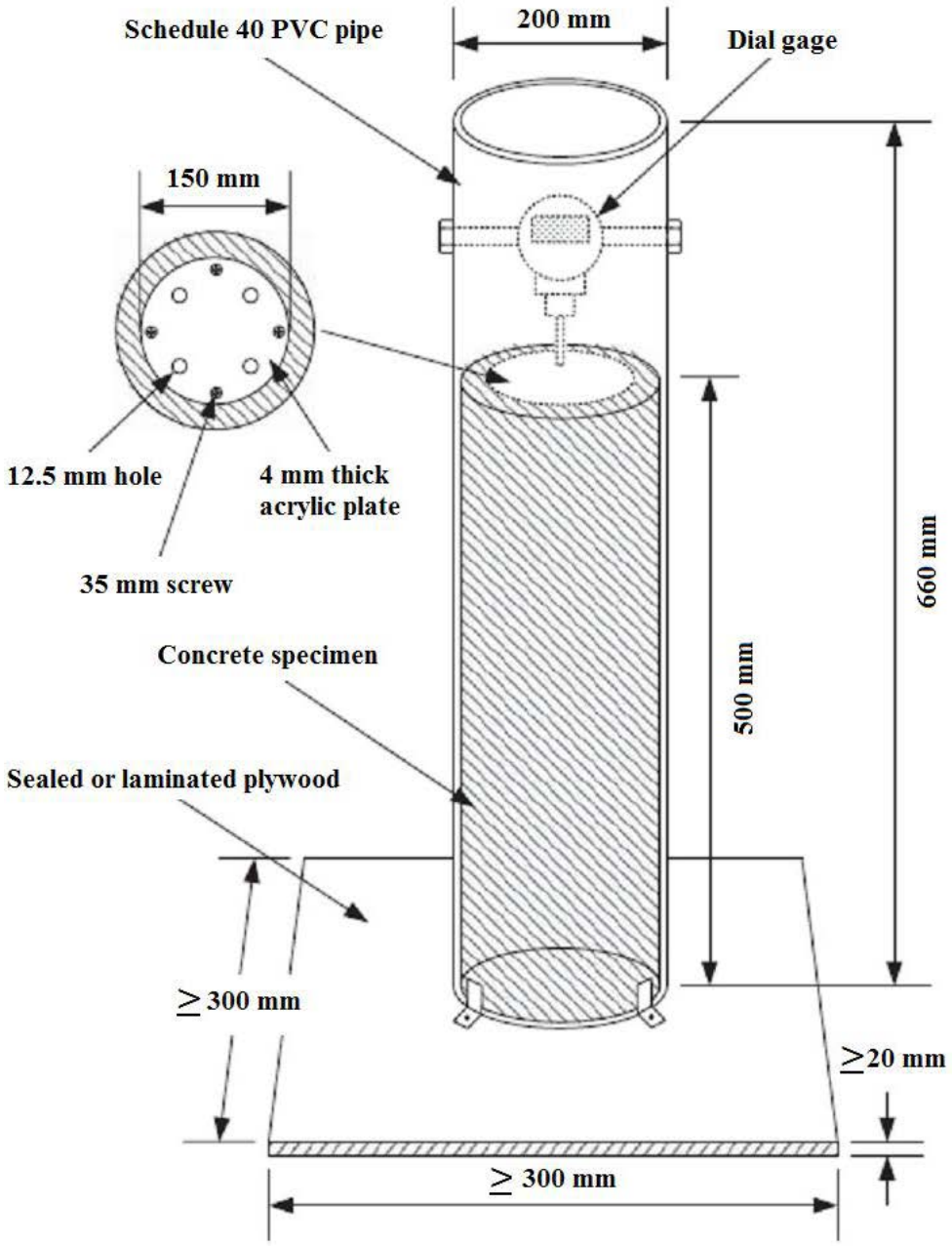

Figure B.3: Surface settlement test apparatus

APPENDIX C: BP COEFFICIENT OF DETERMINATION (ω_{BP})

The BP Coefficient of Determination (ω_{BP}) was developed by Bazant and Panula (1978) to indicate the error between measured time-dependent deformation data and values predicted at each time step. Data points are grouped by logarithmic decade: 0–9.9 days, 10–99.9 days, etc. Weights are determined based on the number of decades and number of points within each decade. Errors in both an individual dataset and all comparable datasets can then be calculated using the following equations:

$$\varpi_{ij} = \frac{n}{n_d n_k}$$

$$\overline{O_j} = \frac{1}{n_w} \sum_{i=1}^{n} \left(\varpi_{ij} O_{ij} \right)$$

$$\varpi_j = \frac{1}{\overline{O_j}} \sqrt{\frac{1}{n-1} \sum_{i=1}^{n} \varpi_{ij} \left(C_{ij} - O_{ij} \right)^2}$$

$$\varpi_{BP} = \sqrt{\frac{1}{N} \sum_{j=1}^{N} {\varpi_j}^2}$$

Where

ω_{ij} is the weight assigned to the *i*-th data point of dataset *j*,

n is the number of data points in dataset *j*,

n_d is the number of logarithmic-scale decades spanned by the measured data in dataset *j,*

n_k is the number of data points in the *k*-th logarithmic decade,

$\overline{O_j}$ is the weighted average of the measured values of the time-dependent property for the *j*-th dataset,

n_w is the sum of the weights of all data points in an entire dataset,

O_{ij} is the measured value of the time-dependent property for the *i*-th data point in dataset *j*,

ω_j is the coefficient of variation for dataset *j*,

C_{ij} is the predicted value of the time-dependent property for the *i*-th data point in dataset *j*,

ω_{BP} is the overall coefficient of variation, and

N is the number of measured datasets.

APPENDIX D: THERMAL EFFECTS AND GIRDER RESPONSES

Table D.1–Table D.2: Measured and Predicted Prestress Losses

Table D.3–Table D.4: Measured and Predicted Cambers

Table D.1: Measured temperature-corrected losses and losses predicted using ACI 209

Girder	Temperature-Corrected (ksi)			Predicted using ACI 209 (ksi)		
	Initial	56 Days	Deck Add.	Initial	56 Days	Deck Add.
54-1S	12.5	18.9	20.7	11.2	23.8	29.2
54-2S	12.0	17.4	19.5	11.4	24.2	29.7
54-3S	12.6	18.4	20.3	11.2	23.8	29.2
54-4S	11.6	18.5	20.5	11.2	23.8	29.2
54-5S	13.4	21.0	21.6	11.4	24.2	29.7
54-6S	12.5	18.0	20.1	11.4	24.2	29.7
54-7S	12.9	20.3	22.3	11.6	24.2	29.8
54-1V	-	-	-	N.A.	N.A.	N.A.
54-2V	12.5	20.2	20.9	10.0	21.3	26.2
54-3V	13.4	20.4	21.8	10.6	22.2	27.2
54-4V	13.4	20.4	22.0	10.6	22.2	27.2
54-5V	12.0	17.7	18.6	10.0	21.3	26.2
54-6V	11.6	18.6	19.3	10.0	21.3	26.2
54-7V	12.6	18.8	20.6	11.0	23.5	28.9
72-1S	14.2	23.4	26.9	13.2	26.8	31.8
72-2S	14.2	23.4	26.5	13.1	26.5	31.6
72-3S	14.3	20.2	24.7	13.0	26.4	31.4
72-4S	13.5	18.7	22.7	13.0	26.4	31.4
72-5S	13.4	18.8	23.0	13.1	26.5	31.6
72-6S	14.4	21.5	25.3	13.4	26.8	31.9
72-7S	14.8	21.8	26.3	13.2	26.8	31.8
72-1V	13.1	20.7	24.0	11.4	23.5	28.0
72-2V	14.0	21.0	24.6	10.9	22.6	27.0
72-3V	13.1	18.8	21.9	11.3	23.2	27.8
72-4V	13.4	19.3	22.7	11.3	23.2	27.8
72-5V	13.5	19.5	22.9	10.9	22.6	27.0
72-6V	12.7	18.3	21.3	11.6	23.5	28.0
72-7V	12.9	19.9	23.1	11.4	23.5	28.0

Note: - = not available due to gauge failure; N.A. = not applicable due to absence of measured response

Table D.2: Prestress losses predicted using AASHTO 2013 and MC 2010

Girder	Predicted using AASHTO 2013 (ksi)			Predicted using MC 2010 (ksi)		
	Initial	56 Days	Deck Add.	Initial	56 Days	Deck Add.
54-1S	11.2	24.4	28.3	11.2	22.9	28.1
54-2S	11.4	24.7	28.3	11.4	23.3	28.5
54-3S	11.2	24.4	28.3	11.2	22.9	28.1
54-4S	11.2	24.4	28.3	11.2	22.9	28.1
54-5S	11.4	24.7	28.3	11.4	23.3	28.5
54-6S	11.4	24.7	28.3	11.4	23.3	28.5
54-7S	11.6	25.3	29.9	11.6	23.8	29.1
54-1V	N.A.	N.A.	N.A.	N.A.	N.A.	N.A.
54-2V	10.0	22.5	26.2	10.0	21.0	26.0
54-3V	10.6	24.1	28.6	10.6	22.8	28.2
54-4V	10.6	24.1	28.6	10.6	22.8	28.2
54-5V	10.0	22.5	26.2	10.0	21.0	26.0
54-6V	10.0	22.5	26.2	10.0	21.0	26.0
54-7V	11.0	23.9	27.8	11.0	22.8	28.1
72-1S	13.2	28.0	32.0	13.2	26.3	31.2
72-2S	13.1	27.7	31.8	13.1	26.0	30.8
72-3S	13.0	28.0	32.4	13.0	25.8	30.6
72-4S	13.0	28.0	32.4	13.0	25.8	30.6
72-5S	13.1	27.7	31.8	13.1	26.0	30.8
72-6S	13.4	29.5	34.7	13.4	27.3	32.4
72-7S	13.2	28.0	32.0	13.2	26.3	31.2
72-1V	11.4	25.1	28.8	11.4	23.5	28.0
72-2V	10.9	23.9	27.3	10.9	22.5	27.0
72-3V	11.3	24.9	28.8	11.3	23.2	27.7
72-4V	11.3	24.9	28.8	11.3	23.2	27.7
72-5V	10.9	23.9	27.3	10.9	22.5	27.0
72-6V	11.6	25.7	30.1	11.6	24.0	28.6
72-7V	11.4	25.1	28.8	11.4	23.5	28.0

Note: N.A. = not applicable due to absence of measured response

Table D.3: Measured temperature-corrected cambers and cambers predicted using ACI 209

Girder	Temperature-Corrected (in.)			Predicted using ACI 209 (in.)		
	Initial	56 Days	Deck Add.	Initial	56 Days	Deck Add.
54-1S	1.31	1.51	1.57	1.43	2.02	2.19
54-2S	1.73	1.91	2.05	1.47	2.06	2.24
54-3S	1.19	1.39	1.48	1.43	2.02	2.19
54-4S	1.13	1.46	1.61	1.43	2.02	2.19
54-5S	1.27	1.26	1.35	1.47	2.06	2.24
54-6S	1.85	1.91	1.91	1.47	2.06	2.24
54-7S	1.31	1.76	1.80	1.48	2.07	2.25
54-1V	1.45	1.67	1.77	1.37	1.94	2.12
54-2V	1.38	1.78	1.71	1.28	1.83	2.00
54-3V	1.56	1.77	1.94	1.37	1.94	2.12
54-4V	1.53	1.72	1.88	1.37	1.94	2.12
54-5V	1.07	1.32	1.24	1.28	1.83	2.00
54-6V	1.34	1.65	1.68	1.28	1.83	2.00
54-7V	1.24	1.56	1.60	1.42	2.09	2.30
72-1S	2.33	2.47	2.55	2.06	2.77	2.98
72-2S	1.82	2.47	2.55	2.05	2.76	2.97
72-3S	2.50	2.43	2.50	2.03	2.74	2.95
72-4S	2.29	2.28	2.22	2.03	2.74	2.95
72-5S	1.86	2.17	2.14	2.05	2.76	2.97
72-6S	2.18	2.64	2.72	2.10	2.82	3.04
72-7S	2.09	2.02	2.34	2.06	2.77	2.98
72-1V	2.00	2.13	2.15	1.78	2.44	2.64
72-2V	1.70	2.02	2.00	1.70	2.33	2.53
72-3V	1.82	2.35	2.45	1.76	2.42	2.63
72-4V	1.90	2.34	2.37	1.76	2.42	2.63
72-5V	1.81	2.02	2.09	1.70	2.33	2.53
72-6V	1.76	2.31	2.28	1.80	2.46	2.66
72-7V	1.91	2.13	2.09	1.78	2.44	2.64

Table D.4: Cambers predicted using AASHTO 2013 and MC 2010

Girder	Predicted using AASHTO 2013 (in.)			Predicted using MC 2010 (in.)		
	Initial	56 Days	Deck Add.	Initial	56 Days	Deck Add.
54-1S	1.36	2.06	2.23	1.55	2.10	2.31
54-2S	1.40	2.10	2.26	1.59	2.16	2.38
54-3S	1.36	2.06	2.23	1.55	2.10	2.31
54-4S	1.36	2.06	2.23	1.55	2.10	2.31
54-5S	1.40	2.10	2.26	1.59	2.16	2.38
54-6S	1.40	2.10	2.26	1.59	2.16	2.38
54-7S	1.41	2.15	2.35	1.62	2.20	2.43
54-1V	1.30	2.00	2.20	1.50	2.08	2.31
54-2V	1.22	1.85	2.00	1.39	1.89	2.09
54-3V	1.30	2.00	2.20	1.50	2.08	2.31
54-4V	1.30	2.00	2.20	1.50	2.08	2.31
54-5V	1.22	1.85	2.00	1.39	1.89	2.09
54-6V	1.22	1.85	2.00	1.39	1.89	2.09
54-7V	1.34	2.01	2.18	1.53	2.09	2.31
72-1S	1.97	2.85	3.09	2.22	2.91	3.18
72-2S	1.96	2.84	3.08	2.20	2.88	3.15
72-3S	1.94	2.85	3.11	2.19	2.85	3.12
72-4S	1.94	2.85	3.11	2.19	2.85	3.12
72-5S	1.96	2.84	3.08	2.20	2.88	3.15
72-6S	2.01	3.00	3.32	2.29	3.04	3.33
72-7S	1.97	2.85	3.09	2.22	2.91	3.18
72-1V	1.69	2.48	2.69	1.92	2.52	2.76
72-2V	1.62	2.35	2.54	1.83	2.41	2.64
72-3V	1.68	2.47	2.69	1.89	2.49	2.73
72-4V	1.68	2.47	2.69	1.89	2.49	2.73
72-5V	1.62	2.35	2.54	1.83	2.41	2.64
72-6V	1.72	2.53	2.78	1.95	2.58	2.82
72-7V	1.69	2.48	2.69	1.92	2.52	2.76